Strengenthening of concrete bridges using reinforced sprayed concrete under state and fatigue loading.

Dung, Pham-Thanh

STRENGTHENING OF CONCRETE BRIDGES USING REINFORCED SPRAYED CONCRETE UNDER STATIC AND FATIGUE LOADING

BY

DUNG PHAM-THANH

A THESIS SUBMITTED FOR THE DEGREE OF
DOCTOR OF PHILOSOPHY OF
THE UNIVERSITY OF LONDON

DEPARTMENT OF CIVIL ENGINEERING
UNIVERSITY OF LONDON
QUEEN MARY & WESTFIELD COLLEGE

NOVEMBER 1997

A THESIS DEDICATED TO

THE NEED

TO STRENGTHEN

HIGHWAY BRIDGES

THROUGHOUT

THE UNITED KINGDOM 'S

MOTORWAY NETWORK

NCE
3 July 1997

Cash crisis forces county to risk bridge overloading

NORTHUMBERLAND COUNTY Council is flouting government-set safety guidelines by allowing over 180 "understrength" bridges regularly to carry heavy lorries up to 38t, it emerged this week.

The bridges have all failed strengthening tests for vehicle loads above 13t, but carry no weight restrictions.

Engineers claim that a severe cash crisis in the Department of Transport's nationwide bridge strengthening programme, coupled with an "onerous" technical assessment regime, has forced the council to adopt what it sees as a "practical and responsible approach to the problem".

Northumberland Council bridges manager Greg Perks said: "The guidelines say we should impose weight or lane restrictions on any bridge that fails the assessment, but this would effectively gridlock much of the county's freight traffic and impose major economic and social hardship on rural communities."

"We have no option but to allow unrestricted use, but we carry out regular bridge inspections to ensure continued structural safety," he explained.

The council argues that access by heavy goods vehicles to industrial and agricultural outlets in this vast but essentially rural county – which boasts over 5,000km of road network – is essential for its economic survival.

To strengthen all 188 failed bridges to carry European Union-demanded 40t loading by January 1999 would cost £20M. But this year the council received just £1M in government grant – a fifth the sum it requested.

The council has already spent over £1M analysing nearly all 813 bridges in its strengthening assessment programme. And of the 269 that failed the 40t test, 81 on strategic routes have already been strengthened.

Most of the rest should, according to DoT rules, now carry 7.5t weight restrictions, with around 50 bridges failing even that loading restriction.

"If we continue to receive government funding at the current rate, all our allocation until 1999 will be committed to just one major strengthening operation on the Royal Tweed bridge, an essential route across the river," claimed Perks. "We regard unrestricted use of these bridges as an interim measure, but one that could remain interim for quite a while."

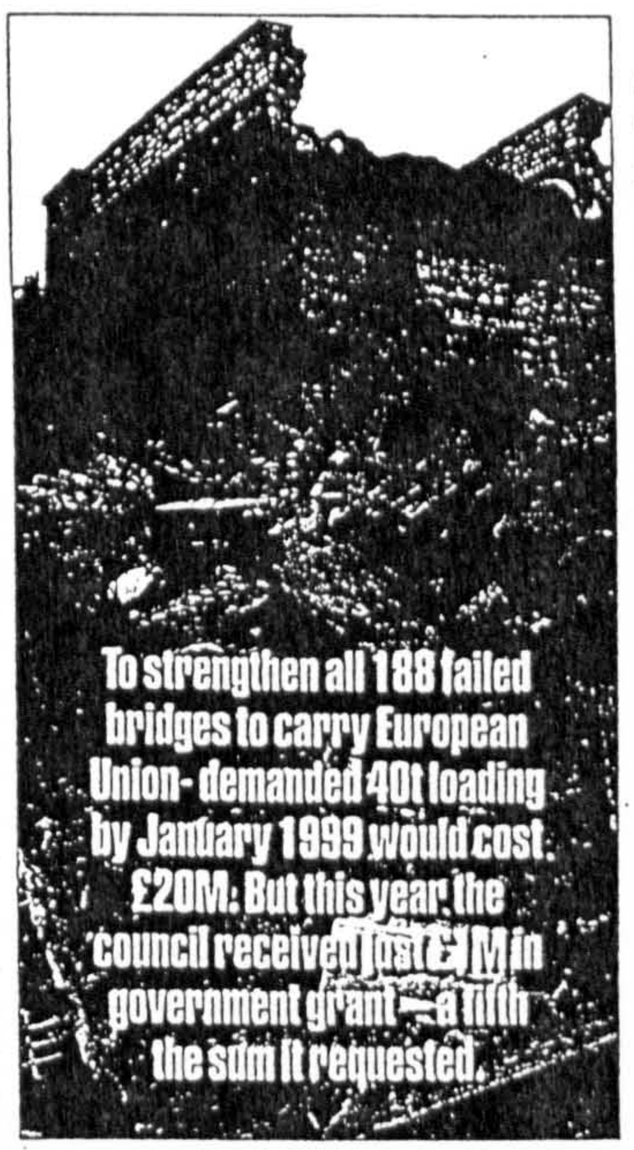

Perks stressed that detailed structural checks were now carried out at three to six month intervals on all failed bridges and any that showed signs of distress would immediately be closed or weight restricted. "Safety remains paramount," he insisted.

In common with most bridge authorities, Northumberland has used the DoT's 1993 bridge assessment codes which, according to Perks, take scant account of actual traffic conditions. Three months ago new, more flexible, DoT guidelines were issued which allow real traffic flow considerations to reduce any loading requirement by up to 15%.

The council now plans to reassess some of the failed bridges to the new code "as soon as funding is available".

"But the guidelines to which most councils have worked are onerous and too harsh," said Perks. "And it is unfortunate that the new more relaxed code has come out so late, after the majority of bridge assessments have been completed."

David Hayward

London's bridges fail weight test

ONLY NINE of London's 19 road bridges are capable of carrying the new generation of 40t lorries due in 1999, an *NCE* survey has revealed this week.

And by the time the new supertrucks hit British roads the total will have risen to just 11 at most, with only three more ready by the turn of the century. The rest will remain restricted to light traffic for the foreseeable future.

Four bridges on major trunk roads, Kingston, Twickenham, Waterloo and Lambeth, failed their initial assessments, with the Highways Agency still waiting for the results of the assessment on Chiswick Bridge. All the rest have long term restrictions which are unlikely to be lifted; from 2t on the Albert Bridge to 17t on Tower Bridge.

Twickenham Bridge, the responsibility of the Agency, has already been strengthened, and a three year, £12.5M contract to strengthen and widen Kingston Bridge will be let by the local authority later this year. Its initial assessment highlighted the need for a 3t weight limit. But with more than 50,000 vehicles a day using the crossing and no sign of serious distress to the masonry arches, engineers opted to keep it unrestricted until work was complete.

Work is also due to begin on Lambeth Bridge, although there is still no guarantee that the £800,000 needed to bring it up to the latest standards will be forthcoming from central government.

(see *Commentary* page 10.)

TABLE OF CONTENTS

ACKNOWLEDGEMENTS

The work described in this thesis is part of a research programme supported by the Engineering and Physical Science Research Council. A very major contribution to the work was made by Tarmac Structural Repairs Limited in carrying out all the concrete spraying, supplying materials and advising on the test programme. In particular the advice offered by Mr. P. J. Quarton has contributed significantly to the success of the investigation. The contribution of Elkem Materials Limited and Ready Mixed Concrete Limited who also supplied materials and equipment is also gratefully acknowledged.

I would like to express my most sincere appreciation and gratitude to Dr. E. Burley, former head of the department and Mr. S. R. Rigden, senior lecturer and consulting engineer for their enthusiastic support and keen supervision in this research programme.

Thanks are also due to all members of staff and technicians for their contributions in the experimental work.

Finally, I would like to thank my girlfriend for her encouragement and support.

SYNOPSIS

The Department of Transport's bridge assessment programme has revealed that a significant number of bridges are not strong enough to carry the much heavier commercial axle loads that will soon be applied to UK bridges.

To address this problem, this research investigates a technique of strengthening concrete bridges by bonding and encapsulating an extra layer of reinforcement using sprayed concrete to the soffit of the bridge to increase the flexural capacity.

An experimental investigation on approximately one eighth scale reinforced concrete slabs strengthened by different amounts of reinforcement placed at varying depths below the soffit and encapsulated by professionally applied dry-mix sprayed concrete, have shown that increased flexural capacity of up to eight times the original capacity is possible with no sign of breakdown of the bond at the soffit interface. Separate interface shear tests both direct and indirect were carried out and showed high shear capacities were obtained in all specimens. The susceptibility to weathering causing a breakdown of the interface bond was investigated by freeze-thaw tests.

Fatigue load tests have also shown that the strengthened slabs have a similar life span to that of normal reinforced concrete. An analytical study was carried out, complemented by the fatigue load test results, to assess the life span of two highway bridges when subjected to fluctuating traffic loading, taking into account the proposed increasing use of heavier axle loads.

All the slabs tested to failure under both static and fatigue loading failed in flexure and extremely good bond between the sprayed concrete layer and its substrate concrete was maintained right up to failure, even without shear connectors. The potential use of this technique in practice was therefore well demonstrated.

CHAPTER 1

INTRODUCTION

An extensive Department of Transport bridge assessment programme has revealed that there is a significant number of highway bridges that are deficient in their load carrying capacity to cope with the expected implementation of the EC directive in the UK which would result in much heavier commercial axle loads being applied to UK bridges. It has been recognised by many bridge owning authorities that there is extreme urgency for their bridge stock to be strengthened to meet this requirement. Currently bridges can only be strengthened by gluing steel plates onto the soffit of the bridge in the critically deficient moment region to increase their moment capacities. At the Department of Civil Engineering of Queen Mary & Westfield college, an alternative technique has been researched which was developed from a previous research programme [1] which found that by simply casting a new section of concrete, encasing reinforcement onto the soffit of a plain concrete member produced the same flexural capacity as a homogeneously cast reinforcement concrete beam of the same overall dimensions. From the authors contacts with industry, it became apparent that the majority of slab bridges failing the Department of Transport bridge assessment programme do so due to the lack of flexural capacity, not shear capacity. It was, therefore considered that a feasible strengthening technique could be based on bonding and encapsulating an extra layer of reinforcement using sprayed concrete to the soffit of a slab bridge.

In order to make the spraying procedure as practical as possible within the a university laboratory environment, it was proposed to simulate the technique by strengthening and testing approximately one eighth scale slabs of dimensions 2.4 x 1.0 x 0.1 metres.

A total of eighteen reinforced concrete slabs were cast to act as the base slabs and one of these was left unstrengthened as a control test slab. The remainder were all strengthened and from these, fourteen were tested under static loading and three were under fatigue, all to failure. The variables considered in both the static and fatigue

loading tests were the amount of mesh reinforcement, the thickness of the sprayed concrete layer and the mix used for the sprayed concrete.

The mechanical properties of the hardened sprayed concrete were measured and a petrographic examination was conducted together with measurement of chloride ingression.

One of the most influential factors affecting of the success of this technique of strengthening is the horizontal shear capacity developed at the substrate/sprayed concrete interface and this is governed by the type of surface preparation of the substrate concrete. In this research grit blasting was used throughout although in three test slabs shear connectors were incorporated in addition to grit blasting. To investigate the shear capacity of the substrate/sprayed concrete interface, experiments were conducted as follows:

1. Using slabs with and without shear connectors.
2. Increasing the shear at the interface by enhancing the reinforcement in the sprayed concrete layer by up to four times the reinforcement in the base slab in test slabs without shear connectors.
3. Conducting slant shear tests, double shear tests and direct shear tests.

The fatigue work undertaken in this research showed that a conservative practical useful life span of 50 years can be achieved using this technique to strengthen a concrete bridge. The steps undertaken were:

1. To establish a table of load range versus the number of cycles to failure. This was obtained by drawing a series of Goodman diagrams for different number of cycles to failure, which were abstracted from an assumed S-N curve obtained from the American Concrete Institute code ACI 215R-74(Revised 1986)[39] and a suitably modified version of the commercial vehicle axle load spectrum of BS 5400: Part 10: 1980[38].
2. Using Miner's hypothesis to assess the total life span of a typical concrete highway bridge which is carrying the modified load spectrum and whose fatigue life is predicted by the assumed S-N and the modified Goodman diagrams.
3. From the table discussed in (1.) a load range was chosen which gave an expected life and which could be reasonably accommodated by the limited time scale of this research with which to fatigue test three slabs. These results were then used in

conjunction with the analytical S-N study to predict fatigue life span of typical bridges.

A method of predicting the induced stresses due to the shrinkage of the sprayed concrete layer is recommended and its application on a typical highway concrete bridge is also presented.

CHAPTER 2

LITERATURE REVIEWS

2.1 SHOTCRETE ORIGINS

There are many legends and stories about how and why the cement gun was developed. The only thing these stories have in common is that they attribute the invention of the cement gun to Carl E. Akeley, a well known explorer and naturalist who was associated for many years with the field museum of Natural History in Chicago[2].

Akeley made attempts at using sprayed plaster for his animal models. He experimented with a pressure tank in which water and plaster of Paris were mixed and then blown through a hose. These trials were unsuccessful because he could not overcome the problem of hose plugging. It appears this process which we in later years would call wet-mix sprayed concrete had been used by contemporaries of Akeley for various purposes. However, Akeley overcame the problem of plugging by adapting the pressure tank to handle dry plaster which was blown through a hose with water added at the nozzle end. This simple yet ingenious device became the precursor of the cement gun and gunite or dry -mix sprayed concrete in today 's terminology. Akeley then developed a working model which would spray a plastic mixture of sand, cement and water onto a surface. By 1908 Akeley had experimented sufficiently to apply for a patent of a device that could successfully spray plaster mortar. In 1920 the cement gun was introduced to the construction industry at the New York Cement show in Madison Square Garden.

Akeley 's first successful practical work with the cement gun was the covering of the old Field museum with a coat of gypsum stucco. In February 1911 Akeley received a patent for the equipment, a single chamber gun with a vertical feedwheel; and the method, a process for producing and depositing plastic or adhesive mixtures. This device could be used only intermittently because it was a single chamber machine and had to be shutdown and re-loaded when empty. However, a second patent was issued in May 1911 for an apparatus that would mix and apply plastic adhesive materials. This

second patent was for equipment only, a variation of the original gun or device differing in two critical respects. First, a double chamber was substituted for the single chamber, which provided continuous flow allowing the lower chamber to operate while the upper was being loaded. Second, the vertical feedwheel was changed in design and moved into a horizontal position providing improved material flow and control. Today, this basic configuration with double chamber and horizontal feedwheel is essentially the same as in this second patent.

It is a matter of interest that at around the same time when Akeley's device was patented, there existed a European patent for a similar gun which were owned by Joseph Von Vass. It appears then that the cement gun concept was not necessarily an American original.

In 1916 Traylor Engineering & Manufacturing Co. of Allentown, PA, purchased the rights to the cement gun in the United States and began manufacturing and marketing the machine.

Sprayed concrete 's early history was the history of the cement gun since it was the most dominant process in existence, at least in the united States, if not in Europe. Many publications were undertaken in those early days but the process did not take hold until the 1920's after considerable research and development had been undertaken by the Cement Gun Co. From then until the post World War II period, a strong technical foundation as being laid to prepare for the revolution that was to take place in the 1950's.

2.2 SPRAYED CONCRETE DEVELOPMENT

In 1912 the word "Gunite", a trade name, was invented to describe the sand-cement product of the cement gun, focusing on its mortar like properties. This description of gunite seems to be the earliest definition of the material we call "fine aggregate dry-mix" shotcrete. Several other names, guncrete (1925) and pneucrete (1929) also appeared in the literatures to describe what is generally called "pneumatically placed mortar"[2], "pneumatically applied mortar" or "sprayed mortar". With regard to the fine aggregate wet-mix shotcrete; apparently during the 1910's or 1920's, a pneumatic concrete device developed by C. Weber was being used by the shotcrete industry

although the name wet-mix was not known at the time, its existence was approximately at the same time as dry-mix shotcrete.

In the early 1930's, the American Railway Engineering Association introduced the term " shotcrete " which they defined as pre-mixed dry portland cement and sand pneumatically ejected from a machine through a hose and a discharge nozzle where water is added, all under regulated pressure. This definition applied to all gunned applications with a mortar consisting of sand, cement and water using delivering equipment similar to the double chambered cement gun and it was enforced until the post World War II when the concrete technology and shotcrete underwent major changes and innovations.

In 1951 the ACI Committee 805-51 on Pneumatically Placed Mortar (now ACI Committee 506) published a standard "Recommended Practice for the Application of Mortar by Pneumatic Pressure"[3]. The standard defined pneumatically placed mortar as mortar which is projected by an air jet directly onto a surface to which it is to be applied irrespective of the type and manufacture of the mixing and placing apparatus. However, the term shotcrete was used for convenience instead of " pneumatically placed mortar " in the standard " Recommended Practice for the Application of Mortar by Pneumatic Pressure ". The ACI 805 's shotcrete definition was to be changed as it applied only to dry-mix process with fine aggregate, not coarse aggregate, even though a Swiss-made cement gun, the Aliva BS-12 had been used for gunning coarse aggregate dry-mix for almost ten years outside the United States.

In 1966 the ACI Committee 506-66 on shotcrete superseded the ACI 805-51 and produced the ACI standard " Recommended Practice for Shotcreting ". This new standard accounted for the many changes that were occurring in shotcrete technology during the years after World War II. With this new standard, the definition of shotcrete was modified to: mortar or concrete conveyed through a hose and pneumatically projected at high velocity onto a surface. The inclusion of the word " concrete " therefore recognised that coarse aggregate dry-mix shotcrete is a shotcrete process.

This revised standard also described and made comparisons between wet-mix and dry-mix processes in detail as well as standardising both coarse and fine aggregates gradations for shotcrete. The term ' shotcrete ' now adequately describes and defines the technology as it existed in the middle of the 1960 's.

About ten years on, the shotcrete technology continued expanding and the expansion brought with it more imprecisions and ambivalence. In 1977 the ACI 506.2 re-defined shotcrete, removing the part " conveyed through a hosė " to become " mortar or concrete pneumatically projected at high velocity onto a surface " and since then, this definition has been continued through many ACI 506 s' revisions to date.

According to current practice in the USA, mortar or concrete projected onto a surface at high velocity is referred to as shotcrete. Here in the UK, the process is referred to as sprayed concrete and the author would like to clarify to readers that this term is used from this point throughout the thesis. However, if the maximum aggregate size is less than 10mm it is referred to as gunite and shotcrete as in the USA if the size is greater than 10mm. For a type of mortar or concrete to be referred to as shotcrete, gunite or sprayed concrete, it should at least be shot, gunned or sprayed:

1. in a horizontal, vertical or overhead position without forms except in those cases where a single backing form is required.
2. without sloughing on vertical surfaces or sagging on overhead surfaces.
3. in any thickness especially in thin layers in the range of 4mm to 100mm.
4. in any shape or configuration, uniform or non-uniform thickness.
5. using liquid or powder accelerator to provide, if required any initial set, from 1 to 3 minutes.
6. using any combination of aggregate, binder or liquid.

2.2.1 Velocity of spraying concrete

Perhaps it would be agreed by most practising sprayed concrete engineers that if concrete cannot be sprayed at high velocity, in order to satisfy the six aforementioned conditions then sprayed concrete would have to be considered as just another routine method for the placing of concrete. Therefore there is an important question of what is meant by 'high velocity' or how low can high velocity be and still make the definition of sprayed concrete valid ? Ordinary pumped concrete has a very low exit velocity; could it be classified as sprayed concrete ? Similarly, could a mortar with air added at the nozzle impart sufficient velocity to the material to be classified as sprayed concrete ?

There are some sprayed concrete users who believe that the quality of *in situ* sprayed concrete, including durability is directly proportional to the exit velocity from the nozzle. Glassgold[2] indicated that in the case of dry-mix sprayed concrete, most of

the literature and experimental data available supports the principle that the higher the exit velocity, the better the sprayed concrete quality. In the case of the wet-mix process, it is generally agreed that the method of placement, except when using pneumatic feed equipment, does not improve the properties of the *in situ* sprayed concrete as it does in dry-mix. There have been unpublished reports, that if the exit velocity is increased in the we-mix process, there is an improvement in the properties of the sprayed concrete, however there are no published data to support this conclusion.

In attempting to investigate the question of exit velocity, the findings from various researchers are being reported as follows:

Stewart[4] conducted an experiment to measure the nozzle exit velocity of the sprayed concrete used in a reservoir re-lining job. The velocity at each nozzle used was read at the gun by means of a single manometer and a suitably calibrated scale. The results of the experiment indicated that sprayed concrete strength increases as exit velocity increases to an optimum level and that smaller diameter nozzles tend to achieve optimum strength at lower velocities. Figure 2.1 illustrates this results.

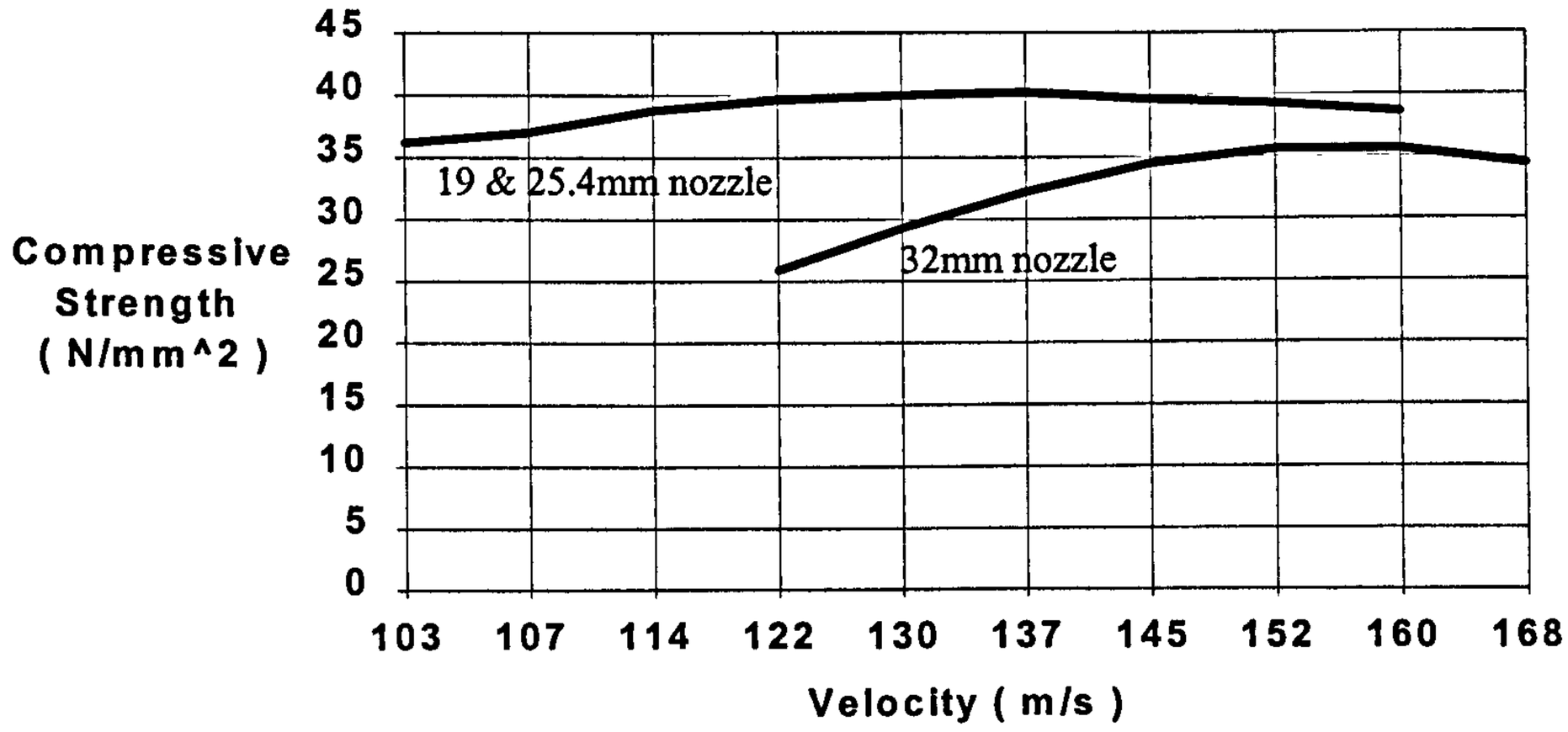

Figure 2.1 - Sprayed concrete velocity versus compressive strength for three sizes of nozzles, Stewart[4].

Clearly from Figure 2.1 the optimum sprayed concrete strength can be achieved with the smaller diameter nozzle at the operating velocity range from 122 to 145 m/s.

Ward and Hills[5] also indicated a correlation between exit velocity and strength similar to that of Stewart, that is the higher the nozzle exit velocity the higher the strength and density of the *in situ* sprayed concrete. However, the measured mean velocity is considerably less than that of Stewart at 35m/s measured from high-speed

photography. It must be pointed out that the velocity data here was incomplete as there were indications that the sprayed concrete strength and density was still increasing, though at a decreasing rate when the measurements ceased.

Parker[6] stated that measurement of the air stream using the stop-action photographic method indicated that particles were moving toward the wall at a rate of 30 to 60m/s. Although this finding tends to confirm Ward and Hills findings, there were indications that the statement was inconclusive and conflicts to some degree with his results reported in Department of Transportation report USA[7].

Valencia[8] stated that the material velocity is approximately 135m/s, is similar to Stewart's measurements. The method of velocity measurement was not described however.

Blumel, Lutsch and Stehno[9] stated that the nozzle velocity of the material is considered to be another crucial factor which influences the quality of sprayed concrete and the average nozzle velocity is in the range of 27 to 35m/s, the method of velocity measurement here was also not clearly described.

Ryan[10] stated that high nozzle velocity results in sprayed concrete of exceptional compaction, while low velocity sprayed concrete is less compacted in comparison but nevertheless exhibits the typical features of sprayed concrete. He indicated 90 to 120m/s for high velocity but gave no values for low velocity or how the velocity was measured.

There is obviously no unique answer to the question of nozzle exit velocity, although there is a general agreement that high nozzle velocity yields high quality *in situ* sprayed concrete. Perhaps in view of the variable opinions expressed in the literature reviews in-depth research into this particular subject using high-speed photography should be undertaken.

2.3 SPRAYED CONCRETE PROPERTIES

Sprayed concrete is a structurally sound and durable construction material. It exhibits very good bonding characteristics with concrete and many other construction materials. It also has many good physical properties which are comparable or superior to those of conventional concrete having the same composition. However, nearly all the good physical properties and performance of sprayed concrete are contingent on good

specifications, materials, proper surface preparation, mixing, competence and the experience of the application crew.

2.3.1 Bond strength

ACI 506R-90[11] contains recent data obtained from tests in which the load was applied parallel to the bond interface. Table 2.1 shows the data.

Table 2.1 - Bond strength of dry-mix sprayed concrete on old concrete.

Sample No.	Compressive strength of sprayed concrete cores (N/mm^2)	Bond strength in shear (N/mm^2)
1	40.3	5.0
2	49.2	4.1
3	40.7	2.9
4	37.3	3.6
5	48.7	6.0
6	31.9	2.8
7	31.6	3.5

Notes:

1. All test specimens are 150mm diameter cores.
2. All surface preparation are grit blasted.
3. Bond strength was maintained by "guillotine" method where shear bond is applied parallel to the bonded interface.

2.3.2 Water/cement ratio and drying shrinkage

The cement content of the *in situ* sprayed concrete is usually higher than in the designed composition due to the rebound and this, coupled with the generally low water/cement ratio potentially increases the strength of the sprayed concrete, it can however cause increased drying shrinkage. The use of joint spacing, reinforcing bars or mesh reinforcement can minimise this problem is recommended. Table 2.2 illustrates some typical values extracted from ACI 506R-90 and Schrader and Kaden[12].

Table 2.2. - Typical w/c ratio and drying-shrinkage of sprayed concrete.

Water/cement	Cement content (kg/m^3)	Shrinkage	Source
0.37	504	$9x10^{-4}$	Dry-mix sprayed concrete Schrader and Kaden
0.48	341	$5x10^{-4}$	Conventional concrete Schrader and Kaden
0.3 - 0.5 (*in situ*)	-	$(6\text{-}10)x10^{-4}$	Dry-mix sprayed concrete ACI 506R-90

2.3.3 Compressive strength and modulus of elasticity

From Schrader and Kaden, for a typical portland cement dry-mix sprayed concrete, approximately:

w/c = 0.37

Compressive strength (N/mm^2) = 55

Modulus of Elasticity (N/mm^2) = 34000

and these properties are very similar to conventional concrete as in Table 2.3.

Table 2.3 - Modulus of Elasticity versus strength BS 8110:Part 2: cl 7.2[13].

Compressive Strength (N/mm^2)	Typical range of Modulus of Elasticity (N/mm^2)
40	22000 - 34000
50	24000 - 36000
60	26000 - 38000

Clearly there is a similarity in the modulus of Elasticity between conventional and sprayed concrete.

2.3.4 Coefficient of thermal expansion

Although not given, ACI 506R-90 stated that generally the coefficient of thermal expansion of sprayed concrete approximates to that of reinforcing steel, thereby minimising internal stress development.

2.3.5 Permeability

Generally the values permeability of sprayed concrete are very low. Schrader and Kaden quoted the following typical figures:

Strength range from 21 to 83 N/mm^2

Permeability range from $3x10^{-8}$ to $3x10^{-11}$ cm/sec.

By comparison, conventional concrete of the similar strength range may have very slightly higher permeability values.

The low permeability of sprayed concrete is generally desirable (assuming that this is achieved without the detrimental effects of a mix that develops greater crack potential). However, one ought not to overlook the " side-effect " of having low

permeability sprayed concrete. Schrader and Kaden pointed out that when sprayed concrete is used in a moisturised zone such as to replace spalled concrete on the side or the bottom of a concrete pier cap, or the submerged surface of the wall for a water retaining structure, if moisture has been slowly migrating into and through the substrate concrete and if it continues to do so after application of the sprayed concrete, it will be restricted from escaping out of the sprayed concrete layer at the same rate that it previously did. Without an alternative escape route for the moisture, it may begin to build up pressure and/or trap contaminates such as chlorides behind the sprayed concrete. In some cases, this has no significant consequences. However, it is possible for serious damage to occur in the forms of debonding of the sprayed concrete from the substrate concrete or concealing the corrosion in the reinforcement in the substrate concrete.

There are indications (Schrader and Kaden, ACI 506R-90) that certain latex formulations can be added to portland cement sprayed concrete, a product called polymer-modified sprayed concrete, to enhance its impermeability, flexural, tensile and bond strengths. However, Glassgold quoted "in his opinion, there are problems attendant to polymer sprayed concrete installation that include its inherent curing characteristic, incompatibility with portland cement concrete matrices, an absence of structural design criteria and a need for special equipment. These and overall lack of conformity with established shotcrete placement and finishing techniques made him question its suitability and viability as a sprayed concrete material". Also, Marusin[14] found that layering occurred in latex-modified dry-mix sprayed concrete. He found that, trapped in between these layers are the non-absorptive polymer rich films which are smooth and dense produced by Latex migration. These films prevent bonding between the applied sprayed concrete and the substrate concrete and resulted in delamination as well as early shrinkage.

2.4 SPRAYED CONCRETE MATERIALS

Standard portland cement sprayed concrete using such basic material as cement, aggregate and water have provided in most cases, durable and effective sprayed concrete. However, new material developments can provide beneficial improvements.

2.4.1 Microsilica

Microsilica or silica fume is supplied in either dry form or slurry form. It is a by-product of the reduction of high-purity quartz with coal in electric arc furnaces in the production of silicon metal. The use of microsilica in concrete was pioneered in Norway in the early 1950s, but not until 1980 was microsilica used in sprayed concrete applications, in several Scandinavian countries. In 1983 a Canadian consulting engineering firm Hardy Associates (1978) Ltd, in Vancouver, B.C., conducted extensive laboratory and field investigations into the incorporation of microsilica in dry-mix sprayed concrete, very positive results were found. Extreme fineness and a high glass content in microsilica results in a very efficient pozzolanic material i.e. it is able to react very efficiently with the products of hydration of portland cement to create secondary cementitious materials in hydrating concrete and sprayed concrete. This results in a product with very low permeability and absorption and enhanced resistance to deterioration in a variety of chemically aggressive environments (deterioration of the sprayed concrete matrix is caused by the breakdown of the calcium hydroxide component of hydrated portland cement).

Glassgold's test results as shown in Table 2.4 on microsilica dry-mix sprayed concrete agree with the above and indicate that a nominal addition of microsilica to standard portland cement mixes has very beneficial effects on the durability properties of dry-mix sprayed concrete.

Table 2.4. - Test results, microsilica sprayed concrete

			Compressive strength		Freeze-Thaw		Chloride permeability	
Test	Cement /Sand ratio	Microsilica %	7-Day (N/mm^2)	28-Day (N/mm^2)	Cycles achieved from 300 total	Weight loss, %	Coulombs	Rating
1	1:4.5	0	19	28	188	6.9	4732@207 mins.	High
2	1:4.2	7.5	36	54	297	0.54	514	Very low
3	1:5.2	7.5	37	51	290	0.24	715	Very low

Additionally, Glassgold pointed out that microsilica when added to sprayed concrete mixture does not have most of the drawbacks associated with polymer modified sprayed concrete. While certain minimal adjustments have to be made in application

procedures, they are well within the expertise of the average applicator and require little change in his skill.

2.4.2 Fibre reinforcement

In the form of steel or polypropylene (sometimes called synthetic) fibres can be integrally mixed with sprayed concrete. In 1968 polypropylene fibre reinforced sprayed concrete was first placed in Europe. Sprayed concrete experiments utilising steel fibres were first conducted in North America in 1971 and in the later years the technology was adopted in Europe (ACI 506.1R-84)[15].

The addition of polypropylene fibres to sprayed concrete tends to give good cohesive and plastic properties to the amalgam but does not improve the flexural strength of the matrix to any great extent. Steel fibres on the other hand, up to 2 percent by volume of the total mixture, would enhance flexural strength, ductility and toughness. It has been found that by incorporating steel fibres, the residual load carrying capacity of sprayed concrete after first cracking can be enhanced.

2.4.3 Steel fibre and mesh reinforced sprayed concrete: a comparison

Kirsten[16] in his attempt to address the answer to the question of the structural performance of steel fibre reinforced sprayed concrete compared to that of steel mesh reinforced sprayed concrete found that mesh reinforcement was more superior to fibre reinforcement for both uniformly distributed and point loading. This was due to the more effective location of the mesh within the section of the sprayed concrete with regard to bending and catenary action (catenary action is the mechanism in which the in-plane tensile forces generated at large deflections are resisted by a compression ring which develops around the tension zone). Kirsten also pointed out that generally when incorporating steel fibres into the sprayed concrete mixture, there are no modifications to the sprayed concrete pump, equipment or application procedures required. However, it appears that the sophisticated attributes of steel fibre reinforced sprayed concrete can only be effectively exploited in civil engineering applications in which quality assurance is subjected to explicit contractual control.

2.5 DURABILITY OF SPRAYED CONCRETE

There is a general agreement that sprayed concrete placed using sound materials in the proper portions and applied by an experienced sprayed concrete crew, can provide a high strength durable concrete.

The contents of this section is not intended to praise or to discredit the good performance of sprayed concrete it is to review the results of the research conducted by experienced sprayed concrete users with the hope that the information reinforces the general agreement above and because of the controversy encountered over the past 15 to 20 years[2], these results tend to focus more on the lack of air entrainment and the freeze-thaw durability of dry-mix sprayed concrete than other properties.

Glassgold revealed that from extensive investigations since the middle of 1950s, it appeared that if dry-mix sprayed concrete contained any air voids, they were resulted from entrapment rather than from being purposely entrained.

Litvin and Shideler[17] in their report in ACI SP-14[18] stated: sprayed concrete could be durable and that the physical entrainment of specified amounts of air was not absolutely necessary to ensure this durability.

Reading[19] concluded that it is possible to produce both wet and dry sprayed concretes that will survive the highly aggressive natural freezing and thawing conditions typically 250 cycles of freezing and thawing every two years.

Some sprayed concrete users had reported that the ASTM C666[46] rapid freezing and thawing standard appears to be more severe than some of the harshest freezing and thawing in nature, therefore one ought to be cautious in analysing data from tests conforming to this standard.

Reading quoted " most sprayed concrete durability failure do not involve failure of the material itself. Generally there is a peeling off of the sound concrete because of bond failure ". Therefore one should be very careful to provide a good, clean bonding surface. The ACI 506R-90 contains a definition of the concrete surface preparation. However, in the experiments described in this thesis, grit blasted concrete surface preparation is perfectly adequate to maintain extremely good bond between the sprayed concrete layer and the substrate concrete surface.

Apparently most sprayed concrete that has performed well in freezing-thawing environments was not saturated because it contains a satisfactory system of entrapped air voids in the case of dry-mix, and entrained air voids for the case of wet-mix.

In this author 's opinion, if microsilca had been used in Schrader and Kaden 's experiment, perhaps the results would have been much improved. This can be illustrated by a pier project in Western Canada[20] which involved repair of corrosion deteriorated and construction damaged piles, pile caps, beams, slab soffits and sea wall. Many of these structural elements were in the inter-tidal zone. In this project, dry-mix microsilica sprayed concrete was used. The feedback revealed consistently higher compressive strengths and lower permeability in the *in situ* sprayed concrete as measured by the volume of permeable voids. Additionally, it was found that the incorporation of microsilica at 12% by weight of portland cement substantially enhanced initial set and therefore the use of an accelerator was not necessary.

To sum up on the issue of durability of sprayed concrete, the author of this thesis would like to emphasise that there are significant studies indicating that certain dry-mix sprayed concrete (non-air-entrained) can be a durable, freeze-thaw resistance material and that sprayed concrete in general could replace existing conventional concrete subjected to its feasible economic evaluation. Berkovitch[21] reported on Humphries' paper[22] which presents information on the question of relative costs, see Figure 2.2, though this must be interpreted in terms of the date when considering the absolute levels, it indicates that cost per square metre of sprayed concrete equals that of normal placed concrete at about 150mm thickness and exceeds it at greater thicknesses. Also, the author would like to stress that the freeze-thaw phenomenon is not as great a threat in the UK as elsewhere generally suffers winter which are relatively mild compared to those of some of its European neighbours and parts of North America. Therefore the durability of sprayed concrete under freeze-thaw conditions should not be the prime criterion in the decision making process for its use on a particular maintenance job in the UK. However, two important issues needed careful consideration to make this possible:

1. Applicator workmanship has to improve providing new and consistent levels of sprayed concrete quality, especially now that the use of sprayed concrete is rapidly expanding.

2. Sprayed concrete engineers must learn and understand all aspects of the process from design through to construction.

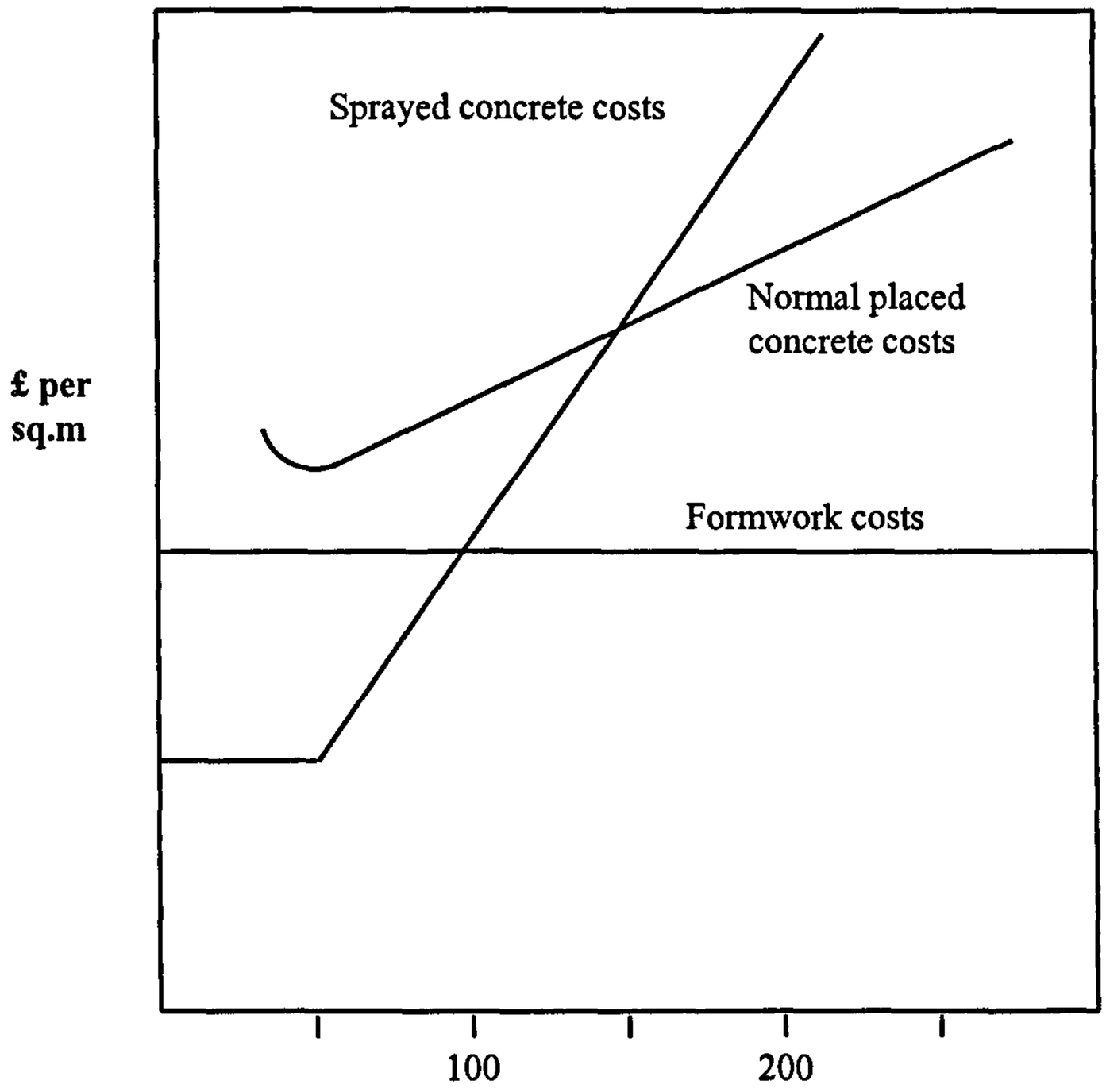

Figure 2.2 - Relationship between costs of sprayed concrete and those for normal placed concrete and formwork, Berkovitch[21].

CHAPTER 3

THE TEST SLABS FOR FATIGUE AND STATIC LOAD TESTING

3.0 GENERAL

The proposed test slab bridge was modelled to the maximum size allowed by the laboratory working area and the simulation of the strengthening technique undertaken on the modelled slab bridge was made as realistic as far as possible in terms of:

1. Spray concrete mix
2. Spray concrete depth
3. Spray concrete reinforcement
4. Surface preparation
5. Spraying process

The modelled strengthened slab bridge was then tested under static loading to study its ultimate flexural capacity and under fatigue loading to evaluate the useful life span of the technique taking into account the current commercial axle load spectrum in the UK. This chapter describes the stages leading to the production of the sprayed concrete strengthened R-C slabs. There were in total eighteen strengthened slabs (also referred to as test slabs) and these were tested as follows:

1. One slab was left unstrengthened and used as a control base slab, this was subsequently tested statically.
2. Fourteen of the strengthened slabs were tested statically.
3. Three of the strengthened slabs were tested under fatigue loading.

3.1 BASE SLAB DETAILS

3.1.1 General details

Eighteen base slabs 2.4 x 1.0 x 0.1 m were cast in the laboratory, using a designed C35 concrete supplied by Ready Mixed Concrete Limited. This concrete had a slump of

125mm and a maximum aggregate size of 10mm. To reinforce the base slabs, A193 mesh reinforcement with deformed bars was used

After the concrete was placed, curing was carried out by spraying a membrane of Concure Clear 90 compound over the placed concrete surface and the slabs were left to cure under laboratory conditions.

3.1.2 Soffit preparation

After curing for 28 days, the eighteen base slabs were then de-moulded and placed side by side on scaffolding at a height of two metres to simulate as near as possible the conditions under which a bridge soffit would be sprayed, see Figure 3.1. This also shows the partition boards, which served to guide the nozzleman to spray the required thickness and also to prevent adjacent slabs bonding together as the sprayed concrete layer set.

Figure 3.1a - Base slab positioned on scaffolding, plastic sheeting required to contain dust.

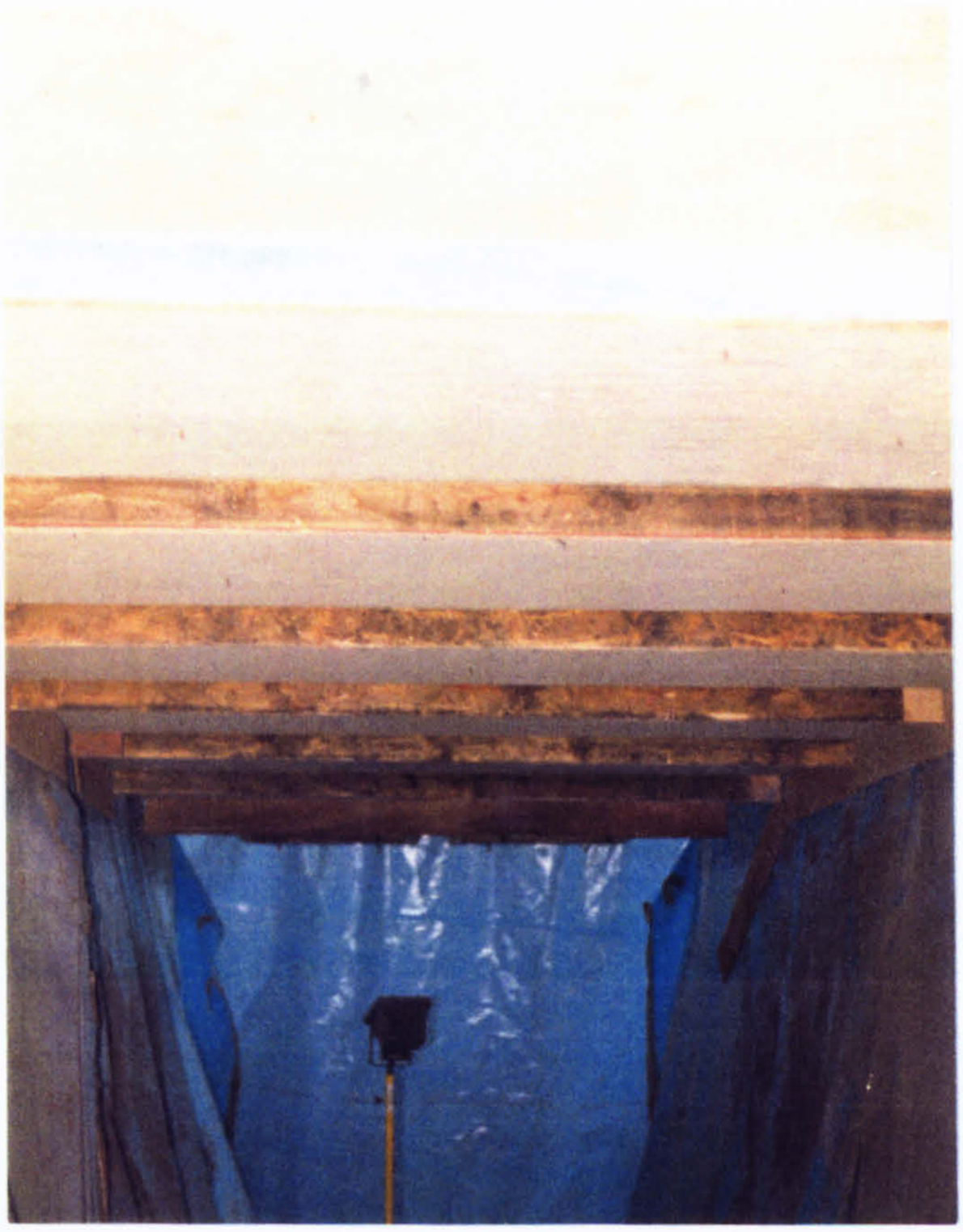

Figure 3.1b - The precast R-C base slabs positioned on scaffolding at two metre height (looking from below soffit level, inside the plastic sheeting).

Figure 3.1 - Preparing the precast R-C base slabs for the spraying operation.

One base slab was kept aside as an unstrengthened, control slab and the soffits of the remaining seventeen base slabs were prepared by grit blasting, see Figure 3.2.

Figure 3.2a - Base slab soffit, formwork finished (the contractor decided to fix the mesh reinforcement before spraying the concrete for this slab).

Figure 3.2b - A sprayed concrete crew member grit blasting the soffit.

Figure 3.2c - The grit blast prepared soffit (looking from below soffit).

Figure 3.2 - The grit blasting process.

As can be seen from Figure 3.2c, the extent of grit blasting was just sufficient to remove the concrete laitance so that the aggregate was exposed. Hilti metal hangers (type HA8L1) were then fixed to the underside of the slabs and the mesh reinforcement rigidly secured to them. Timber spacer blocks of the correct size were used to set the mesh reinforcement at the pre-determined depth relative to the over all pre-determined thickness of the strengthened slab. The seventeen slabs were then sprayed with concrete so as to encapsulate the mesh reinforcement on their soffits, see Figure 3.3. The entire strengthening process was performed by Tarmac Structural Repairs Limited, the next section describes the sprayed concrete procedures

Figure 3.3a - Mesh reinforcement and spacer blocks being secured to the slab soffit.

Figure 3.3b - Sprayed concrete encapsulating the mesh reinforcement.

Figure 3.3c - The strengthening process completed.

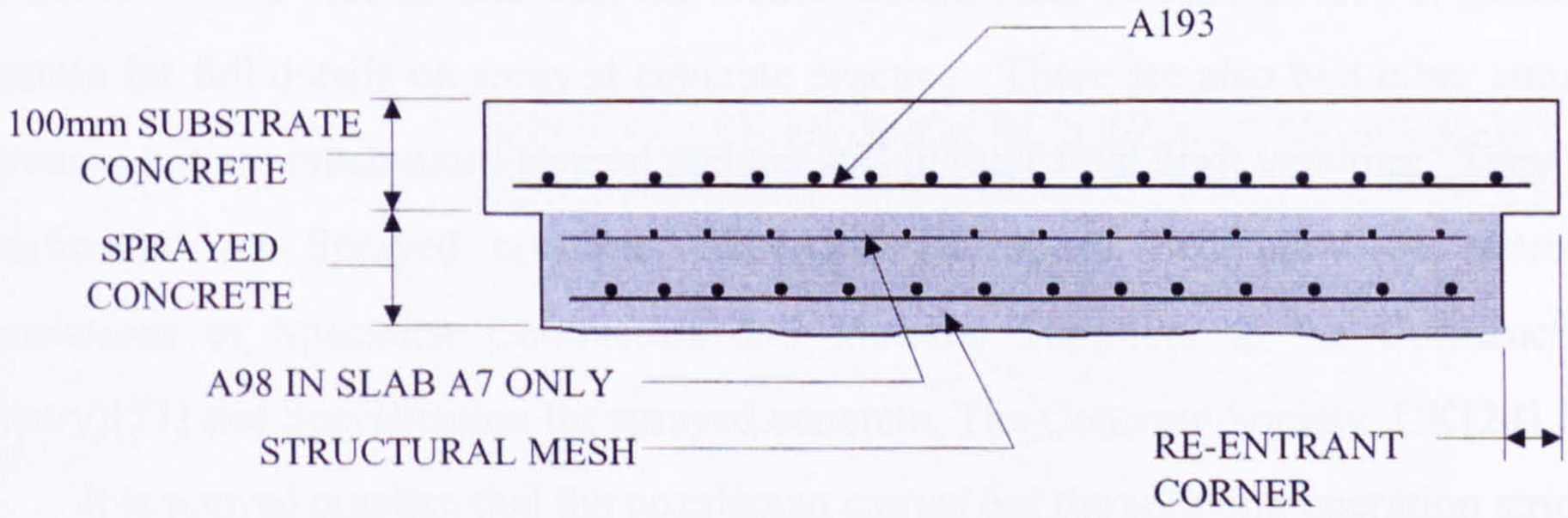

Figure 3.3d - Typical test slab reinforcement details, note that the re-entrant corners (75mm) are created by the supporting timber beam.

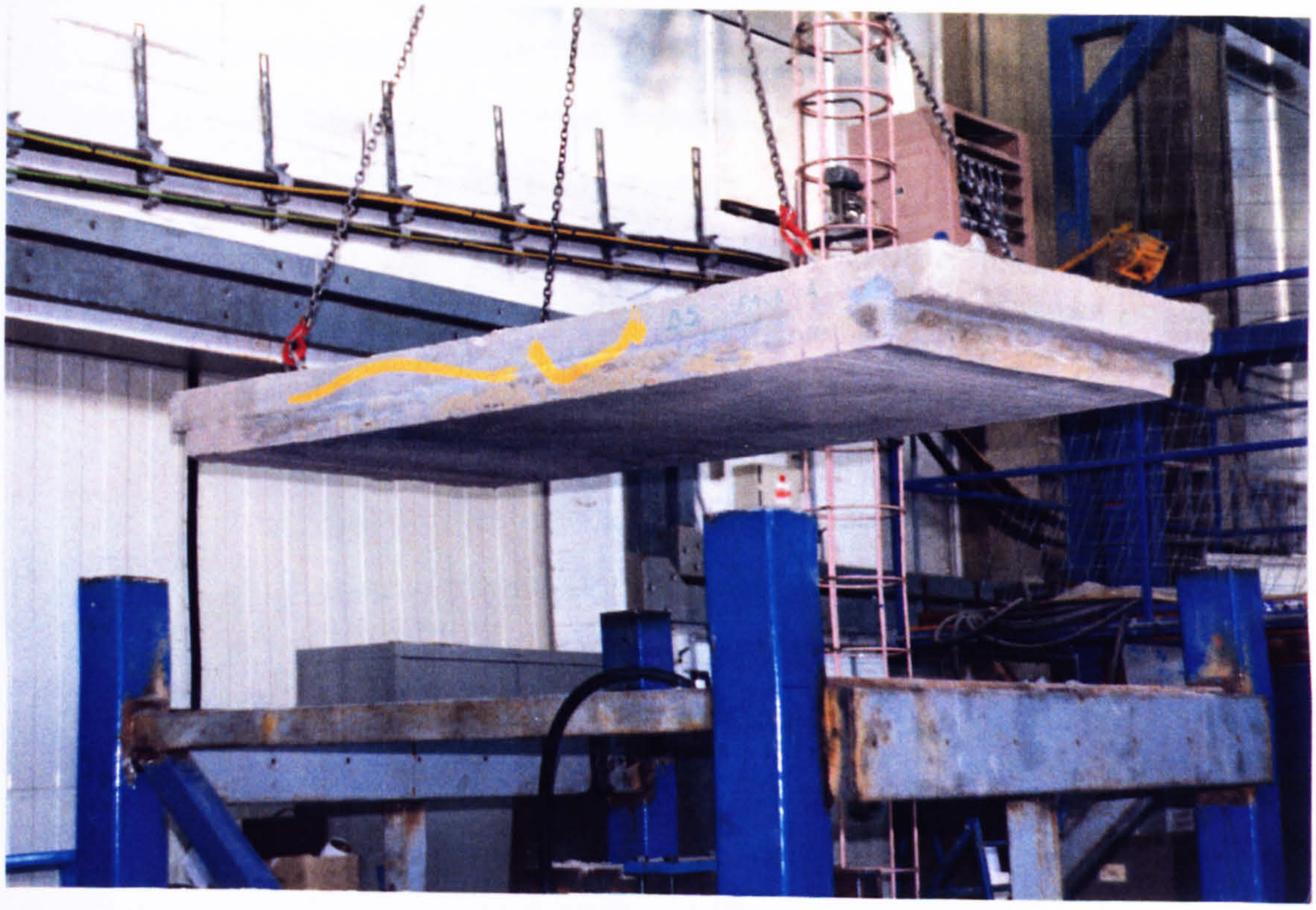

Figure 3.3e - A typical test slab being lifted off the scaffolding onto the loading frame for static/fatigue load testing.

Figure 3.3 - Strengthening of the precast R-C base slab.

3.1.3 Sprayed concrete practice

The author would recommend that the reader should refer to ACI 506R-90, guide to shotcrete for full details on sprayed concrete practice. There are also two other similar references but are much more general and are still in their final draft versions. They are Specification for Sprayed concrete, EFNARC (European Federation of National Associations of Specialist Contractors and Material Suppliers to the Construction Industry)[23] and Specification for sprayed concrete, The Concrete Society, UK[24].

It is normal practice that the nozzleman carries out the spraying operation strictly in accordance with the recommended guide lines detailed in the code such as the ACI 506R-90 and that his competence should be assessed from the certification code ACI 506.3R-82 (Guide to Certification of Concrete Nozzleman)[25]. The nozzleman used in this research was professionally experienced and was appointed by Tarmac Structural

Repairs' Operation Manager, therefore the competence of the nozzleman was guaranteed.

The following are questions which the author addressed to the nozzleman during the spraying concrete operation, being reported here in an attempt to describe the sprayed concrete practice relevant to this research.

1. Question - What is the approximate water-cement ratio of the dry mix sprayed concrete ?

   Answer - Because this is the dry-mix process, the mixing water is controlled by the nozzleman at the nozzle (see Figure 3.4) and this depends on his observation of the rebound (rebound is sprayed concrete material which has rebounded off the receiving surface and falls to the ground). In this work the w/c ratio was 0.3 approximately.

ACI 506R-90 states:

> The water-cement ratio for dry-mix shotcrete in-place normally falls within a range of 0.3-0.5 by weight.

Figure 3.4 - The nozzle used in this work (being replaced), to the left of photo is nozzle tip and to the right is material hose, water control tap is the top attachment.

2. Q. - Velocity of spraying the concrete, is this to be stated in the specification ?

   A. - The average velocity is about 30m/s and this is the approximate figure for this work. Velocity of spraying concrete is judged by the nozzleman and for the dry-mix process, the variation can be made by adjusting the air pressure.

3. Q. - Is there a minimum and optimum velocity for spraying the concrete ?

   A. - No. However this is adjusted by adjusting the air pressure depending on the visual judgement of the nozzleman.

4. Q. - How important is the velocity of the spraying the concrete with respect to its ultimate properties ?

   A. - If velocity is low then compaction is low, if velocity is high then rebound is high. Therefore velocity of spraying should be just sufficient for concrete to adhere with a minimum rebound and this depends on the mix being used and largely on the judgement of the nozzleman.

ACI 506R-90 states:

> The velocity of the material at impact is an important factor in determining the ultimate properties of the shotcrete. Consideration must also be given to the fact that increasing velocity means increasing rebound.
>
> In dry-mix shotcrete with given delivery equipment, the factors that determine material velocity at the nozzle are volume and pressure of available air, hose diameter and length, size of nozzle tip, type of material and the rate it is being gunned. These factors allow for great flexibility and versatility in that large, intermediate, or small volumes of material can be gunned at low, medium and high velocities according to the immediate needs of the application. Small or large variations in flow, water content and velocity can be made on order from the nozzleman.

5. Q. - What precautions can be taken to prevent 'void-pockets' forming behind the reinforcement.

   A. - For 10mm diameter bars (maximum bar size in this research) void-pockets forming is extremely low - spray at an angle to get behind the bars.

ACI 506R-90 states:

When shooting through and encasing reinforcing bars the nozzle should be held closer than normal (normally 0.6 to 1.8m) and at a slight upward angle to provide better encasement of horizontal steel (or slightly sideward angle for vertical steel) and minimise the accumulation of rebound.

6. Q. - What is the nozzle size used in this work ?

   A. - Standard nozzle size is used in this work and this is 38mm inside diameter/58mm outside diameter, see Figure 3.4.

ACI 506R-90 states:

Although the standard nozzle size is not stated, a useful guide line is: discharge nozzles consisting of a nozzle body and nozzle tip are attached to the end of the material delivery hose to inject water or air into the moving stream of materials, to premix water and solids, and to provide uniform distribution of the mixture. Ideally, the nozzles should pattern the discharge as a uniform inner core consisting primarily of solids and some water spray surrounded by a thin outer core which is mainly water spray. The nozzle tip size should not exceed the diameter of the hose and often is smaller.

3.2 THE SPRAYED CONCRETE LAYER DETAILS

The sprayed concrete variable parameters considered in investigating the performance of this strengthening technique are:

1. The size of the mesh reinforcement
2. The amount of mesh reinforcement
3. The thickness of the sprayed concrete layer
4. The concrete mix in the sprayed concrete layer
5. Shear connectors.

The following sections describes these parameters.

3.2.1 Reinforcement in the sprayed concrete layer

The quantity of reinforcement to be encapsulated in the sprayed concrete layer is governed by the required strengthening factor and this varies vastly as several considerations need to be fulfilled prior to its determination and on a real bridge, it has been generally found that from the bridge assessment programme that the maximum

strength increase required is 30%. This therefore should be easily achieved by adding a single layer of reinforcement just below the existing soffit and encasing this with a layer of sprayed concrete of suitable thickness for weathering protection. However, in order to fully test the shear capacity of the interface and to establish the effects of the variables listed, significant extra reinforcement was added in some test slabs and significant changes to the lever arm of the added steel was also incorporated in other test slabs to cause a large increase in flexural capacity.

Table 3.1 tabulates the sprayed concrete variable parameters of all the seventeen test slabs.

Table 3.1 - Test slabs details

Slab	Sprayed Concrete Thickness (mm)	Reinforcement in the Sprayed Concrete	Mesh Sizes Normal Pitch of Bars		Cross Sectional Area per Metre Width		Size of Bars		Main Bars as % of Concrete
			Main (mm)	Cross (mm)	Main (mm^2)	Cross (mm^2)	Main (mm)	Cross (mm)	
Control	-	-	-	-	-	-	-	-	-
A1	75	A193	200	200	193	193	7	7	0.22
A2	75	A193	200	200	193	193	7	7	0.22
A3	75	A193 (Shear Connected)	200	200	193	193	7	7	0.22
A4	75	A393	200	200	393	393	10	10	0.33
A5	75	A393 (Shear Connected)	200	200	393	393	10	10	0.33
A6	50	A193	200	200	193	193	7	7	0.26
A7	100	A193 & A98	200	200	193	193	7	7	0.19
A8	100	A193 (Shear Connected)	200	200	193	193	7	7	0.19
B1	75	B785	100	200	785	252	10	8	0.56
B2	75	B785	100	200	785	252	10	8	0.56
B3	75	B503	100	200	503	252	8	8	0.4
B4	75	A393	200	200	393	393	10	10	0.33
B5	75	B503	100	200	503	252	8	8	0.4
B6	75	A393	200	200	393	393	10	10	0.33
B7	75	A393	200	200	393	393	10	10	0.33
B8	75	A393	200	200	393	393	10	10	0.33
B9	75	A393	200	200	393	393	10	10	0.33

Note:
All mesh reinforcement are deformed bars except for A98 and total percentage of steel is based on total cross-section of the composite slab

3.2.2 Shear connectors

In order to see whether horizontal shear capacity at the substrate/sprayed concrete interface of the strengthened slabs would be enhanced, mechanical shear connectors were incorporated in the three test slabs listed in Table 3.1. Figure 3.5 shows the details of these shear connectors.

The number of shear connectors was determined in accordance with BS 8110: Part 1: cl 5.4.7.3[26] which states that the nominal links (shear connectors) is 0.15% of the contact area, this gives:

$$\text{Shear Connectors} = 0.0015 \times 1000 \times 1000 \text{ mm}^2/\text{m}^2$$

$$\text{Shear Connectors} = 1500 \text{ mm}^2/\text{m}^2$$

$$\text{Shear Connectors} = 20 \text{ T10 bars/m}^2 \ (1571\text{mm}^2/\text{m}^2)$$

$$\text{Shear Connectors} = \text{T10 bars @ 200 centres.}$$

In this research shear connectors were provided throughout the soffit of the test slab, although the requirement is greater at both ends of the slab as in these areas the horizontal shear is high and these are the initiation points for the 'peeling-off' of the sprayed concrete layer, if the horizontal shear capacity of the interface is exceeded i.e. if composite action broke down and debonding occurred.

Figure 3.5a - Shear connectors fixed before the concrete spraying process.

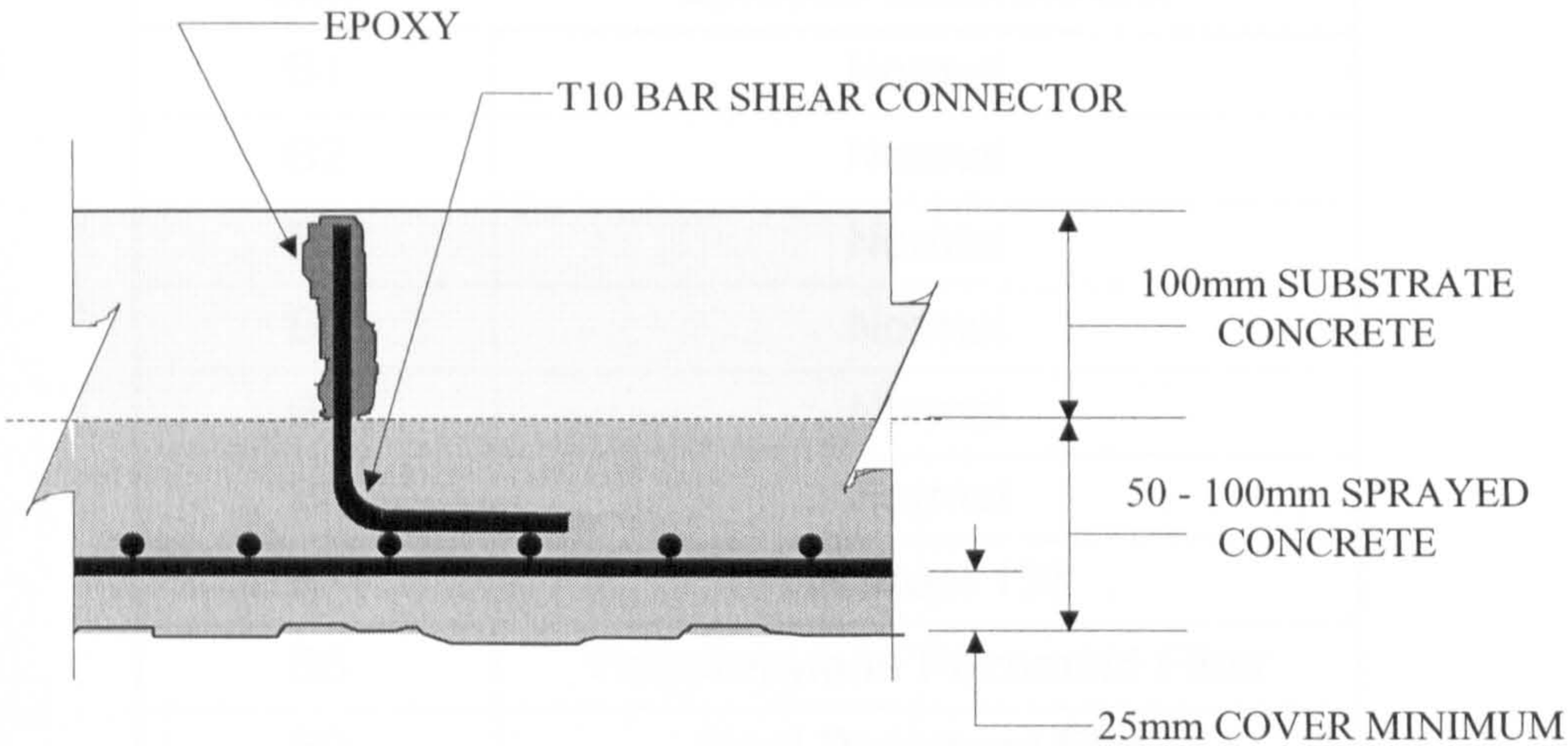

Figure 3.5b - Shear connector details.

Figure 3.5 - Shear connectors.

3.2.3 Concrete mix in the sprayed concrete layer

Slabs A1 to A8 inclusive were sprayed with the following concrete mix which is referred to as the Normal Mix:

- Cement to sand ratio 1:3, both cement and sand were supplied pre-packed. The pre-packed sand contained angular aggregates ranging up to 5 mm in diameter.
- Microsilica in slurry form was added to the water at 7 % dosage by weight of water.

In spraying slabs A1 to A8, Elkem Materials Limited, who supplied the microsilica supplied their mixing machine which regulated the supply of water and microsilica to the spraying nozzle, thereby ensuring the 7 % dosage of microsilica.

Slabs B1 to B9 inclusive were sprayed with the following three proprietary concrete mixes, as well as the normal mix, tabulated in Table 3.2. The mix proportions and the 7% microsilica dosage were the same as in the case of the normal mix and they were also supplied in pre-packed form.

Table 3.2 - Concrete mixes of slab B1 - B9 inclusive	
Slab	Sprayed Concrete Mix
B1	Normal
B2	Normal
B3	Normal
B4	Normal
B5	Normal
B6	Normal
B7	Sikacem 133
B8	Polypropylene Pozament Fiber
B9	Steel Pozament Fiber

Purely for the reason of economy and because of the experience of the sprayed concrete crew, the dosing of microsilica at 7 % added at the nozzle was achieved by manually setting the appropriate pressure of a mobile pump and therefore the special Elkem mixing machine was not necessary.

3.3 PRE-CONSTRUCTION TEST

For the purpose of material testing and, to provide an indication of the quality to be expected in the test slabs, a total of twelve pre-construction test panels measuring 600 x 600 x 50 - 100 mm were sprayed using, the same concrete mixes as those used in the test slabs, the same equipment and the same crew. The method of curing was also the same as that used in the test slabs i.e. sprayed membrane curing. The details of the twelve pre-construction test panels are as shown in Table 3.3 below.

Table 3.3 - details of the twelve pre-construction test panels			
Pre-Construction Panel	Concrete Mix	Sprayed Thickness	Direction Sprayed
1	Normal	50	Vertical
2	Normal	75	Vertical
3	Normal	100	Horizontal
4	Normal	100	Horizontal
5	Normal	100	Horizontal
6	Normal	100	Horizontal
7	Normal	100	Vertical
8	Normal	100	Vertical
9	Normal	100	Horizontal
10	Steel Fiber	100	Horizontal
11	Sikacem 133	100	Horizontal
12	Polypropylene Fiber	100	Horizontal

From the pre-construction test panels listed in Table 3.3 and some statically load tested slabs, cores and prismatic specimens were extracted for the following tests:

1. Mechanical testing
2. Material analysis
3. Petrographic examination
4. Chloride ingression.

3.3.1 Mechanical test results

All mechanical tests concluded on cores and prisms extracted from the pre-construction test panels are as shown in Table 3.4 (although the pull-off and slant shear tests are being reported here, the tests were actually done from a statistically load tested slab, the slant shear test shall be presented again in more details in the Horizontal Shear Study, chapter 7.

Table 3.4 - Mechanical test results (results for normal sprayed concrete mix, unless stated otherwise)

Test	Age	Specimen Size (mm)	No. of Specimen	Overhead/Horizontal Sprayed	Results
Compressive Strength	40 day core	Ø=74.0,L=75.9 L/Ø=1.0	4	Overhead	35.0 N/mm^2
	40 day estimated cube strength	-	-	-	32.5 N/mm^2
	40 day core	Ø=74.1,L=81.1 L/Ø=1.1	4	Horizontal	35.9 N/mm^2
	40 day estimated cube strength	-	-	-	34.2 N/mm^2
	84 day core	Ø=50.8,L=55.5 L/Ø=1.1	2	Horizontal	41.4 N/mm^2
	84 day estimated cube strength	-	-		39.6 N/mm^2
Tensile Splitting, Cores Drilled Parrallel to Direction of Spraying	40 day core	Ø=99.8,L=103 L/Ø=1.0	3	Horizontal	3.6 N/mm^2
	40 day cube	98 x 98 x 98	4	Horizontal	4.9 N/mm^2
Tensile Splitting Loaded Parallel to Horiz't Plane of Layering	84 day core	Ø=74.4,L=73.9 L/Ø=1.0	4	Overhead	6.2 N/mm^2
	84 day core	Ø=74.2,L=75.8 L/Ø=1.0	4	Horizontal	5.0 N/mm^2
Static Modulus of Elasticity	84 day	32.5 x 31.6 x 96.0	1	Horizontal	24.1 kN/mm^2
Pull-Off	84 day	Ø=50	6	Overhead	1.1 N/mm^2
Slant Shear Test	84 day	57.75 x 55.77 x 150	1	-	37.6 N/mm^2
Coefficient of Linear Thermal Expansion	70 day	-	-	-	1.26×10^{-5} /°C

Table 3.4 - Mechanical test results continued.

			Compressive		Tensile Splitting	
Concrete Mix	Specimen Size (mm)	Age (days)	Overhead Sprayed	Horizontally Sprayed	Overhead Sprayed	Horizontally Sprayed
Normal	75Ø	47	26.5	26.1	3.7	3.5
Sikacem 133	75Ø	47	-	35.4	-	4.7
Steel Fiber	75Ø	47	40.6	47.6	7.7	7.3
Poly Fiber	75Ø	47	-	33.1	-	4.2

Modulus of Elasticity (kN/mm^2)			Overhead Sprayed	Horizontally Sprayed
Normal	32 x 32	-	21	24.1
Sikacem 133	32 x 32	-	-	22.5
Steel Fiber	32 x 32	-	26.8	22
Poly Fiber	32 x 32	-	-	19.9

All mechanical tests were conducted in accordance with the following British Standards except the pull-off test and measurement of the coefficient of Linear Thermal Expansion for which details are given below:

1. Compressive Strength BS 1881: Part 120: 1983 [27]
2. Tensile Splitting BS 1881: Part 117: 1983 [28]
3. Static Modulus of Elasticity: Part 121: 1983 [29]
4. Slant Shear BS 6319: Part 4: 1984 [30].

The pull-off test

The test was conducted according to CIRA Technical Note No. 139[31] and the apparatus used is shown in Figure 3.6.

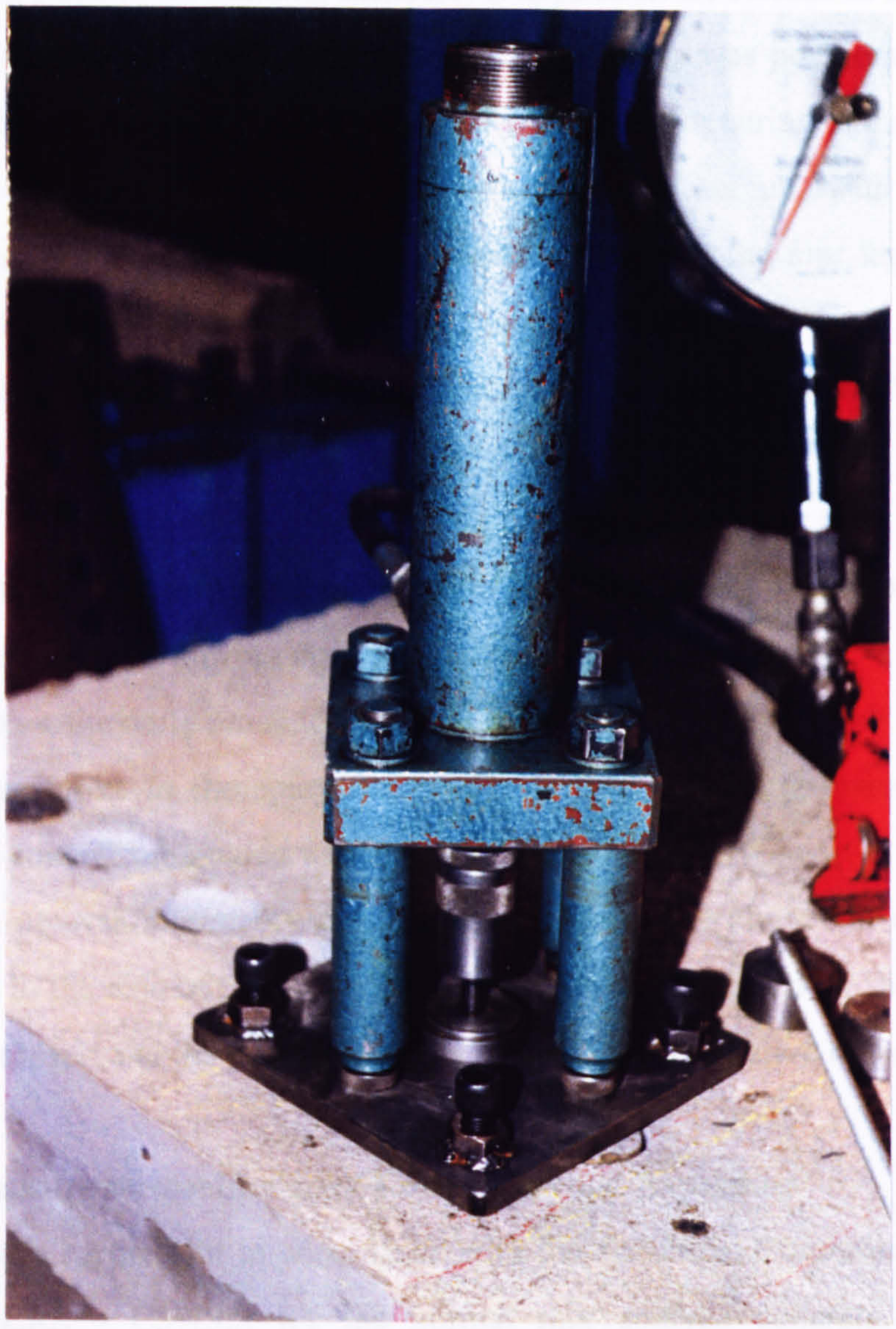

Figure 3.6 - The pull-off test apparatus.

The test procedures:

1. The tested slab was placed on level surface (the laboratory floor).
2. 50mm diameter coring slots were made through the sprayed concrete thickness and 10mm into the substrate concrete.
3. A steel cylinder (size to suit) was made and hand slotted into the core (the internal wall of the steel cylinder was greased). This cylinder served to ensure that the axis of the core is in alignment with the axis of the steel dolly.

4. A film of Sika Dur 31 (a two parts adhesive compound recommended by Tarmac Structural Repairs for bonding concrete) is applied to the surface of the core enclosed by the steel cylinder, following which the steel dolly was positioned over the Sika Dur 31 film and the preparation was left for 24 hours for curing of the adhesive.
5. After 24 hours curing, the pull-off apparatus was set up, with the steel dolly connected to the pulling rod of the apparatus (note that the four legs of the pull-off apparatus rest on a steel plate which has four levelling bolts).
6. The pull-off apparatus was levelled relative to the steel plate and the pulling force applied.

The pull-off test was performed on a total of six cores, giving the average bond strength of 1.1 N/mm^2. The following observations were made after the test.

a) In all cores, the dolly remained bonded.
b) All cores broke in the sprayed concrete portion, indicating lower strength in the sprayed concrete compared with the substrate concrete.
c) The set up was reasonably accurate as seen from the alignment of the dolly axis relative to the axis of the core. This alignment was achieved by the use of the steel cylinder insert and the perpendicularity of this cylinder relative to the steel plate.

Test to measure the coefficient of Linear Thermal Expansion

This test was carried out in accordance with the American Corporations of Engineers Standard CRS - C39[32] for the normal mix sprayed concrete (for other three proprietary mixes, supplied in pre-packed form, the coefficients can be obtained from the manufacturers). There were four specimens each of dimensions 40 x 40 x 160 mm. Demec points were placed on the surface of the specimens at 100 mm centres.

The specimens were first placed in water at 20°C for four hours and initial readings were taken, the specimens were then placed in a water bath at 50°C for four hours before another set of readings were taken, the difference representing the expansion of the specimens.

The specimens were then moved back to the 20°C water bath and left there for four hours before another set of readings were taken and the difference between the 50°C and the 20°C readings were taken as the contraction of the specimens. The same procedures were repeated to give results for four cycles.

Each specimen has four sets of readings. Therefore the mean of sixteen measurements was calculated to give the coefficient of Linear Thermal Expansion of 1.26 x 10^{-5}/°C. This marginally exceeded the range expected by Tarmac Structure Repair 's Ltd of 0.8 to 1 x 10^{-5}/°C for this material to satisfy a durability specification but is very similar to the value for normal concrete.

3.3.2 Material analysis

Material analysis, petrographic examination (section 3.3.3) and chloride ingression testing (section 3.3.4) were carried out by a specialist company. The purpose of these tests were:

1. To study the constituents of the hardened sprayed concrete.
2. To assess the quality of the sprayed concrete at microscopic level.
3. To examine the effectiveness of the sprayed concrete in encapsulating the reinforcement when sprayed in the overhead position.

For material analysis six 50mm diameter cores from the pre-construction test panels were extracted and air void content and air void parameter were determined in accordance with ASTM C457-82[33] as shown in Table 3.5. Full details of the test procedures can be found in Appendix A.

Table 3.5 - Air void content and parameter

Sample	1	2	3	4	5	6
Aggregates	57.2	57.2	54.7	54.6	54.4	57.4
Paste	38.9	38.5	41.3	40.9	42.3	39.6
Total air void content	3.9	4.3	4	4.4	3.3	3
Number of Voids per mm (per inch)	0.23 (5.8)	0.27 (6.9)	0.21 (5.3)	0.16 (4.1)	0.19 (4.8)	0.17 (4.3)
Average chord intercept	0.17	0.16	0.19	0.27	0.18	0.17
Specific surface in mm to -1	23.3	24.7	21.5	14.8	22.6	22.9
Spacing factor (mm)	0.34	0.27	0.34	0.51	0.33	0.34
Entrained air to paste/ratio	0.1	0.11	0.1	0.11	0.08	0.08

Table 3.5 shows that dry mix sprayed concrete does contain air voids and the author stresses that no air entrainment was performed (air entraining is not applicable for dry-mix sprayed concrete) the most probable explanation to the reported air content is due to air entrapment resulted from the 'bombardment' of concrete sprayed at

approximately 30m/s (velocity approximated by an experienced nozzleman). This results is a favourable finding of the sprayed concrete in this research as SP-14[18] reports that although dry-mix sprayed concrete cannot be purposely air-entrained, it does contain the air voids similar in size and spacing to those in air-entrained concrete and that, this is one of the durability characteristics of dry-mix sprayed concrete.

So, how are the results of the air void content and parameter of Table 3.5 compared to those in properly air-entrained concrete ? From the Design and Control of Concrete Mixtures, 13th Edition, PCA[34], the four generally accepted criteria for properly air-entrained concrete are:

1. (Table 3.5) - Average spacing factor = 0.36, range 0.27 to 0.51.
   (PCA) - Spacing factor less than 0.20mm.
2. (Table 3.5) - Average specific surface = 21.6, range 14.8 to 24.7
   (PCA) - Specific surface greater than 23.6mm^2/mm^3.
3. Recommended number of voids per linear inch equals 1.5 or 2.0 times (say 1.5) greater than the numerical value of air void content:
   (Table 3.5) Average air void content = 3.8%
   1.5 x Average air void content = 5.7% per linear inch
   (Table 3.5) Average air void content per inch = 5.2%, range 4.1% to 6.8%
4. (Table 3.5) -Average air content = 3.8%, range 3.0% to 4.4%
   (PCA) - An air content ranging from 4.5% to 7.5% for severe exposure.

The comparison shows that the sprayed concrete in this research is marginally less favourable than the properly air-entrained concrete. However, Seegebrecht, Litvin and Gebler[35], in their investigation into the durability of dry-mix sprayed concrete reported similar air void content and parameter to those in Table 3.5 and that the sprayed concrete in their investigation was durable in the ASTM 's severe freeze-thaw testing as shown in Table3.6. In their investigation three pre-construction test panels were sprayed from which specimens were extracted and tested. The findings after 300 cycles of freezing and thawing in accordance with ASTM C666 - 84[46] were:

> After 300 cycles of freezing and thawing tests conducted in fresh water indicated excellent relative dynamic moduli of elasticity with minimal expansions and relatively low weight losses (3-7% maximum) and the air void content and parameter are in Table 3.6.

Table 3.6 - Air-void characteristics of hardened dry-mix shotcrete[35]				
Panel	Air content, %	Spacing factor, inch (mm)	Specific surface, $inch^2/inch^3$ (mm^2/mm^3)	Voids per linear inch (mm)
A	3.6	0.011 (0.28)	482 (19)	4.4 (0.17)
B	3	0.008 (0.20)	687 (27)	5.1 (0.2)
C	3.8	0.008(0.20)	683 (27)	6.6 (0.26)

3.3.3 Petrographic examination

A single composite prismatic sample was extracted from one of the statically load tested slabs and the following samples were prepared:

1. The polished surface - examined by a binocular microscope,
2. The thin section - examined with a Zeiss petrological photomicroscope,
3. The remainder of the sample was examined as hand specimens with a binocular microscope.

An in depth report including photograph from petrographic examination can be seen in Appendix A. only the important findings are discussed here:

1. A layer of approximately 5mm was seen (can also be seen from observing the broken face of a load tested slab with an unaided eye). This layer was reported as a dark layer, indicating a high concentration of microsilica and contains no coarser size ranges of the aggregate but has a normal component of fines, it also has much more unhydrated cement than the remainder of the sprayed concrete.

   This layer was formed within approximately 5mm from the prepared soffit of the substrate concrete and its formation can be explained from reviewing the process spraying: during the initial phase of building up the thickness, the coarser size ranges material tend to loose cohesion from the body of the spray concrete as thickness is still low and as a result rebound from the surface being sprayed and therefore leaving the fines material adhering to the surface, microsilica is the finest component in the entire range of constituents of the sprayed concrete and therefore is the first to be deposited closest to the receiving surface i.e. the soffit of the base slab, as the spraying process continues more and more material is deposited,

increasing the thickness of sprayed concrete and therefore microsilica becomes more evenly distributed into the mass of the sprayed concrete. Therefore, within the short initial period of spraying, when the thickness is still low, the coarser material rebounded off the surface, leaving the finest material intact - the 5mm dark layer containing largely microsilica.

2. Although strongly bonded to the substrate concrete, the sprayed concrete shows very slight variation in colour and appearance, this is an indication of layering over the depth of the sprayed concrete, resulted from the normal practice of intermittently spraying for overhead work. In this work, layering of 35mm and 60mm was reported and is perfectly acceptable, as ACI 506 states:

   > Overhead work is gunned in layers just thick enough to prevent sagging or dropouts, usually 25 to 50mm at a time.

3. Quoting from the report incorporated in Appendix A:

   > The level of microcracking within the sample of sprayed concrete is exceptionally low. The majority of the sprayed concrete is compact and contains voids which range up to 12mm in diameter, but which are mostly less than 0.5mm in diameter. The void content is of the order of 4% by volume. However, there are areas of sprayed concrete, particularly behind the reinforcement bars, where the material contains voids and cavities.

To sum up, petrographic examination has revealed that quality dry-mix sprayed concrete can be achieved and has been achieved despite the finding of cavities behind the reinforcement which is covered by site tolerance.

3.3.4 Chloride Ingression

Five 75mm diameter cores were extracted from the pre-construction test panels and were tested for chloride ingression and the effective diffusion coefficient was calculated. Appendix B gives full details of the test procedures and data analysis, in this section the results of the test are quoted:

- The diffusion coefficient is 1.02×10^{-12}m/s compared to Tarmac Structural Repairs Ltd 's expected value of 0.7×10^{-12}m/s. The diffusion coefficient tends to increase slightly with depth into the concrete and to decrease slightly with time.

- On comparison, the profile of chloride concentration versus depth is almost identical to that expected for high quality normal concrete.

3.3.5 Results from Pre-construction testing

The majority of tests listed in section 3.3 were performed on specimens taken from the pre-construction test panels and the results are reported in sections 3.3.1 to 3.3.4. The results show that in almost every area of testing, the dry-mix sprayed concrete in this research performed very well in comparison with either any good quality normal concrete or any other good quality dry-mix sprayed concrete.

CHAPTER 4

THE PERFORMANCE OF THE TECHNIQUE UNDER STATIC LOADING

4.0 GENERAL

After a minimum of 28 days of curing, each test slab in turn was lifted off the scaffold supporting frame onto a fabricated steel loading frame for load testing.

The details of the fourteen test slabs and the control slab tested under static loading are shown in Table 4.1. The slabs are denoted as A-type (A1 to A8) and B-type (B1, B3, B4, B7, B8 and B9) where, B-type are test slabs with the higher levels of reinforcement in the sprayed concrete and A-type define all other with and without shear connectors.

Test slabs B1, B3 and B4 were used to provide the ultimate static failure load for identical slabs B2, B5 and B6 which were subjected to fatigue loading.

Table 4.1 - Test slabs for static load testing

Slab	Sprayed Concrete Mix	Shear Connectors	Sprayed Concrete Thickness (mm)	Reinforcement Encapsulated in Sprayed Concrete (total steel as % of total concrete)
Control	-		-	-
A1	Normal		75	A193 (0.22)
A2	Normal		75	A193 (0.22)
A3	Normal	✓	75	A193 (0.22)
A4	Normal		75	A393 (0.33)
A5	Normal	✓	75	A393 (0.33)
A6	Normal		50	A193 (0.26)
A7	Normal		100	A193 & A98 (0.19)
A8	Normal	✓	100	A193 (0.19)
B1	Normal		75	B785 (0.56)
B3	Normal		75	B503 (0.4)
B4	Normal		75	A393 (0.33)
B7	Sikacem 133		75	A393 (0.33)
B8	Poly Fiber		75	A393 (0.33)
B9	Steel Fiber		75	A393 (0.33)

4.1 EXPERIMENTAL PROCEDURES

The experimental set up and instrumentation was relatively simple and this comprised:

- A fabricated steel loading frame,
- A servo controlled hydraulic loading jack,
- An electronic control unit which operates the hydrostatic loading jack,
- Three dial gauges,
- A data acquisition system

The slabs were positioned on the loading frame over a span of 1956 mm with the support bearings placed underneath the sprayed concrete layer as shown in Figure 4.1.

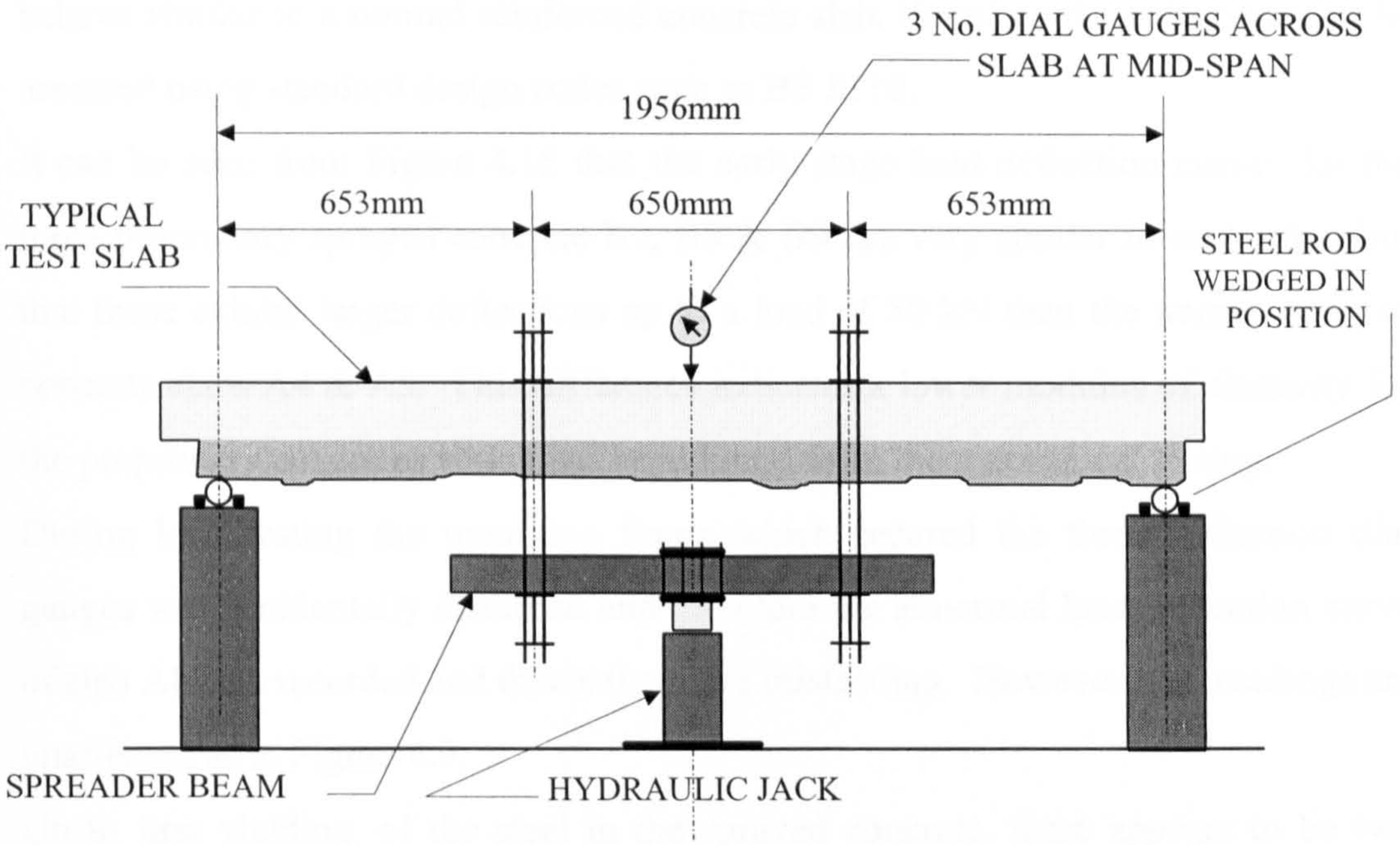

Figure 4.1 - Set up for static load testing.

The set up was such that the jack which was clamped down to the heavy rails built into the strong floor of the laboratory could exert a pulling force from underneath the slab.

For the control slab and A-type test slabs, data logging was carried out manually, taking readings from a set of three dial gauges positioned securely across the slab width at mid-span to monitor the average mid-span deflection versus the applied load read from the electronic control unit. For all B-type test slabs, data logging was automated with the use of a data acquisition system, this was necessary for safety reasons as the load intensity applied to these test slabs was much higher than those of the A-type. In all cases the load was applied in 5 kN increments up to failure.

4.2 EXPERIMENTAL RESULTS - STATIC

4.2.1 Deflection behaviour

The load versus average mid-span deflection curves of individual test slabs (strengthened) compared with the base slab (unstrengthened) are shown in Figures 4.2 to 4.14. In order to compare the deflection behaviour of the different test slabs, all the individual curves are superimposed as shown in Figure 4.15.

In studying the load-deflection curves, the following points can be deduced:

- The curves of load versus average mid-span deflection show that all test slabs behave similar to a normal reinforced concrete slab, therefore the behaviour can be assessed using standard design codes such as BS 8110.
- It can be seen from Figure 4.15 that the early stage load-deflection curves for the three proprietary sprayed concrete B7, B8 & B9 are very similar to each other but that these exhibit larger deflections up to a load of 50 kN than the normal sprayed concrete slabs A4 & A5. This difference indicates a lower modulus of elasticity for the proprietary concretes which has been found from the mechanical testing.
- During load testing the mounting frame which secured the three deflection dial gauges was accidentally disturbed and therefore the abnormal load-deflection curve of slab A8 was recorded and this is therefore misleading. However load readings are unaffected as in Figure 4.9.
- Up to first yielding, of the steel in the sprayed concrete, there appears to be two types of behaviour, that of the A-type slabs and that of the B-type slabs, in which the initial loading in the A-type is more linearly elastic up to first yield point, which is therefore a distinct point between elastic and plastic behaviour compared with the B-type which shows a more gradual change over the entire range.
- Beyond first yield of the steel and up to failure, all test slabs behave in a similar way.
- The superimposed curves diagram also shows that for similar test slabs the B-type test slabs displayed larger deflections at the ultimate state compared to the A-type test slabs.

Figure 4.2 - Test slab A1 and base slab.

Figure 4.3 - Test slab A2 and base slab.

Figure 4.4 - Test slab A3 and base slab.

Figure 4.5 - Test slab A4 and base slab.

Figure 4.6 - Test slab A5 and base slab.

Figure 4.7 - Test slab A6 and base slab.

Figure 4.8 - Test slab A7 and base slab.

Figure 4.9 - Test slab A8 and base slab.

Figure 4.10 - Test slab B1 and base slab.

Figure 4.11 - Test slab B3 and base slab.

Test slab B4 and base slab. Data was lost due to damaged disk.

Figure 4.12 - Test slab B7 and base slab.

Figure 4.13 - Test slab B8 and base slab.

Figure 4.14 - Test slab B9 and base slab.

Figure 4.15 - All test slabs superimposed for comparison.

Figure 4.2 - Slab A1 / Base Slab

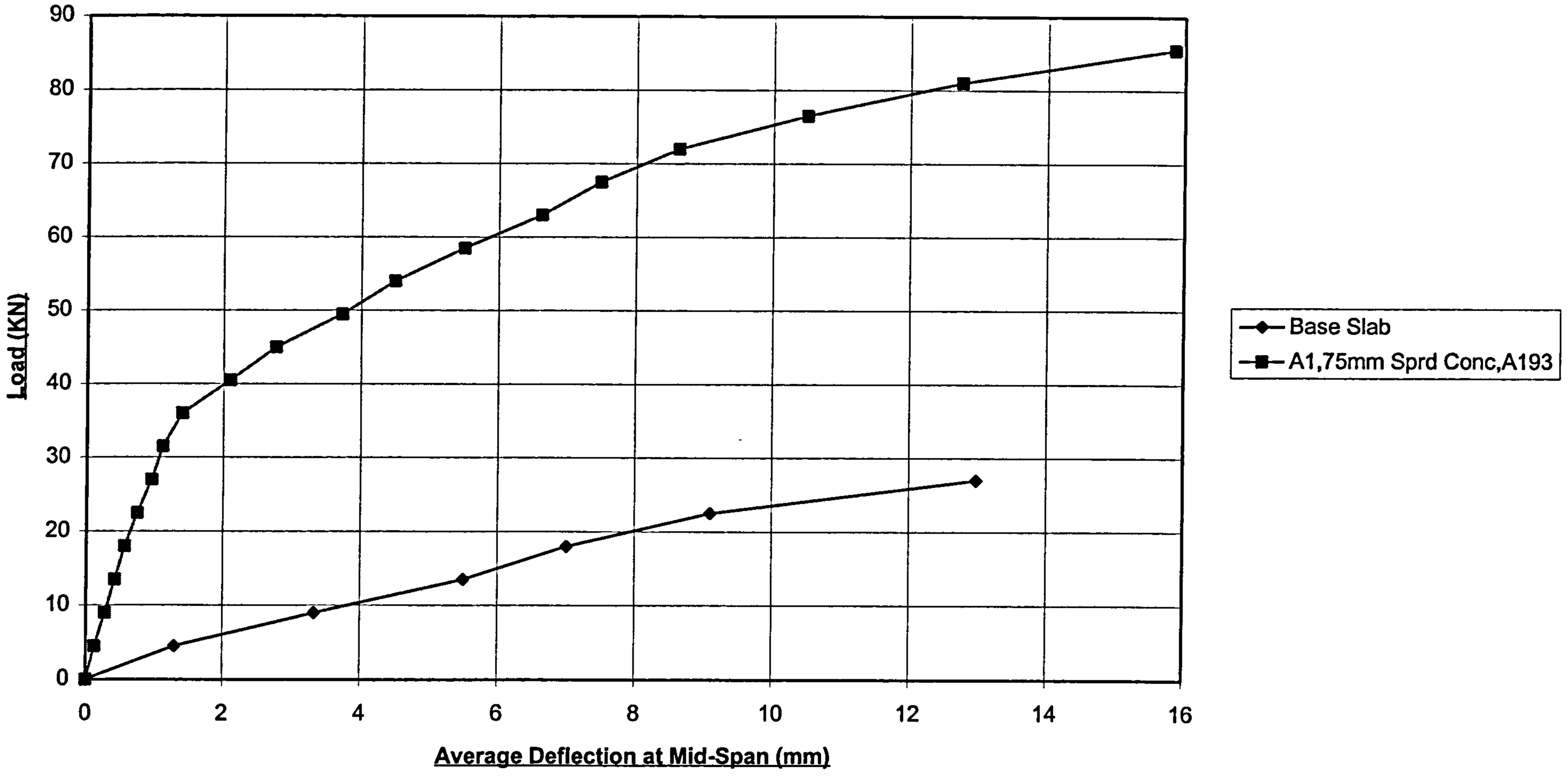

Figure 4.3 - Slab A2 / Base Slab

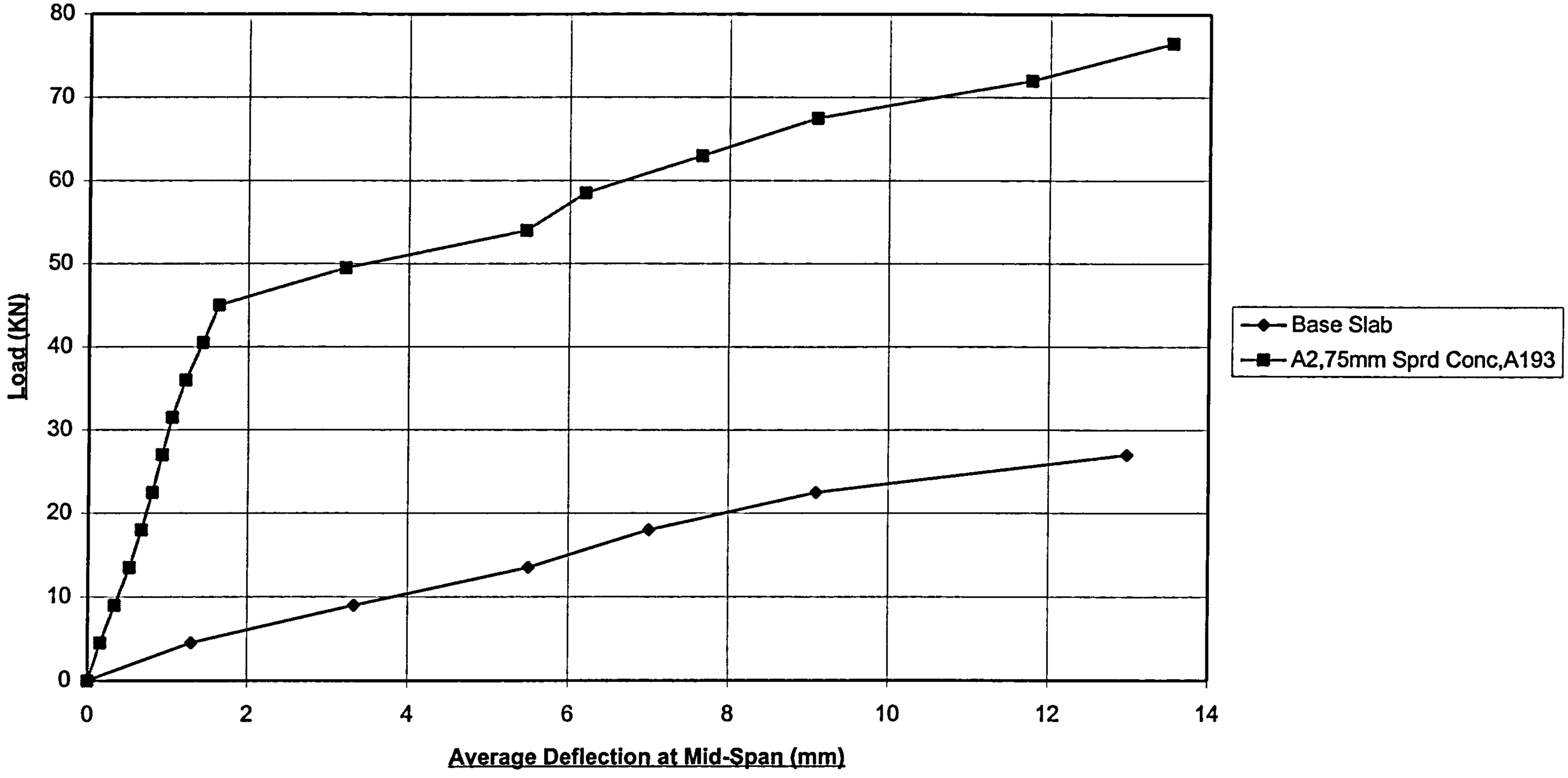

Figure 4.4 - Slab A3 / Base Slab

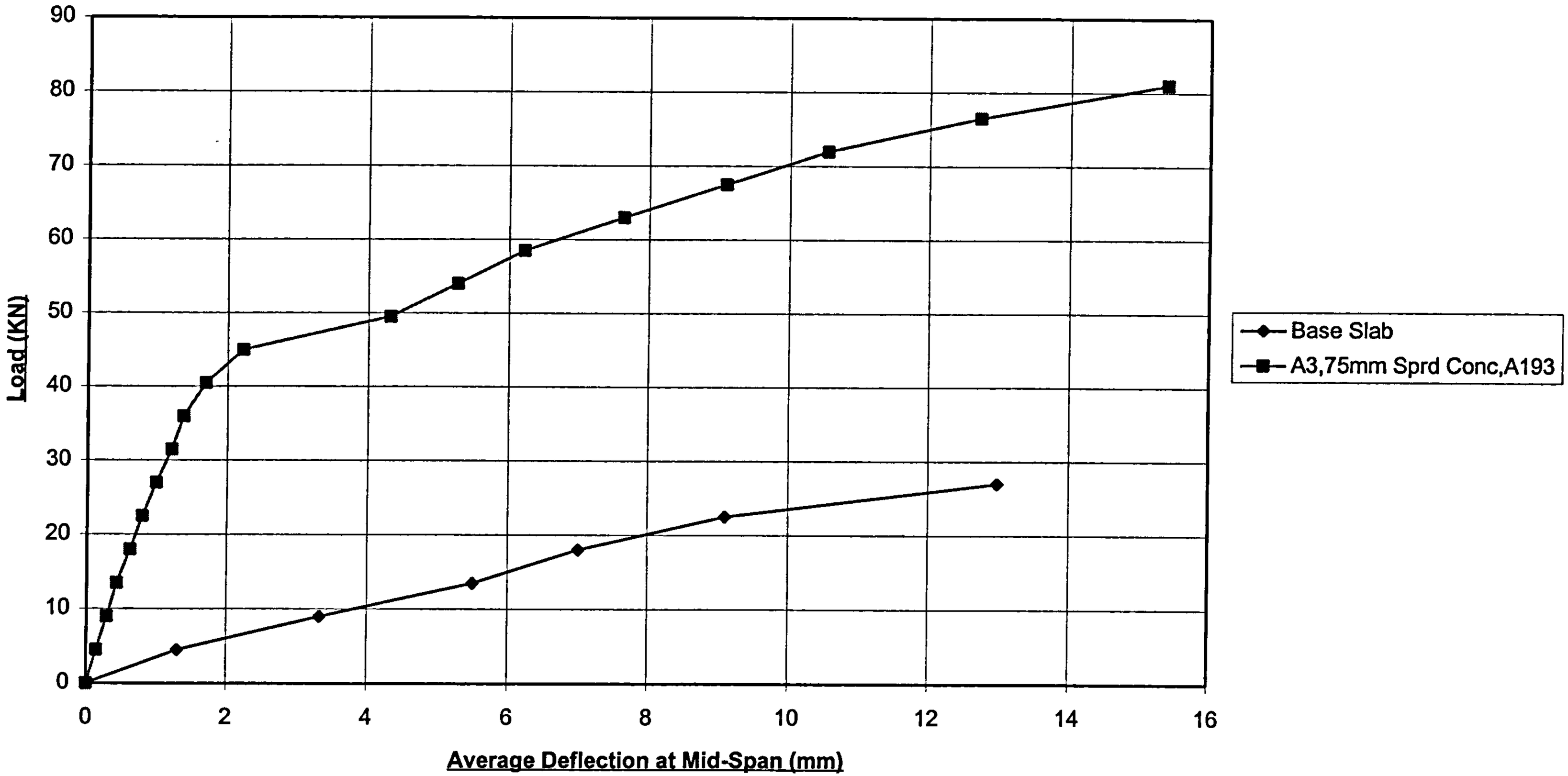

Figure 4.5 - Slab A4 / Base Slab

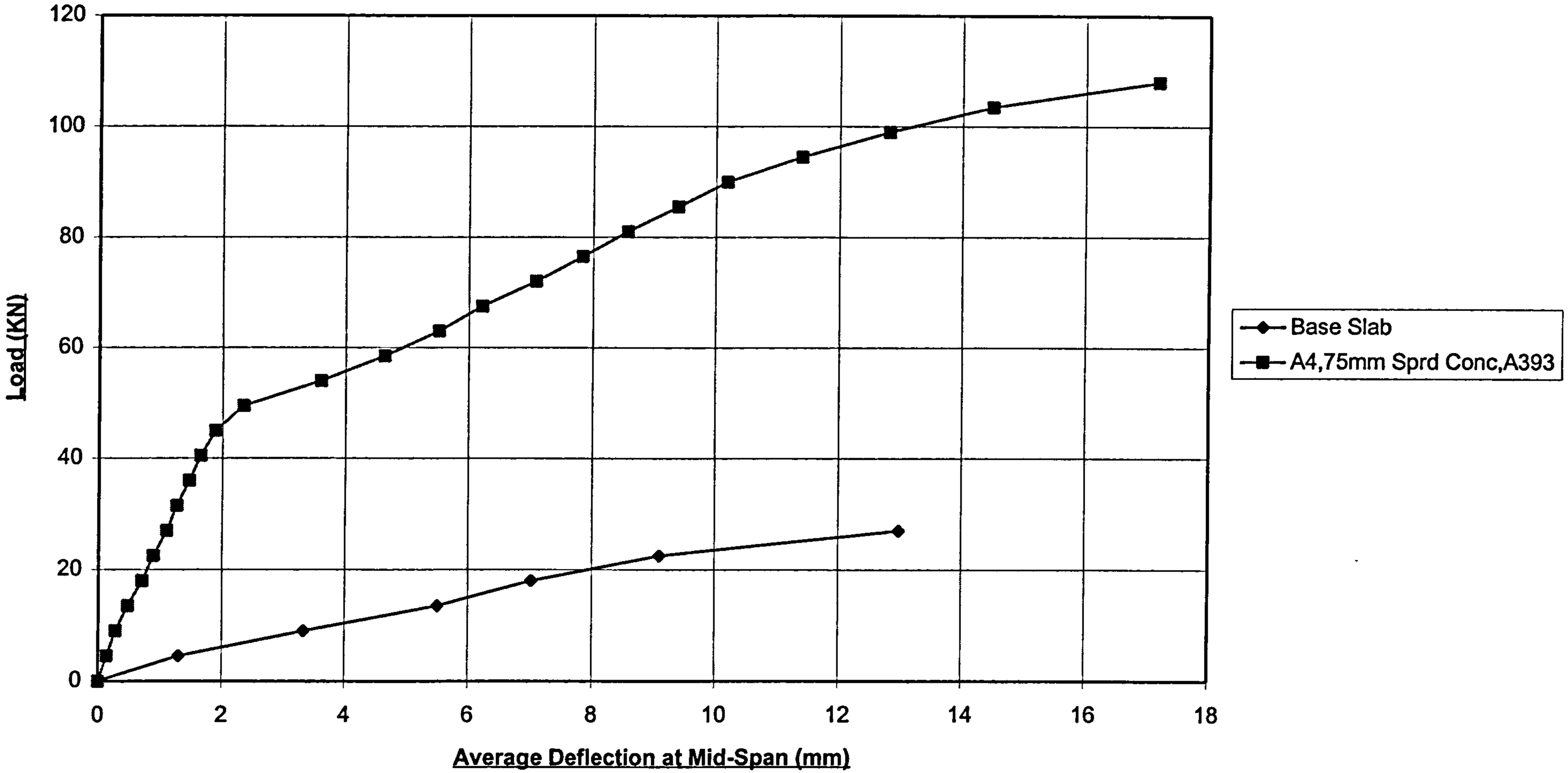

Figure 4.6 - Slab A5 / Base Slab

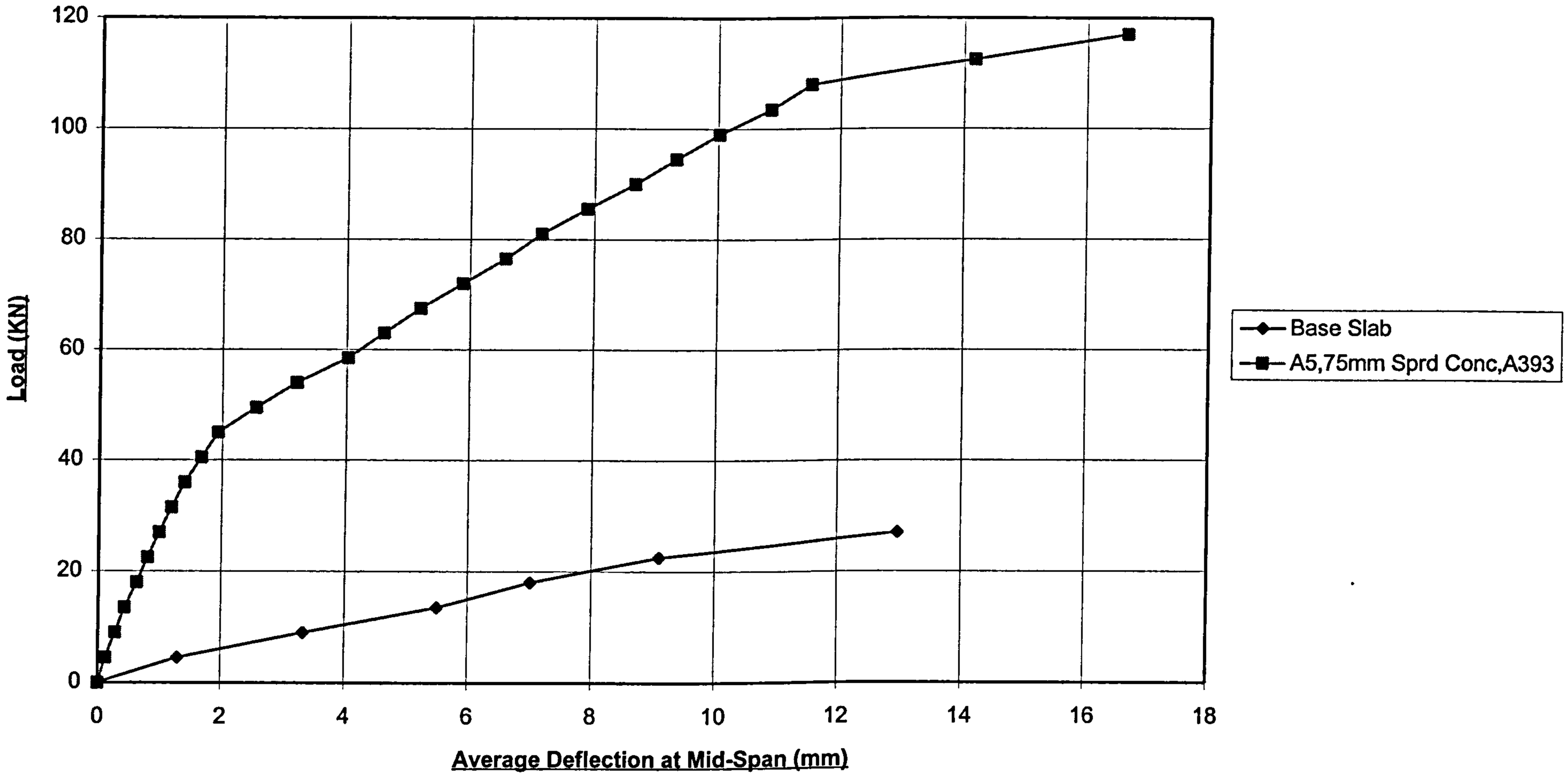

Figure 4.7 - Slab A6 / Base Slab

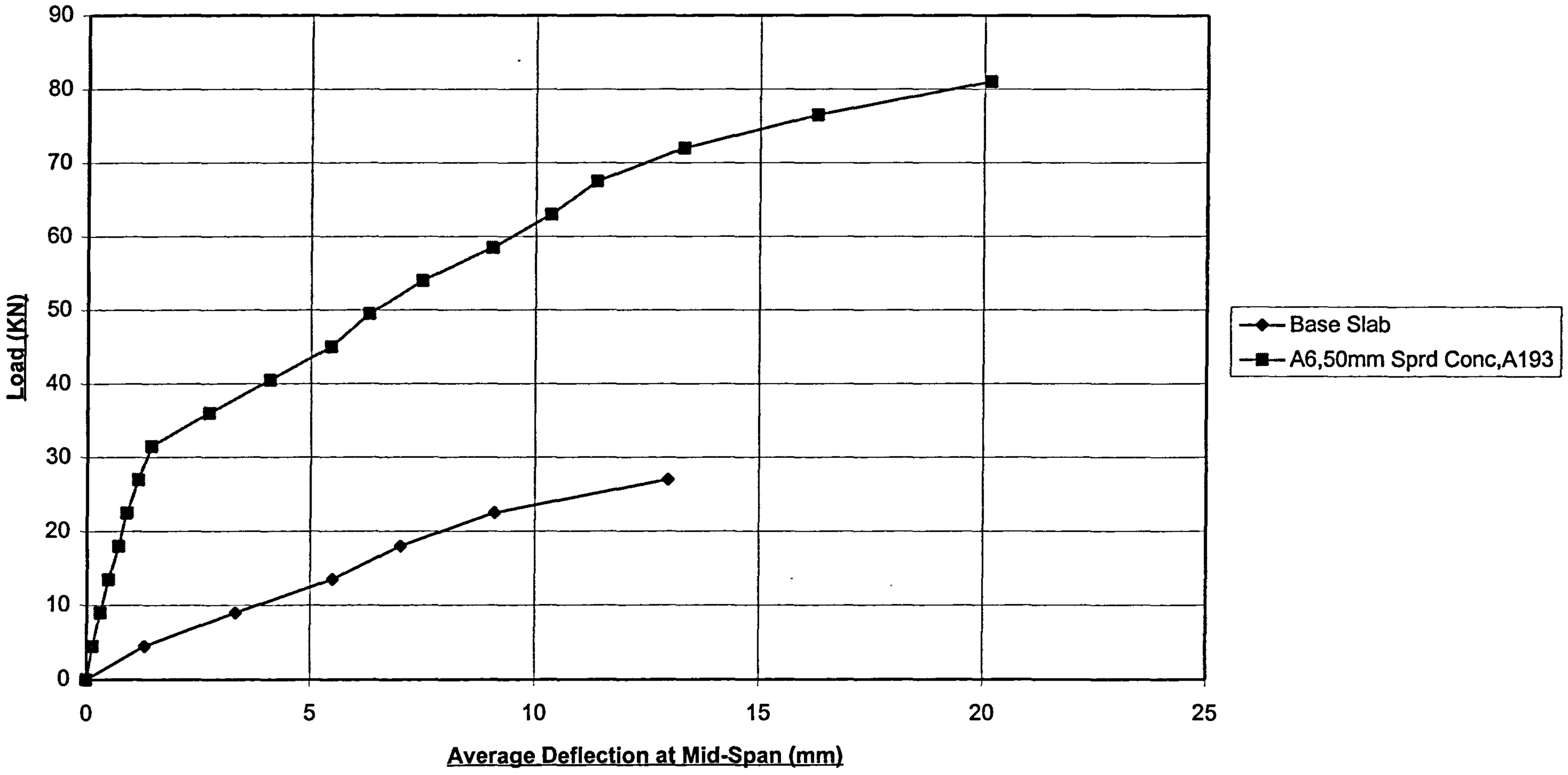

Figure 4.8 - Slab A7 / Base Slab

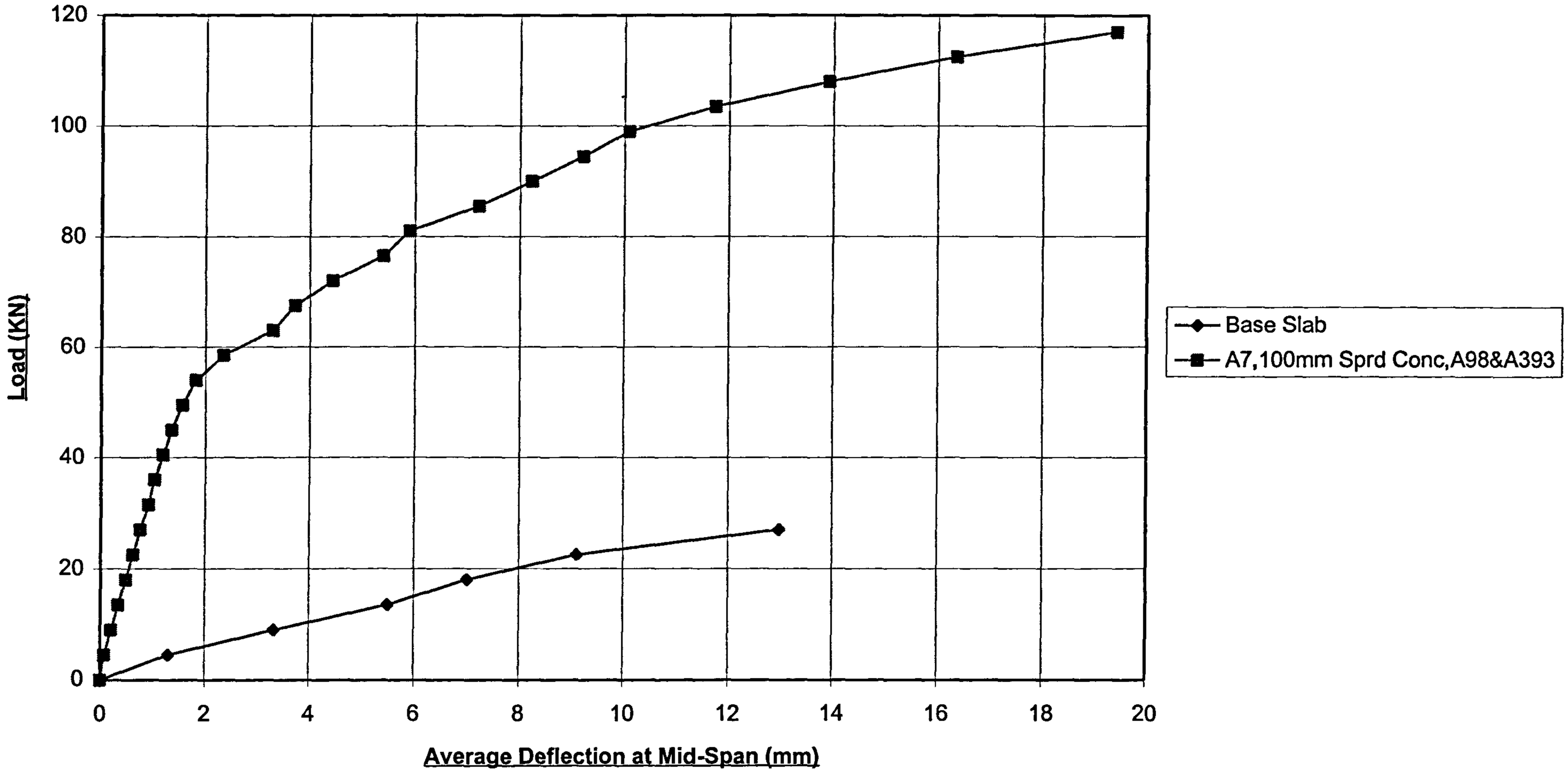

Figure 4.9 - Slab A8 / Base Slab

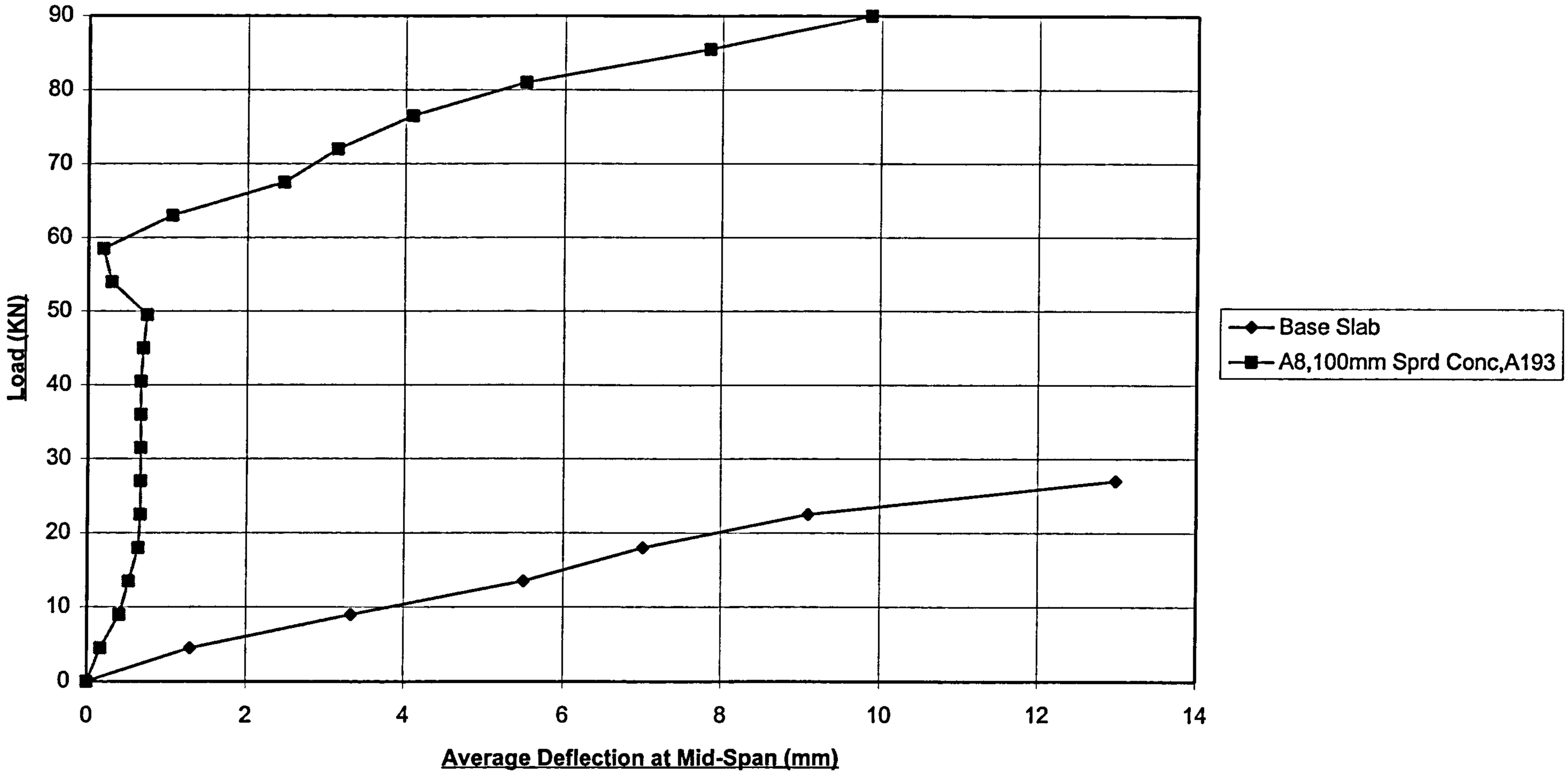

Figure 4.10 - Slab B1 / Base Slab

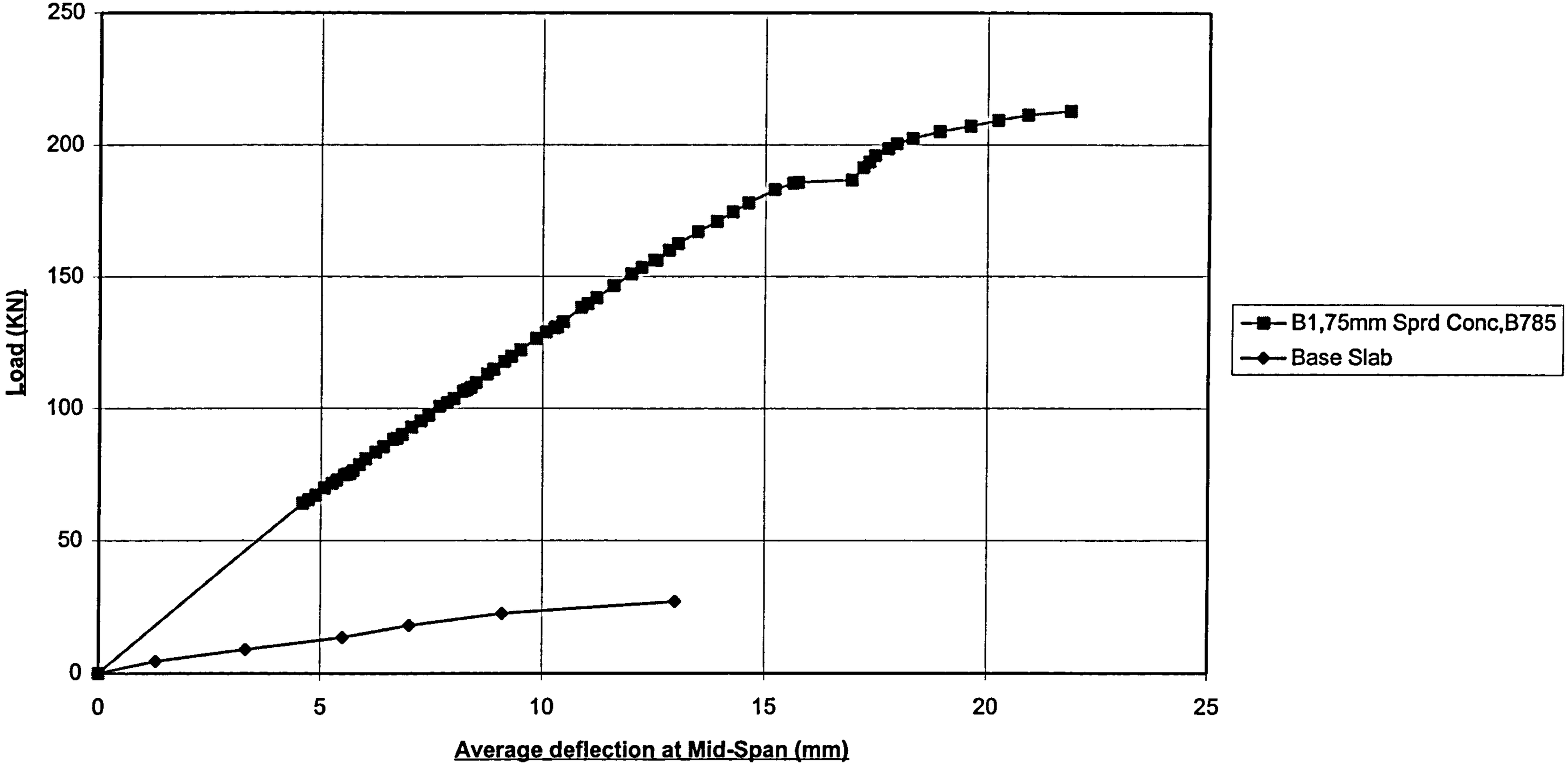

Figure 4.11 - Slab B3 / Base Slab

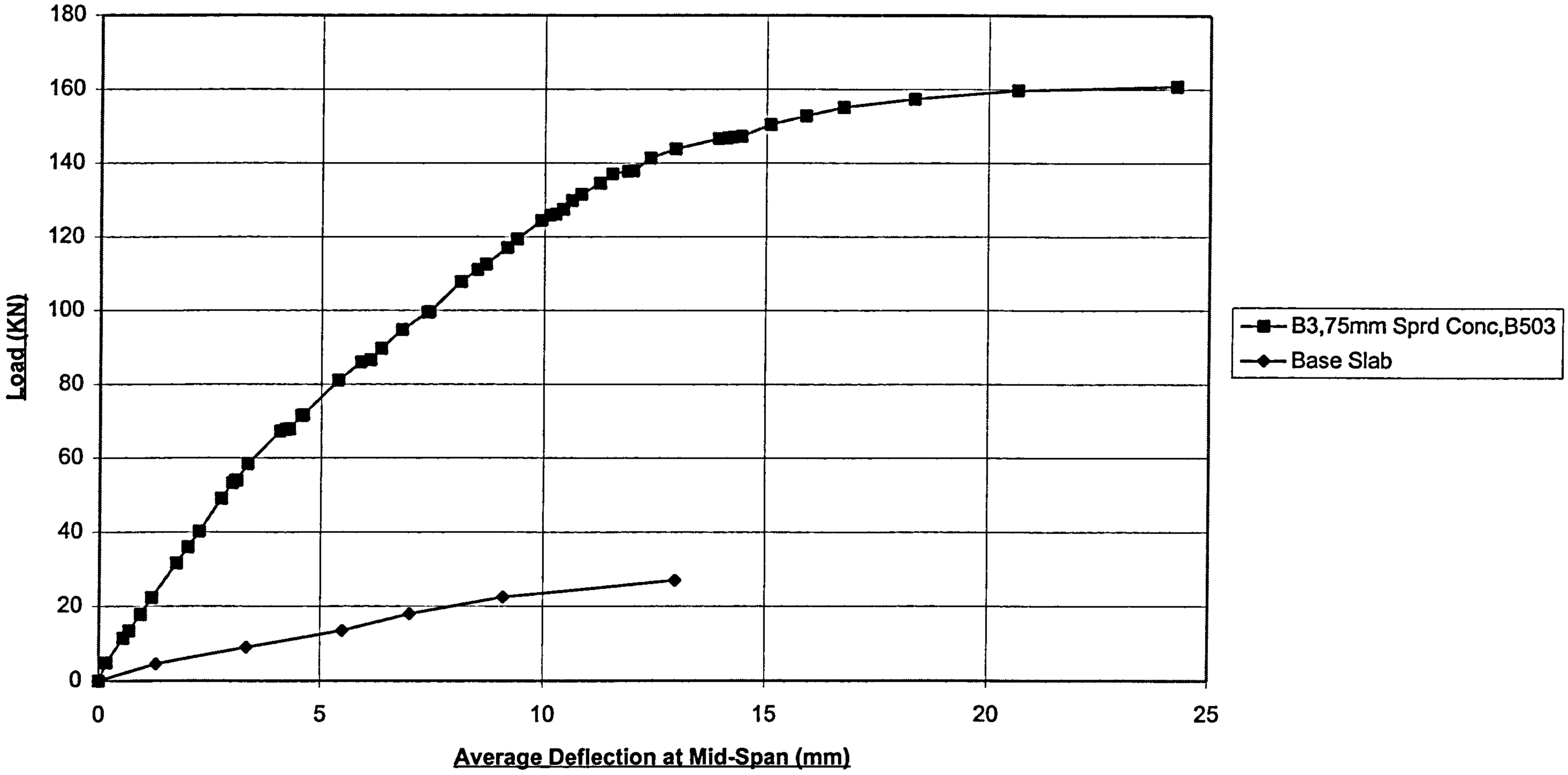

Figure 4.12 - Slab B7 / Base slab

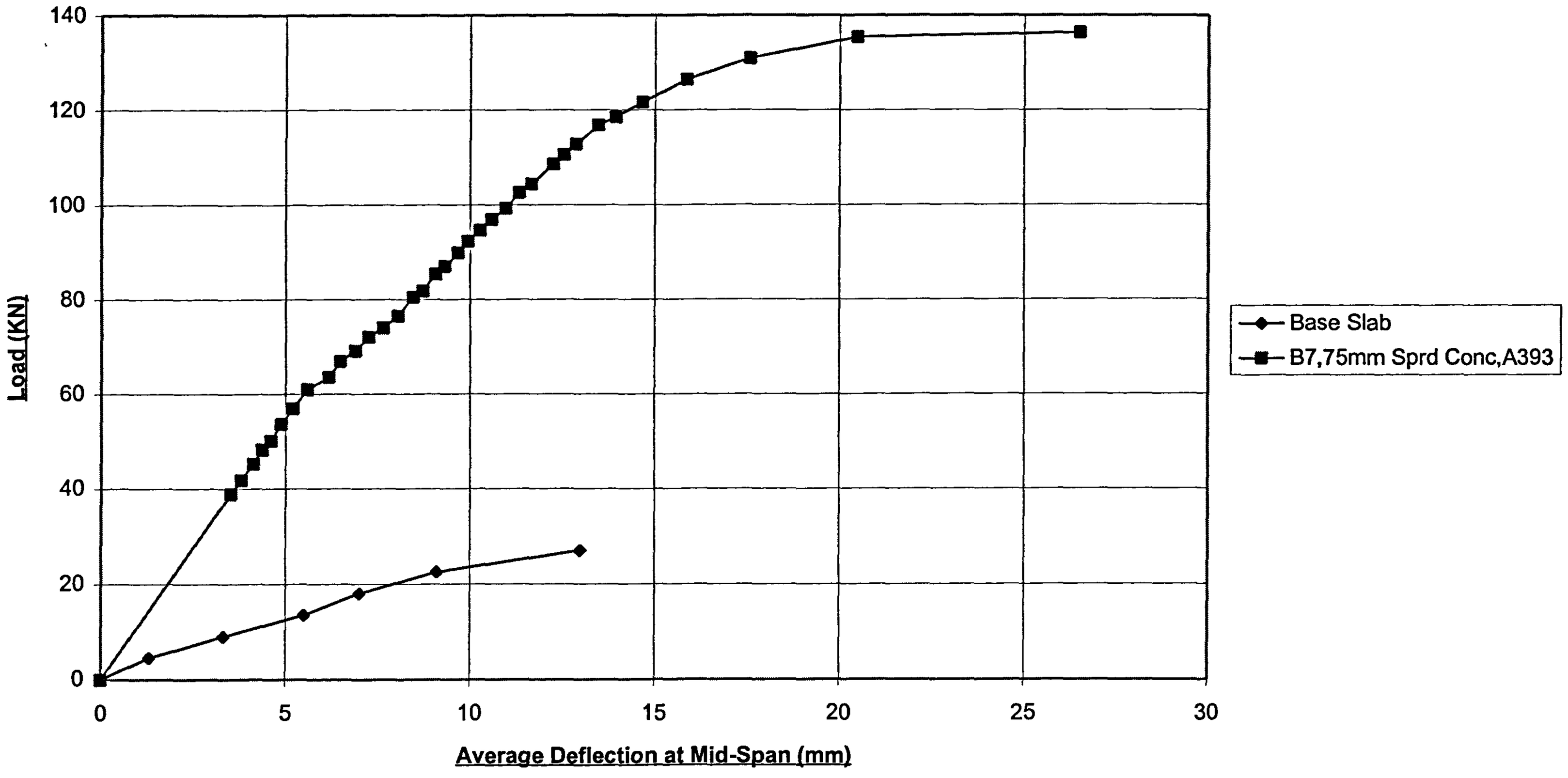

Figure 4.13 - Slab B8 / Base Slab

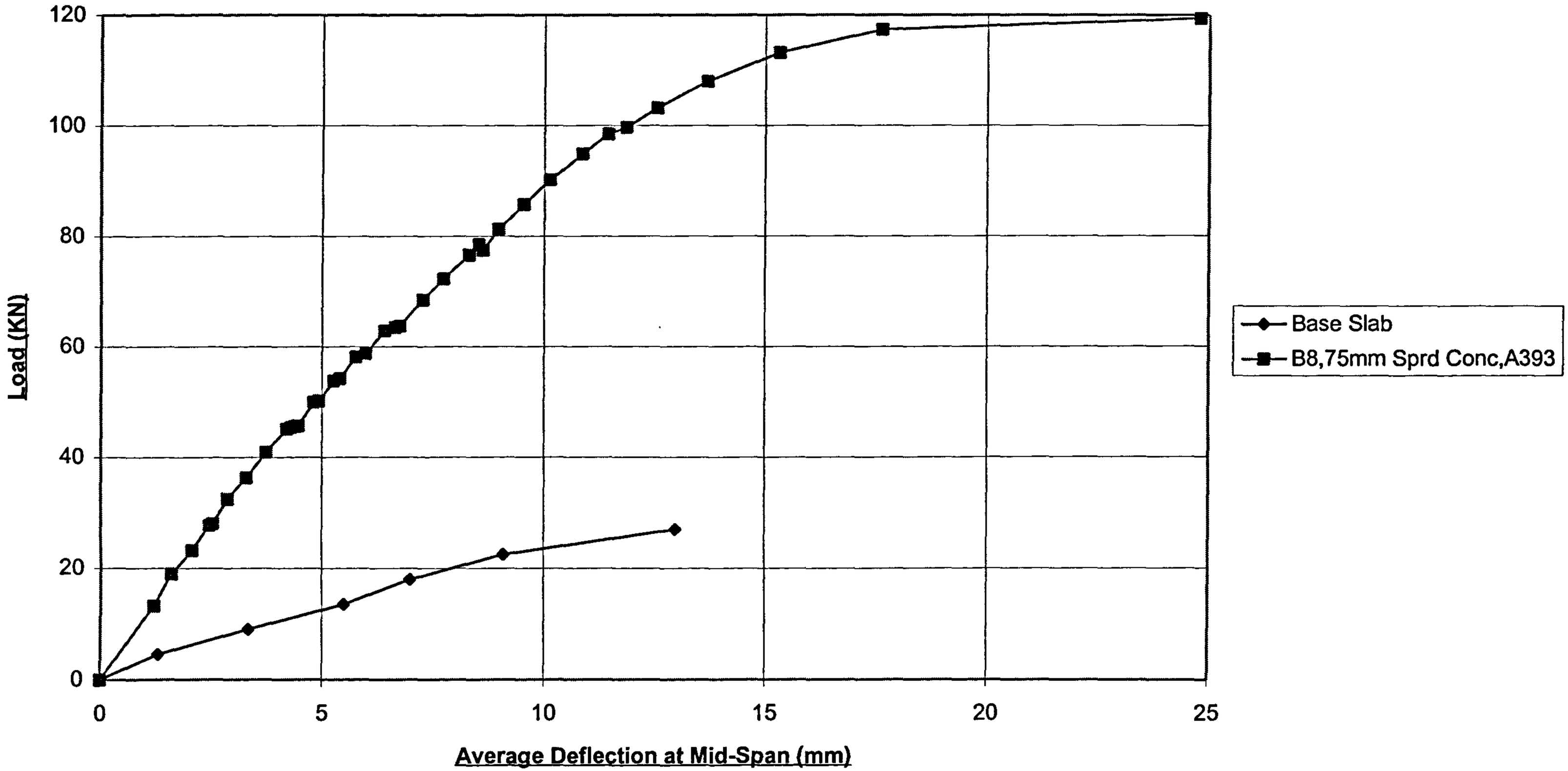

Figure 4.14 - Slab B9 / Base Slab

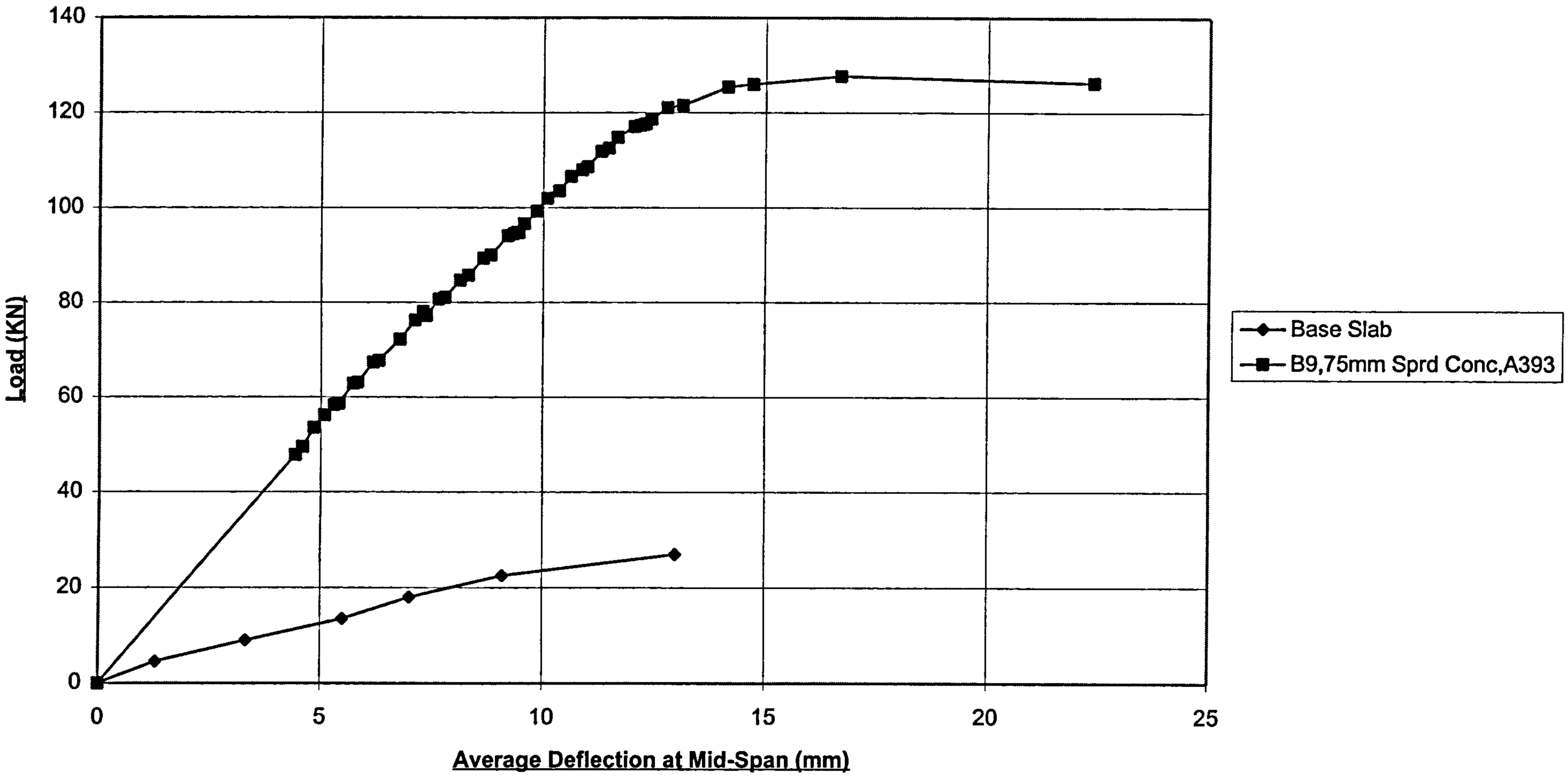

Figure 4.15 - All Test Slabs Under Static Loading

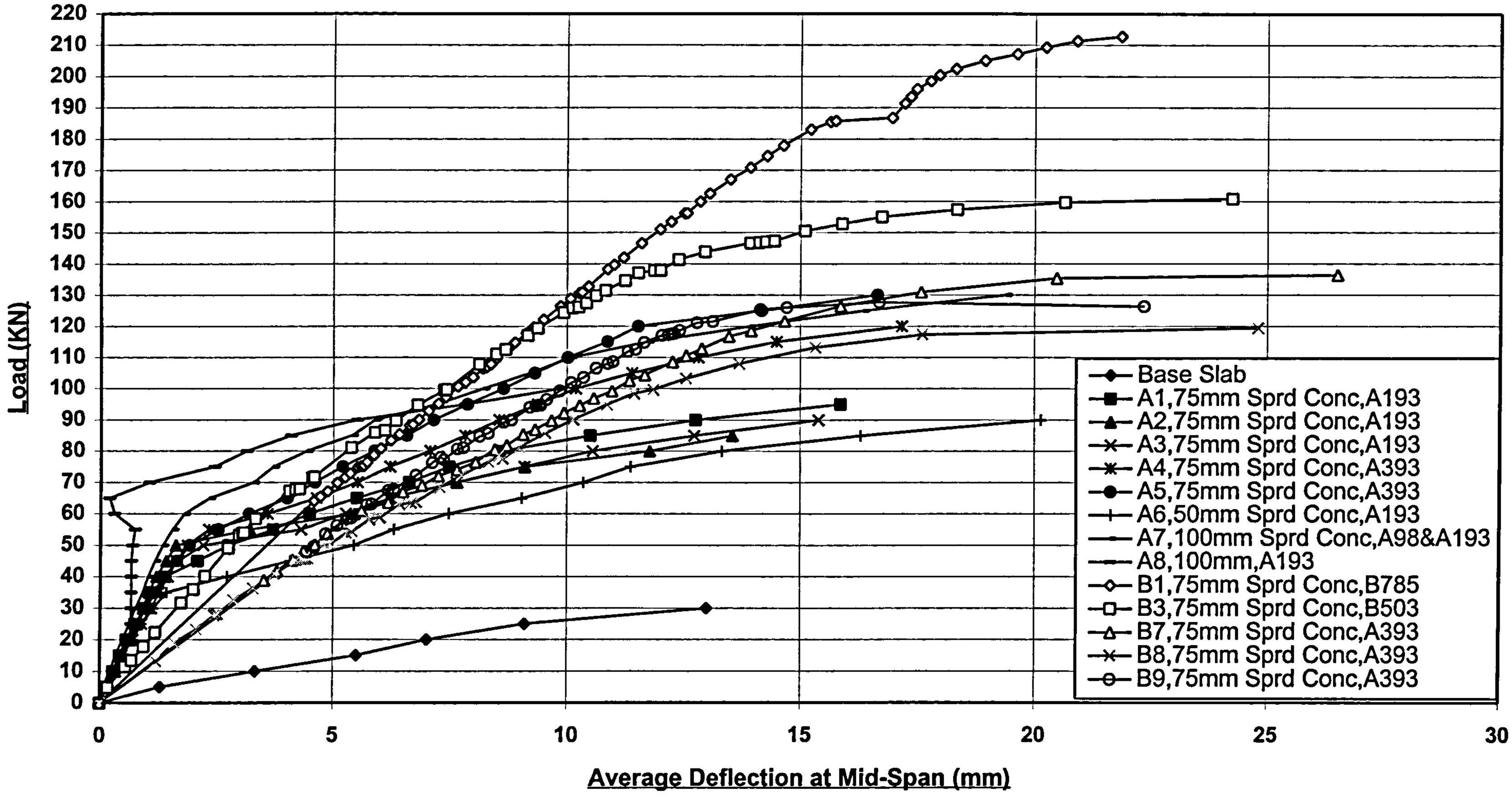

4.2.2 Ultimate strength of test slabs - static

All statically load tested slabs have their experimental failure loads recorded in Table 4.2 and these values are compared with the predicted values in accordance with simple R-C slab design theory as defined in BS 8110: Part 1: 1985[26]. The following points are applicable to Table 4.2,

1. Factors γ_m of 1.5 for f_{cu} and 1.15 for f_y are not included in calculating the theoretical values.
2. A98 in slab A7 assisted structurally in carrying load and was considered in the calculation.
3. All theoretical values are determined based on the actual effective depths of reinforcement layers as measured manually from the broken faces of the tested slabs.
4. A5 failed in a ductile manner and the slab remained intact therefore the actual effective depth could not be determined, but it was assumed to be similar to slab A4.
5. The design ultimate strength of all reinforcement was used in the moment capacity calculations and this is 460 N/mm^2.
6. The design cube strength in the base slab was used for all test slabs and this is 35 N/mm^2.

The predicted or theoretical flexural M_{cap} were determined assuming that the reinforcement in both the sprayed concrete layer and the base concrete (or substrate concrete) had yielded and that the bond at the substrate/sprayed concrete interface is fully maintained. Appendix C shows the details of the typical design calculation leading to the theoretical failure loads of the strengthened slabs in accordance with BS 8110: Part 1: 1985.

From the results tabulated in Table 4.2, the following points can be deduced:

- The load deflection curves of all test slabs show that the strengthening process had resulted in the slab being significantly stronger in flexure - up to nearly eight times stronger, (comparing B1, M = 212.8 kNm and control, M = 27 kNm)
- Comparison of similar slabs with and without shear connections in Table 4.2 (A1, A2 & A3 and A4, A5 & B4) shows that the inclusion of shear connectors does not cause any increase in strength. Comparison of A7 & A8 is more difficult since it was thought necessary to include a subsidiary mesh near the interface due to the

thickness of the sprayed concrete layer, when shear connectors were not present and this extra reinforcement is the main reason for the increase in strength.

- All test slabs failed at loads greater than predicted from BS 8110 with the ratio of M_{expt}/M_{8110} ranging from 1.07 to 1.53. The design calculations were carried out in accordance with BS 8110 except that partial material load factors were taken as one. A reinforcement design strength of 460 N/mm^2 (actual strength measured in air was 654 N/mm^2) was taken since this material was high tensile. The design cube strength was taken as 35 N/mm^2, the specified strength for a C35 concrete. The actual depth of the reinforcement (marginally greater than the designed depth) was used. The possible explanations for the disagreement between M_{expt} and M_{8110} are:

1. Actual strength of the base slab concrete at the time of testing was significantly greater than the value used in the calculations and this averaged 46 N/mm^2 for all test slabs.
2. The ratio of actual steel breaking strength to the design strength is 1.42, but take into account the fact that, though not recorded, the rate of load testing the test slabs was comparatively greater than the rate of tensile testing the reinforcement in air and Park and Paulay[36] state that:

> The effect of a fast rate of loading is to increase the yield strength of the steel, for example, it has been reported by ACI 439[37] that for a strain rate of 0.01/sec the lower yield strength may be increased by up to 14%.

Therefore making the ratio 1.62. Clearly, from Table 4.2 the ratio lies within this range, from 1.07 to 1.53 but much more distinctly from 1.20 to 1.53. The ratio 1.07 indicates relative weakness of this test slab compared with the others and is most likely due to the following reasons:

- Weakness in the mesh reinforcement perhaps caused by spot welding occurring at the critical section.
- Greater effect from torsion caused by the test slab not sitting uniformly flat on the loading frame causing possible overstressing of reinforcement in parts of the slab, leading to premature failure.
- Possible difference in bond between the mesh reinforcement and sprayed concrete caused by local variations in density of sprayed concrete around the bars, see section 3.3.3.

Table 4.2 - Experimental and theoretical failure loads of the strengthened slabs

Slab	Concrete Mix	Sprayed Concrete Thickness (mm)	Reinforcement in sprayed concrete	Shear connectors	Theoretical M_{cap1} (kNm)	Experimental Failure Jack load (kN)	Experimental M_{cap2} (kNm)	Ratio of M_{cap2}/M_{cap1}
Control	-	-	-		7.0	27.0	8.8	1.26
A5	Normal	75	A393	✓	31.8	117.0	38.2	1.20
A4	Normal	75	A393		31.8	104.0	34.0	1.07
A7	Normal	100	A193 & A98		27.1	117.0	38.2	1.41
A8	Normal	100	A193	✓	21.7	90.0	29.4	1.35
A1	Normal	75	A193		19.5	85.5	27.9	1.43
A3	Normal	75	A193	✓	19.5	76.5	25.0	1.28
A2	Normal	75	A193		19.5	81.0	26.4	1.36
A6	Normal	50	A193		17.3	81.0	26.4	1.53
B1	Normal	75	B785		55.2	212.8	69.5	1.26
B3	Normal	75	B503		38.7	160.8	52.5	1.36
B4	Normal	75	A393		31.8	144.0	47.0	1.48
B7	Sikacem 133	75	A393		31.8	136.4	44.5	1.40
B8	Poly Fiber	75	A393		31.8	119.4	39.0	1.23
B9	Steel Fiber	75	A393		31.8	127.7	41.7	1.31

4.2.3 Cracking and modes of failure

- All test slabs displayed flexural crack patterns, see Figure 4.16.
- All test slabs failed when one of the cracks widened under load and propagated across the substrate/sprayed concrete interface into the substrate concrete and then to failure. The propagation of the flexural crack crossing the substrate/sprayed concrete interface can be seen from one of the slabs which remained intact, see Figure 4.17 and upon examination of the two halves of a broken slab, see Figure 4.18, which shows a 'a clear' (flexural) failure without any sign of vertical separation at the interface.
- The finding that at failure, a flexural crack crossed the substrate/sprayed interface with no initiation of the crack horizontally at the interface shows that grit blasting even without shear connectors was sufficient for the sprayed concrete layer to be fully bonded to the substrate concrete, thereby maintaining composite action throughout loading until failure.
- All test slabs exhibited a tension failure mode, only one slab (A5) failed in a ductile manner and remained intact, the remaining slabs failed in a brittle manner, with the slabs broken into two halves. Although the majority of test slabs exhibited this brittle failure manner, they were all under-reinforced with the maximum total steel content of 0.56%. The probable reason for the brittle failure was because all the reinforcement in the slabs was high tensile and therefore exhibited little yield, therefore near the ultimate condition, the bottom reinforcement (in the sprayed concrete) was close to fracturing, the upper reinforcement (in the base slab concrete) was close to yield and as soon as the bottom reinforcement reached its breaking value and broke, the upper reinforcement was unable to sustain much further stress and this therefore also broke apparently instantaneously.

The following photographs describe the above points:

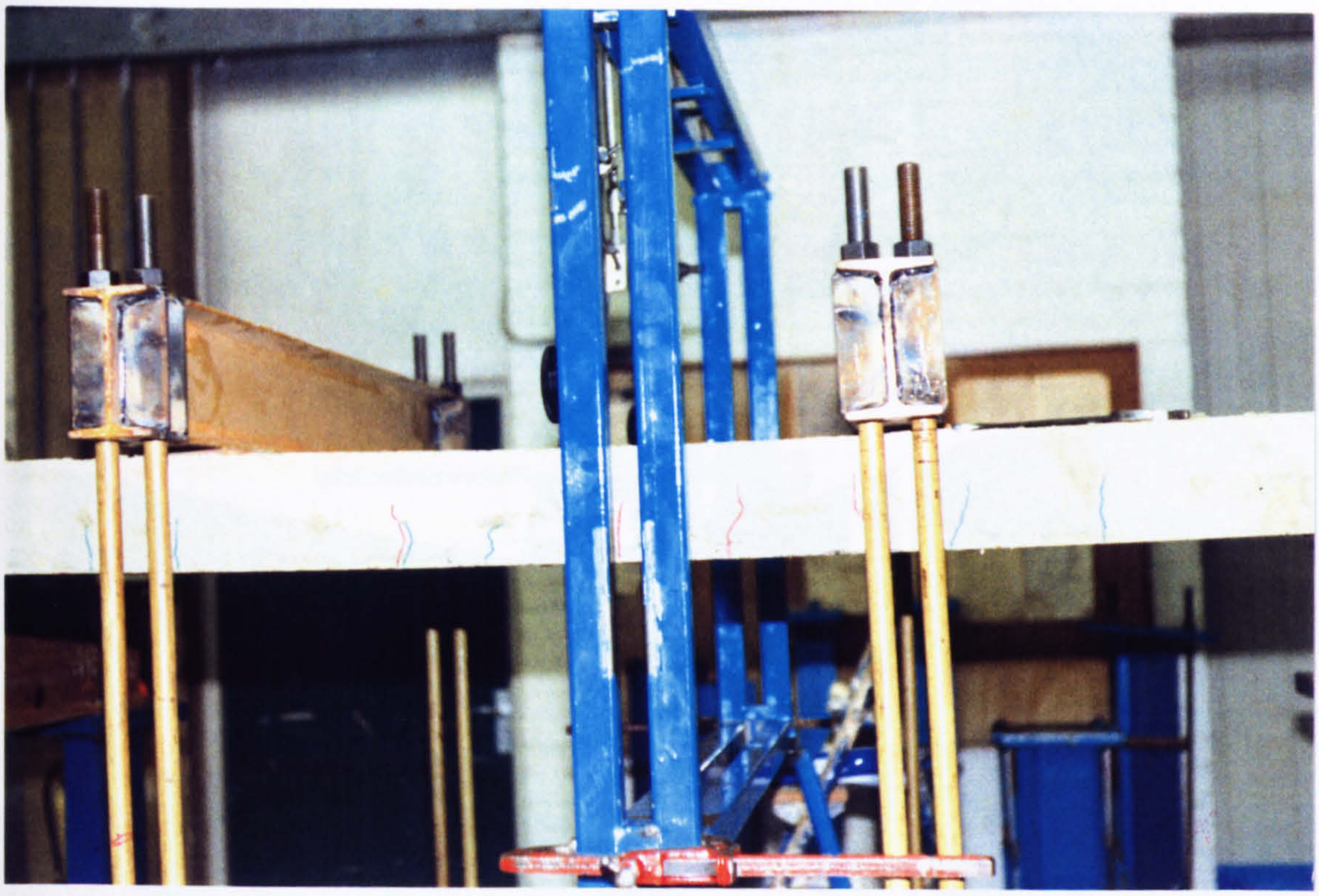

Figure 4.16a - Flexural crack pattern in control slab.

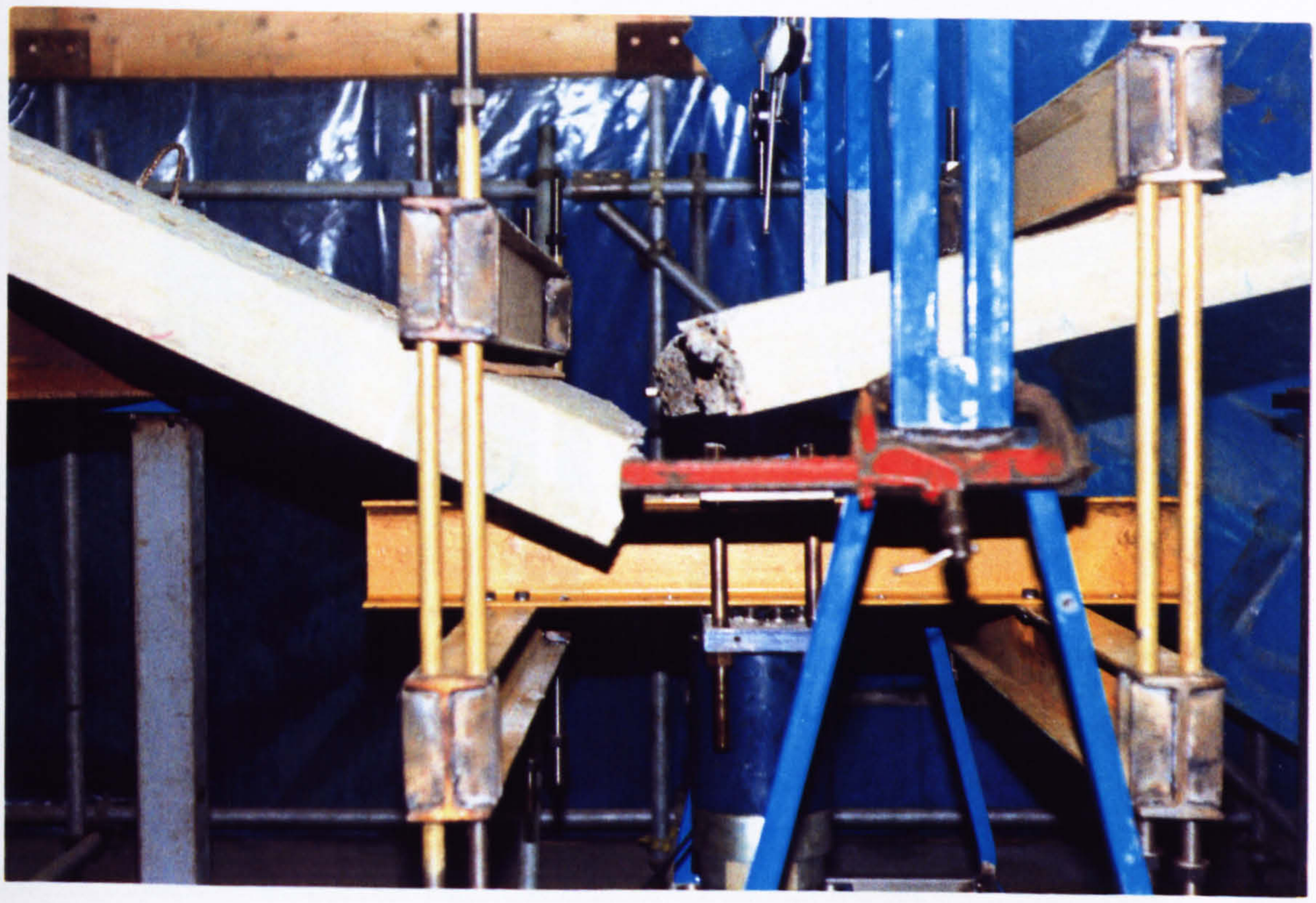

Figure 4.16b - Flexural failure in control slab.

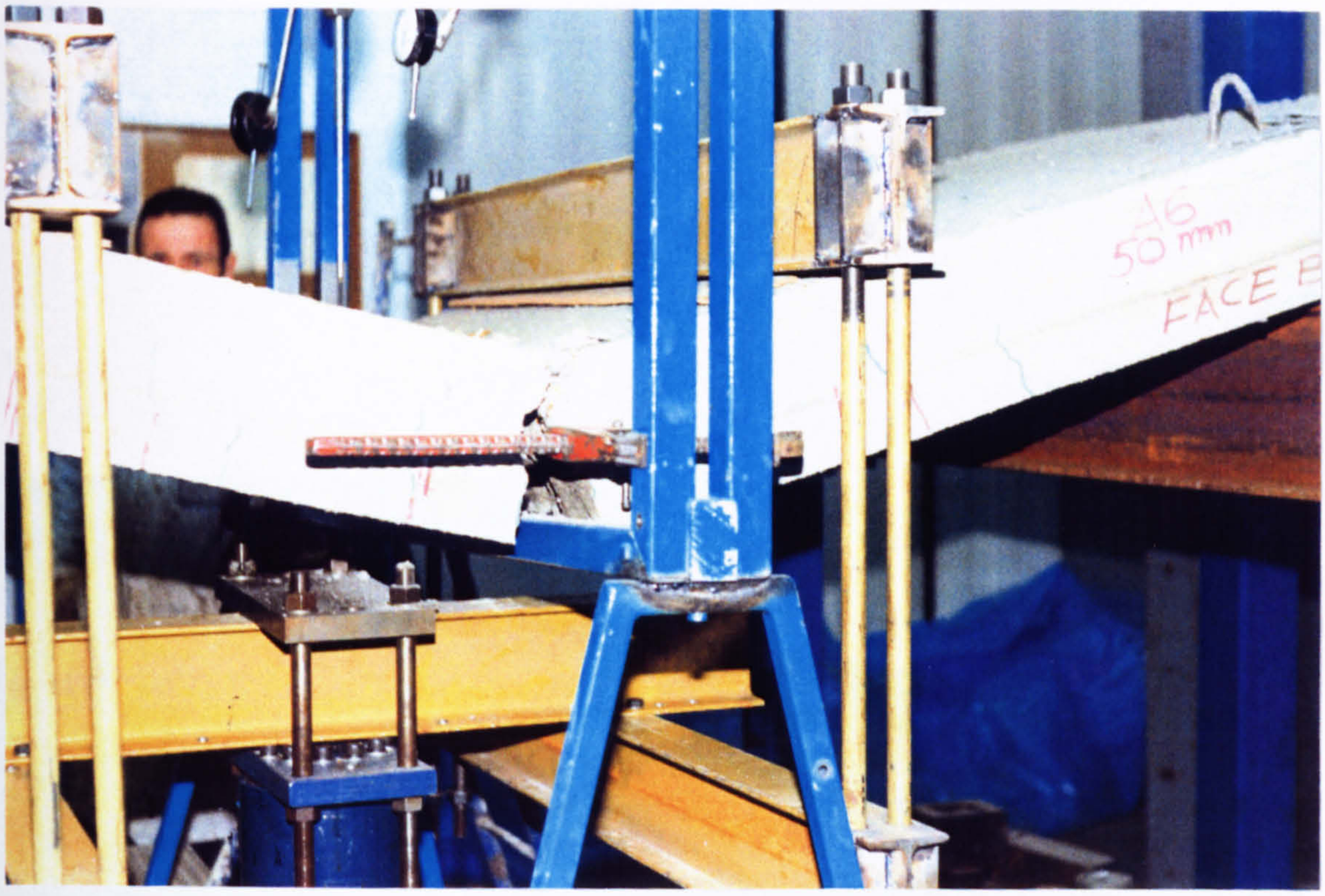

Figure 4.16c - Flexural failure in a typical test slab.

Figure 4.16 - Mode of failure in the control and a typical test slab.

Figure 4.17 - Ductile failure of test slab A5.

Figure 4.18 - Examining the 'broken' faces of the test slab.

CHAPTER 5

FATIGUE LOADING - AN ANALYTICAL STUDY

5.0 GENERAL

Nowadays, the methods of analysis for structures are becoming more exact and as a result, there is a need for more fundamental information on the behaviour of concrete structures under loads other than simple static loads. Highway engineers have been aware of the need to understand the fatigue of concrete in roads and bridges for many years.

In 1961 in the UK, the committee on bridges of the former Road Research Board formed a panel to look into the performance of highway bridges under fatigue loading and a conclusion drawn from the investigation was that for concrete bridges fatigue problems were unlikely to occur with the existing methods of design outlined in BS 5400: Part 10: 1980[38], either for reinforced or prestressed construction, although the experience in prestressed structures was relatively limited. However, subsequent investigations indicated that fatigue life might not be sufficiently long for the problem to be ignored. The work being reported in this chapter attempts to address fatigue life of a concrete bridge strengthened using reinforced sprayed concrete.

5.1 SCOPE OF FATIGUE CONSIDERATION

This chapter describes how the load range to be applied to the test slabs was determined. This load range is intended to be equivalent to that imposed on a typical trunk road bridge during its 120 years life span. In order to fulfil this intention, the current suitably modified and updated load spectrum tabulated in BS 5400[38] is used in conjunction with a simplified S-N curve obtained from the American Concrete Institute code ACI 215R-74 [39] and the series of Goodman diagram obtained from this S-N curve. It is pointed out that although the original diagrams were produced for plain concrete, it will be shown in chapter 6 that their use in this research is conservative.

The structure of this chapter follows the following sequence:

1. Using the commercially available structural analysis program QSE to calculate the ultimate design moment capacity of the typical trunk road bridge.
2. Using simple statics to calculate the dead load and live load moments on the bridge. The live load moment is based on the updated commercial vehicle wheel load spectrum of BS 5400: Part 10.
3. Nominal load range was derived, from which the test slabs were fatigue load tested for one million cycles.
4. Analytical study undertaken to show how the analytical table of load range versus the number of cycles to failure was obtained, based on the simplified S-N diagram and the range of Goodman diagrams.
5. The expected total number of cycles (N) to failure for a particular load range is obtained from Table 5.8 and the number of vehicles passes (n) for the appropriate vehicle grouping associated with this range are obtained from Table 5.12 which is in turn obtained from Table 5.11 and Table 10 of BS 5400: Part 10. Using Miner's summation hypothesis of total (n/N) ≤ 1 shows that the 15 m bridge example is the most critical and for this bridge, the greatest contribution to this summation is given by the 18GT-H commercial vehicle type. The final fatigue load range was therefore based on the range corresponding to this commercial vehicle type, but had to be reduced to 40 - 70% due to oil flow limitations.

5.2 HIGHWAY BRIDGE LOADING

Fatigue loading consists of a sequence of load repetitions that may cause a fatigue failure in about 100 or more cycles and on highway bridges this sequence of load repetitions is from moving traffic.

Basically, for design purposes the fatigue load range can be represented by the minimum load being the bridge dead load and the maximum load being the summation of the dead and live loads.

From the literature reviews, it appears that BS 5400 has not so far been superseded, however in using this standard, the author has accounted for the increasingly common commercial vehicle type 6A-M with a projected 44 tons total wheel load (see Appendix D) and this standard is used in conjunction with Department

of Transport Standard BD 37/88[40] to configure the fatigue load to the following two types of highway bridges:

I. A 15m span two lane single carriageway slab bridge shown in Figure 5.1

II. A 20m span two lane dual carriageway slab bridge shown in Figure 5.2

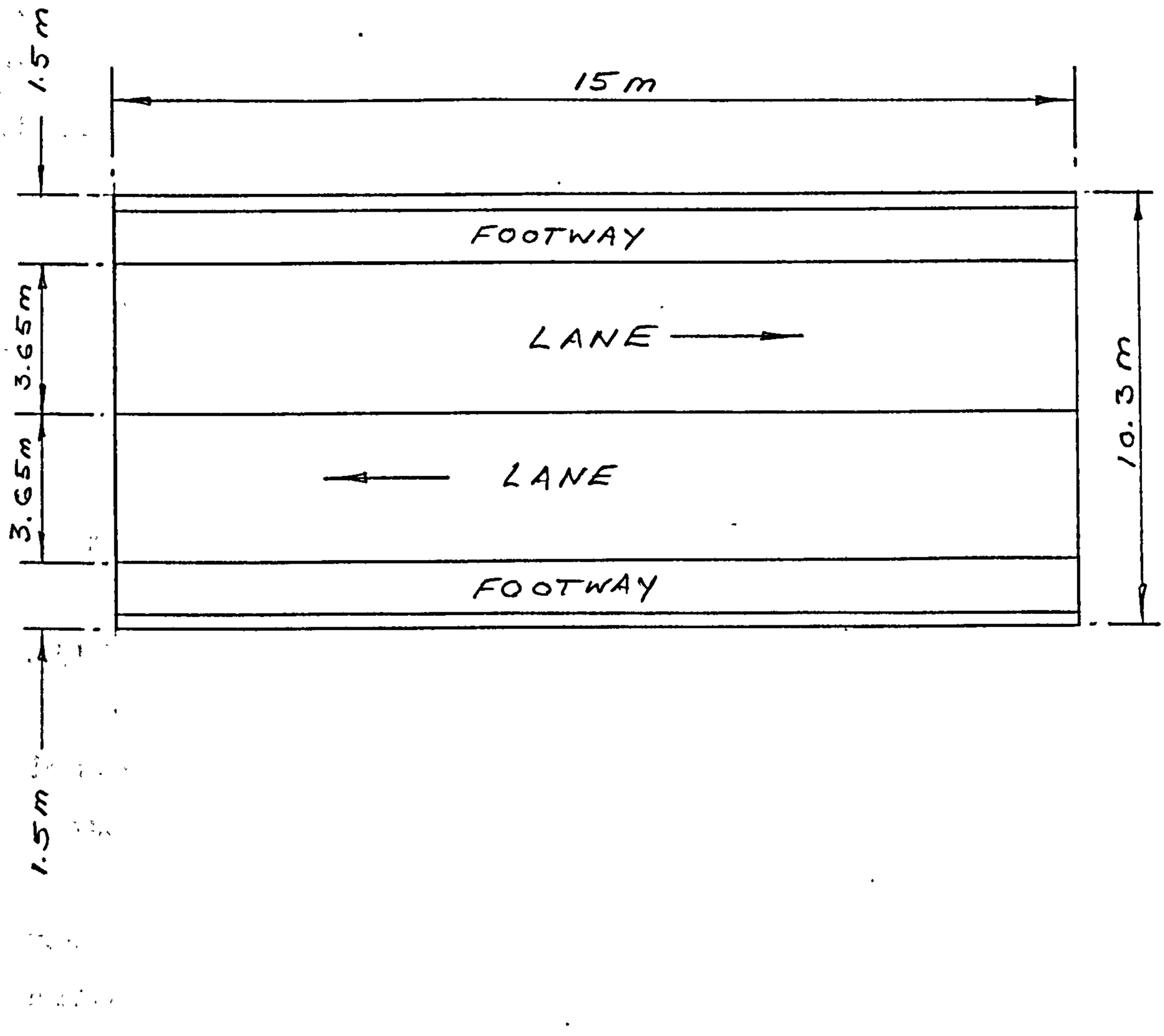

Figure 5.1 - A 15m span two lane single carriageway slab bridge.

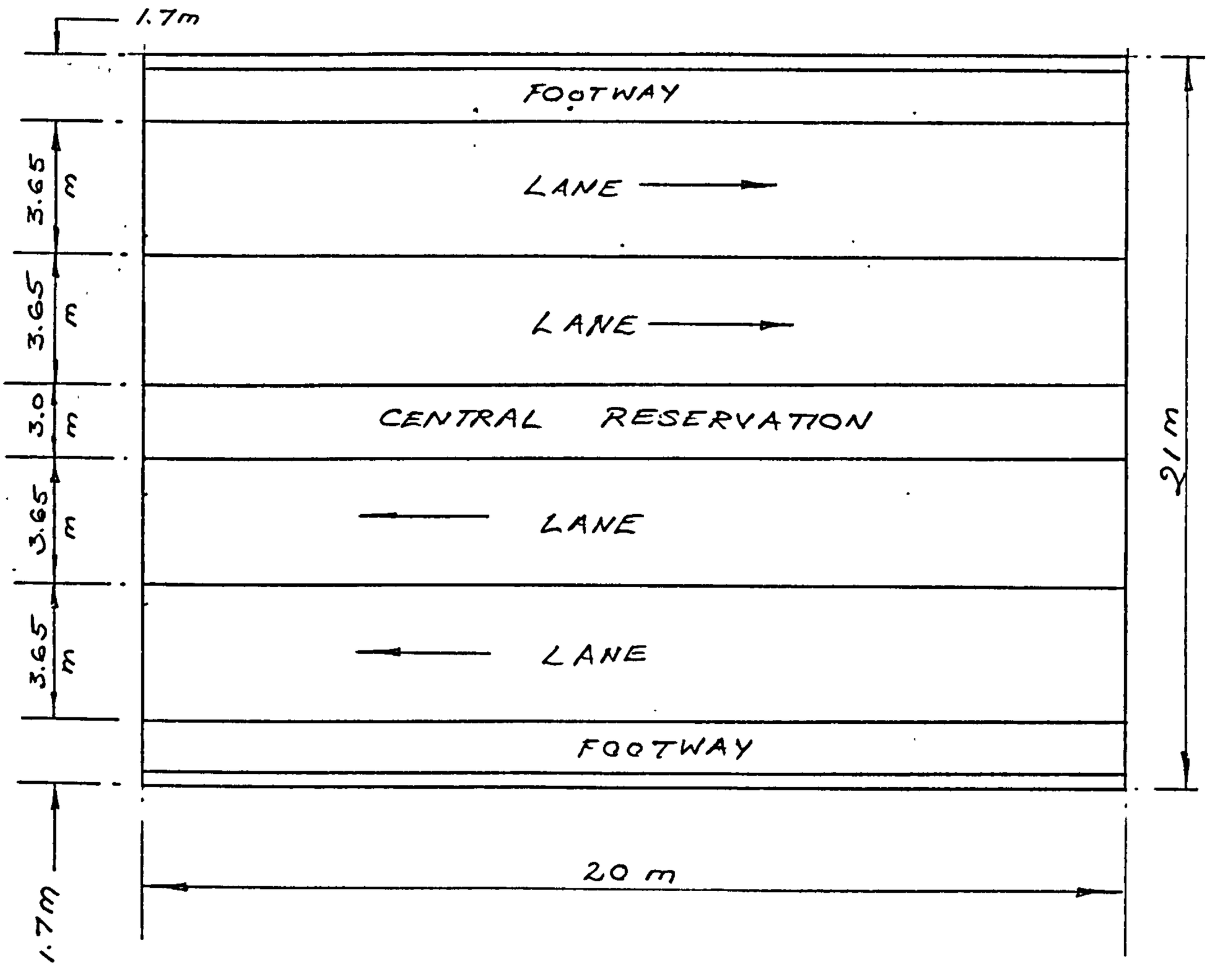

Figure 5.2. - A 20m span two lane dual carriageway slab bridge.

5.2.1 The Ultimate bridge loading

The ultimate bridge loading being used here is described in the Department of Transport's document BD 37/88 which states the application of type HA loading in combination with type HB loading as follows:

Where the HB vehicle lies wholly within the notional lane or where the HB vehicle lies partially within a notional lane and the remaining width of the lane, measured from the side of the HB vehicle to the edge of the notional lane, is less than 2.5 metres, type HB loading is assumed to displace part of the HA loading in the lane or straddled lanes it occupies. No other live loading shall be considered for 25 metres in front of the loading axle to 25 metres behind the rear axle of the HB vehicle. The

remainder of the loaded length of the lane or lanes thus occupied by the HB vehicle shall be loaded with HA udl load only; HA KEL shall be omitted.

The ultimate load configuration is applied to two different bridges as shown in Figures 5.1 and 5.2 and then analysed using QSE Structural Analysis computer program. In the analysis, the bridges were modelled as shown in Figures 5.3 and 5.4 for the 15 m single carriageway and the 20 m dual carriageway respectively.

Appendices E and F give the details of the load configurations and the derivation of the longitudinal ultimate bending moments for the two bridges.

The 15m span single carriageway.

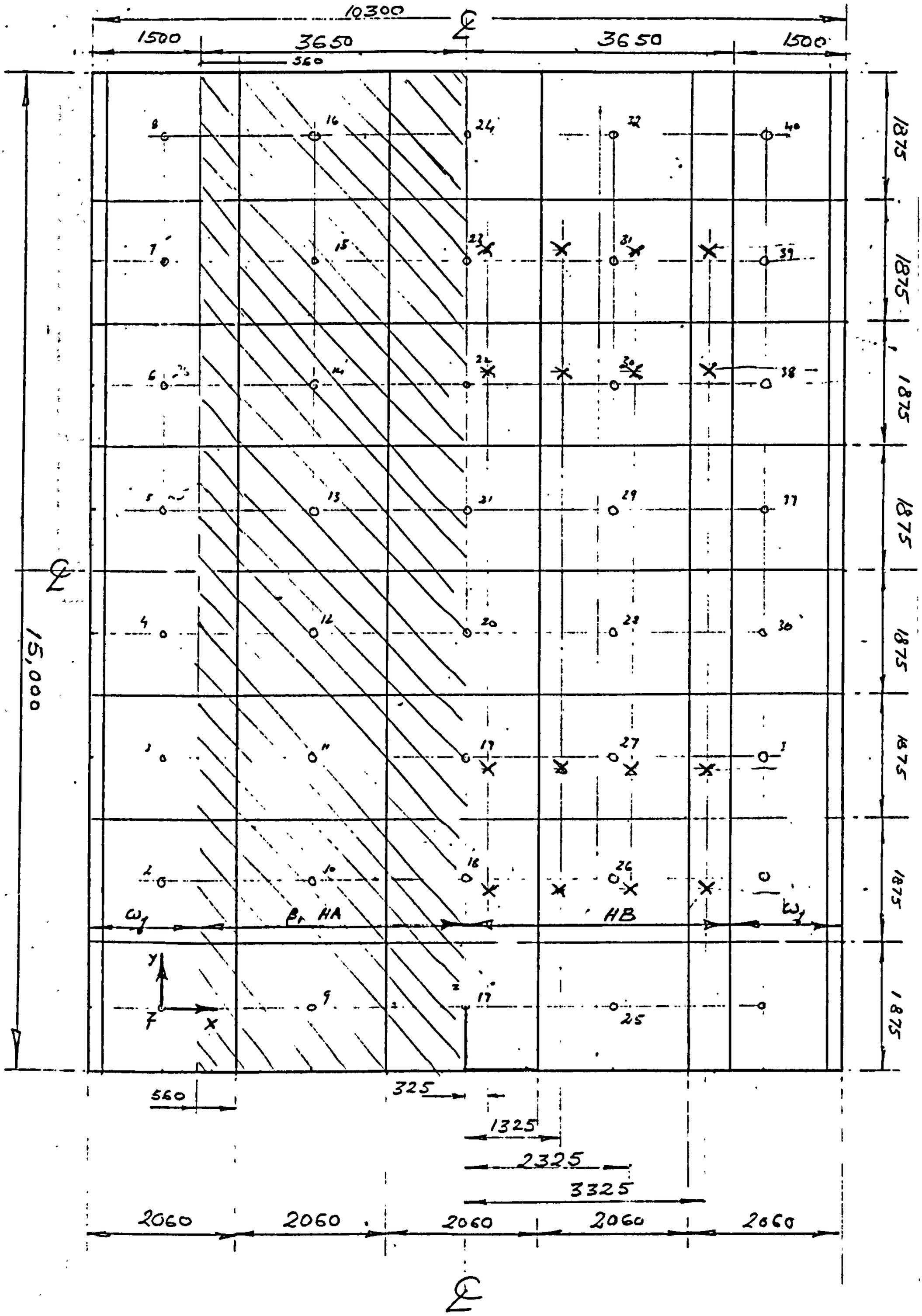

Figure 5.3 - Applying HA and HB on the modelling of the 15m span single carriageway slab bridge.

From the computer analysis, the longitudinal ultimate bending across mid-span of the bridge deck are given in Table 5.1:

Table 5.1 - Ultimate moment of the 15 m span single carriageway slab bridge

	Member across Mid-Span				
	M4	M15	M30	M45	M60
Nodal Ultimate Bending Moment from QSE (kNm)	1872	1946	1985	1987	2136
Udl Input per Member (kN/m)	57.6	86.1	66	45.9	46.7
Moment due to Udl on each member (L=1.875m)	25.3	37.8	29.0	20.2	20.5
Ultimate Moment at center of member corrected for Udl (kNm)	1897	1984	2014	2007	2157

The 20m span dual carriageway.

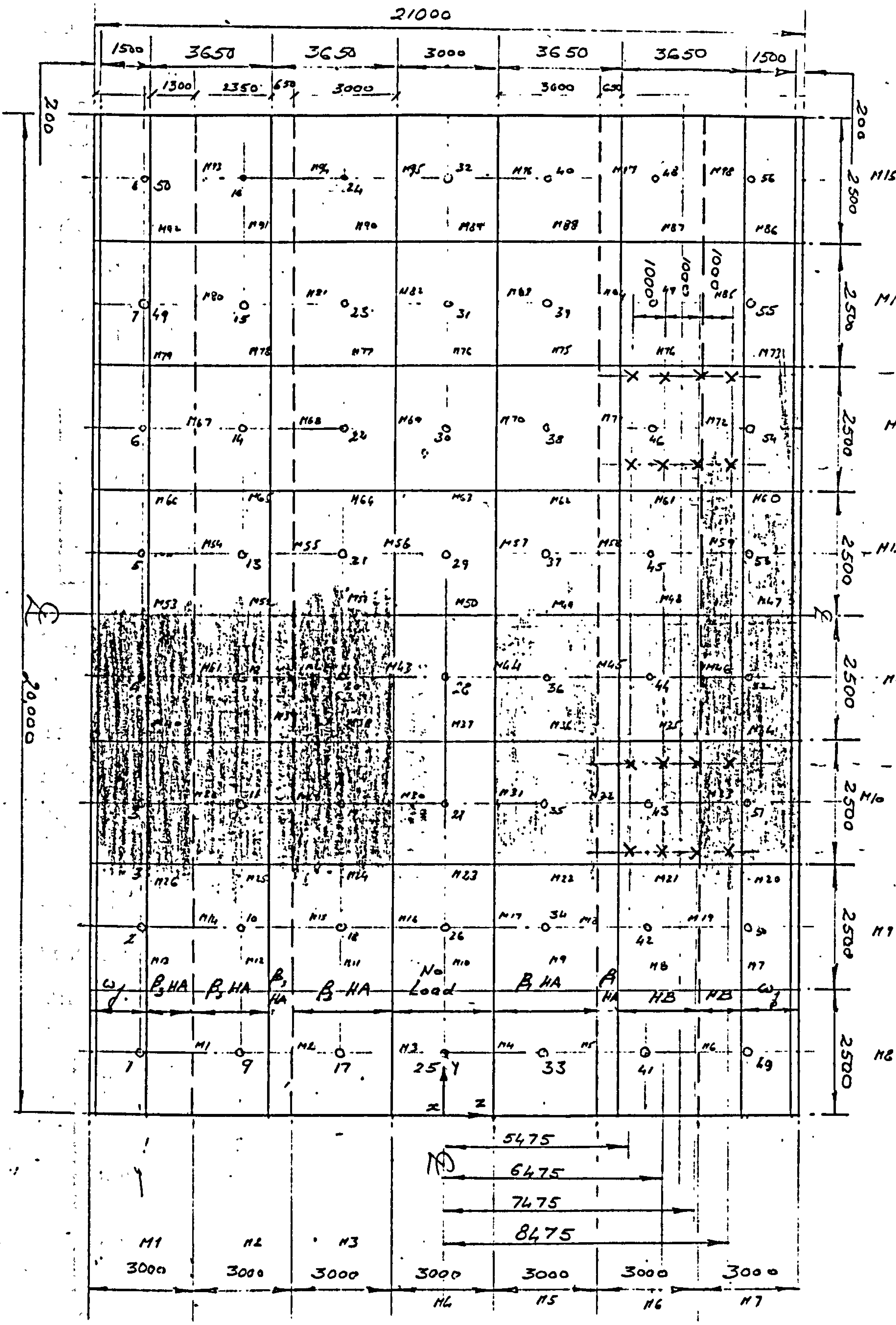

Figure 5.4 - Applying HA & HB on the modelling of the 20m span dual carriageway slab bridge.

Similarly, Table 5.2 is obtained for the case of the 20 m span dual carriageway slab bridge.

Table 5.2 - Ultimate moment of the 20 m span dual carriageway slab bridge

	Member across Mid-Span						
	M4	M15	M30	M45	M60	M75	M90
Nodal Ultimate Bending Moment from QSE (kNm)	4130	4466	4882	5309	5605	5757	6013
Udl Input per Member (kN/m)	79.7	124.8	124.8	106.8	144	106.3	79.9
Moment due to Udl on each member (L=2.5m)	62.3	97.5	97.5	83.4	112.5	83.0	62.4
Ultimate Moment at center of member corrected for Udl (kNm)	4192	4564	4980	5392	5718	5840	6075

5.2.2 Load cases to obtain the design ultimate moment capacity of the bridge

Case I

The corrected ultimate moments obtained from the longitudinal members in Tables 5.1 and 5.2 are from the ultimate loads of BD 37/88, with the HB vehicle on the lane. Since the HB vehicle could equally be travelling in the other direction then load case I assumes that for a lower bound, the longitudinal beams are to have ultimate bending capacities, arranged symmetrically, thus accounting for the situation where the HB vehicle may be positioned on either side of the bridge deck, Table 5.3 shows this arrangement.

Table 5.3 - Symmetrical moment capacity arrangement

	Member across mid-span						
	M4	M15	M30	M45	M60	M75	M90
Ultimate Moment 15m Span (kN)	2157	2007	2014	2007	2157	-	-
Ultimate Moment 15m Span (kN)	6075	5840	5718	5392	5718	5840	6075

Case II

For an upper bound it is assumed that all the longitudinal beams carry the maximum ultimate moment. An assumption which most practising engineers would adopt on the grounds that, it is reasonable to calculate the maximum ultimate moment and then design all the beams for this moment, Table 5.4 shows this arrangement.

Table 5.4 - Maximum moment capacity arrangement

	Member across mid-span							
	M4	M15	M30	M45	M60	M75	M90	Total moment
Ultimate Moment 15m Span (kN)	2157	2157	2014	2157	2157	-	-	10642
Ultimate Moment 20m Span (kN)	6075	6075	6075	5392	6075	6075	6075	41842

5.2.3 The bridge live loading

This load is based on the typical traffic loading detailed in Table 11 of BS 5400: Part 10: 1980, see appendix D, this table gives the axle loads and axle spacing of typical commercial vehicle groups in the UK, from which the maximum moments due to a single commercial vehicle in each group imposed on the two types of bridges, have been calculated and tabulated in Table 5.5.

Table 5.5 - Maximum moment due to commercial vehicle groups

Traffic Type	Maximum moment due to a single commercial vehicle from each group	
	15m span single carriageway	20m span dual carriageway
18GT - H	3780	5820
18GT - M	1275	2090
9TT - H	3308	5093
9TT - M	1260	2075
7GT - H	1950	2900
7GT - M	1150	1775
7A - H	1560	2210
6A - M	845	1335
4R - H	768	1125
3R - H	713	1010

5.2.4 Load range for experimental fatigue loading

Based on Table 11 of BS 5400: Part 10, a range of loads can be established, from which experimental fatigue loading can be conducted on three reinforced sprayed concrete strengthened slabs.

It is intended that the peak loads that these test slabs received from the fatigue load test are representatives of the peak loads that a typical highway bridge on trunk roads in the UK are receiving from the traffic that it carries.

The load range is calculated based on the following equations and the results are tabulated in Table 5.6.

$$\text{Min}\% = \frac{\text{Dead Load Moment}}{\text{Ultimate Design Load Moment}}$$

$$\text{Max}_1\% = \frac{\text{Dead Load Moment + Live Load } M_1}{\text{Ultimate Design Load Moment}}$$

$$\text{Max}_2\% = \frac{\text{Dead Load Moment + Live Load } M_2}{\text{Ultimate Design Load Moment}}$$

Where:

Dead Load Moment = Moment due to the self weight of the slab + Highway surfacing, unfactored, calculated from Appendices E & F.

Ultimate Design Load Moment = Moment due to HA + HB loadings as specified in BD 37/88 calculated from QSE grillage analysis, the values are given in Table 5.4.

Live Loads M_1 & M_2 = Moment due to the situation where one and two Nos. respectively of the most frequently seen commercial vehicles on UK roads. The likely introduction of the 44 tons HGV is classified here as the 6A-M vehicle type.

A further explanation of Live Loads M_1 & M_2,

From the author's observation and judgements, it appears that the commercial vehicle type 6A-M with six axles giving a total of 40 tons of wheel load is most frequently seen on the road and it is this combination increased to 44 tons which is the minimum required highway bridge assessment loading criterion imposed by the UK's Department of Transport. In this research, for the purpose of examining the severity of the upper loading level of the experimental fatigue load test, it is proposed that M_1 is the moment due to a single commercial vehicle of type 6A-M alone imposed on the two types of slab bridges under consideration and similarly M_2 is the moment due to two commercial vehicles of the type 6A-M.

Table 5.6 - Stress range for experimental fatigue load test

Slab Bridge Type	Dead Load Moment	Live Load Moment	Ultimate Design Moment	Min %	Max_1 %	Max_2 %
15m Span Single Carriageway	4270	845	10642	40.1	48.1	56.0
20m Span Dual Carriageway	15600	1335	41842	37.3	40.5	43.7

From Table 5.6, the author exercised engineering judgement and proposed that the appropriate load range to be used should be as follows:

Load Range = 40-50% of the designed failure load of the test slab for 1×10^6 cycles of fatigue load.

It is pointed out that the one million cycles imposed as above is taken from a conclusion drawn by Hanson[54] in his accounts on the Design for Fatigue, that:

> There is a limiting stress range which may be considered to be a fatigue limit. At stress ranges above this limit, a reinforcing bar will have a finite life. Below this limit, the bar will have a long life and may be able to sustain a virtually unlimited number of cycles . The transition from the finite life to long life region occurred in the range of one or two million cycles.

Although the above load range will yield useful experimental results, it appears to be at a nominal level and certainly the effect of abnormal loadings has not been considered, a phenomenon which would be detrimental if not considered at the design stage. One of the causes of abnormal loadings on highway bridges is from the probable lateral co-incidence of heavily loaded (overloaded even) traversing commercial vehicles in the adjacent lanes and in time the resulting damage accumulates, leading to the reduction in fatigue life. In view of this issue, it was thought necessary that the experimental fatigue testing and the associated analytical study should address the useful life span of a typical highway bridge with consideration for this abnormal loading effect.

It is therefore proposed that the test slabs are to be fatigue tested first at the nominal load range of 40 - 50% of the design failure load (DFL) for one million cycles and then at the higher load range, the results are then associated with an analytical fatigue study which would have accounted for the effect of the abnormal loading.

The method of determining the higher load range for further fatigue testing is being described in later sections of this chapter.

5.2.5 Fatigue load in concrete in general

In this sub-section, the ultimate aim is to derive at the analytical relationship between the load range versus the number of cycles to failure so that further fatigue testing can be performed, but first the study into the influential factor of load range on the fatigue strength is being presented, based on which the ultimate aim was fulfilled.

5.2.5.1 The S-N curves or Wöhler curves

The S-N curves or Wöhler curves are defined as a set of curves representing the linear relationship between the relative upper load level (i.e. stress level) versus the logarithm of the number of cycles to failure. These S-N curves characterise the fatigue behaviour of concrete (other materials as well) in that, the number of load cycles N that the concrete member can withstand before failure occurs increases for a decreasing upper load level. Figure 5.5 shows this typical linear relationship.

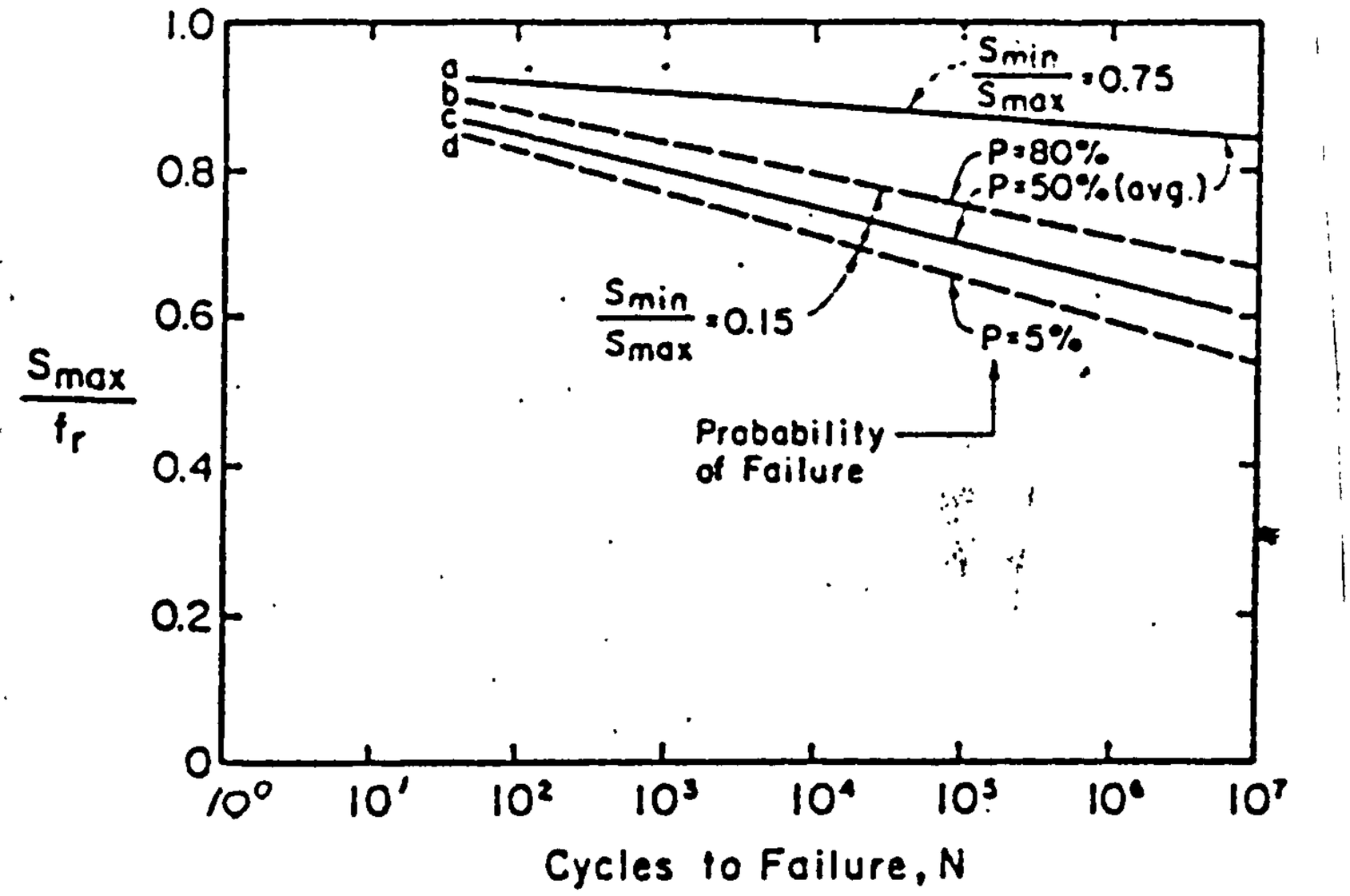

Figure 5.5 - Fatigue strength of plain concrete beams (ACI 215R - 74[39]).
S_{min} = Minimum stress, S_{max} = Maximum stress and f_r = Static strength

A definition of fatigue strength can now be introduced, this is defined as a fraction of the static strength that can be supported repeatedly for a given number of load cycles, this can be taken from the S-N curve.

Generally, the number of cycles to failure in the fatigue load results are very variable, this is largely due to the variations in the static strength. As opposed to steel, concrete has no fatigue limit, although fatigue strength in compression for two million cycles and zero lower load level ranges from 57 to 67% of the static strength.

5.2.5.2 The Goodman diagram

As well as other influential factors such as rate of loading, eccentricity of loading, load history, material properties and environmental conditions, the range of load is significantly important in evaluating the fatigue strength of a concrete member. This can be represented by Cornelissen's work[41]:

Cornelissen arrived at the following graphical results from his work in fatigue behaviour of concrete.

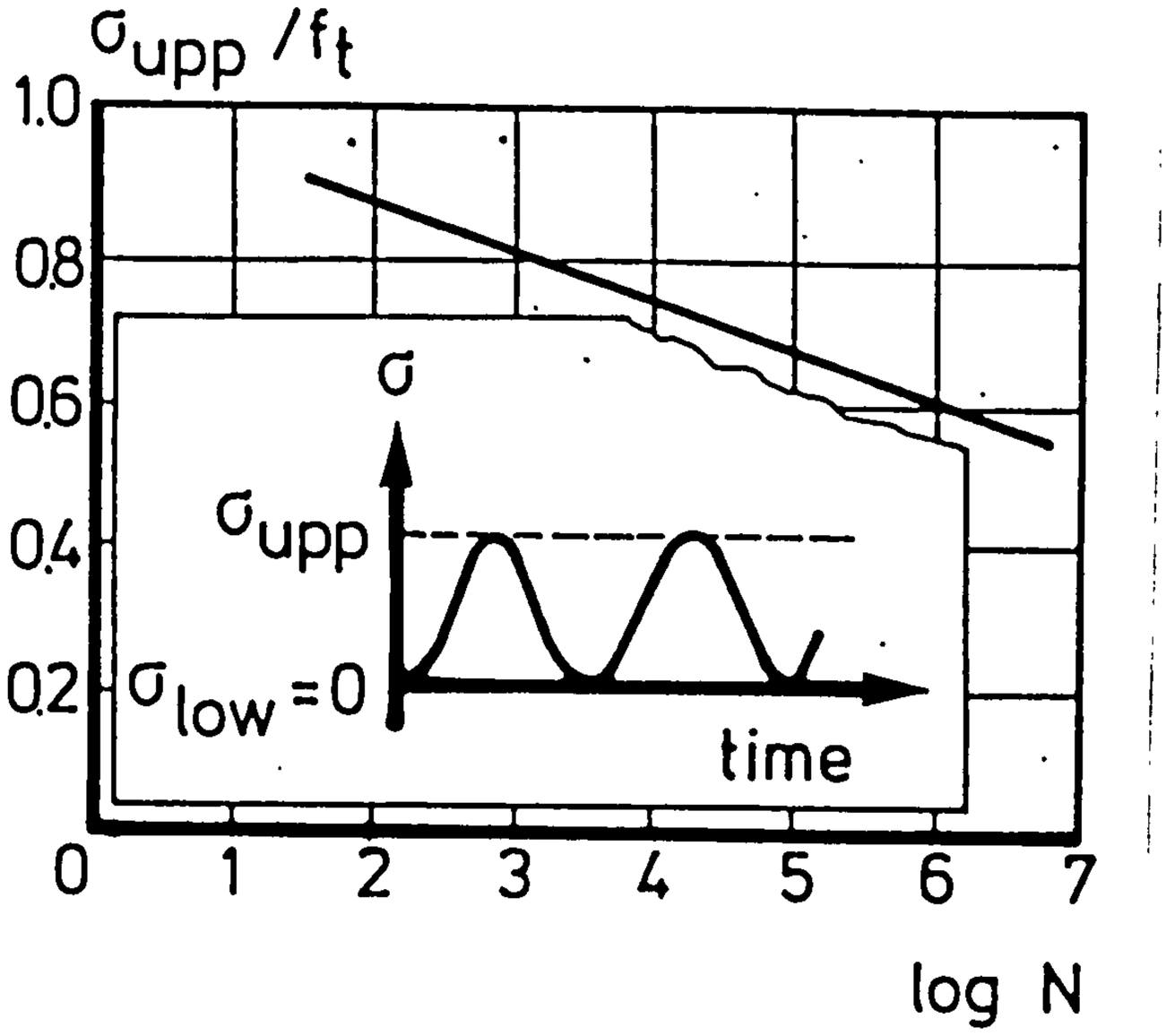

Figure 5.6a - Relationship between relative upper stress level and number of cycles to failure.

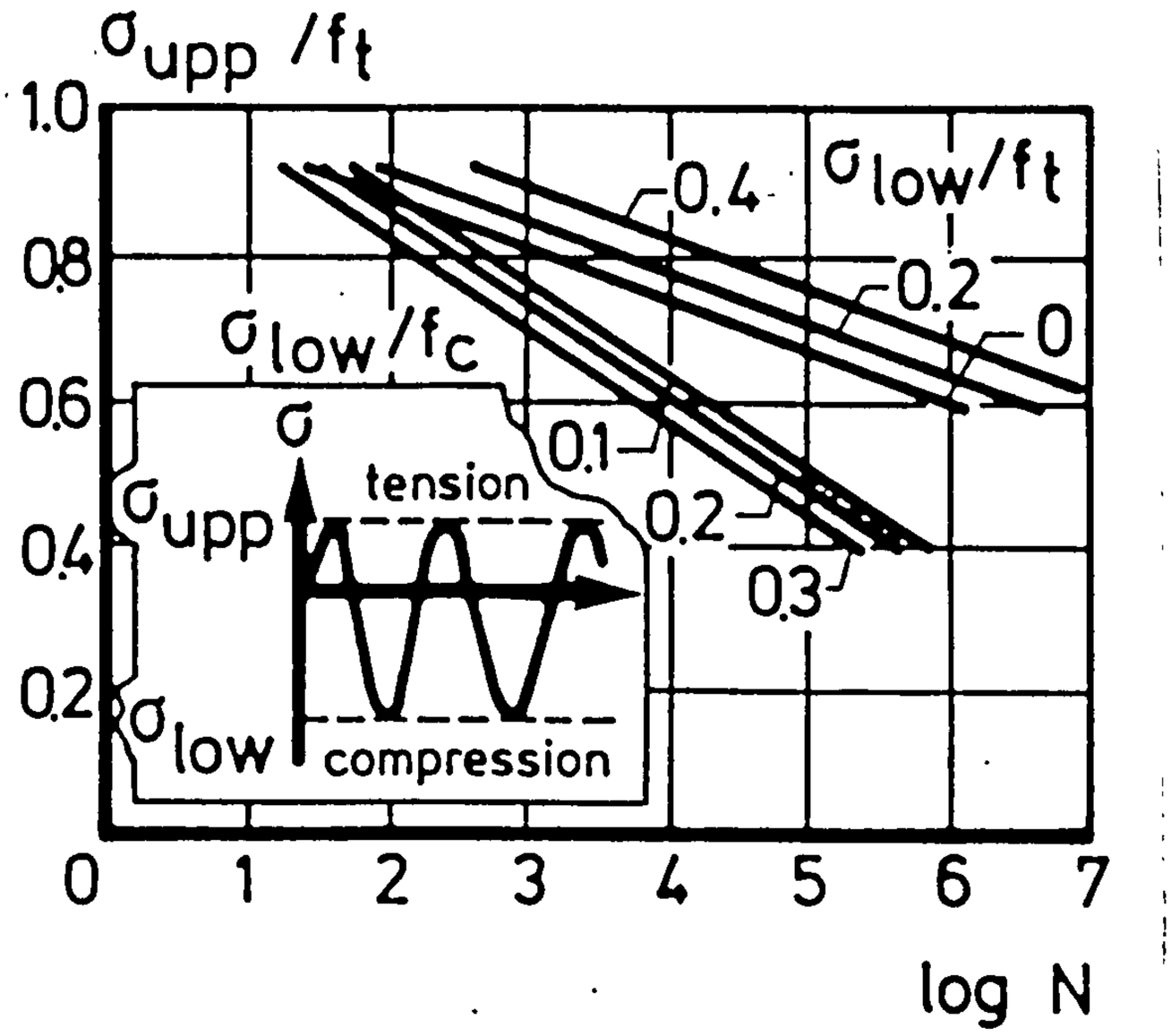

Figure 5.6b - The influence of stress levels.

Figure 5.6 - Cornelissen 's work on fatigue behaviour of concrete[41].

It can be seen from Figure 5.6a that for one million cycles and a zero lower stress level, the fatigue strength is equal to 60% of the static strength, while for a small lower stress level, this value can reduce to about 40% of the static strength. As can be seen in Figure 5.6b, a decreasing lower stress level results in a decreasing number of cycles to failure.

The influence of upper and lower stress (or load) levels is usually presented on the Goodman diagram or the Smith diagram as shown in Figure 5.7 (ACI 215) i.e. for a zero minimum stress level, the maximum stress level the concrete can support for one million cycles without failure is taken conservatively as 50% of the static strength and as the minimum stress level is increased, the stress range that the concrete can support decreases.

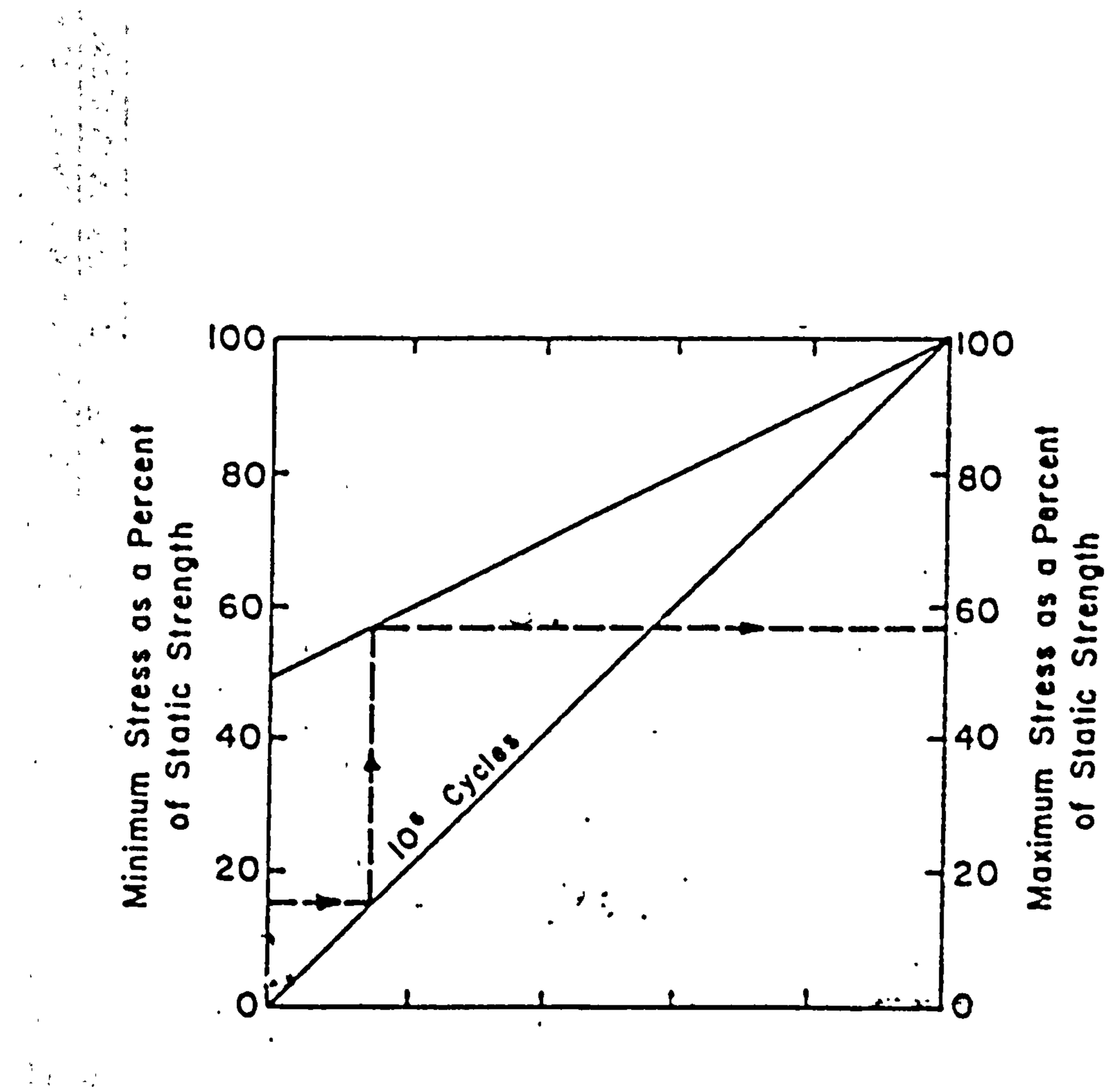

Figure 5.7 - Fatigue strength of plain concrete in flexure.

5.2.5.3 The modified Goodman diagram

In the work being presented here, the Goodman diagram in Figure 5.7 is used and a single S-N curve is produced from it on the assumption that the line intercepts the vertical axis at the maximum load = 100% of static failure load.

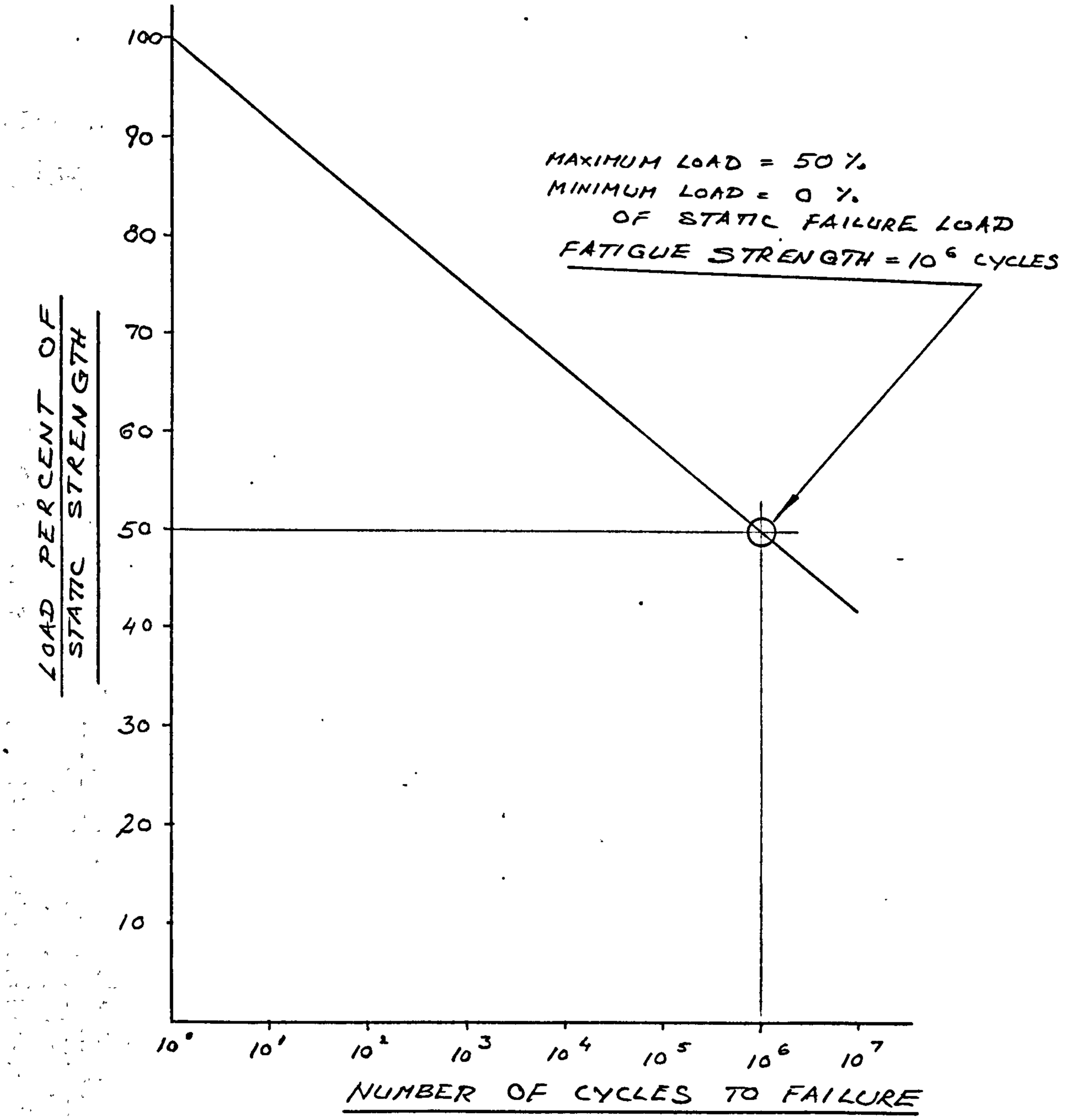

Figure 5.8 - The assumed S-N curve.

An important feature of Figure 5.8 in comparison with the established ACI 215 's S-N curves is that for the number of cycles to failure N less than 10^6, Figure 5.8 would provide an upper bound load range and from this, it was attempted to produce a modified Goodman diagram for different number of cycles to failure and the procedures are detailed as follows:

Figure 5.8 represents the case of zero lower load level and a linear relationship between the upper load level and the number of cycles to failure N i.e.

$$\text{Upper load} = -\frac{50}{6}\log N + 100 \qquad \text{(5.1)}$$

$$\text{Lower load} = \text{Zero}$$

From equation (5.1), a series of co-ordinates can be plotted on the Goodman diagram of Figure 5.7 For example,

$$\text{At } N = 10^5, \text{ Lower load} = 0\% \text{ and Upper load} = (175/3)\%$$

$$\text{At } N = 10^4, \text{ Lower load} = 0\% \text{ and Upper load} = (150/3)\%$$

This process is continued to produce a Modified Goodman diagram for a range of N values as shown in Figure 5.10.

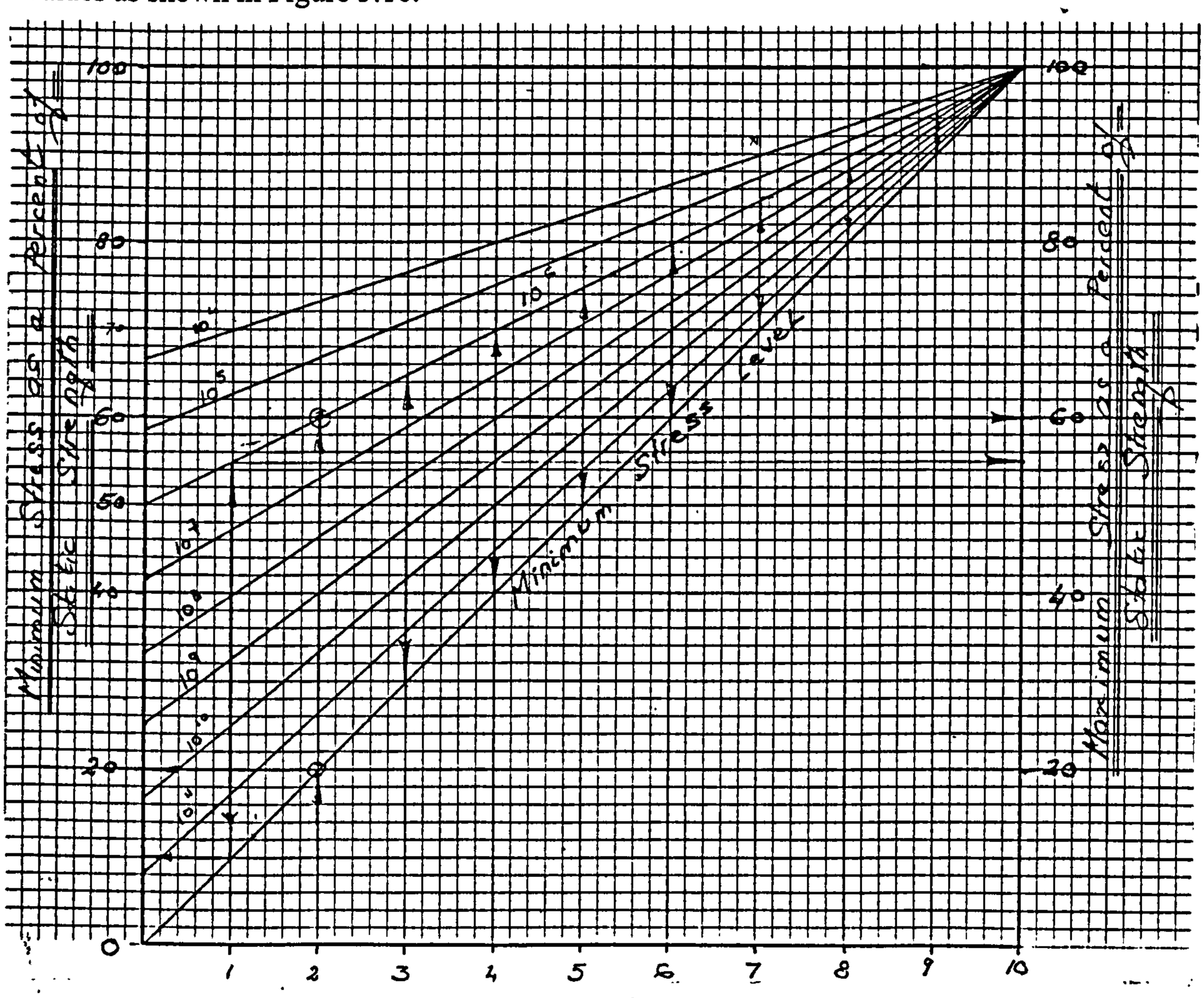

Figure 5.10 - The Modified Goodman diagram for a range of N values.

Having established the Modified Goodman diagram as shown in Figure 5.10, it is possible now to use the information from this diagram to produce an S-N diagram containing a set of curves that can be used to derive a comprehensive load range table corresponding to the expected fatigue strength i.e. N. Again it is stressed that the assumption of all S-N curves passing through the Upper load level at 100% still holds good.

From equation (5.1),

$$\text{Upper load} = -\frac{50}{6}\log N + 100 \qquad \text{(5.1)}$$

$$\text{Lower load} = \text{Zero}$$

and from Figure 5.10, it can be seen that within the envelope bounded by,

$$\text{Upper load} = 0\%$$

$$\text{and Lower load} = 50\%,$$

$$N \text{ is equal to } 10^6.$$

However if still within this envelope,

$$\text{The lower load} = 10\%$$

$$\text{This gives the upper load} = 55\%$$

$$\text{Therefore the ratio of } \frac{\text{Lower Load}}{\text{Upper Load}} = 0.18$$

$$\text{and } N = 10^6$$

Similarly if still within this envelope,

$$\text{The lower load} = 20\%$$

$$\text{This gives the upper load} = 60\%$$

$$\text{Therefore the ratio of } \frac{\text{Lower Load}}{\text{Upper Load}} = 0.33$$

$$\text{and } N = 10^6$$

The process is continued for various load ranges and the data obtained is presented graphically in the form of the S-N curves as shown in Figure 5.11.

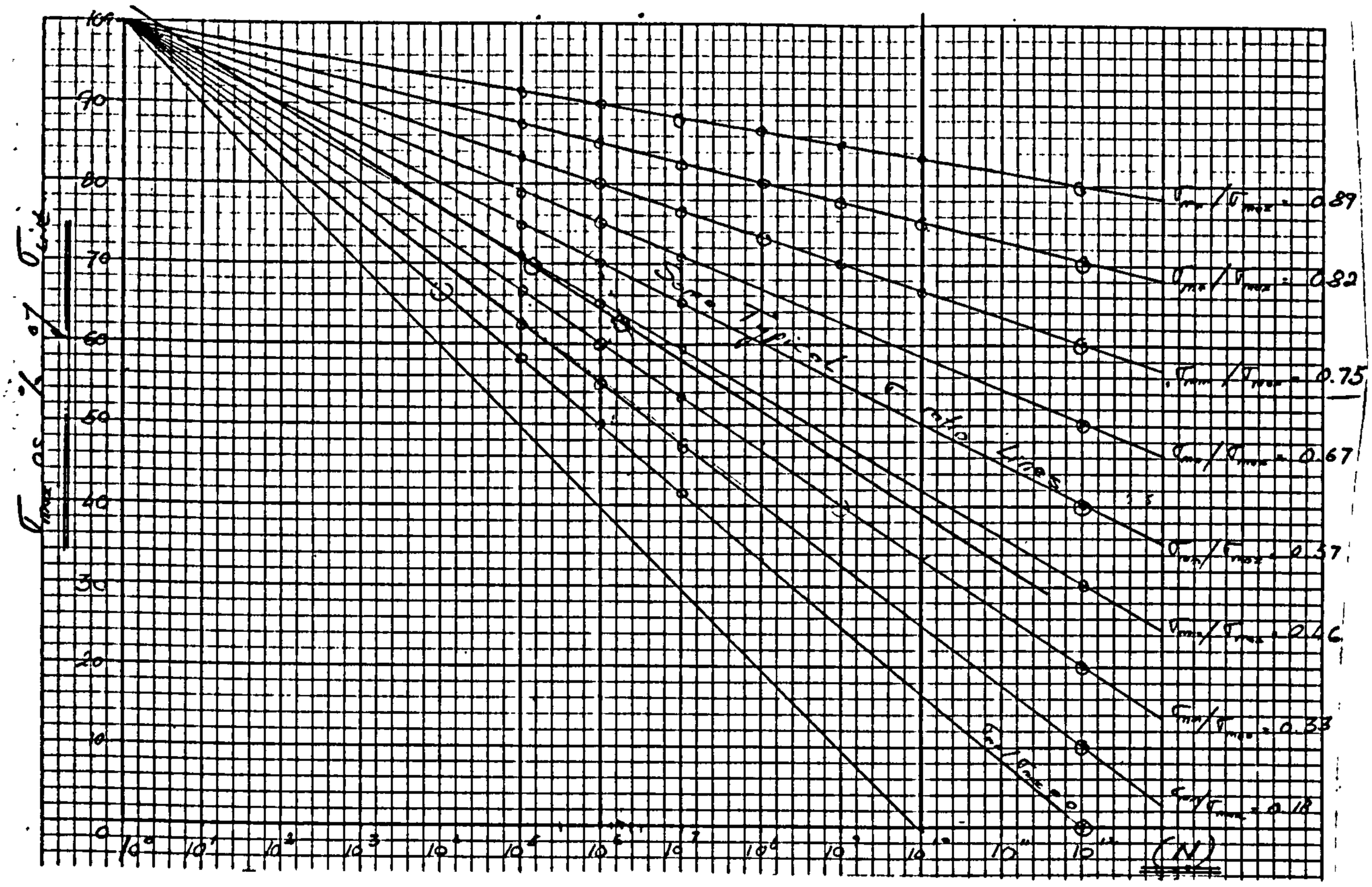

Figure 5.11 - S-N curves.

It is useful, that the above data can also be presented in tabular form as shown in Table 5.7,

Table 5.7 - Load ranges at $N = 10^6$

Load ratio	Equation of the S-N curves (max load)	$N=10^6$	
		Min%	Max%
(Min/Max)=0	$\sigma_0=100-(50/6)\text{Log}N$	0	50
(Min/Max)=0.18	$\sigma_{0.18}=100-(45/6)\text{Log}N$	10	55

It is equally useful to be able to established the load range corresponding to various N values. This can be obtained simply by calculating the co-ordinates of the points that intersect the vertical line drawn at the corresponding N value, see Figure 5.11. As an

example, the vertical lines at $N = 10^5$ and $N = 10^7$ are drawn in Figure 5.11 and the co-ordinates are calculated as follows:

At $N = 10^5$,

On the load ratio line of zero,

$$\text{The upper load} = 100 - \left(\frac{50}{6}\right)\log 10^5 = 58.3\%$$

Therefore giving,

$$\text{The lower load} = 0 \times 58.3 = 0\%$$

Consider another point on the vertical line,

At $N = 10^5$,

On the load ratio line of 0.18,

$$\text{The upper load} = 100 - \left(\frac{45}{6}\right)\log 10^5 = 62.5\%$$

Therefore giving,

$$\text{The lower load} = 0.18 \times 62.5 = 11.3\%$$

Similarly,

At $N = 10^7$,

On the load ratio line of zero,

$$\text{The upper load} = 100 - \left(\frac{50}{6}\right)\log 10^7 = 41.7\%$$

Therefore giving,

$$\text{The lower load} = 0 \times 41.7 = 0\%$$

Consider another point on the vertical line,

At $N = 10^7$,

On the load ratio line of 0.18,

$$\text{The upper load} = 100 - \left(\frac{45}{6}\right)\log 10^7 = 47.5\%$$

Therefore giving,

$$\text{The lower load} = 0.18 \times 47.5 = 8.6\%$$

In tabular form, the above calculations are presented in Table 5.8.

Table 5.8 - Table of load range versus number of cycles to failure

σ_{max} as % of σ_{ult}	Number of cycles to fatigue failure, N															
	$N=10^4$		$N=10^5$		$N=10^6$		$N=10^7$		$N=10^8$		$N=10^9$		$N=10^{10}$		$N=10^{11}$	
	Max	Min	Max	Min	Max	Min	Max	Min	Max	Min	Max	Min	Max	Min	Max	Min
σ_0=100-(50.6)logN	66.7	0.0	58.3	0.0	50.0	0.0	41.7	0.0	33.3	0.0	25.0	0.0	16.7	0.0	8.3	0.0
$\sigma_{0.35}$=100-(45.6)logN	70.0	12.7	62.5	11.4	55.0	10.0	47.5	8.6	40.0	7.3	32.5	5.9	25.0	4.5	17.5	3.2
$\sigma_{0.33}$=100-(40.6)logN	73.3	24.4	66.7	22.2	60.0	20.0	53.3	17.8	46.7	15.6	40.0	13.3	33.3	11.1	26.7	8.9
$\sigma_{0.30}$=100-(39.56)logN	74.0	26.7	67.5	24.3	61.0	22.0	54.5	19.7	48.0	17.3	41.5	15.0	35.0	12.6	28.5	10.3
$\sigma_{0.29}$=100-(38.6)logN	74.7	28.9	68.3	26.5	62.0	24.0	55.7	21.5	49.3	19.1	43.0	16.6	36.7	14.2	30.3	11.7
$\sigma_{0.28}$=100-(37.6)logN	75.3	31.1	69.2	28.5	63.0	26.0	56.8	23.5	50.7	20.9	44.5	18.4	38.3	15.8	32.2	13.3
$\sigma_{0.27}$=100-(36.6)logN	76.0	33.3	70.0	30.6	64.0	28.0	58.0	25.4	52.0	22.8	46.0	20.1	40.0	17.5	34.0	14.9
$\sigma_{0.26}$=100-(35.6)logN	76.7	35.4	70.8	32.7	65.0	30.0	59.2	27.3	53.3	24.6	47.5	21.9	41.7	19.2	35.8	16.5
$\sigma_{0.25}$=100-(34.6)logN	77.3	37.5	71.7	34.7	66.0	32.0	60.3	29.3	54.7	26.5	49.0	23.8	43.3	21.0	37.7	18.3
$\sigma_{0.24}$=100-(33.6)logN	78.0	39.6	72.5	36.8	67.0	34.0	61.5	31.2	56.0	28.4	50.5	25.6	45.0	22.8	39.5	20.0
$\sigma_{0.23}$=100-(32.6)logN	78.7	41.6	73.3	38.8	68.0	36.0	62.7	33.2	57.3	30.4	52.0	27.5	46.7	24.7	41.3	21.9
$\sigma_{0.22}$=100-(31.56)logN	79.0	42.7	73.8	39.8	68.5	37.0	63.3	34.2	58.0	31.3	52.8	28.5	47.5	25.7	42.3	22.8
$\sigma_{0.21}$=100-(31.6)logN	79.3	43.7	74.2	40.8	69.0	38.0	63.8	35.2	58.7	32.3	53.5	29.5	48.3	26.6	43.2	23.8
$\sigma_{0.20}$=100-(30.6)logN	80.0	45.7	75.0	42.9	70.0	40.0	65.0	37.1	60.0	34.3	55.0	31.4	50.0	28.6	45.0	25.7
$\sigma_{0.19}$=100-(29.6)logN	80.7	47.7	75.8	44.9	71.0	42.0	66.2	39.1	61.3	36.3	56.5	33.4	51.7	30.6	46.8	27.7
$\sigma_{0.18}$=100-(28.56)logN	81.0	48.7	76.3	45.9	71.5	43.0	66.8	40.1	62.0	37.3	57.3	34.4	52.5	31.6	47.8	28.7
$\sigma_{0.17}$=100-(28.6)logN	81.3	49.7	76.7	46.9	72.0	44.0	67.3	41.1	62.7	38.3	58.0	35.4	53.3	32.6	48.7	29.7
$\sigma_{0.16}$=100-(27.6)logN	82.0	51.7	77.5	48.8	73.0	46.0	68.5	43.2	64.0	40.3	59.5	37.5	55.0	34.7	50.5	31.8
$\sigma_{0.15}$=100-(26.6)logN	82.7	53.6	78.3	50.8	74.0	48.0	69.7	45.2	65.3	42.4	61.0	39.6	56.7	36.8	52.3	33.9
$\sigma_{0.14}$=100-(25.56)logN	82.9	54.8	78.7	52.0	74.5	49.2	70.1	46.3	65.9	43.5	61.6	40.7	57.3	37.9	53.1	35.0
$\sigma_{0.13}$=100-(25/6)logN	83.3	55.6	79.2	52.8	75.0	50.0	70.8	47.2	66.7	44.4	62.5	41.7	58.3	38.9	54.2	36.1
$\sigma_{0.12}$=100-(24/6)logN	84.0	57.1	80.0	54.4	76.0	51.7	72.0	49.0	68.0	46.3	64.0	43.5	60.0	40.8	56.0	38.1
$\sigma_{0.11}$=100-(23.5/6)logN	84.3	58.2	80.4	55.5	76.5	52.8	72.6	50.1	68.7	47.4	64.8	44.7	60.8	42.0	56.9	39.3
$\sigma_{0.10}$=100-(23/6)logN	84.7	59.3	80.8	56.6	77.0	53.9	73.2	51.2	69.3	48.5	65.5	45.9	61.7	43.2	57.8	40.5
$\sigma_{0.75}$=100-(20/6)logN	86.7	65.0	83.3	62.5	80.0	60.0	76.7	57.5	73.3	55.0	70.0	52.5	66.7	50.0	63.3	47.5
$\sigma_{0.82}$=100-(15/6)logN	90.0	74.1	87.5	72.1	85.0	70.0	82.5	67.9	80.0	65.9	77.5	63.8	75.0	61.8	72.5	59.7
$\sigma_{0.89}$=100-(10/6)logN	93.3	83.0	91.7	81.5	90.0	80.0	88.3	78.5	86.7	77.0	85.0	75.6	83.3	74.1	81.7	72.6

5.3 HIGHER LOAD RANGE FOR FATIGUE LOAD TESTING - A STUDY

With reference to Table 5.8 derived from the analytical study of the assumed S-N and the Modified Goodman diagrams, it is proposed that using this Table in conjunction with Tables 1 and 10 of BS 5400: Part 10, an assessment of the actual commercial traffic distribution is presented and from which a higher load range can be determined to perform the fatigue load test on the test slabs.

5.3.1 Fatigue loading on existing bridges

On existing bridges here in the UK, there are occasions when passing commercial vehicles are 'abnormally' heavily loaded and with the forecast of traffic being on an increasing trend, these occasional heavy commercial vehicle loads can be expected to increase and can at some points substantially exceed the design load capacity and it appears that, if it was possible to design a highway bridge on the basis that fatigue failure would not occur after random loadings i.e. due to the occasional heavy commercial vehicle loadings of the entire load spectrum that are possible and probable during the life expectancy of the bridge, with the varying intensities and frequencies, then the factor of safety to a static failure loading is not necessary.

To investigate this phenomena, it is attempted in this work to present an analytical study which relates the cumulative effect of fatigue loading on the test slabs tested under laboratory conditions to that on a typical highway bridge. In this analytical study, Table 5.8 is used in conjunction with BS 5400: Part 10: 1980.

The concept of occasional heavy load on existing bridges is influenced by several factors, including the following:

- Vehicle headway and queuing and,
- Vehicle coincidence.

The significance of these two factors on fatigue loading of existing highway bridges can be an extensive area for investigation and the time scale is limited in this research therefore only the second factor is considered.

The fatigue loading on existing bridges outlined above can be evaluated by using the Palmgren-Miner hypothesis, this is an empirical approach which utilises the S-N curves and is described in the following section.

5.3.2 Palmgren-Miner hypothesis

Fatigue loadings on a real structure vary greatly, in magnitude, number and sequence, generally very random and so in order to study the effect of fatigue loading, it is necessary to study the cumulative effect of its variation in the entire load spectrum.

The failure criterion due to fatigue loading is:

$$\sum_{i=1}^{k} \frac{n_i}{N_i} \leq 1$$

Where: n_i = The number of cycles at the load range i.

N_i = The number of cycles to failure at load range i.

The ratio effectively means that the same fatigue resistance can be obtained for reduced number of cycles over greater loading ranges, provided that the sum of the proportions of applied cycles to the number of cycles that the structural member can withstand never exceeds unity.

5.3.3 Load range due to traffic loading

From Tables 5.3 and 5.4, the load ranges due to traffic loading are calculated and these are tabulated in Table 5.9, according to the following equations:

Case I - When a single commercial vehicle is on the bridge.

$$\text{Min\%} = \frac{M_{DL}}{M_{ULT}}$$

$$\text{Max\%} = \frac{M_{DL} + M_{CV}}{M_{ULT}}$$

Case II - When two commercial vehicles coincide on the bridge simultaneously (Note, it is very conservatively assumed that the maximum moment caused by the commercial vehicle M_{CV} occurs when the vehicle is fully on the bridge).

$$\text{Min\%} = \frac{M_{DL}}{M_{ULT}}$$

$$\text{Max\%} = \frac{M_{DL} + [2 \times M_{CV}]}{M_{ULT}}$$

Where:

M_{DL} = Moment due to the unfactored dead load calculated in Appendices E for the 15m span and F for the 20m span bridges.

M_{CV} = Moment due to the commercial vehicle in each group as detailed in Table 11 of BS 5400 and tabulated in Table 5.5.

M_{ULT} = Ultimate moment calculated from grillage analysis as tabulated in Table 5.4.

1. Also given in Table 5.9 are the load ranges extracted from Table 5.8 which are obtained from the modified Goodman diagram, that are the nearest equivalent to the load ranges calculated from cases I & II s' equations. Also given in square brackets are the corresponding expected number of cycles to failure - the intention here is to co-relate the load ranges from the actual commercial vehicle spectrum to the analytical load ranges given in Table 5.8 (which was derived from assumed S-N curves and the modified Goodman diagram) so that the higher load range for fatigue load testing can be obtained.

Table 5.9 - Load range due to traffic loading

Traffic Type	Load Range			
	15m Span		20m Span	
	Load Range From Cases I and II	Equivalent Range From Goodman Diagram (Table 5.8)	Load Range From Cases I and II	Equivalent Range From Goodman Diagram (Table 5.8)
18GT - H	40.2 - 75.7 -	39.8 - 78.0 [10^4]	37.3 - 51.2 37.3 - 65.1	37.1 - 65.0 [10^7]
18GT - M	40.2 - 52.6 40.2 - 65.0	40.1 - 66.8 [10^7]	37.3 - 42.3 37.3 - 47.3	37.1 - 55.1 [10^{11}]
9TT - H	40.2 - 71.3 -	40.0 - 70.0 [10^6]	37.3 - 49.5 37.3 - 61.6	37.2 - 62.0 [10^8]
9TT - M	40.2 - 52.0 40.2 - 63.9	40.3 - 64.0 [10^8]	37.3 - 42.2 37.3 - 47.2	37.1 - 55.1 [10^{11}]
7GT - H	40.2 - 58.5 40.2 - 76.8	40.8 - 60.0 [10^{10}]	37.3 - 44.2 37.3 - 51.1	37.1 - 55.1 [10^{11}]
7GT - M	40.2 - 52.5 40.2 - 63.6	40.3 - 64.0 [10^8]	37.3 - 41.5 37.3 - 45.8	37.1 - 55.1 [10^{11}]
7A - H	40.2 - 54.8 40.2 - 69.5	40.5 - 57.8 [10^{11}]	37.3 - 42.6 37.3 - 47.8	37.1 - 55.1 [10^{11}]
6A - M	40.2 - 48.0 40.2 - 56.1	40.5 - 57.8 [10^{11}]	37.3 - 40.5 37.3 - 43.7	37.1 - 55.1 [10^{11}]
4R - H	40.2 - 47.4 40.2 - 54.6	40.5 - 57.8 [10^{11}]	37.3 - 40.0 37.3 - 42.7	37.1 - 55.1 [10^{11}]
3R - H	40.2 - 49.7 40.2 - 59.2	40.8 - 60.0 [10^{10}]	37.3 - 39.7 37.3 - 42.1	37.1 - 55.1 [10^{11}]

5.3.4 Traffic distribution

Using Tables 1 and 10 of BS 5400: Part 10, see appendix D, the number of occurrences of each type of commercial vehicle over a design life span of 120 years can be evaluated for the two types of bridges being considered i.e. the 15m span single carriageway bridge and the 20m span dual carriageway bridge.

Assumptions made:

1. The 15 span bridge is an all purpose two lane single carriageway. Therefore from Table 1 of BS 5400, there are:

1×10^6 commercial vehicles in each direction per year.

2. The 20m span bridge is on a motorway dual carriageway with two lanes per carriageway. Therefore from Table 1 of BS 5400, there are:

$(1.5 + 1.0) \times 10^6 = 2.6 \times 10^6$ commercial vehicles in each direction per year.

3. The vehicle types with the corresponding axle loads and number of occurrence detailed in Table 11 of BS 5400 are re-grouped as in the following Table 5.10. Only vehicle types lighter than the 7GT-M are re-grouped.

The evaluation of the number of occurrences of commercial vehicles n is based on the following formula, n is tabulated in Table 5.10.

$$n = \frac{LS \times N_{vpm} \times V_d}{1 \times 10^6}$$

Where:

LS = Life span of the bridge.

N_{vpm} = Number of commercial vehicles in each group per million commercial vehicles.

V_d = Commercial vehicles distribution as defined in assumptions 1. and 2.

Table 5.10 - Occurance number of commercial vehicles over a 120 year design life

Vehicle Group	Flow of Commercial Vehicle over a 120 Year Design Life [V_d x 120]		Total Number in each Group per Million Commercial Vehicles	No. of Occurances of Commercial Vehicles Over a 120 Year Design Life [n]	
	15m Span	20m Span		15m Span	20m Span
18GT - H	120×10^6	300×10^6	10	1200	3000
18GT - M	120×10^6	300×10^6	30	3600	9000
9TT - H	120×10^6	300×10^6	20	2400	6000
9TT - M	120×10^6	300×10^6	40	4800	12000
7GT - H	120×10^6	300×10^6	30	3600	9000
7GT - M	120×10^6	300×10^6	70	8400	21000
7A - H	120×10^6	300×10^6	300	36000	90000
6A - M	120×10^6	300×10^6	299500	35.9×10^6	89.9×10^6
4R - H	120×10^6	300×10^6	135000	16.2×10^6	40.5×10^6
3R - H	120×10^6	300×10^6	565000	67.8×10^6	169.5×10^6

5.3.5 Cumulative effect of traffic loading

From Table 5.10 there are ten types/groups of commercial vehicle that are imposing axle loads on UK bridges and it is a reasonable proposition that co-existence of any combination (of these groups of commercial vehicle) is possible, depending upon its weight restriction and its width. This possible coexistence, therefore, subjects the bridges to different values of maximum loads i.e. random fatigue loading.

The effect of this random fatigue loading can be evaluated, although not always conservatively, using Miner's hypothesis, from section 5.3.2:

$$\sum \left[\frac{n_i}{N_i}\right] \leq 1 \qquad (5.2)$$

Where:

n_i = Number of cycles of a definite load range applied for which the structure can withstand N_i cycles before fatigue failure.

Equation (5.2) effectively means that the same fatigue resistance can be obtained for a reduced number of cycles with greater loading ranges, provided that the sum of the proportions of applied cycles to the total number of cycles that the structure can sustain for each separate load range does not exceed unity.

Using Miner 's hypothesis to evaluate the cumulative effect of the load cycles due to each types/groups of commercial vehicle tabulated in Table 5.10 versus the corresponding expected number of cycles over the design life of 120 years in Table 5.9 gives the figures in Table 5.11.

Table 5.11 - Values of n and N for different types of traffic.

Traffic Group	15m Span Single Carriageway			20m Span Dual Carriageway		
	n, From Table 5.10	N, From Table 5.9	n/N	n, From Table 5.10	N, From Table 5.9	n/N
18GT - H	1200	10^4	0.12	3000	10^7	3×10^{-4}
18GT - M	3600	10^7	3.6×10^{-4}	9000	10^{11}	9×10^{-8}
9TT - H	2400	10^6	2.4×10^{-3}	6000	10^8	6×10^{-5}
9TT - M	4800	10^8	4.8×10^{-5}	12000	10^{11}	12×10^{-8}
7GT - H	3600	10^{10}	3.6×10^{-7}	9000	10^{11}	9×10^{-8}
7GT - M	8400	10^8	8.4×10^{-5}	21000	10^{11}	21×10^{-8}
7A - H	36000	10^{11}	3.6×10^{-7}	90000	10^{11}	90×10^{-8}
6A - M	35.9×10^6	10^{11}	3.6×10^{-4}	89.9×10^6	10^{11}	89.9×10^{-5}
4R - H	16.2×10^6	10^{11}	1.6×10^{-4}	40.5×10^6	10^{11}	40.5×10^{-5}
3R - H	67.8×10^6	10^{10}	6.8×10^{-3}	168.5×10^6	10^{11}	16.9×10^{-4}

Table 5.11 is now reduced further to arrive at different sets of combinations of commercial vehicles. These combinations are based on the same N values and they would also represent the typical cases of random loading on highway bridges. Miner 's hypothesis to evaluate the cumulative effect is illustrated in Table 5.12 as follows:

Table 5.12 - Miner 's Hypothesis

Group	Traffic Group	Load Range	Sum of [n/N]	
			15m Span	20m Span
(I)	18GT - H	39.8 - 78.0	0.12	3.0×10^{-4}
(II)	9TT - H	40.0 - 70.0	2.4×10^{-3}	6.0×10^{-5}
(III)	18GT - M	40.1 - 66.8	3.6×10^{-4}	9.0×10^{-8}
(IV)	9TT - M 7GT - M	40.3 - 64.0 40.3 - 64.0	4.8×10^{-5} $\underline{8.4 \times 10^{-5}}$ 1.3×10^{-4}	12×10^{-8} $\underline{21 \times 10^{-8}}$ 33×10^{-8}
(V)	3R - H 7GT - H	40.8 - 60.0 40.8 - 60.0	6.8×10^{-3}	16.9×10^{-4} $\underline{9 \times 10^{-8}}$ 16.9×10^{-4}
(VI)	7A - H 6A - M 4R - H	40.5 - 57.8 40.5 - 57.8 40.5 - 57.8	3.6×10^{-7} 3.6×10^{-4} $\underline{1.6 \times 10^{-4}}$ 5.2×10^{-4}	90×10^{-8} 89.9×10^{-5} $\underline{40.5 \times 10^{-5}}$ 130.5×10^{-5}
			Σ [n/N] = 0.13	**Σ [n/N] = 33.6×10^{-4}**

5.3.6 Higher load range fatigue loading

Using Table 5.12, it is proposed that the higher load range to be used for further fatigue loading on the slabs would be:

39.8 - 78 percent of the static failure load.

The reasons for the above proposal are:

1. Miner hypothesis indicates that the load range from the 18GT-H vehicle type is most severe.
2. The limiting fatigue load cycles of 10^4 can be accommodated in the testing program, within the limited time scale of this research.

CHAPTER 6

THE PERFORMANCE OF THE TECHNIQUE UNDER FATIGUE LOADING

6.0 GENERAL

This chapter intends to show that :

- Given the commercial axle load spectrum of BS 5400: Part 10 to establish that the number of passes (n) from BS 5400 divided by the number of cycles to failure for the same loading (N) summed for all loads is less than one.
- To verify that the behaviour of this strengthening technique under fatigue loading follows the assumed S-N curves and the modified Goodman diagrams. This is done by mapping the fatigue test results onto the assumed S-N diagram, if the mapping shows close agreement then when the technique is used to strengthen the typical highway bridge, which is expected to be subjected to the current load spectrum (of BS 5400: Part 10) then its life span can be predicted.

The above is also the sequence which the structure of this chapter follows

6.1 LIFE SPAN OF A TYPICAL HIGHWAY BRIDGE UNDER THE CURRENT LOAD SPECTRUM - A PREDICTION

In order to improve the accuracy of the study in this area, it was proposed that, in addition to the current commercial load spectrum of BS 5400: Part 10, commercial vehicle coincidence in the adjacent lanes be accounted for and in this study, a single carriageway two lane bridge (one lane in each direction) is considered, therefore the coincident commercial vehicles in this case would be from the opposite direction of the traffic lanes. Without an actual traffic survey on the bridge and detailed statistical analysis on a typical single carriageway two lane bridge, the percentage of commercial vehicles in coincidence is taken as 15% as given in by the Transport and Road Research Laboratory LR 252[42]. However, it is realised that during the useful life span of the bridge, any combinations of classes of commercial vehicle in coincidence are possible

and therefore an attempt to account for as many combinations as practical is also presented.

6.2 FATIGUE TESTING THE STRENGTHENED SLABS

This section, describes the fatigue load tests performed on the strengthened test slabs. The load range for these tests was determined in sections 5.2.4 and 5.3.6 which was derived the assumed S-N curves and the modified Goodman diagrams.

Additionally, one of the test slabs due for fatigue load testing had its reinforcement in the sprayed concrete layer curtailed see Figure 6.1. This was then tested statically prior to fatigue testing to address the concern over the higher longitudinal shear stress concentration that might be caused by the re-entrant corner at each end of the sprayed concrete layer which might cause peeling-off of this layer at the ends. The following section will describe this pre-fatigue test in more details.

It is emphasised that under the higher level of fatigue loading on the slabs in Table 6.1, the fatigue load ranges were determined based on the static failure loads (SFL) of the companion slabs of Table 6.2 and for the lower level of fatigue load testing, the design failure loads (DFL) were used.

Fatigue load testing of the slabs was conducted consecutively at the age of eight months after the strengthening process.

Table 6.1 - Test slabs for fatigue load testing

Slab	Sprayed concrete type	Spayed concrete thickness (mm)	Reinforcement encapsulated in sprayed concrete	Lower fatigue load range level	Higher fatigue load range level
B2	Normal	75	B785 mesh	27% - 33% of SFL (note)	23% - 63% of SFL
B5	Normal	75	B503 mesh	27% - 33% of SFL (note)	30% - 70% of SFL
B6	Normal	75	A393 mesh	-	30% - 70% of SFL

(note) - These are equivalent to 40% - 50% of DFL

Note: DFL = Design failure load of the test slab.

SFL = Static failure load from a companion slab.

Table 6.2 - Companion slabs tested under static loading			
Slab for fatigue load testing	Companion slab tested under static loading		
	Slab	SFL (KN)	DFL (KN)
B2	B1	236.4	169.1
B5	B3	178.7	118.5
B6	A4	160	97.4

6.2.1 Pre-fatigue test on curtailed reinforced sprayed concrete layer

It was realised during the course of the research that when this technique of strengthening is used on existing concrete bridges that the reinforced sprayed concrete layer could only extend to near the points of support and not beyond them. The original bridge bearings would still be used and the critical vertical shear capacity at the supports would not be improved. This was not considered to cause a major problem as the author's understanding is that the majority of slab bridges failing the Department of Transport bridge assessment programme do so due to lack of flexural capacity not shear capacity.

However some concern existed over the higher longitudinal shear stress concentration that might be caused by the re-entrant corner at each end of the sprayed concrete layer which might cause peeling off of this layer at the ends.

In order to investigate this problem, test slab B5 with a large amount of reinforcement in the sprayed concrete layer and therefore a high shear stress at the interface was prepared to simulate the above end conditions by vertically cutting through the new sprayed concrete layer to the depth of the base concrete at the span side of the support, see Figures 6.1 for details. This slab was then subjected to static loading up to 15% beyond its design failure load prior to being tested under fatigue loading.

Figure 6.1a - Reinforced sprayed concrete curtailment - side view.

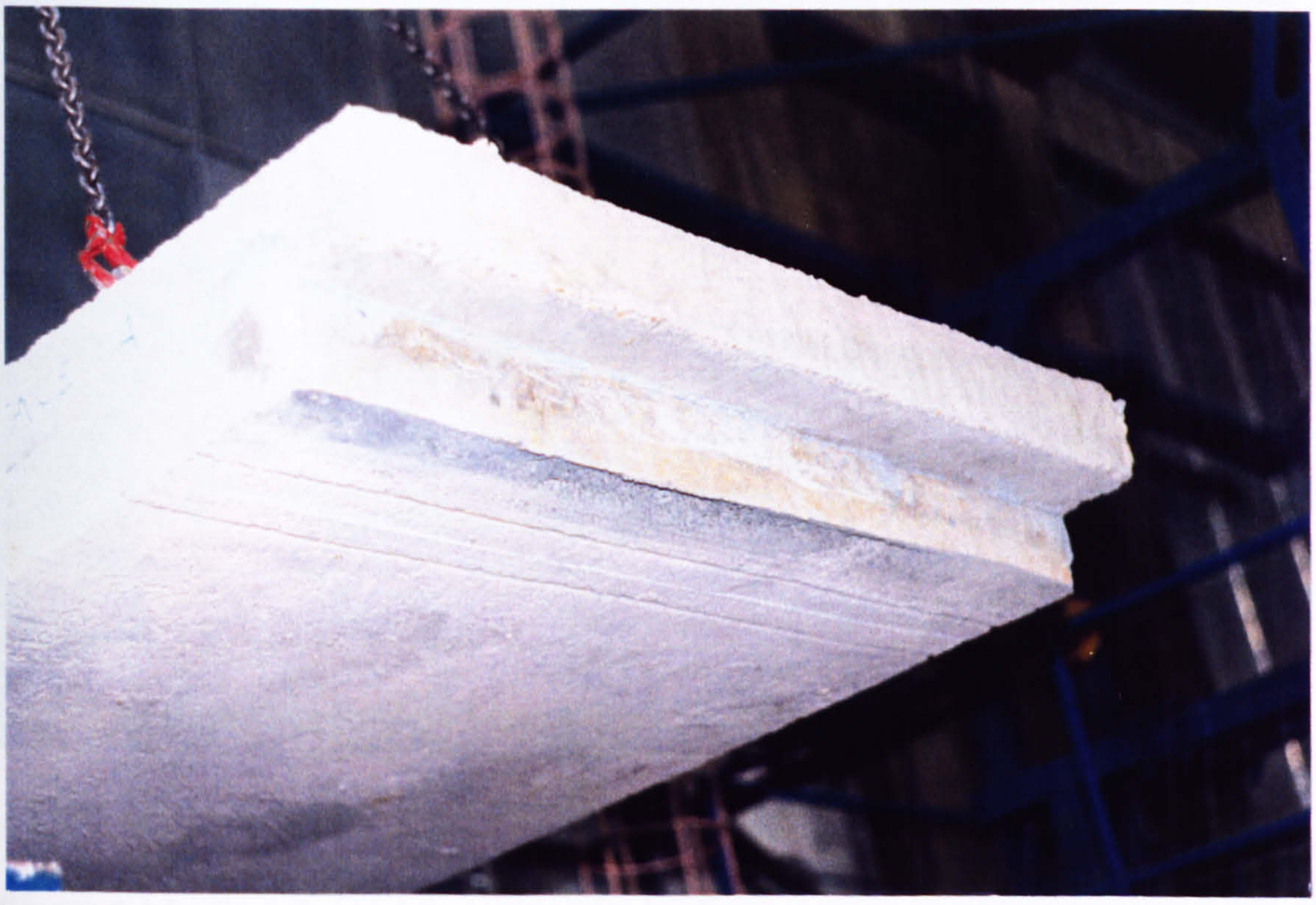

Figure 6.1b - Reinforced sprayed concrete curtailment - underside view.

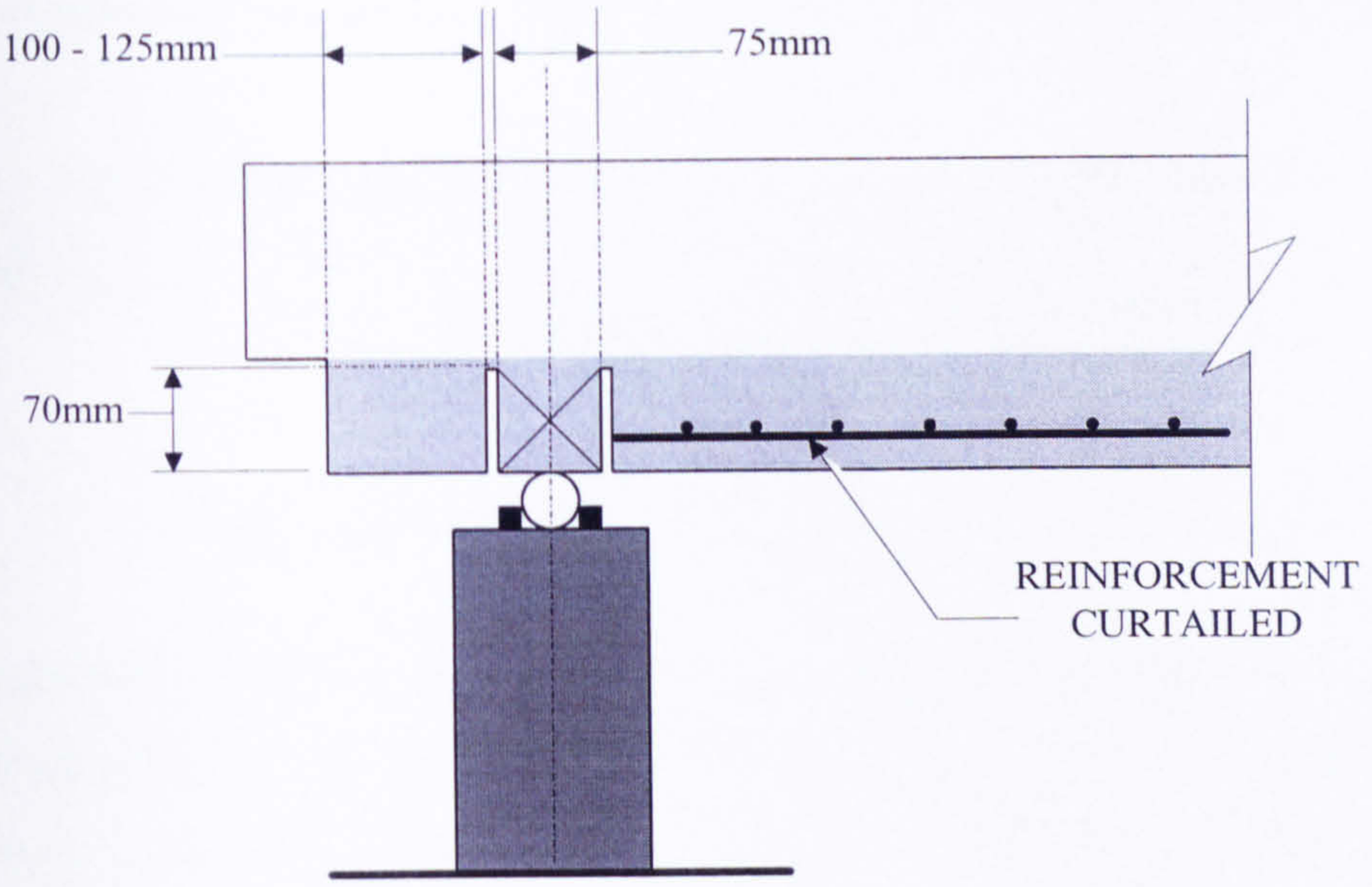

Figure 6.1c - Dimensions of curtailment.

Figure 6.1d - Curtailed slab in position for loading

Figure 6.1 - Reinforced sprayed concrete curtailment (similar detail at opposite end).

6.2.1.1 Test procedures on curtailed test slab.

The test slab under consideration was test slab B5. Prior to the static loading of this slab, an assessment was made to ensure that this static load test limit was less than the SFL.

i.e. DFL + (15% of DFL) must be < SFL

From Table 6.2:

DFL = 118.5 kN

SFL = 178.7 kN

DFL + (15% of DFL) = 136.3 kN _____ < SFL

In the static load test, the load increments of 5 kN was imposed up to 60 kN and then the increments were reduced to 1 kN up to 136.3 kN. This was considered necessary so that any distress in the slab under increasing load could be monitored, particularly at the re-entrant corners.

6.2 2 Instrumentation

As in the static load test, the set up here was also simple, comprising:

- A heavy fabricated steel loading frame.
- A hydraulic jack.
- An electronic control unit which operates the hydraulic jack.
- A data acquisition system.
- A frequency signal generator (to control the fatigue load).

6.2.3 Experimental procedures

The slabs were tested in the same loading frame used for the static tests. The data acquisition system was programmed to record the load range applied to the test slab and the corresponding deflection against time and this recorded continuously until failure of the slab.

6.2.3.1 Fatigue Load frequency

ACI 215 points out that:

> Several investigations indicate that variations of the frequency of loading between 70 and 900 cycles per minute (i.e. 1.2 and 15 cycles per second respectively) have little effect on the fatigue strength provided that the

maximum load level is less then 75 % of the static strength. For higher load levels, a significant influence of rate of loading has been observed.

Due to the limited time scale available, the load frequency used in all fatigue load testing in this work was maintained at one cycle per second, which was the maximum available from the hydraulic pump which oscillated the loading jack

6.3 EXPERIMENTAL RESULTS & DISCUSSION - FATIGUE

The fatigue load test results are given in table form in Table 6.3.

Table 6.3 - Summary of fatigue load test results

Slab	Lower fatigue load range level	No. of cycles tested	Higher fatigue load range level	Failed at cycle N	Test duration	Failure mode
B2	27% - 33% of SFL (*)	$1x10^6$	23% - 63% of SFL	$0.817x10^6$	21 days	Flexural failure No debonding
B5	27% - 33% of SFL (*)	$0.6x10^6$	30% - 70% of SFL	$0.457x10^6$	12 days	Flexural failure No debonding
B6	-	-	30% - 70% of SFL	$0.141x10^6$	12 days	Flexural failure No debonding
(*) - This is equivalent to the 40% - 50% of DFL range						

The graphs of deflection versus number of cycles are given in Figures 6.3 - 6.5.

All slabs failed in flexure and no debonding was observed. In particular, slab B5 with the curtailed reinforcement, no cracks were seen initiating at the points of curtailment. A typical mode of failure is shown in Figure 6.2.

Figure 6.2a - Test slab under fatigue loading.

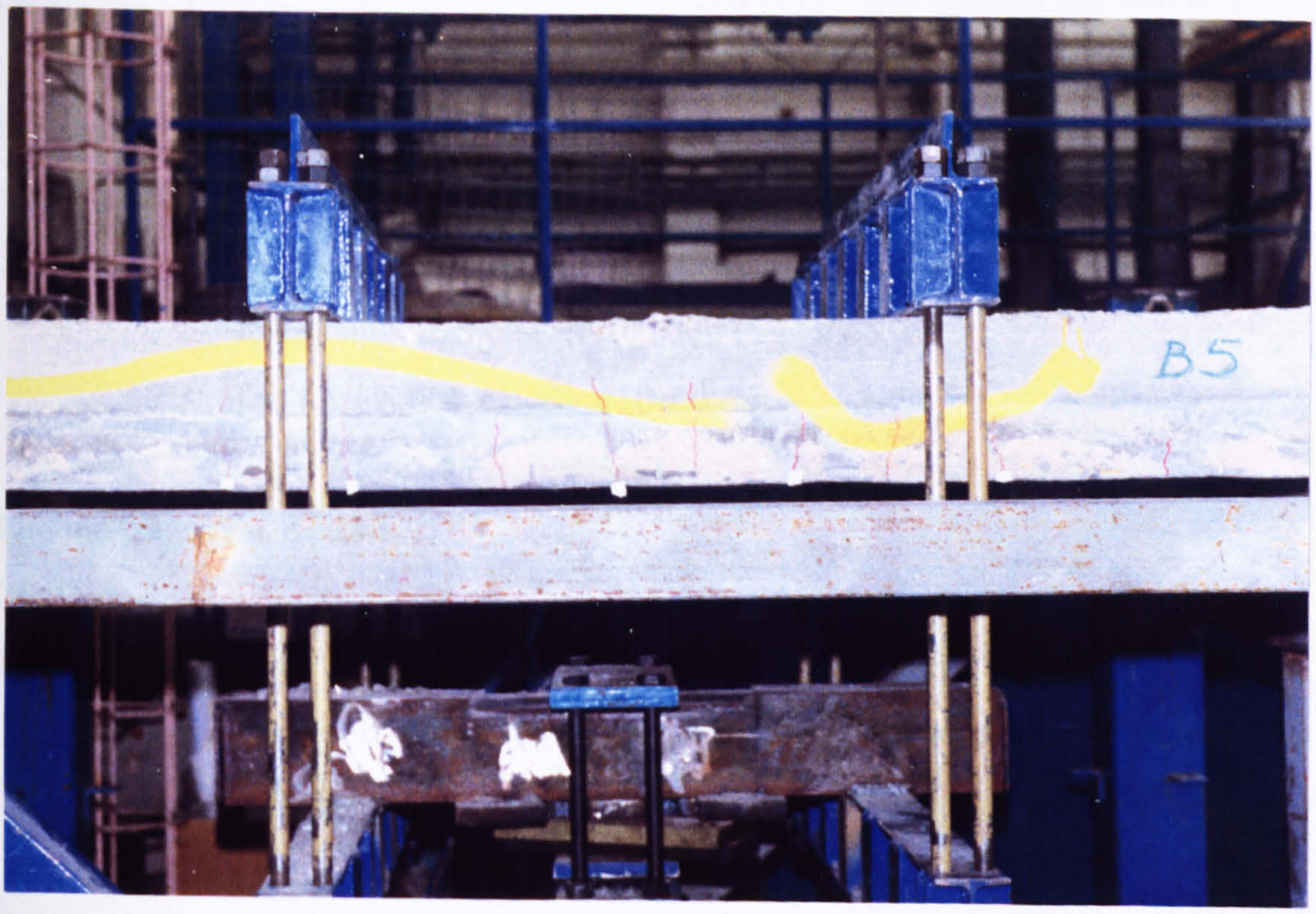

Figure 6.2b - Stable hair line flexural cracks developed.

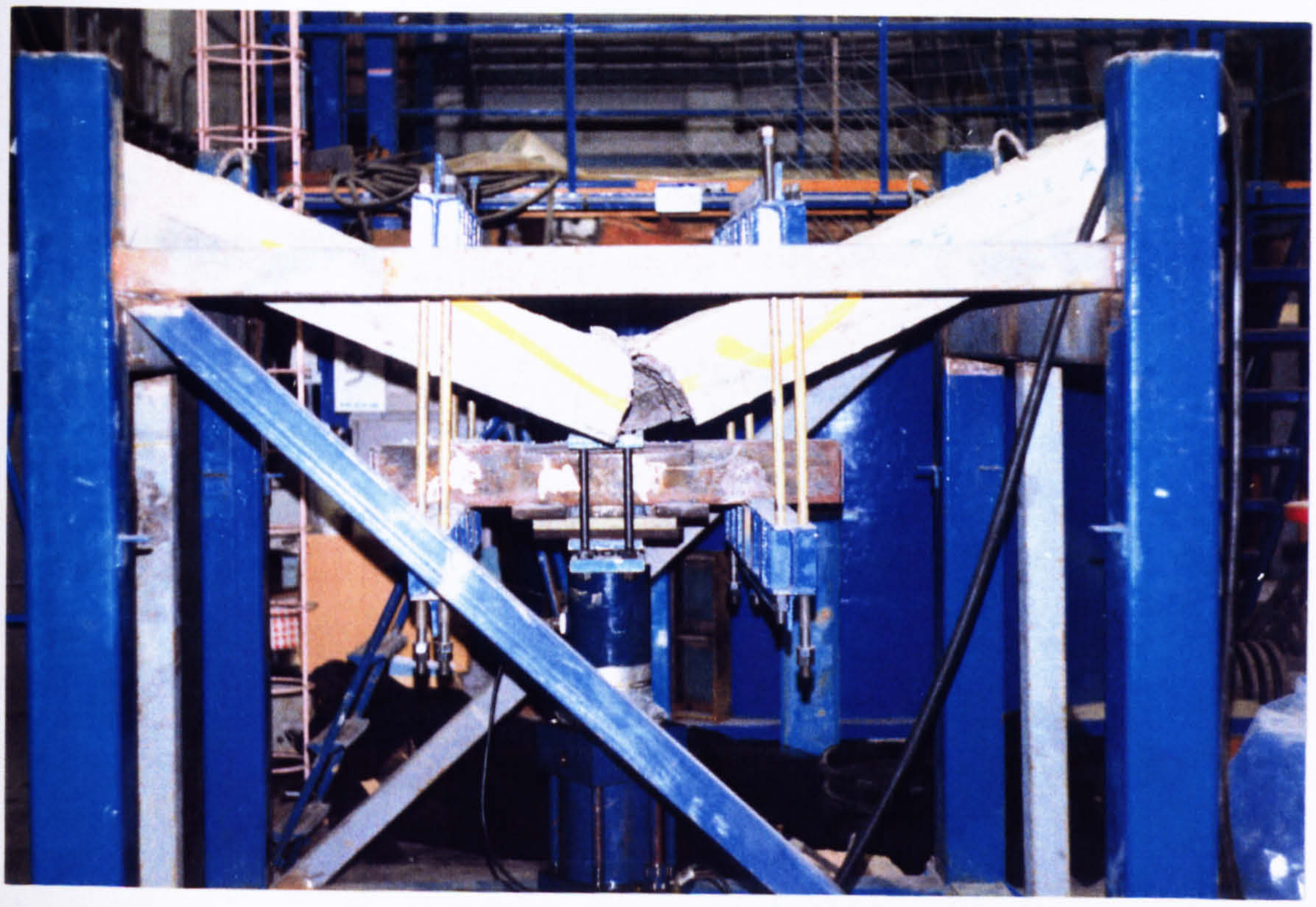

Figure 6.2c - Fatigue failure.

Figure 6.2 - Typical fatigue failure mode - flexural failure slab (shown test slab B5).

The deflection versus the number of cycles of all test slabs exhibit the cyclic creep curve, consisting of three portions:

1. The initial convex portion (initiation of cracking)
2. The straight portion (propagation of cracks)
3. The final concave portion (fracture).

The initial convex portion

B5 (Figure 6.4) &

B2 (Figure 6.5) During the first 200,000 to 250,000 cycles under the 27%-33% of SFL range, the test slabs displayed stable flexural cracks. These cracks opened and closed under the action of fatigue loading.

B6 (Figure 6.3) During approximately the first 25,000 cycles at the higher load range, the slab displayed hair line cracks, these were flexural cracks and were

due to the initial pre-setting of the hydraulic jack at the upper load level of 70% of SFL (i.e. pre-setting the amplitude of oscillation of the hydraulic jack). These cracks continued to open and close under the action of fatigue loading.

The straight and final concave portions

B5 (Figure 6.4) &

B2 (Figure 6.5) Between 250,000 to 600,000 cycles (B5) and 250,000 to 1,000,000 cycles (B2) at the lower load range of 27% - 33% of SFL, the test slabs displayed very little distress apart from the flexural cracks which were stable. It appears that at under this load range, the slab would have continued to sustain a very large number of cycles. This is indicated by the large number of cycles within the straight portion of the diagram before an abrupt change in deflection in response to the increased load range over which steel fracture developed, leading to the slab failure within a relatively small number of cycles (457,000) after the increase, for B5. For B2, from the point of abrupt change of deflection to slab failure the number of cycles was relatively high - 817,000 cycles, during which there was a small decrease in the rate of increasing deflection against the increasing number of cycles.

B6 (Figure 6.3) Between about 25,000 and 100,000 cycles the stress intensity at the crack front reached a critical value and after a further 40,000 cycles the steel fractured and the slab failed.

The following points are also important:

- Between 250,000 to 1,000,000 cycles the slab B2 displayed strength gain (indicated by the decrease in deflection with increasing number of cycles) at around 400,000 cycles under the lower load range. The possible explanation for this strength gain is due to the 24 hours rest period whilst one of the clamp bolts of the apparatus was replaced. A similar report of strength gain was reported by Holmen[43]:

  > In fatigue testing, at the upper stress level of 60%, after twelve million cycles no fatigue occurred, the test was stopped and the specimens were

statically load tested to failure, when comparing the results of these specimens with similar specimens which had not undergone fatigue loading, an increase in strength of about 7% was observed.

- An important observation made from the curtailed steel was that when the reinforcement within the sprayed concrete failed at mid-span, leaving just the reinforcement in the base slab resisting the applying fatigue loading there was no sign of delamination at the substrate/sprayed concrete interface either at mid-span or the curtailed ends. This is further evidence showing the good bond between the sprayed concrete and its substrate.
- Although it was found from examining the broken faces of the fatigue tested slabs that almost every main reinforcement bar failed in between the welded intersections. It is recognised that there may be a concern that the fatigue strength of the steel mesh reinforcement may be influenced by the significant stress concentration caused by welded intersections. This point may therefore be worth further study and account should be taken of ACI 215 which states:

  > Several recent investigations have examined the fatigue characteristics of welded mesh reinforcement and found that the disturbance due to the welded intersection is dominated only if the stress concentration caused by the intersection was greater than the concentration caused by the deformation. The available evidence does not indicate that these effects are additive.

Figure 5.4. - Fatigue test of slab B6
DFL = Designed Failure Load
SFL = Static Failure load

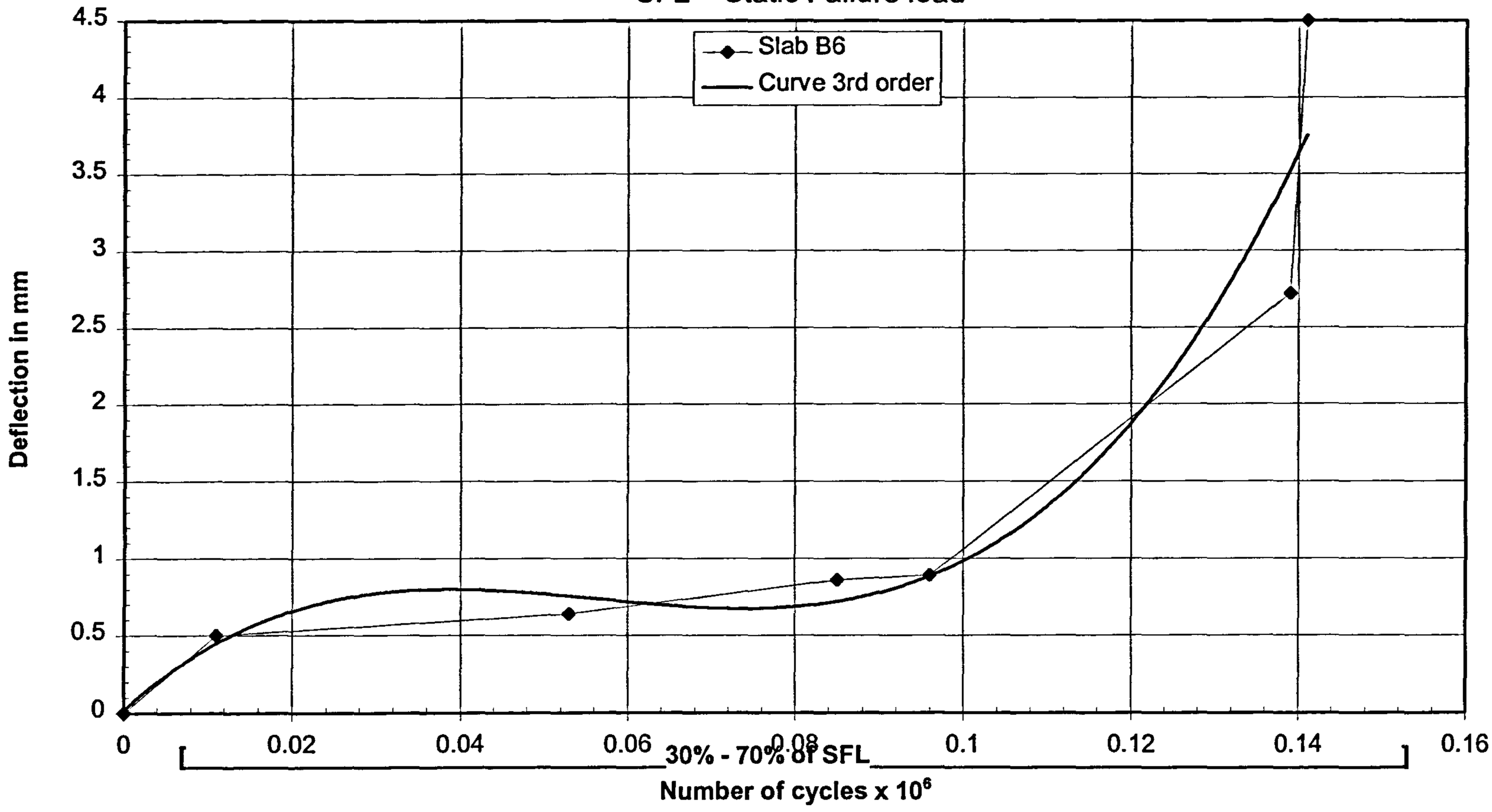

Figure 5.5 - Fatigue test of slab B5
DFL = Designed Failure Load
SFL = Static Failure load

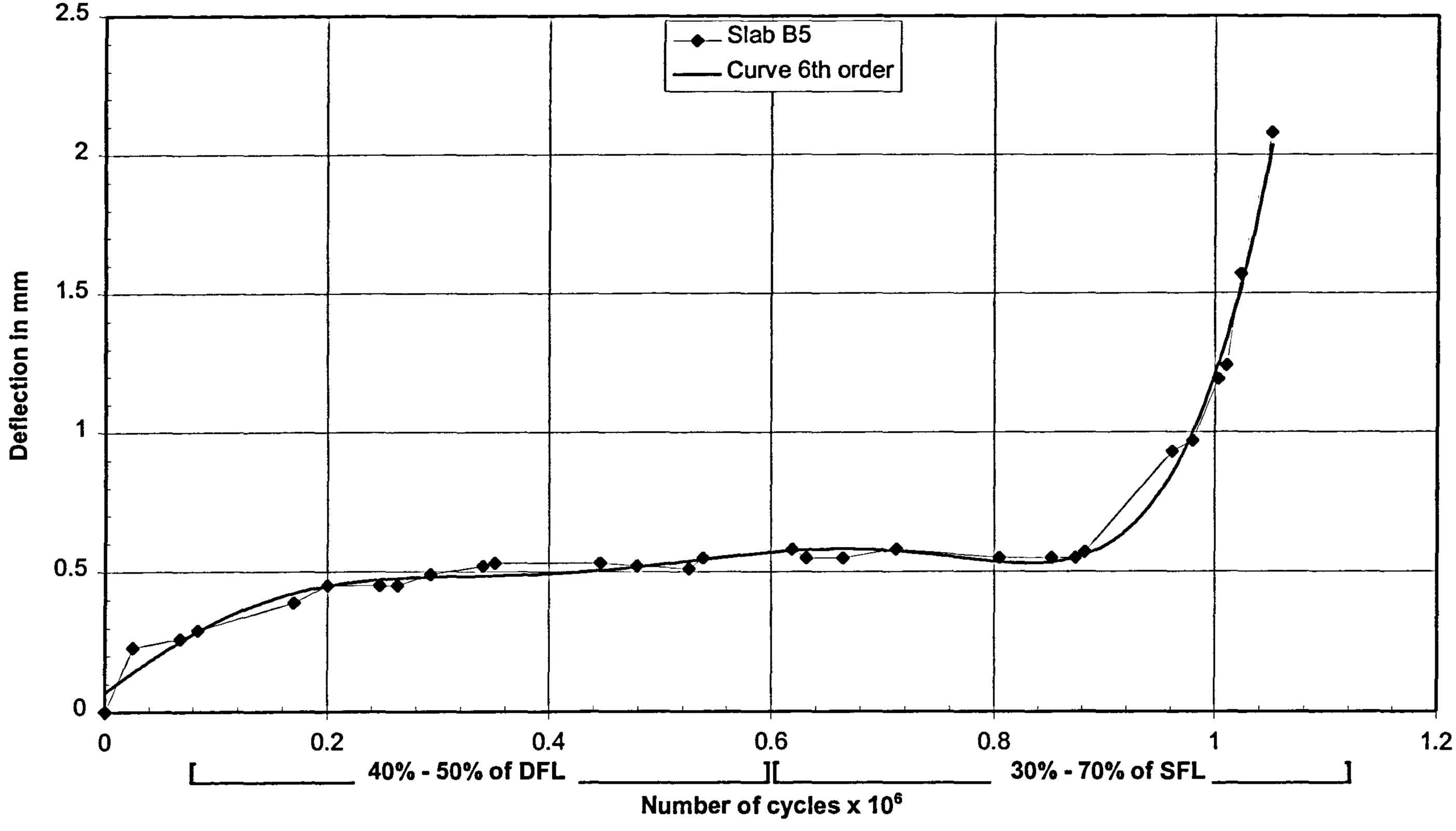

Figure 5.6 - Cyclic test, slab B2
DFL = Designed Failure Load
SFL = Static Failure Load

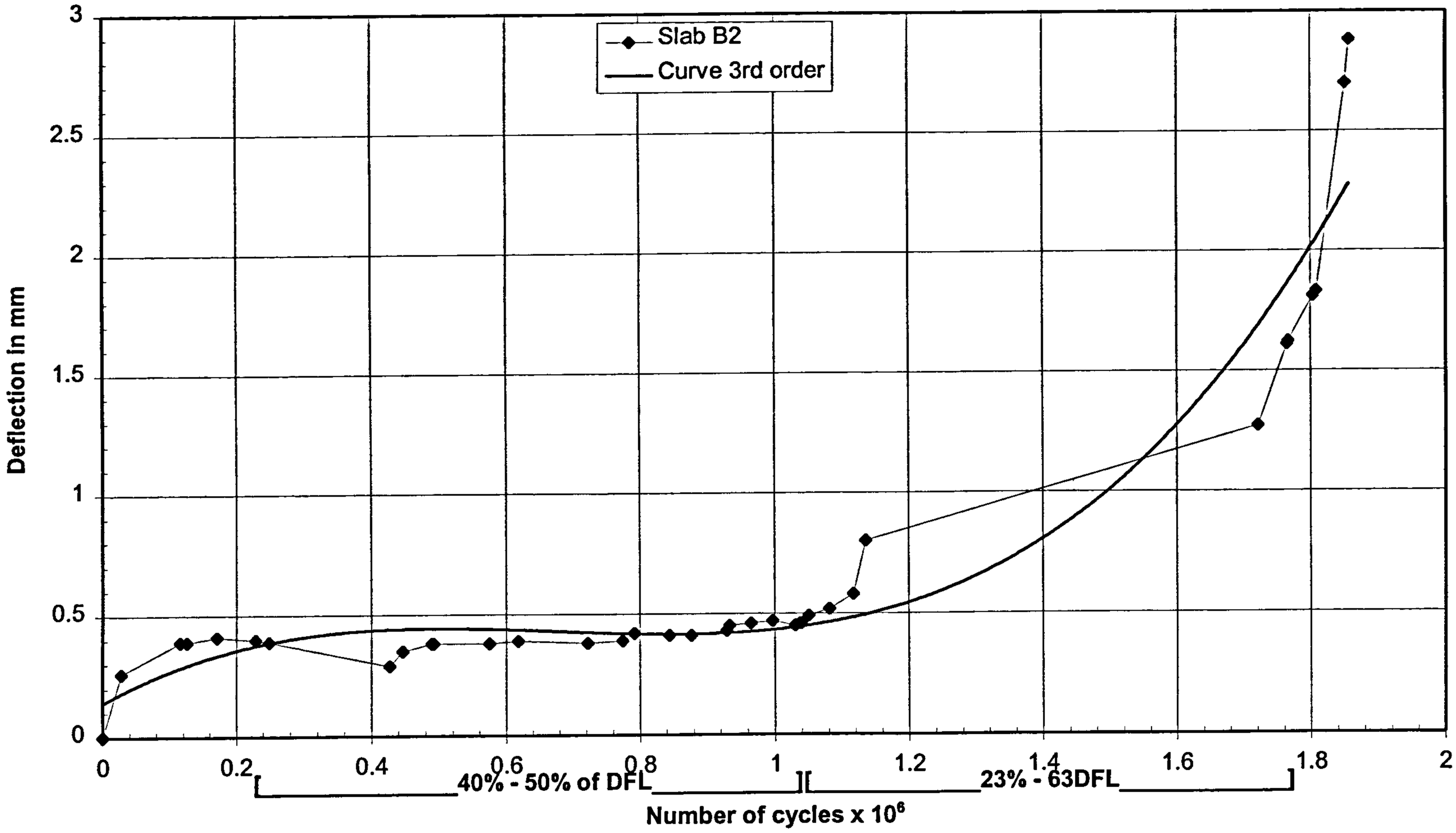

6.3.1 Analytical study of commercial vehicle wheel load on highway bridges

As already stated in section 6.1 the report LR 252 estimates that there is the 15% probability of commercial vehicle coincidence and the currently unsuperseded BS 5400: Part 10 which tabulates the commercial vehicle wheel load spectrum are being used in this analytical study and is based on the following theory:

Considering a single lane dual carriageway, if there is a given class of commercial vehicle traversing the bridge, imposing a maximum moment of (M1) and this has a total number of occurrences on this bridge of (X), it is taken that there is a 15% chance that this class is in coincident with another class of commercial vehicle which imposes a maximum moment (M2) and whose total number of occurrences on this bridge is (Y), traversing in the opposite direction.

From this theory, the followings are deduced:

I. At 15% chance of coincident, the moment imposed on the bridge under consideration is (M1+M2).

II. Given two classes of commercial vehicle, the number of occurrences at 15% (n) is therefore:

a. - n = { 15% } x { The smaller value of X or Y } x { 2 (for both directions) }

b. - n is effectively the number of wheel load of the load range due to the two classes of commercial vehicle that are coincident on the bridge.

III. Given the two classes of commercial vehicle in coincident at 15% on the bridge, they would impose a range of loading which for N cycles would cause failure of the bridge and N is determined from Table 5.8 of chapter 5 which is in fact the results of the assumed S-N curves Figure 5.11 and the Modified Goodman diagram study Figure 5.10, both of chapter 5 as well.

An explanation of to the determination of N is :

The use of Table 5.8 is required and the first step prior to using Table 5.8 would be that the maximum & minimum loads due to the combinations (of CV that are in coincident) as a percentage of the ultimate load of the bridge, be determined first, as an example consider the CV type 18GT-H (which a lone imposes a maximum moment of 3780 kNm on the 15m span two lane single carriageway) in coincident with the 6A-M type CV (which alone imposes a maximum moment of 845 kNm on the same bridge),

$$\text{Max \%} = \frac{\text{DL}}{\text{Ult}} = \frac{4275}{10642} \times 100\,\% = 40.2\,\%$$

$$\text{Mix \%} = \frac{\text{DL} + (\text{combined moment})}{\text{Ult}} \times 100\,\%$$

$$= \frac{4275 + (845 + 3780)}{10642} \times 100\% = 83.6\,\%$$

With the max % and the min % and the aid of Table 5.8, N can be established.

IV. Table 11 of BS 5400: Part 10 has tabulated the number of different classes of commercial vehicle that are expected to be traversing the UK road network. From this table, various possible combinations of commercial vehicle are determined, with the assumption that commercial vehicles of the trailer & tractor type required police supervision of their movement and therefore when traversing certain bridges this will not allow room for passage of a different type of commercial vehicle in the opposite direction and therefore coincident of such types are not considered.

From the points (I) - (IV) deduced above, Table 6.4 is set up for the case of the 15m span two lane single carriageway bridge.

It is obvious that any combinations of commercial vehicle from the list of Table 11 of BS 5400: Part 10 may occur on the bridge and that the resulting load effects are accumulated to contribute to the failure of the bridge by the end its useful design life span and this is a phenomenon of random loading on the bridge.

Based on Miner 's hypothesis, this phenomenon is expressed into a mathematical form to establish an indication of life span of existing UK bridges under the current BS 5400 commercial vehicle wheel load spectrum. The purpose of this life span is that from its comparison to that obtained from the three slabs tested under fatigue loading in the laboratory, an engineering judgement can be made on the efficiency of the strengthening technique.

With reference to Table 5.8 the interpretation of the above phenomenon is:

If (n_i) means that n cycles of a definite load range are applied (i.e. the load range resulted from a given combination or non-combination of commercial vehicle) of which the bridge can withstand (N_i) cycles (i.e. the N cycles to failure due to the combination or non-combination under consideration, obtained from Table 5.8) then from Miner 's hypothesis:

Table 6.4 - Calculation of N for combinations of different classes of Commercial Vehicles

Commercial Vehicles on the Bridge	Coresponding No. of CV in each direction over 120 Year Design Life (Table 5.10,Chapter 5)		Moment due to each individual Class of CV (Table 5.5, Chapter 5)		Min %	Max %	N (Table 5.8)
7A-H & 7A-H	36000	36000	1560	1560	40.2	69.5	1E+06
7A-H & 6A-M	36000	35.9E+06	1560	845	40.2	62.8	1E+09
7A-H & 4R-H	36000	16.2E+06	1560	768	40.2	62	1E+09
7A-H & 3R-H	36000	67.8E+06	1560	713	40.2	61.5	1E+09

$$\sum \frac{n_i}{N_i} \leq 1.0$$

Meaning that the same fatigue life can be obtained for reduced number of cycles over greater load ranges i.e. from the lower (n) of the heavier combinations of commercial vehicle to the larger (n) of the lighter combinations of commercial vehicle, provided that the sum of the proportions of applied cycle n to the number of cycles that the bridge can withstand (N) becomes 1.0

From this, the life span is:

$$LS \times \sum \frac{n_i}{N_i} = 1$$

$$LS = \frac{1}{\sum \frac{n_i}{N_i}}$$

Tables 6.5 to 6.9 tabulate the possible co-existence of commercial vehicle classes on the single lane dual carriageway at 15% probability on the annual basis.

$$\left.\begin{array}{l} 5.847 \times 10^{-8} \\ 4.490 \times 10^{-7} \\ 1.418 \times 10^{-7} \\ 4.789 \times 10^{-7} \end{array}\right\} \Rightarrow \sum \frac{n}{N} = 1.128 \times 10^{-6}$$

For the type of bridge being considered and at the 15% probability of coincident, the co-existence of the heavier classes in this Table are not considered, taking into account such factors as, requiring police escort and overall width restriction of the bridge.

From Table 5.12 of Section 5.3.5, Chapter 5, the $\left[\sum \frac{n}{N}\right]$ ratio for non-coincident CV over the design life span of 120 years is now being combined with that from the co-incident CV.

$$\sum \frac{n}{N} = \frac{0.13}{120}$$

The indication of life span of UK bridges under the current loading spectrum as given in BS 5400: Part 10 is:

$$LS\left[1.128\times10^{-6}+\frac{0.13}{120}\right]=$$

$$LS = 922 \text{ years.}$$

Table 5.12, Section 5.3.5, Chapter 5 - Miner 's Hypothesis

Group	Traffic Group	Load Range	Sum of [n/N]	
			15m Span	20m Span
(I)	18GT - H	39.8 - 78.0	0.12	3.0×10^{-4}
(II)	9TT - H	40.0 - 70.0	2.4×10^{-3}	6.0×10^{-5}
(III)	18GT - M	40.1 - 66.8	3.6×10^{-4}	9.0×10^{-8}
(IV)	9TT - M 7GT - M	40.3 - 64.0 40.3 - 64.0	4.8×10^{-5} 8.4×10^{-5} 1.3×10^{-4}	12×10^{-8} 21×10^{-8} 33×10^{-8}
(V)	3R - H 7GT - H	40.8 - 60.0 40.8 - 60.0	6.8×10^{-3}	16.9×10^{-4} 9×10^{-8} 16.9×10^{-4}
(VI)	7A - H 6A - M 4R - H	40.5 - 57.8 40.5 - 57.8 40.5 - 57.8	3.6×10^{-7} 3.6×10^{-4} 1.6×10^{-4} 5.2×10^{-4}	90×10^{-8} 89.9×10^{-5} 40.5×10^{-5} 130.5×10^{-5}
			Σ [n/N] = 0.13	**Σ [n/N] = 33.6×10^{-4}**

Table 6.5 - Distribution of the re-grouped CV classes (sect 5.3.4 chapter 5)			
From Table 1, BS 5400: Part 10, for the two lane single carriageway there are 0.5×10^6 Commercial Vehicles in each direction per year			
Assuming 15% co-incidence			
Total no. of co-incident passes of all CV = $0.15 \times 0.5 \times 10^6 = 0.075 \times 10^6$			
Total no. of passes of CV over bridge = $(2 \times 0.5 \times 10^6) = 1 \times 10^6$			
Number of single passes of CV over bridge per year = $(1 \times 10^6) - (0.075 \times 10^6) = 0.925 \times 10^6$			
Distribution of CV groups			
CV Class	No. in each group per 10^6 CV	Total No. per year	
		Co-incident with another CV Class	Self-Existance
7A-H	300	$(300/10^6) \times 0.075 \times 10^6 = 22.5$	$(300/10^6) \times 0.925 \times 10^6 = 277.5$
6A-M	2.995×10^5	$(2.995 \times 10^5/10^6) \times 0.075 \times 10^6 = 2.246 \times 10^4$	$(2.995 \times 10^5/10^6) \times 0.925 \times 10^6 = 2.770 \times 10^5$
4R-H	1.35×10^5	$(1.35 \times 10^5/10^6) \times 0.075 \times 10^6 = 1.013 \times 10^4$	$(1.35 \times 10^5/10^6) \times 0.925 \times 10^6 = 1.249 \times 10^5$
3R-H	5.65×10^5	$(5.65 \times 10^5/10^6) \times 0.075 \times 10^6 = 4.238 \times 10^4$	$(5.65 \times 10^5/10^6) \times 0.925 \times 10^6 = 5.226 \times 10^5$

Table 6.6 - n/N ratio of 7A-H co-incident with other classes in the load spectrum				
7A-H with other classes	(p),No. of coincident passes/year	n per year (2 x p)	N (Table 6.4)	n/N
7A-H with 7A-H	$22.5 \times 300/10^6 = 6.75 \times 10^{-3}$	0.014	1E+06	1.35E-08
7A-H with 6A-M	$22.5 \times 2.995 \times 10^5/10^6 = 6.739$	13.478	1E+09	1.3478E-08
7A-H with 4R-H	$22.5 \times 1.35 \times 10^5/10^6 = 3.038$	6.076	1E+09	6.076E-09
7A-H with 3R-H	$22.5 \times 5.65 \times 10^5/10^6 = 12.710$	25.420	1E+09	2.542E-08
Summation				**5.847E-08**

Table 6.7-n/N ratio of 6A-M co-incident with other classes in the load spectrum				
6A-M with other classes	(p),No. of coincident passes/year	n per year (2 x p)	N (Table 6.4)	n/N
6A-M with 6A-M	$2.246 \times 10^4 \times 2.995 \times 10^5/10^6 = 6727$	13454	1E+11	1.3454E-07
6A-M with 4R-H	$2.246 \times 10^4 \times 1.35 \times 10^5/10^6 = 3032$	6064	1E+11	6.064E-08
6A-M with 3R-H	2.246 x 104 x 5.65 x $10^5/10^6 = 12690$	25380	1E+11	2.538E-07
Summation				**4.490E-07**

Table 6.8-n/N ratio of 4R-H co-incident with other classes in the load spectrum				
4R-H with other classes	(p),No. of coincident passes/year	n per year (2 x p)	N (Table 6.4)	n/N
4R-H with 4R-H	$1.013 \times 10^4 \times 1.35 \times 10^5/10^6 = 1368$	2736	1E+11	2.736E-08
4R-H with 3R-H	$1.013 \times 10^4 \times 5.65 \times 10^5/10^6 = 5723$	11446	1E+11	1.145E-07
Summation				**1.418E-07**

Table 6.9-n/N ratio of 3R-H co-incident with other classes in the load spectrum				
3R-H with other classes	(p),No. of coincident passes/year	n per year (2 x p)	N (Table 6.4)	n/N
3R-H with 3R-H	$4.238 \times 10^4 \times 5.65 \times 10^5/10^6 = 23945$	47890	1E+11	4.789E-07
Summation				**4.789E-07**

This life span results reinforces the validity of the commercial vehicle wheel load spectrum tabulated in Table 11 of BS 5400: Part 10: 1980 (with the addition of the 44 tons commercial vehicle type 6A-M).

6.3.2 Plotting the fatigue test results on the assumed S-N diagram

The fatigue test results of slab B2, B5 and B6 are now superimposed onto the analytical S-N diagram for analysis, see Figure 6.7. The tabulated results are re-presented as follows:

Results extracted from Table 6.3		
Slab	Failed at total number of cycles	Higher fatigue load range level
B2	0.817×10^6	23% - 63% of SFL
B5	0.457×10^6	30% - 70% of SFL
B6	0.141×10^6	30% - 70% of SFL

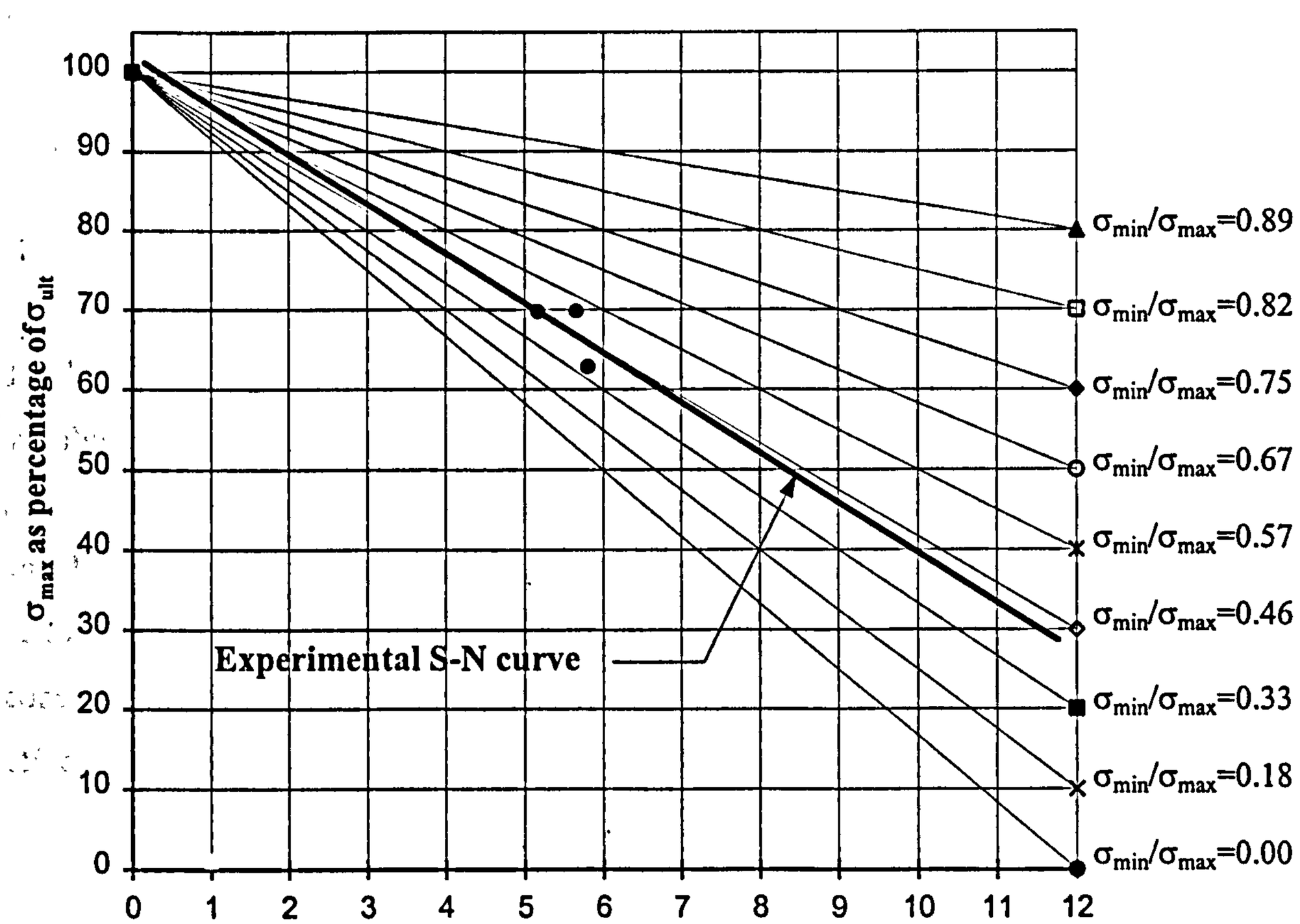

Figure 6.7 - Superimposition of the experimental and analytical S-N curves.

Deductions from Figure 6.7

A best fit straight line through the three experimental results points has a tendency to intersect the axis of σ_{max} as a percentage of σ_{ult} at 100%, this result therefore appears to reflect the agreement between the assumed analytical S-N curves and the experimental S-N curves.

The analytical prediction of the number of cycles to failure in Table 5.8 is clearly seen to be on the conservative side as shown in the following comparison

Slab B2,

Tested: 23%- 63% of SFL

Failed: 0.817×10^6 cycles

Table 5.8 predicted: 0.1×10^6 cycles

Slab B5,

Tested: 30% - 70% of SFL

Failed: 0.457×10^6 cycles

Table 5.8 predicted: 0.1×10^6 cycles

Slab B6,

Tested: 30% - 70% of SFL

Failed: 0.141×10^6 cycles

Table 5.8 predicted: 0.1×10^6 cycles

The behaviour of the strengthened test slabs appear to follow the assumed S-N diagram and the modified Goodman diagram and therefore the implication is that, if the bridge is strengthened (i.e. strengthening factor >1) then under the current commercial vehicles and load spectrum of BS 5400: Part 10, the total expected life should at least be restored. The experimental results also show very similar fatigue behaviour to normal concrete, indicating very strongly that the strengthening technique has no detrimental effect in fatigue behaviour.

CHAPTER 7

HORIZONTAL SHEAR STUDY

7.0 GENERAL

One of the most important factors required for this technique of strengthening to be effective is that the composite action is maintained right up to failure. How well composite action is maintained depends on how well the additional sprayed concrete layer is bonded to the existing concrete member being strengthened i.e. the required horizontal shear capacity at the interface.

The following sections present three experimental investigations which reveal the effectiveness of this strengthening technique as far as horizontal shear capacity is concerned under the loading conditions imposed.

7.1 SLANT SHEAR TEST

This test aims to assess the bond strength between two types of concrete by subjecting the bond interface to a combination of shear and compressive stresses.

When a reinforced concrete member is sustaining a load, the high tensile strength of the reinforcement is mobilised by way of shear stresses in the concrete and shear stresses are also generated as a result of the elastic response of the concrete in the compressive zone. This regime of combined shear and compressive loading is very common in concrete structures. Therefore the shear properties of the bond strength would be representative of the bond strength assessment.

7.1.1 Test preparation

The specimens for this test were extracted from one of the load tested slabs without shear connectors and this was done by first cutting a large but manageable composite block from the test slab, the block was then accurately cut down to dimensions of 55 x 55 x 150 mm such that the substrate/sprayed concrete interface was at 30° to the longitudinal axis of the specimen and that no cracks or reinforcement were present.

Two test specimens and four control specimens (monolithic, base slab concrete) were prepared and tested in accordance with BS 6319: Part 4: 1985. Due to the high labour intensity required, it was only possible to extract two composite test specimens.

7.1.2 Slant shear test results

The specimens were tested and the results are tabulated in Table 7.1.

Table 7.1 - Slant shear test results.

Slant Shear Bond Strength (quoted as compressive strength)	
Composite Specimen	Monolithic Specimen
Specimen extracted from a tested slab	Specimen extracted From a tested Slab
Normal Mix Sprayed Concrete	All Substrate Concrete
Dimensions 55 x 55 x 150mm	Dimensions 55 x 55 x 150mm
1 No. Specimen at 84 day age, failed at **37.6 N/mm^2** in compression	4 Nos. Specimens at 19 month age **47.1 N/mm^2** average compression failure
1 No. Specimen at 21 month age, failed at **43.7 N/mm^2** in compression	

The slant shear test results are quoted as the compressive strength - in accordance with BS 6319. The intention of recording the failure of the specimens in terms of compressive strength to assess the bond strength at the interface can be explained from the following principle of the code:

> Failure of the joint (at the substrate/sprayed concrete interface) at a stress of say, x N/mm^2 before concrete failure occurs could be taken as an indication that the joining composition and procedure employed would only give monolithic failure of a composite prism if the hydraulic cement concrete was of compressive strength x N/mm^2 .

In this work, monolithic failure of the composite prism was achieved as explained in section 7.1.3 (Mode of failure) and the compressive strength of the composite prism is 25 percent less than the monolithic prism at the age of 84 days and 8 percent at 21 months.

7.1.3 Mode of failure

Figures 7.1 and 7.2 show the test specimens before and after undergoing the slant shear test. It was found that on failure of the test specimen the fracture lines were distributed uniformly and symmetrically relative to the longitudinal axis of the specimen and with fracture lines crossing the slanted interface in the direction of the longitudinal axis of the specimen, a mode of failure that would be expected if a similar test specimen was fabricated monolithically. Figure 7.2 also shows the fracture lines crossing the slanted interface in the direction of the longitudinal axis of the specimen. It therefore appears from the results of this test that grit blasting as a means of surface preparation was more than adequate, as extremely good bond was maintained at the substrate/sprayed concrete interface.

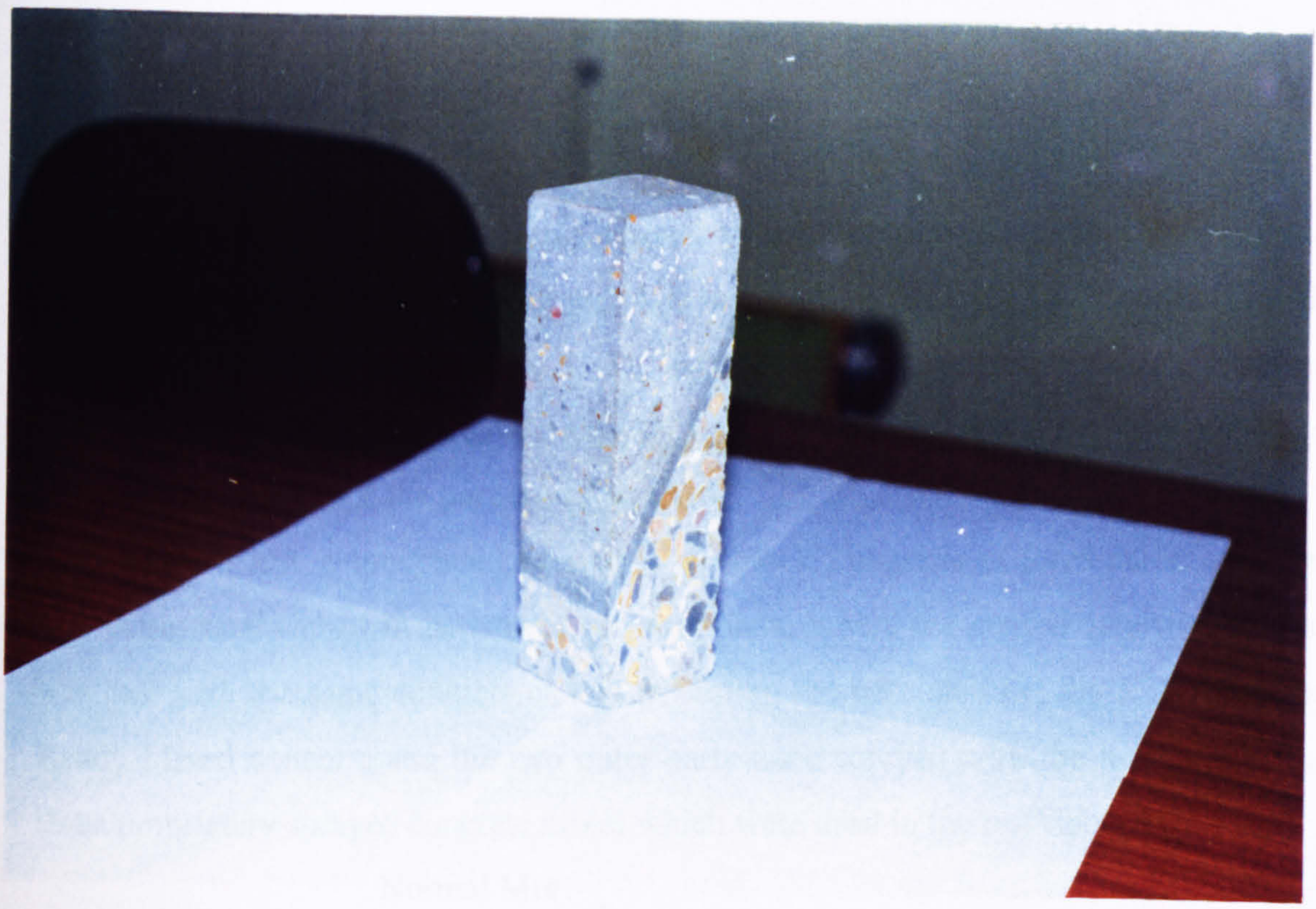

Figure 7.1 - Slant shear test specimen before testing.

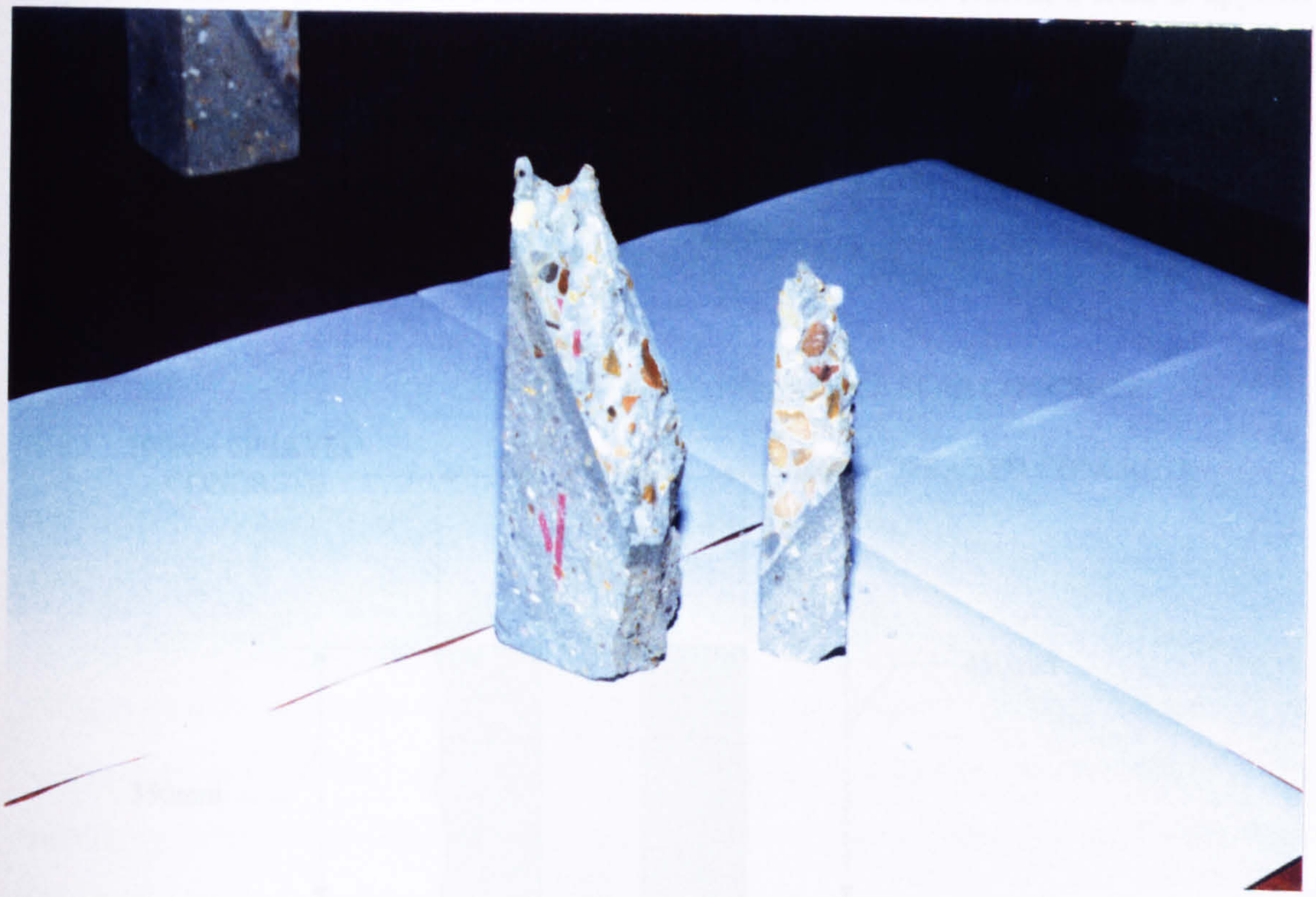

Figure 7.2 - Slant shear test specimen after testing.

7.2 DOUBLE SHEAR TEST

This test aims to simulate the shearing action between the sprayed concrete lager and the base concrete slab under load. Although this test was not conducted in accordance with a specific code of practice, it is a test method adopted by a proprietary concrete supplier - Master Builders Technologies[44] to test the bond between the substrate and a proprietary concrete for the purpose of repair.

In this test, a specimen (referred to as 'block') consists of three parts, a central part being sandwiched in between two outer parts, where the central sandwiched part was cast with the same concrete as that in casting the base slab i.e. the C35 Designed Ready Mixed concrete and the two outer parts were sprayed with the normal and the three proprietary sprayed concrete mixes which were used in the test slab i.e.

Normal Mix

Sikacem133 Mix

Polypropylene Fibre Mix

Steel Fibre Mix

Figure 7.3 shows the detail of a double shear test block. When tested, a load is applied to the central part of the specimen and the polystyrene on its underside will be squashed as the shearing action takes place and the central part moves down relative to the two outer sprayed concrete parts.

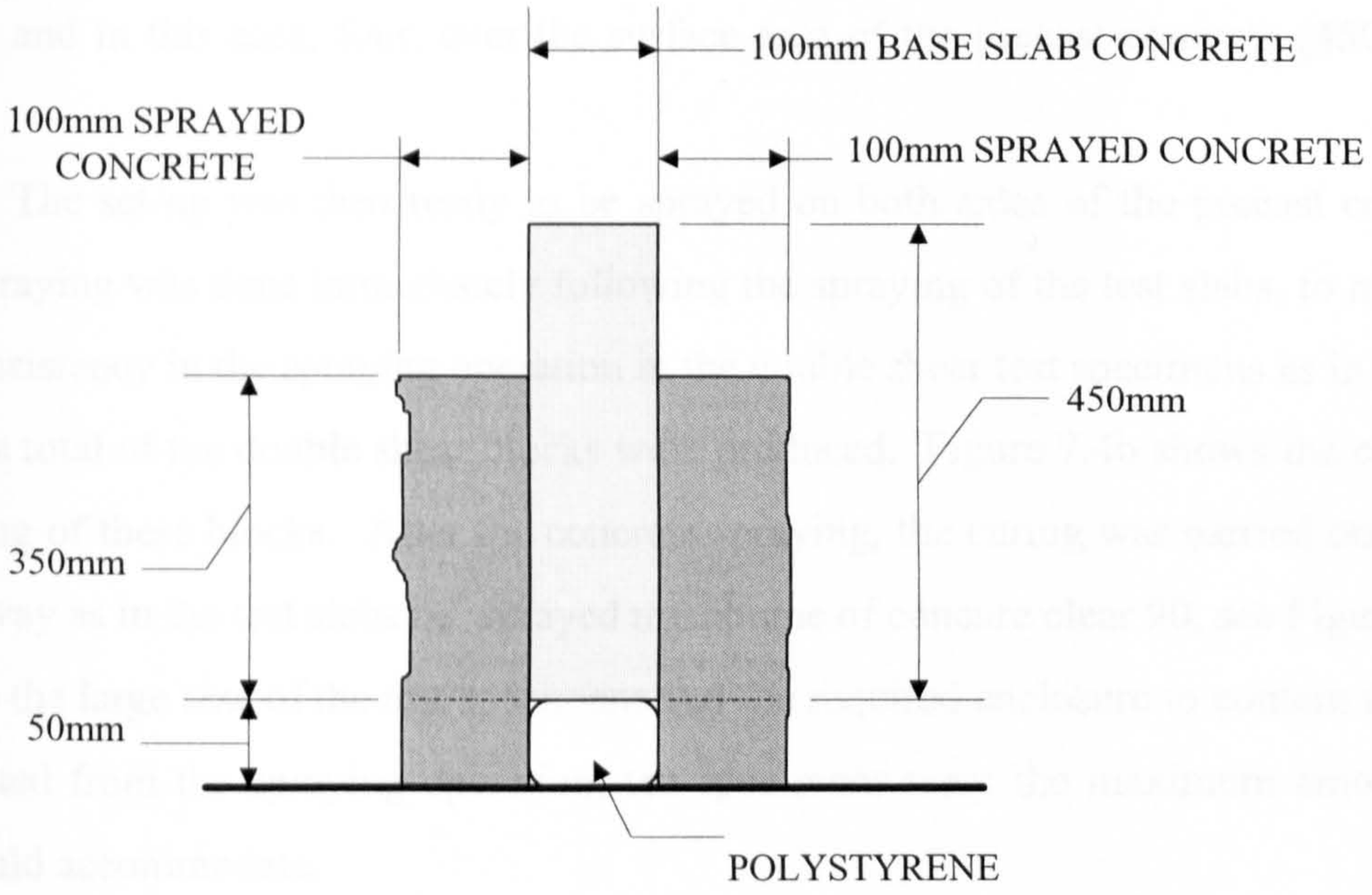

Figure 7.3 - Details of a double shear test block (500mm overall length).

This shearing action is similar to that taken place in the test slab and thus enabled a direct measure of the shear performance at the substrate/sprayed concrete interface.

The polystyrene piece in Figure 7.3 served to create the 50mm vertical travel for the central concrete part during spraying of the two outer parts and was of the soft grade polystyrene so that it did not resist load when the central part concrete was loaded.

7.2.1 Test preparation

Special timber shuttering was made and with the polystyrene in position as shown in Figure 7.4a, the central precast concrete part (100 x 450 x 500mm) was then slotted into the shuttering (a typical central precast concrete outside the shuttering is also shown in Figure 7.4a).

With the precast concrete part in position in the shuttering, identical surface finishes were prepared on both sides of the precast concrete - there were five different surface finishes:

Grit blasted

As cast

Scabbeled

As cast with shear connectors

Grit blasted with shear connectors.

The number of shear connectors were exactly the same as in the test slabs i.e. T10 @ 200c/c and in this case, four, over the surface area of the precast concrete (450 x 500 mm)

The set-up was then ready to be sprayed on both sides of the precast concrete. The spraying was done immediately following the spraying of the test slabs, to maintain the consistency in the spraying operation in the double shear test specimens as in the test slabs, a total of ten double shear blocks were produced. Figure 7.4b shows the concrete spraying of these blocks. After the concrete spraying, the curing was carried out in the same way as in the test slabs i.e. sprayed membrane of concure clear 90, see Figure 7.4c. Due to the large size of the test specimens and the required enclosure to contain the dust generated from the spraying operation, ten specimens were the maximum amount the lab could accommodate.

Figure 7.4a - Shuttering for the sprayed concrete parts of the double shear block.

Figure 7.4b - Spraying concrete for the double block.

Figure 7.4c - Curing the sprayed concrete parts with a concure clear 90 membrane.

Figure 7.4 - Fabrication of the double shear test blocks.

7.2.2 Double shear test results

Of the ten specimens, one was discarded when the precast concrete part was damaged during lifting into the shuttering, the remaining nine were tested and the results are in Table 7.2

Table 7.2 - Double shear test results					
	Type of Surface Preparation				
	Grit Blasted	Scabbled	As cast with Shear Connectors	As cast	Grit Blasted with Shear Connectors
Bond Area (mm^2)	300 x 500	300 x 500	300 x 500	300 x 500	300 x 500
Age (days)	100	100	100	100	100
	Shear Stress at Failure (N/mm^2)				
Normal	2.14 (2)	1.69 (2)	2.00	0.77	2.5
Sikacem 133	5.93	-	-	-	-
Steel Fiber	-	-	-	-	-
Poly Fiber	3.37	-	-	-	-
BS 8110: Prt 1: Cl 5.4.7.2	0.8	0.75	2	0.65	2.5
Note: (2) indicates two identical specimens were test - average results quoted					

Table 7.2 shows that the performance of the normal mix sprayed concrete in bonding to the substrate concrete with different surface finishes is equivalent or exceeds the design ultimate horizontal shear stresses at the interface required by BS 8110: Part 1: 1985: cl 5.4.7.2.

7.2.3 Mode of failure

Figure 7.5 shows the failure mode of the double shear block. Although as already mentioned that the entire test was not in accordance with a specific code of practice, the rate of loading applied to the specimens was taken from BS 1881: Part 120: 1983 (Method of determination of the compression strength of concrete cores) and was 0.3 $N/(mm^2.s)$[27].

On examination of the concrete faces of the grit blast prepared specimens, it was seen that marginally more sprayed concrete was deposited on the substrate concrete and that the depth of concrete removed from either the substrate or the sprayed part was 5 to 10mm, indicating that by grit blasting the surface of the substrate concrete extremely good bond can be achieved.

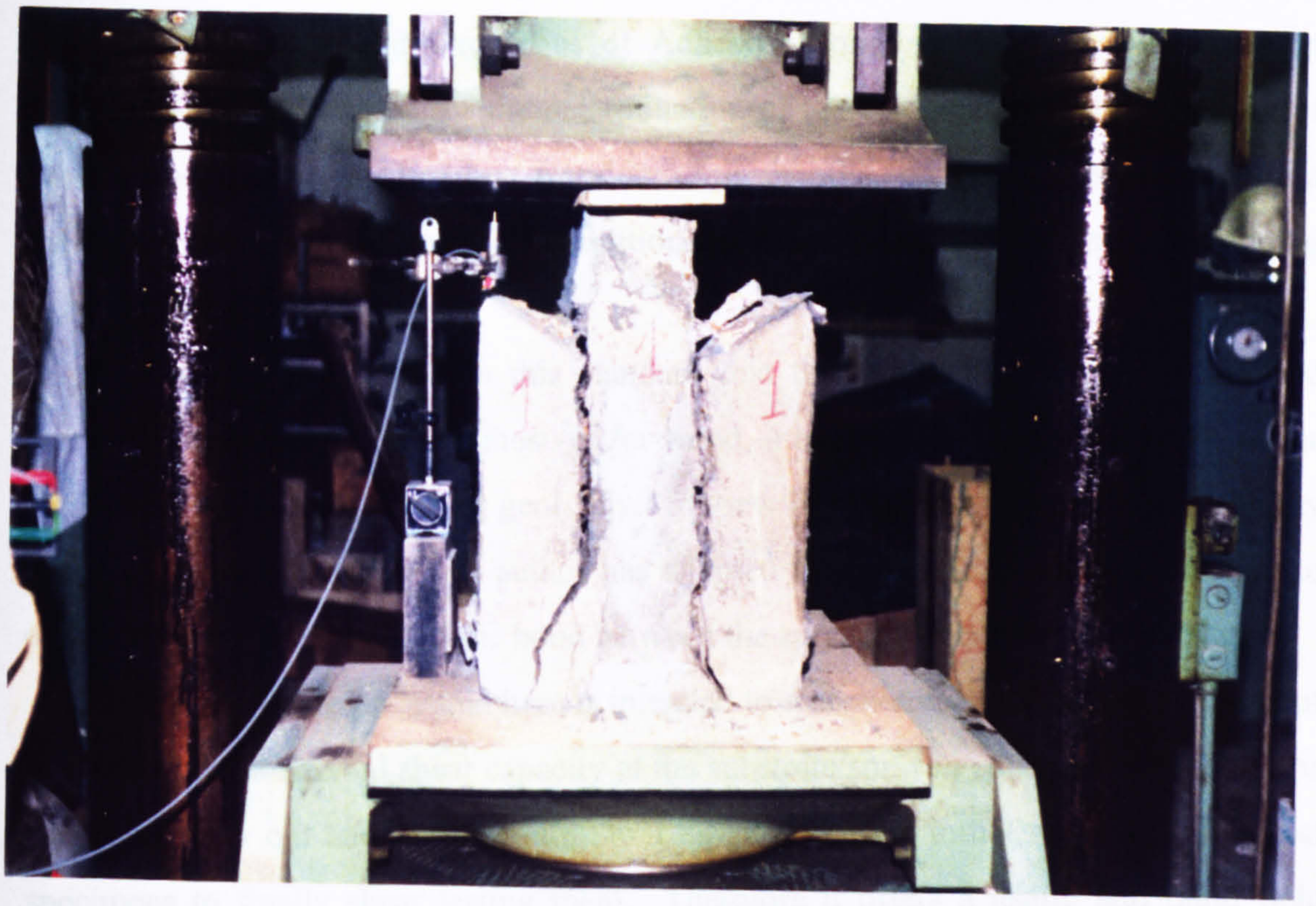

Figure 7.5a - Just after failure.

Figure 7.5b - Observing the interface.

Figure 7.5 - Mode of failure of a double shear test block.

7.3 HORIZONTAL SHEAR STUDY - DIRECT SHEAR TEST

The American Society for testing and Materials standard D 905-89 states, "Standard Test Method for Strength Properties of Adhesive Bonds in Shear by Compression Loading" [45] can be used for the determination of the comparative shear strengths of adhesive bonds used for bonding wood and other similar materials, when tested on a standard specimen under specified conditions of preparation, conditioning and loading in compression.

Although it is stated in this standard that this method of testing is intended primarily as an evaluation of adhesives for wood, it has also stated the suitability of the method for monitoring bonding generally. In view of this suitability and the simplicity in the experimental set up, the author has adopted the principle of this test method to evaluate the shear strength of the bond between the sprayed concrete and its substrate.

The test being presented here is intended to a economical but effective means of evaluating the horizontal shear capacity at the substrate/sprayed concrete interface. It is simple to carry out and requires minimum labour from the initial stage of coring test specimens to finally shear testing them. Therefore it offers a useful and rapid field verification test.

In this test, the composite concrete specimen with its sprayed portion (or its substrate portion) would be held rigidly in position in a clamp which is readily available in any mechanical testing laboratory. The positioning of the specimen is such that the plane of the substrate/sprayed concrete interface coincides with the plane of the shearing force.

7.3.1 Test preparation

From the load tested slabs, 75mm diameter cores were extracted by through drilling perpendicular to the horizontal plane of the slab, each core therefore has the substrate/sprayed concrete interface at mid-length. Figure 7.6 shows the extracted cores

Figure 7.6a - Through-Drilling to extract cores.

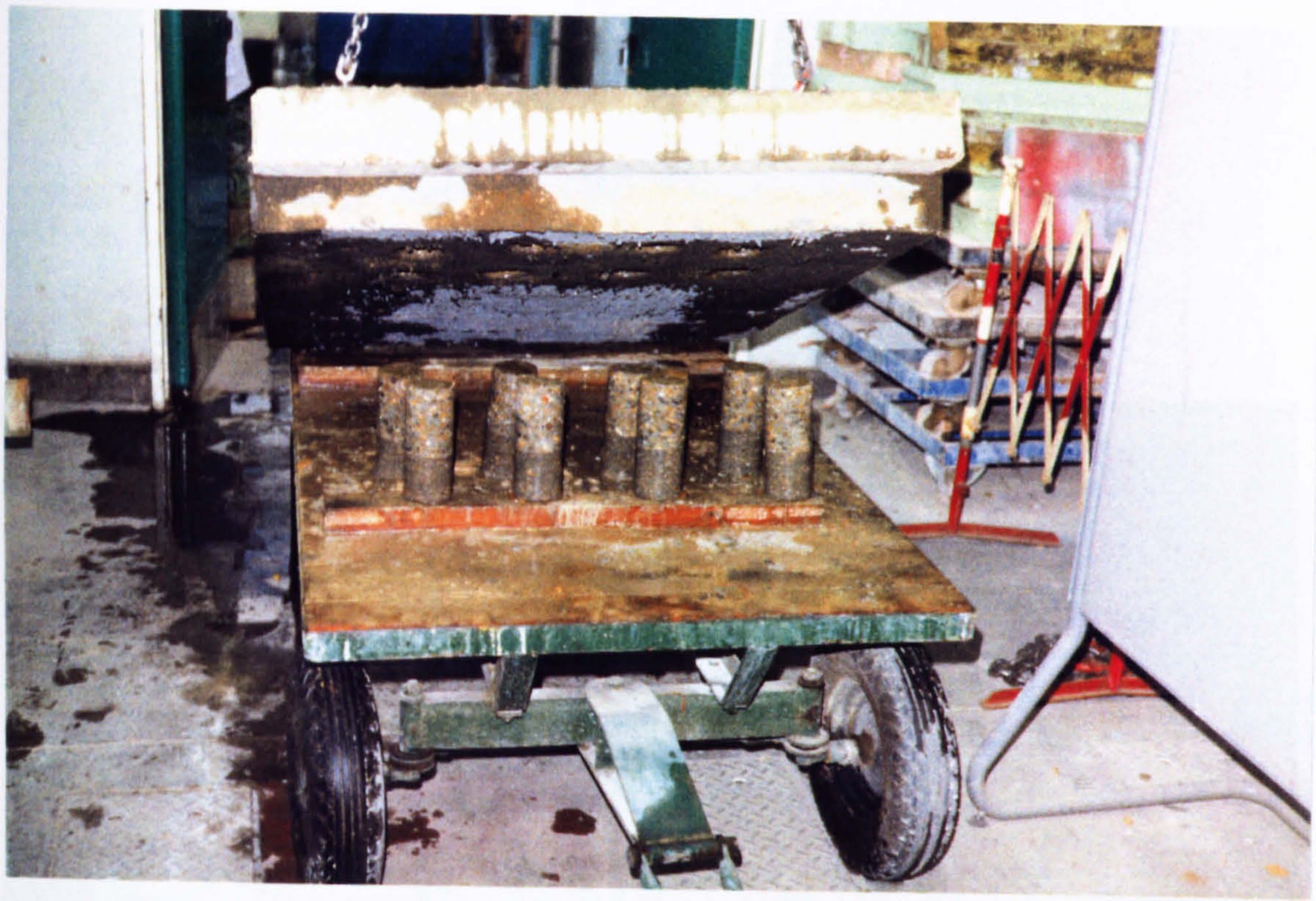

Figure 7.6b - After Through Drilling.

Figure 7.6 - Extracting cores for direct shear testing.

The cores were extracted from the load tested slabs of the four concrete mixes used i.e.

Normal Mix

Sikacem 133 Mix

Steel Fibre Mix

Polypropylene Fibre Mix

Monolithic core specimens from an all base slab concrete were also extracted for comparison. The cores were then trimmed down to prismatic shaped specimens for clamping into the shear loading device.

The prepared cores are identical to those shown in Figure 7.7 but with reduced length i.e. 25mm sprayed concrete and 50mm base slab concrete - The cores shown are those being used for freeze-thaw testing.

Figure 7.7 - Prepared direct shear specimens.

After preparation , the specimen were then loaded in shear as shown in Figure 7.8.

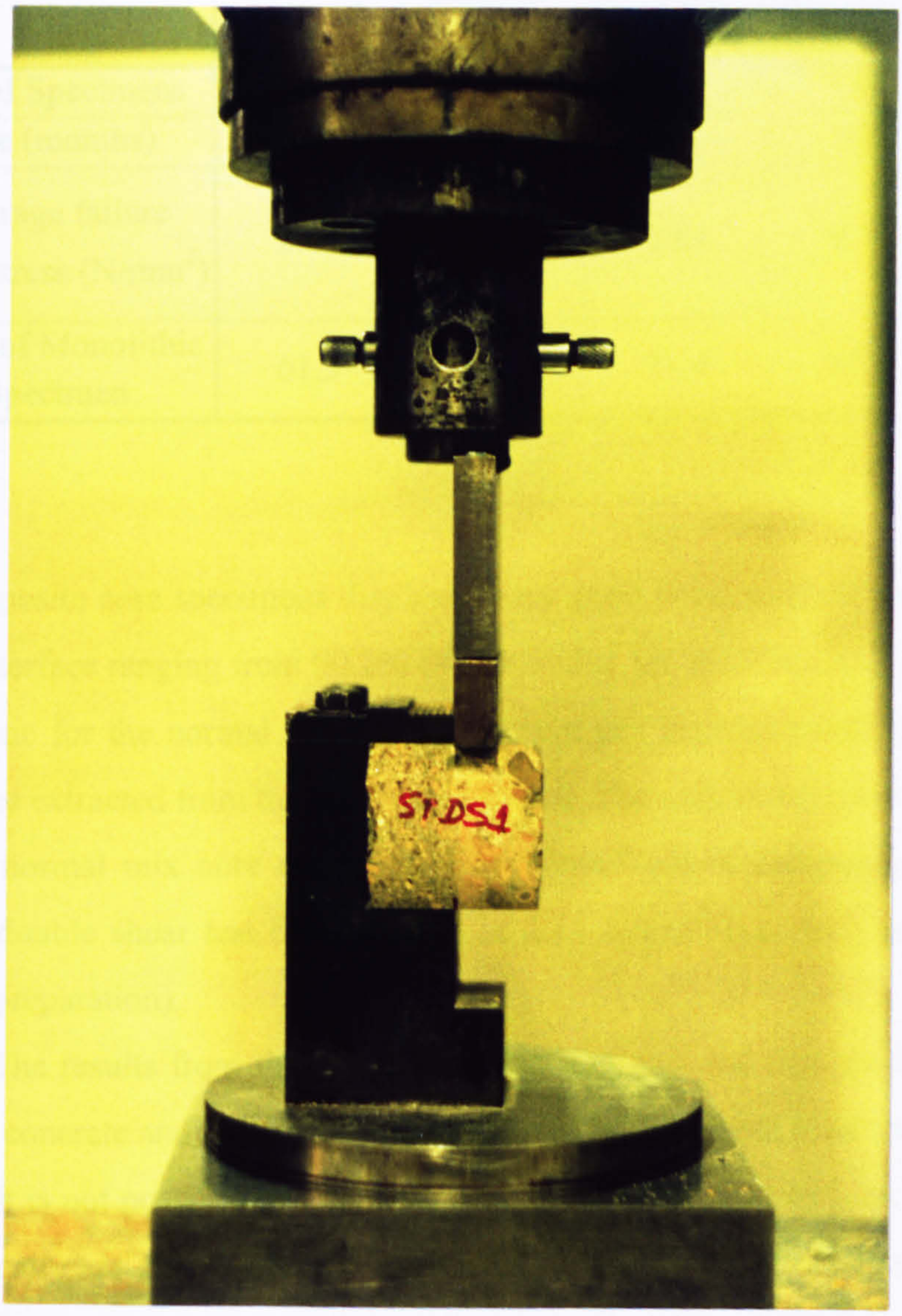

Figure 7.8 - A direct shear specimen being tested.

7.3.2 Direct shear results and mode of failure

All cores failed at the interface as intended and the shear stresses at failure are tabulated as in Table 7.3

Table 7.3 - Direct shear test results.

	Concrete Mix				
	Normal	Sikacem 133	Steel Fiber	Poly Fiber	Monolithic Specimen
No. of Specimens	3	4	3	4	4
Age (months)	19	19	19	19	19
Average failure shear stress (N/mm^2)	2.44	3.59	2.84	2.77	3.98
As % of Monolithic Specimen	61.3	90.2	71.4	69.6	100.0

All composite core specimens displayed very good bond with the failure shear stresses at the interface ranging from 90.2% of monolithic for the Sikacem 133 mix to 61.3% of monolithic for the normal mix (all cores have grit blast prepared interfaces - because they were extracted from the load tested slabs). The only results that could be compared are the normal mix core results of 2.44 N/mm^2 which compare very well with the similar double shear test block results of 2.14 N/mm^2 (i.e. with normal mix and grit blasted preparation).

The results from the direct shear test again shows that good bond between the sprayed concrete and its substrate was achieved with just grit blast surface preparation.

It is not possible to compare the direct shear results with the slant shear results, which really are only useful for comparing different surface preparations and those are not much use to a designer who wishes to know what actual shear stress a particular type of interface will support which can be offered by the direct shear test

CHAPTER 8

FREEZE - THAW DURABILITY

8.0 GENERAL

This chapter reports on the experimental investigation into the performance of the bond between the sprayed concrete layer and the precast concrete base slab when subjected to rapidly repeated cycles of freezing and thawing.

The experimental investigation was conducted in accordance with ASTM C666-84, Procedure A: Rapid Freezing and Thawing in water[46]. However, it is pointed out that this standard is primarily for the determination of the resistance of monolithic concrete specimens to rapidly repeated cycles of freezing and thawing in the laboratory. For the purpose of this research work, only the test procedures of the standard were used and applied to composite core specimens extracted from the load tested slabs and the resistance of the cores to the rapidly repeated cycles of freezing and thawing was assessed in terms of the direct shear test results and the measured velocity of ultrasonic pulses (BS 8110: Part 203: 1987 [47]).

The intention of measuring the velocity of ultrasonic pulses in the freezing and thawing cycles tested core was to enable the following items to be addressed:

1. The detection of the presence and approximate extent of cracks, voids and other defects.
2. The correlation of pulse velocity and strength as a measure of concrete quality.

8.1 EXPERIMENTAL PREPARATION

The test specimens to be used for this test were core specimens extracted from the load tested slabs at the same time as those core specimens for the direct shear test (Chapter 7, section 7.3.1) using the same approach i.e. drilling perpendicularly through the horizontal plan of the slab and trim the cores to prismatic dimension of 50 x 50 x 100mm (with the substrate/sprayed concrete interface at mid-length).

The length of the specimens was such that all composite specimens from the four mixes can be accommodated in the freeze-thaw chamber i.e.

Normal Mix (6 cores)

Sikacem 133 Mix (6 cores)

Steel Fibre Mix (5 cores)

Polypropylene Fibre Mix (3 cores)

Figure 8.1 shows the composite core specimens prepared for freeze-thaw cycle testing.

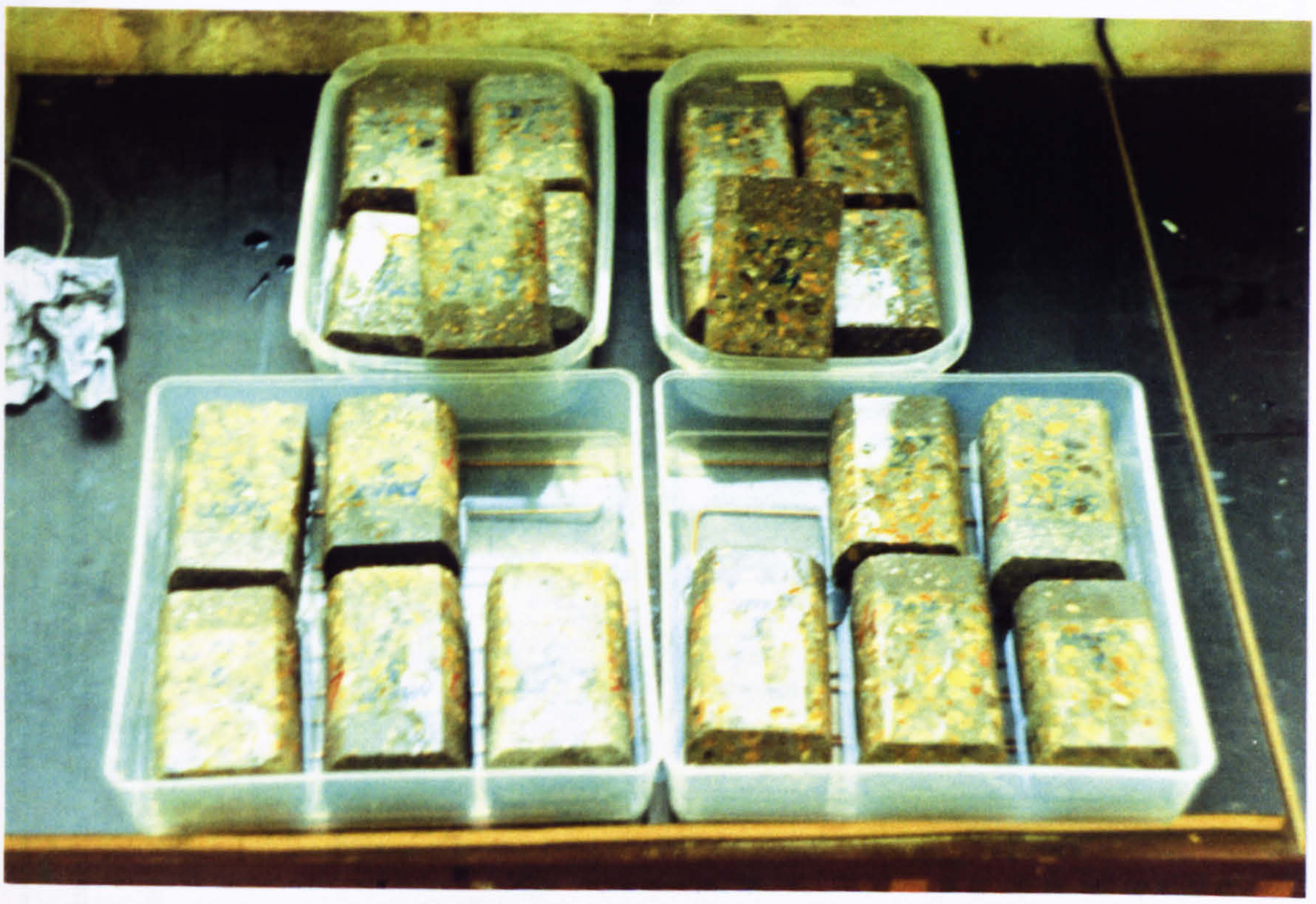

Figure 8.1 - Specimens for freeze-thawing testing.

The experimental procedures were carried out in accordance with ASTM C 666[46] test procedure A which states that, the number of cycles required in this standard was 300 cycles and the temperature limits required versus those achieved in the test are as shown in Figure 8.2. The Velocity of Ultrasonic Pulses[47] and length change in the test specimens were measured throughout the test duration. On completion of the freeze-thaw test, all specimens were subjected to the direct shear test (see chapter 7 for details of this test).

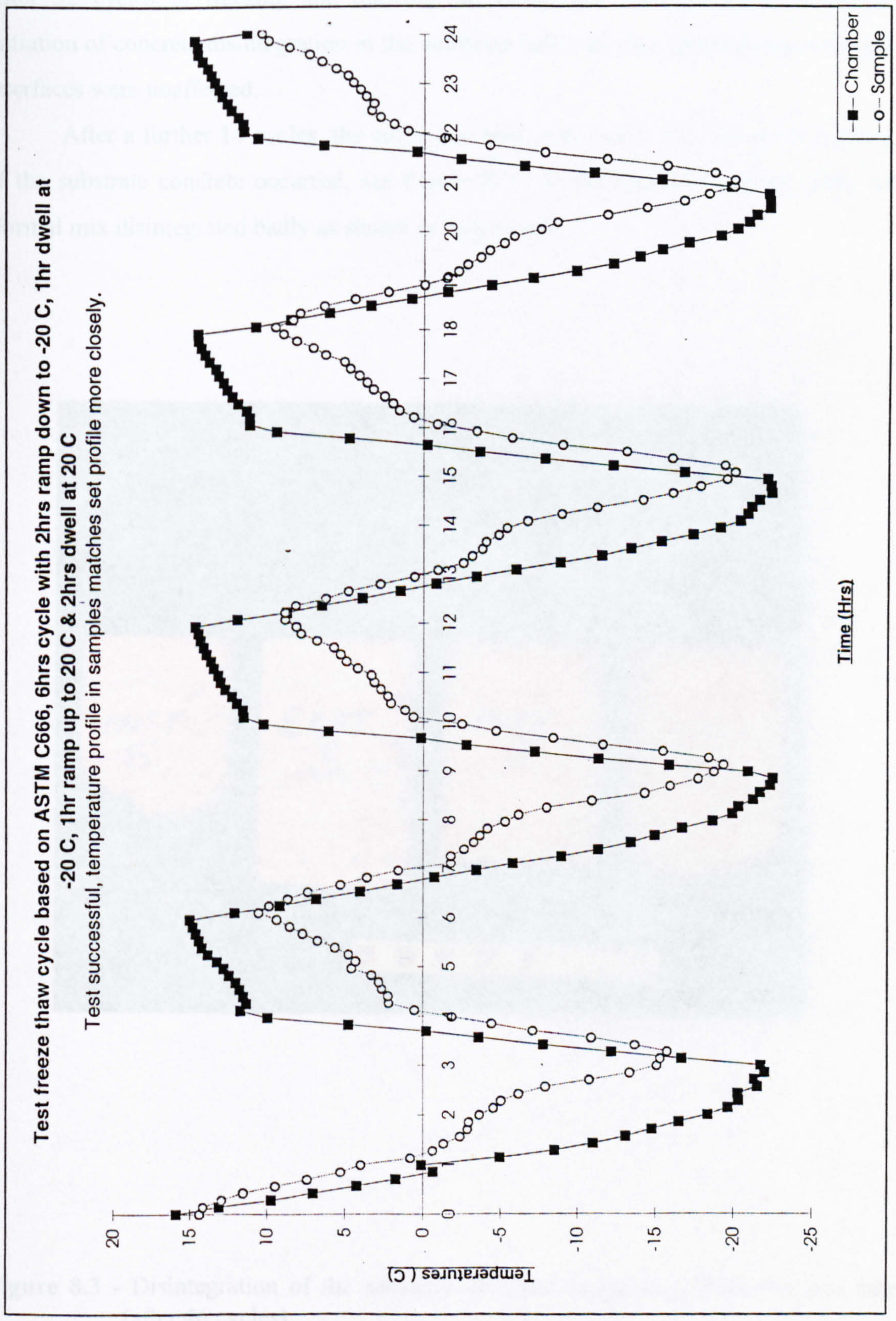

Figure 8.2 - Temperature profile for freeze-thaw testing.

8.2 EXPERIMENTAL RESULTS

After 32 cycles of freezing and thawing, all composite core specimens displayed initiation of concrete disintegration in the substrate half only, the sprayed concretes and interfaces were unaffected.

After a further 14 cycles, the entire test was terminated as severe disintegration of the substrate concrete occurred, see Figure 8.3. In the sprayed concrete, only the Normal mix disintegrated badly as shown in Figure 8.4.

Figure 8.3 - Disintegration of the substrate concrete, progressing from the end face (after 46 cycles)

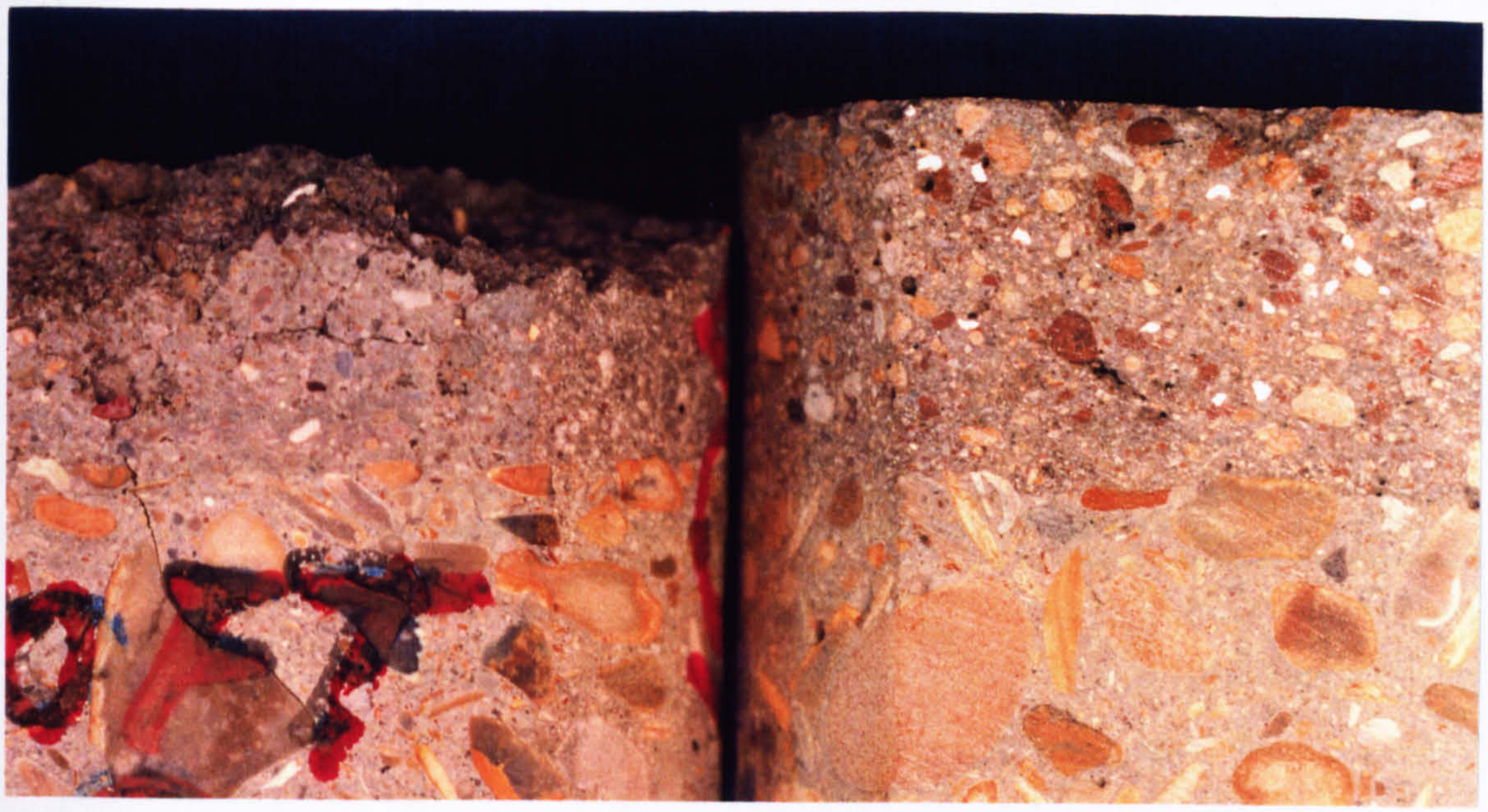

Figure 8.4 - Normal mix sprayed concrete tested (left) untested (right)

Due to the poor resistance of the base specimen particularly under freeze-thaw action, full assessment from the limited velocity of ultrasonic pulses data obtained, cannot be analysed. However, direct shear testing after the test termination are summarised in Table 8.1. The test procedures are already described in section 7.3 of chapter 7.

Where a freeze-thaw tested specimen had severe concrete disintegration, capping was carried out to make up for the lost concrete so that the specimen can be secured into the clamp of the direct shear test apparatus.

Test specimen identification:

Normal Mix: NOFT1 to NOFT6

Sikacem 133 Mix: SKFT1 to SKFT6

Polypropylene Fibre Mix: POFT1 to POFT3

Steel Fibre Mix: STFT1 to STFT5.

Table 8.1 - Direct shear test results.

Specimens NOT tested for freeze-thaw (reproduced from Table 7.3)					
	Normal	Sikacem 133	Steel Fibre	Poly Fibre	Monolithic Specimen
No. of Specimens	3	4	3	4	4
Age (months)	19	19	19	19	19
Average failure shear stress (N/mm^2)	2.44	3.59	2.84	2.77	3.98
As % of Monolithic Specimen	61.3	90.2	71.4	69.6	100.0
Specimens after 46 cycles of freezing and thawing					
No. of Specimens	6	6	5	3	-
Age (months)	19	19	19	19	-
Average failure shear stress (N/mm^2)	1.47	1.6	1	1.08	-

The rapidly repeated cycles of freezing and thawing of ASTM C666-84 have caused:

1. Early deterioration of the base concrete and the Normal mix sprayed concrete.
2. Sikacem 133, Polypropylene and Steel Fibre mixes displayed only slight surface deterioration.
3. In all composite specimens, the disintegration progressed from the substrate concrete ends (see Figure 8.3), although the specimens were partially submerged in 3mm of water.
4. Cracks were observed in most specimens but were at random as shown in Figure 8.4
5. The stiffness of the normal concrete and the substrate concrete were almost lost as the body of the concrete can be chipped away by hand.
6. Significant loss of the bond strength is as shown in the direct shear test result comparisons in Table 8.1, this was due to the cycles of freezing and thawing causing relative thermal deformation between the sprayed concrete and the substrate concrete. However, the normal and sikacem mixes retained their bond strength quite well, this is attributed to them having similar mechanical properties to those of the substrate concrete, see Table 8.2.

Table 8.2 - Some mechanical properties of Sikacem 133 and Normal mixes		
Concrete	Coefficient of linear thermal expansion	Static modulus of elasticity
Normal mix	12.6×10^{-6} /°C (Table 3.4)	24.1 N/mm^2
Sikacemm 133 mix	8×10^{-6} /°C (from supplier)	22.5 N/mm^2 (Table 3.4)
Substrate concrete (C35) standard concrete	12×10^{-6} /°C (Neville[48])	27 N/mm^2 (Kong & Evans[49])

The reported observations clearly show that the composite specimens cannot withstand the cycles of freezing and thawing of ASTM C666. However, the failure was largely due to early deterioration in the substrate concrete portion (which was of the standard ready mixed concrete C35) and therefore the results in this freeze-thaw testing should not penalise the long term durability assessment of the sprayed concrete.

In a study reported by Reading[19] in which sprayed concrete specimens were exposed to cycles of freezing and thawing on site by placing them in the intertidal range of the river, where the typical exposure was about 250 cycles of freezing and thawing in every two years (reportedly a highly aggressive natural freezing and thawing conditions). The analysis of the test results from this site exposure showed that all sprayed concrete specimens performed considerably better than those equivalent specimens tested to ASTM C666, Procedure A - from which Reading concluded that:

> It is possible to produce both dry and wet mix sprayed concrete that will survive the highly aggressive natural freezing and thawing conditions on site. The ASTM S666 Procedure A, rapid freezing and thawing to 300 cycles test, appears to be even more severe than some of the harshest freezing and thawing conditions existing in nature.

CHAPTER 9

THE TIME DEPENDENT PROPERTIES

9.0 GENERAL

This chapter attempts to look into the time dependent properties of the strengthened slab by calculating the stresses in the composite section of the slab caused by the shrinkage and creep as a result of the strengthening sprayed concrete layer.

First, an analytical approach is presented, which is then compared with the experimental results and finally a calculation is performed to indicate the practicality of this technique of strengthening and its potential use in view of the time dependent behaviour.

9.1 ANALYTICAL STUDY OF THE TIME DEPENDENT PROPERTIES

The related analytical studies already published by L. Yam[50] and D. W. Hobbs[51] are referred to and from these a deduction is made on an approach which best represents the behaviour of the strengthened slab under investigation in this research.

9.1.1 Slab dimensioning

Figure 9.1 below shows the cross-section of a metre strip of test slab B6 which was strengthened and was selected for the study being presented in this chapter. This test slab is also referred to as the composite slab.

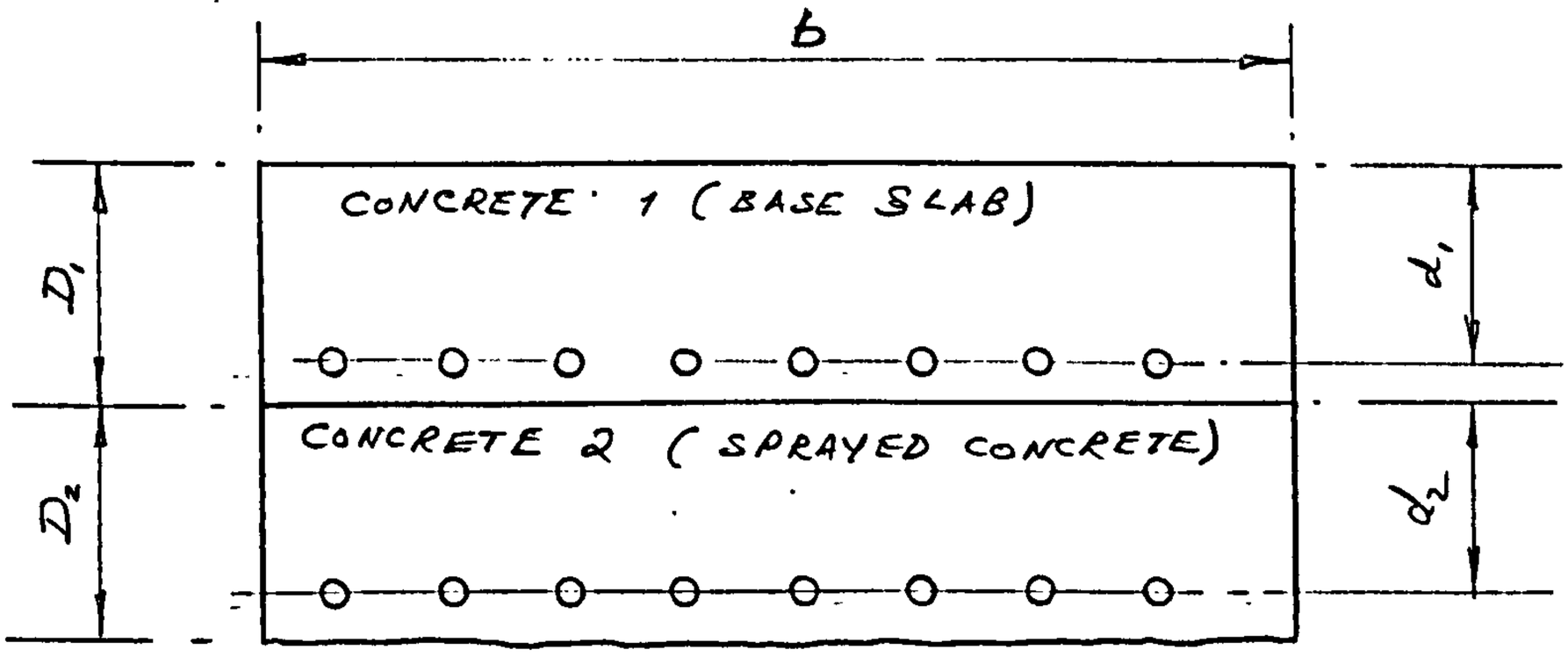

Figure 9.1 - Cross-section of the test slab.

$D_1 = 100$ mm

$D_2 = 75$ mm

$d_1 = 100 - 15 - 3.5 = 81.5$ mm

$d_2 = 75 - 25 - 5 = 45$ mm

$\gamma_1 = E_s/E_{c1} = 205/30 = 6.83$ (modular ratio)

$\gamma_2 = E_{c2}/E_{c1} = 25/30 = 0.83$ (modular ratio)

$A_{s1} = 193$ mm^2/m

$A_{s2} = 393$ mm^2/m

9.1.2 Section properties

The cross-section of the composite slab is transformed into the equivalent cross-section shown in Figure 9.2,

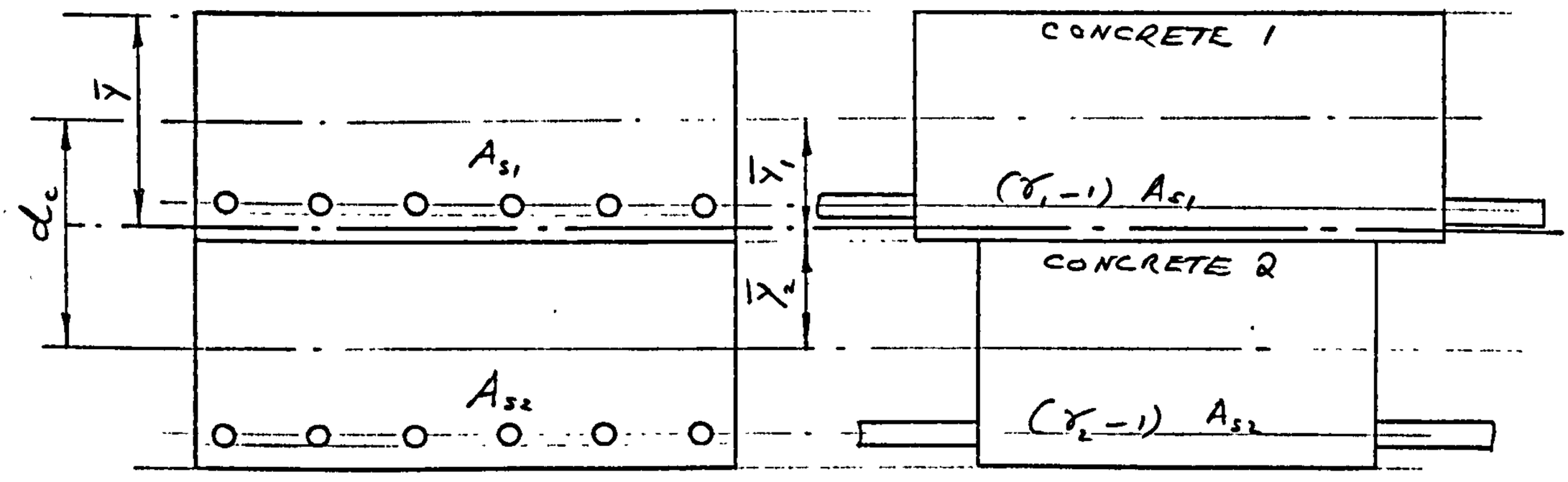

Figure 9.2 - The equivalent transformed cross-section.

Centroid of the composite section ($\bar{y}$)

From Figure 9.2,

$$\bar{y}\,[(1000\times100)+(6.83-1)193+0.83(1000\times75)+(6.83-1)393] = (1000\times100)(50)+$$

$$(6.83-1)(193)(81.5)+(0.83)(1000)(75)\left(100+\frac{75}{2}\right)+(6.83-1)(393)(100+45)$$

$$\bar{y}[1.657\times10^5] = 1.398\times10^7$$

$$\bar{y} = 84.41 \text{ mm}$$

Transformed equivalent areas

$$A_1 = 1000 \text{ x } 100 = 1 \text{ x } 10^5 \text{ mm}^2$$

$$A_2 = 0.83 \text{ [} 1000 \text{ x } 75 \text{]} = 62250 \text{ mm}^2$$

$$(\gamma_1 - 1)A_{s1} = (6.83 - 1)193 = 1125.19 \text{ mm}^2$$

$$(\gamma_1 - 1)A_{s2} = (6.83 - 1)393 = 2291.19 \text{ mm}^2$$

Centroids of the individual concrete sections about the interface

$$\bar{y}_1 \left[[(1000 \times 100) + (6.83 - 1)193]\right] = (1000 \times 100 \times 50) + (6.83 - 1)(15 + 3.5)193$$

$$\bar{y}_1 = 49.65 \text{ mm}$$

$$\bar{y}_2 \left[[(1000 \times 75)0.83 + (6.83 - 1)393]\right] = (1000 \times 75 \times 0.83 \times 37.5) + (6.83 - 1)(45)393$$

$$\bar{y}_2 = 37.77 \text{ mm}$$

$$d_c = \bar{y}_1 + \bar{y}_2 = 49.65 + 37.77 = 87.42 \text{ mm}$$

Second moment of areas about the centroidal axis

From Figure 9.2,

$$I_{c1} = \frac{(1000 \times 100^3)}{12} + (6.83 - 1)(193)(49.65 - 18.5)^2 + (1000 \times 100)(50 - 49.65)^2$$

$$I_{c2} = 8.44 \text{ x } 10^7 \text{ mm}^4$$

$$I_{c2} = \frac{(1000 \times 75^3)}{12} + (6.83 - 1)(193)(45 - 37.77)^2 + (1000 \times 75)(37.77 - 37.5)^2$$

$$I_{c1} = 3.53 \text{ x } 10^7 \text{ mm}^4$$

Young 's modulii

$$E_{c1} = 30{,}000 \text{ N/mm}^2$$

$$E_{c2} = 25{,}000 \text{ N/mm}^2$$

$$E_s = 205{,}000 \text{ N/mm}^2$$

9.1.3 Yam's Theory

In Yam's theory, the concept of free strain is considered for the strain at a point in the material which is free from stresses under the actions of

1. Shrinkage
2. Creep
3. Temperature effect

The composite section is assumed to be unstressed in the initial state and to have developed the following strains after a period of time

$$e_f = e_s + e_c + e_t$$

where e_f = free strain corresponding to zero stress

e_s = strain due to shrinkage

e_c = compressive strain due to creep

e_t = strain due to decrease in temperature

As time increases, deformation becomes more pronounced (relative deformation of base concrete and sprayed concrete) and provided the horizontal shear stress capacity at the interface is not exceeded, i.e. no slippage at the interface, the composite section is constrained against deformation and consequently the initial unstressed state has now become stressed due to this constraint.

Therefore, if the composite section is free to deform, planes will remain plane, the deformation can be defined by an imposed uniform strain (due to axial compression) together with an imposed curvature due to pure bending about the neutral axis, provided there is no interface slippage:

For equilibrium, the deformations are:

- A uniform axial e_n at the neutral axis

$$C_f = e_n (E_s A_s + A_c E_c)$$

Compression due to the free strain = Compression due to imposed axial strain

- A curvature K

$$M_f = K (1 + \alpha) (E_s I_s + E_c I_c)$$

Moment due to free strain = Imposed moment, hence curvature

where:

α = composite stiffness factor

e_n = axial strain at neutral axis

E_s = Young's Modulus of steel reinforcement

E_c = Young's Modulus of concrete

I_s = Second moment of area of steel reinforcement

I_c = Second moment of area of concrete.

9.1.3.1 Stress parameters

The composite factor (α)

$$\alpha = \left[\frac{(E_{c1}\,A_{c1})(E_{c2}\,A_{c2})}{E_{c1}\,A_{c1} + E_{c2}\,A_{c2}}\right] \times \left[\frac{d_c^{\,2}}{E_{c1}\,I_{c1} + E_{c2}\,I_{c2}}\right]$$

From Yam 's theory, α depends only on the section properties and shows the extent of the composite action and was derived from the assumption that full composite action is maintained between the two concretes.

$A_{c1} = bD_1 + (\gamma_1 - 1)A_{s1} = (1000)(100) + (6.83-1)193 = 101125\ mm^2$

$A_{c2} = bD_2 + (\gamma_1 - 1)A_{s2} = (1000)(75) + (6.83 - 1)393 = 77291 mm^2$

$d_c = 87.42\ mm$

$I_{c1} = 8.44 \times 10^7\ mm^4$

$I_{c2} = 3.53 \times 10^7\ mm^4$

Giving α,

$$\alpha = \frac{30000 \times 101125 \times 20000 \times 77291 \times 87.42^2}{[(25000 \times 77291) + (30000 \times 101125)] \times [(30000 \times 8.44 \times 10^7) + (25000 \times 3.53 \times 10^7)]}$$

$$\alpha = 2.642$$

Direct forces in the concrete (C) due to shrinkage of the sprayed layer

The induced compressive force in the base slab due to the shrinkage of the sprayed concretes can be evaluated from Yam 's theory:

From longitudinal equilibrium, the tension in the shrinking concrete must be equal and opposite to this compression as,

$$C = -\frac{(E_{c1}\,A_{c1})(E_{c2}\,A_{c2})\,e_1}{(E_{c1}\,A_{c1} + E_{c2}\,A_{c2})(1+\alpha)}$$

Where e_1 = Free shrinkage strain, taken from L. J. Parrott[52].

$$e_1 = 100 \times 10^{-6}$$

$$C = -\frac{30000 \times 101125 \times 25000 \times 77291 \times 100 \times 10^{-6}}{[(30000 \times 101125) + (25000 \times 77291)] \times [1 + 2.64]}$$

$$C = -32429\ N$$

9.1.3.2 Curvature due to shrinkage (K)

Due to the shrinkage of the sprayed concrete layer, the composite slab will develop an upward curvature of ,

$$K = \frac{\alpha\, e_1}{(1+\alpha) d_c} = \frac{2.64 \times 100 \times 10^{-6}}{(1+2.64)\,(87.42)}$$

$$K = 0.83 \times 10^{-6}$$

Elastic section modulii (Z)

The Z values are determined for the composite slab shown in Figure 9.3.

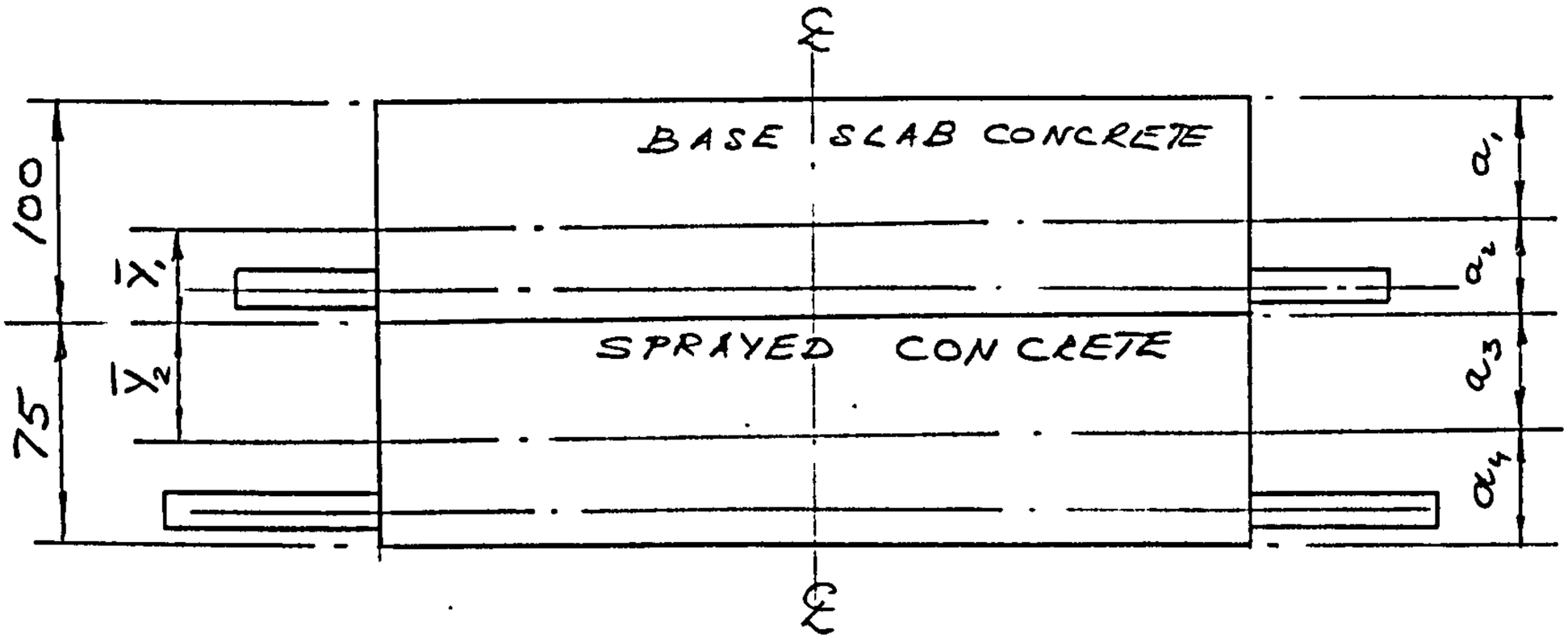

Figure 9.3 - Z value determination for the composite slab.

Top of the base concrete, $$Z_{c1} = \frac{I_{c1}}{a_1} = \frac{8.44 \times 10^7}{100 - 49.65} = 1.676 \times 10^6 \text{ mm}^3$$

Underside of the base concrete, $$Z_{c2} = \frac{I_{c1}}{a_2} = \frac{8.44 \times 10^7}{49.65} = 1.700 \times 10^6 \text{ mm}^3$$

Top of the sprayed concrete, $$Z_{c3} = \frac{I_{c2}}{a_3} = \frac{3.53 \times 10^7}{37.77} = 0.935 \times 10^6 \text{ mm}^3$$

Top of the sprayed concrete, $$Z_{c4} = \frac{I_{c2}}{a_4} = \frac{3.53 \times 10^7}{75 - 37.77} = 0.948 \times 10^6 \text{ mm}^3$$

Stresses in the composite section - from L. Yam 's theory

This calculation combines the direct stresses with the flexural stresses caused by the curvature.

Top of the base concrete,
$$\sigma_1 = \frac{-C}{A_{c1}} - \frac{K E_{c1} I_{c1}}{Z_{c1}}$$
$$\sigma_1 = \frac{32429}{101125} - \frac{8.3 \times 10^{-7}\left(8.44 \times 10^7\right)30000}{1.676 \times 10^6} = -0.93 \text{ N / mm}^2$$

Underside of the base concrete,
$$\sigma_2 = \frac{-C}{A_{c1}} + \frac{K E_{c1} I_{c1}}{Z_{c2}}$$
$$\sigma_2 = \frac{32429}{101125} + \frac{8.3 \times 10^{-7}\left(8.44 \times 10^7\right)30000}{1.700 \times 10^6} = 1.56 \text{ N / mm}^2$$

Top of the sprayed concrete,
$$\sigma_3 = \frac{C}{A_{c2}} - \frac{K E_{c2} I_{c2}}{Z_{c3}}$$
$$\sigma_3 = -\frac{32429}{77291} - \frac{8.3 \times 10^{-7}\left(3.53 \times 10^7\right)25000}{0.935 \times 10^6} = -1.2 \text{ N / mm}^2$$

Underside of the sprayed concrete,
$$\sigma_4 = \frac{C}{A_{c2}} + \frac{K E_{c2} I_{c2}}{Z_{c4}}$$
$$\sigma_4 = -\frac{32429}{77291} + \frac{8.3 \times 10^{-7}\left(3.53 \times 10^7\right)25000}{0.948 \times 10^6} = 0.36 \text{ N / mm}^2$$

In a later section of this chapter, the calculated stresses shall be superimposed on a stress diagram with those calculated from Hobbs' theory from which the significance of the stress values will be assessed and a recommended theory shall be presented.

9.1.4 D. W. Hobbs' Theory

9.1.4.1 Induced moment due to the shrinkage of the sprayed concrete

Consider Figure 9.4, the sprayed concrete is first assumed to be free to shrink and this is only possible if the reinforcement and the substrate concrete are compressed by the fictitious forces are as follow:

$F_1 = \varepsilon_{cs} \cdot A_1 \cdot E_{c1}$ _____Fictitious force acting on the substrate concrete

$F_2 = \varepsilon_{cs} \cdot A_{s1} \cdot E_s$ _____Fictitious force acting on the upper level steel

$F_3 = \varepsilon_{cs} \cdot A_{s2} \cdot E_s$ _____Fictitious force acting on the lower level steel

It is pointed out that these three forces are restraining the sprayed concrete from free shrinkage. Therefore the hypothetical fictitious forces are introduced to allow for the shrinkage of the sprayed concrete.

When the three fictitious are released, the effect is equivalent to eccentric tensile forces:

$$F_1 = \varepsilon_{cs} \cdot A_1 \cdot E_{c1}$$

$$F_2 = \varepsilon_{cs} \cdot A_{s1} \cdot E_s$$

$$F_3 = \varepsilon_{cs} \cdot A_{s2} \cdot E_s$$

being applied to the entire transformed area of the composite concrete section, at the steel levels and the substrate concrete's centroid, as shown below in Figure 9.4.

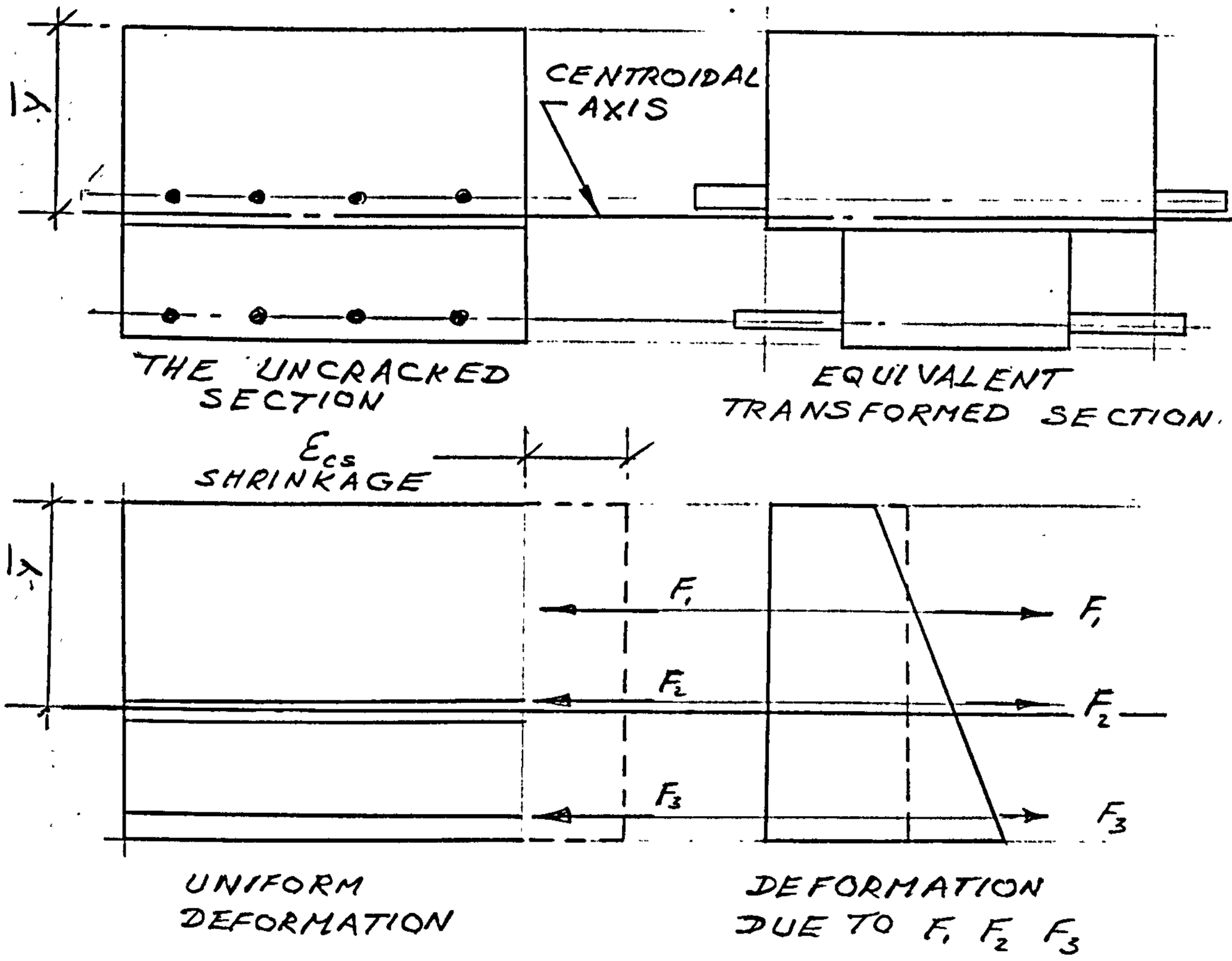

Figure 9.4 - D. W. Hobbs' Theory.

The eccentric forces produce a bending moment and consequently a curvature of the composite concrete section. The bending moment produced by the shrinkage is:

$$M = F_1\left[\bar{y} - \frac{D_1}{2}\right] + F_2\left[\bar{y} - d_1\right] - F_3\left[D_1 + d_2 - \bar{y}\right]$$

Making the above substitution,

$$M = \varepsilon_{cs}\, E_{c1}\, A_1\left[\bar{y} - \frac{D_1}{2}\right] + \varepsilon_{cs}\, E_s\, A_{s1}\left[\bar{y} - d_1\right] - \varepsilon_{cs}\, E_s\, A_{s2}\left[D_1 + d_2 - \bar{y}\right]$$

9.1.4.2 Curvature due shrinkage (K)

$$K = \frac{[1+\psi] M_{cs}}{E_{c2}\ I_u}$$

Where ψ = The creep coefficient

Making the substitution for M above

$$K = \frac{[1+\psi]\varepsilon_{cs}\left[A_1 E_{c1}\left(\bar{y} - \frac{D_1}{2}\right) + A_{s1}E_s(\bar{y} - d_1) - E_s A_{s2}(D_1 - d_2 - \bar{y})\right]}{E_{c2} I_u}$$

Transforming all E(s) to E_{c1} by applying the following modular ratios,

$$\gamma_1 = \frac{E_s}{E_{c1}} \qquad \text{and} \qquad \gamma_2 = \frac{E_{c2}}{E_{c1}}$$

$$E_s = \gamma_1 E_{c1} \qquad E_{c2} = \gamma_2 E_{c1}$$

Giving,

$$K = \frac{\varepsilon_{cs}[1+\psi]\left[A_1\left(\bar{y} - \frac{D_1}{2}\right) + (\gamma_1 - 1)A_{s1}(\bar{y} - d_1) - (\gamma_1 - 1)A_{s2}(D_1 + d_2 - \bar{y})\right]}{\lambda_2\ I_u}$$

$\varepsilon_{cs} = 100 \times 10^{-6}$ assumed from Parrott

$\psi = 2$ from Parrott[52], assuming UK exposure and 80% relative humidity

$A_1 = 1000 \times 100\ mm^2$

$A_{s1} = 193\ mm^2$

$A_{s2} = 393\ mm^2$

I_u = calculated as follows (The uncracked section assumed)

$\gamma_1 = 6.83$

$\gamma_2 = 0.83$

$\bar{y} = 84.41$ mm

$d_1 = 81.5$ mm

$d_2 = 45$ mm

$D_1 = 100$ mm

The second moment of area of the transformed uncracked section about the centroidal axis (I_u)

From Figure 9.4,

$$I_u = \frac{1000 \times 100^3}{12} + (100 \times 1000)(84.41 - 50)^2 + (6.83 - 1)\,193\,(84.41 - 81.5)^2$$

$$(6.83 - 1)\,393\,(145 - 84.41)^2 + 0.83\frac{1000 \times 75^3}{12} + (0.83 \times 1000 \times 75)\left(100 + \frac{75}{2} - 84.41\right)^2$$

$$I_u = 4.15 \times 10^8 \text{ mm}^4$$

Therefore giving K:

$$K = \frac{(1+2)100 \times 10^{-6}\left[1 \times 10^5 (84.41 - 50) + 5.83 \times 193(84.41 - 81.5) - 5.83 \times 393(100 + 45 - 84.4)\right]}{0.83\left(4.15 \times 10^8\right)}$$

$$K = (1+2)\ 0.96 \times 10^{-6}$$

$$K = 2.88 \times 10^{-6}$$

Stresses in the composite section - From Hobbs' theory

Note that in the following stress equations, the physical parameters based from Yam 's theory and the critical curvature K is from Hobbs':

Top of the base concrete,

$$\sigma_1 = \frac{-C}{A_{c1}} - \frac{K\,E_{c1}\,I_{c1}}{Z_{c1}}$$

$$\sigma_1 = \frac{32429}{101125} - \frac{2.88 \times 10^{-6}\left(8.44 \times 10^7\right)30000}{1.676 \times 10^6} = -4.03 \text{ N / mm}^2$$

Underside of the base concrete,

$$\sigma_2 = \frac{-C}{A_{c1}} + \frac{K\,E_{c1}\,I_{c1}}{Z_{c2}}$$

$$\sigma_2 = \frac{32429}{101125} + \frac{2.88 \times 10^{-6}\left(8.44 \times 10^7\right)30000}{1.700 \times 10^6} = 4.61 \text{ N / mm}^2$$

$$\sigma_3 = \frac{C}{A_{c2}} - \frac{K E_{c2} I_{c2}}{Z_{c3}}$$

Top of the sprayed concrete,

$$\sigma_3 = \frac{-32429}{77291} - \frac{2.88\times10^{-6}(3.53\times10^{7})25000}{0.935\times10^{6}} = -3.14\ \mathrm{N/mm^2}$$

Underside of the sprayed concrete,

$$\sigma_4 = \frac{C}{A_{c2}} + \frac{K E_{c2} I_{c2}}{Z_{c4}}$$

$$\sigma_4 = \frac{-32429}{77291} + \frac{2.88\times10^{-6}(3.53\times10^{7})25000}{0.948\times10^{6}} = 2.26\ \mathrm{N/mm^2}$$

9.1.5 Shrinkage stresses using Yam 's theory with effective E value

An immediate comparison can be made between K = 0.83 x 10^{-6} from Yam 's theory (section 9.1.3.2) and K = 2.88 x 10^{-6} from Hobbs' (section 9.1.4.2) which contains the creep coefficient $\psi = 2$, clearly the K value from Hobbs' is sensitive to ψ. Returning to Yam's theory and using the effective (or long term) E value of the base concrete, the value of which is a recommendation of BS 8110: Part 2: cl 3.6 [13] as,

$$E_{eff} = \frac{E_{concrete}}{1+\psi}$$

Assuming $\psi = 1$ so that $E_{eff} = 0.5$ x $E_{concrete}$ and this is the accepted practice in design offices. With this effective E value, the following parameters were re-calculated

$E_{c1} = 15000\ \mathrm{N/mm^2}$	$I_{c1} = 8.57$ x $10^7\ \mathrm{mm^4}$
$E_{c2} = 25000\ \mathrm{N/mm^2}$	$I_{c2} = 3.53$ x $10^7\ \mathrm{mm^4}$
C = -21529 N	$Z_{c1} = 1.689$ x $10^6\ \mathrm{mm^3}$
$A_{c1} = 102445\ \mathrm{mm^2}$	$Z_{c2} = 1.74$ x $10^6\ \mathrm{mm^3}$
$A_{c2} = 79979\ \mathrm{mm^2}$	$Z_{c3} = 0.934$ x $10^6\ \mathrm{mm^3}$
K = 0.86 x 10^{-6}	$Z_{c4} = 0.949$ x $10^6\ \mathrm{mm^3}$

$$\sigma_1 = \frac{-C}{A_{c1}} - \frac{K E_{c1} I_{c1}}{Z_{c1}}$$

Top of the base concrete,

$$\sigma_1 = \frac{21529}{102445} - \frac{8.6\times10^{-7}(8.57\times10^{7})15000}{1.689\times10^{6}} = -0.44\ \mathrm{N/mm^2}$$

$$\sigma_2 = \frac{-C}{A_{c1}} + \frac{K\,E_{c1}\,I_{c1}}{Z_{c2}}$$

Underside of the base concrete,

$$\sigma_2 = \frac{21529}{102445} + \frac{8.6\times10^{-7}\left(8.57\times10^{7}\right)15000}{1.74\times10^{6}} = 0.85\ \mathrm{N/mm^2}$$

$$\sigma_3 = \frac{C}{A_{c2}} - \frac{K\,E_{c2}\,I_{c2}}{Z_{c3}}$$

Top of the sprayed concrete,

$$\sigma_3 = -\frac{21529}{79979} - \frac{8.6\times10^{-7}\left(3.53\times10^{7}\right)25000}{0.934\times10^{6}} = -1.08\ \mathrm{N/mm^2}$$

Underside of the sprayed concrete,

$$\sigma_4 = \frac{C}{A_{c2}} + \frac{K\,E_{c2}\,I_{c2}}{Z_{c4}}$$

$$\sigma_4 = -\frac{21529}{79979} + \frac{8.6\times10^{-7}\left(3.53\times10^{7}\right)25000}{0.949\times10^{6}} = 0.53\ \mathrm{N/mm^2}$$

9.1.6 The recommended theory in predicting shrinkage stresses

First, the stresses in the composite concrete slab due to shrinkage of the sprayed concrete layer, predicted from Yam, Hobbs and Yam 's with effective E values are superimposed as shown in Figure 9.5. The following table summarises the calculated stresses.

Table 9.1 - Three thoeretical calculations of shrinkage stresses

Theory	σ_1 (N/mm^2)	σ_2 (N/mm^2)	σ_3 (N/mm^2)	σ_4 (N/mm^2)
L. Yam	-0.93	1.56	-1.2	0.36
Hobbs, $\psi = 0$	-1.12	1.75	-1.33	0.47
Hobbs, $\psi = 1$	-2.57	3.18	-2.24	1.36
Hobbs, $\psi = 2$	-4.02	4.61	-3.14	2.26
L. Yam (with effective E value)	-0.44	0.85	-1.08	0.53

It can be seen from Table 9.1 that the use of ψ in Hobbs' equation seems to cause too large a change in the curvature K. However, using Yam 's theory with the effective E value only causes a small change in the K value. Therefore Yam 's theory appears suitable to be used for calculation of stresses in the composite section due to the shrinkage of the sprayed concrete layer.

Figure 9.5 - Stresses in the composite concrete slab due to shrinkage

C	A_{C1}	A_{C2}	E_{C1}	E_{C2}	I_{C1}	I_{C2}	Z_{C1}	Z_{C2}	Z_{C3}	Z_{C4}	ψ	k	σ_1	σ_2	σ_3	σ_4
From L. Yam's theory (ψ does not enter the equation of K)												8.30E-07	-0.93	1.56	-1.21	0.35
-32909	101125	77291	30000	25000	8.44E+07	3.82E+07	1.68E+06	1.70E+06	1.01E+06	1.03E+06	0	9.60E-07	-1.12	1.75	-1.33	0.47
-32909	101125	77291	30000	25000	8.44E+07	3.82E+07	1.68E+06	1.70E+06	1.01E+06	1.03E+06	1	1.92E-06	-2.57	3.18	-2.24	1.36
-32909	101125	77291	30000	25000	8.44E+07	3.82E+07	1.68E+06	1.70E+06	1.01E+06	1.03E+06	2	2.88E-06	-4.02	4.61	-3.15	2.25
From L. Yam's theory with reduced E values(ψ does not enter the equation of K)												8.60E-07	-0.44	0.85	-1.08	0.53
													0	100	100	175

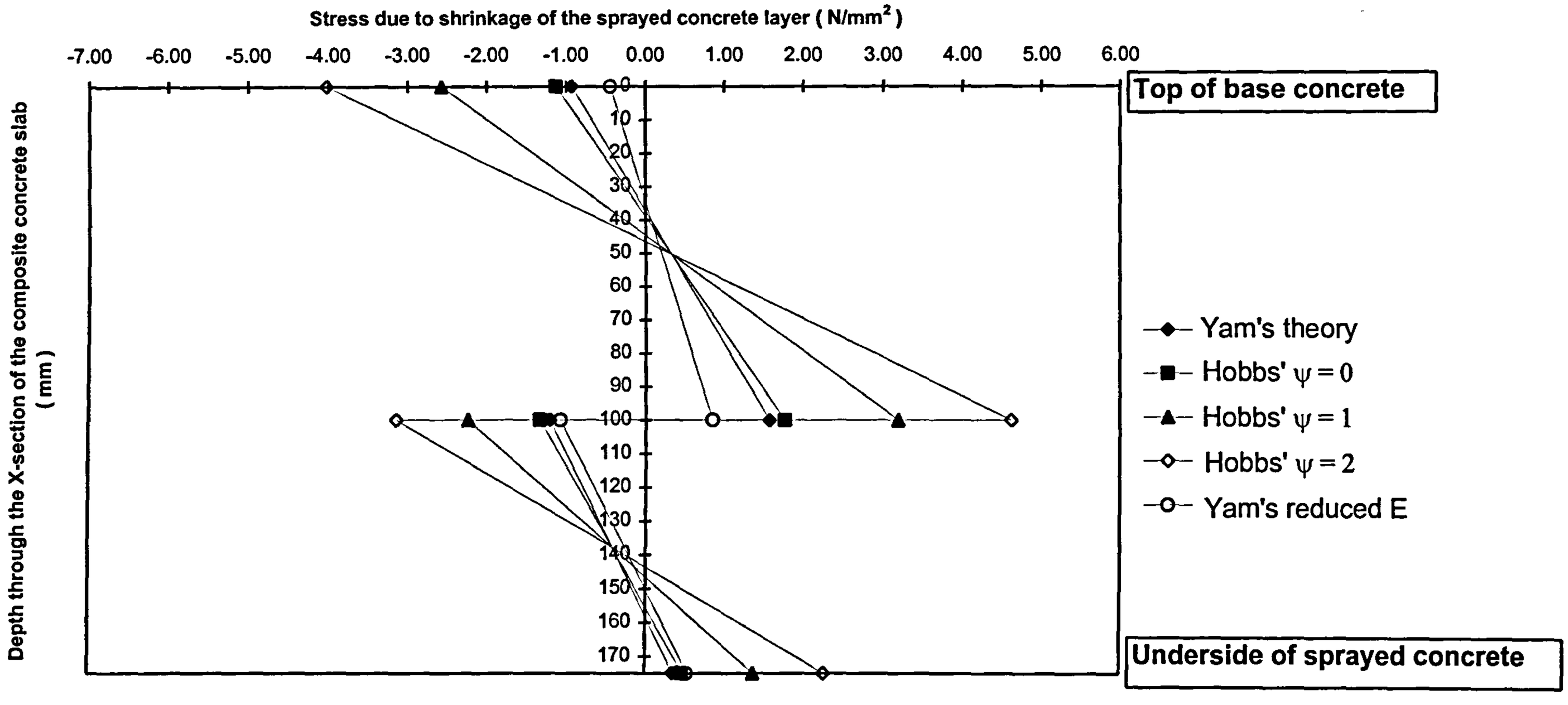

9.2 EXPERIMENTAL INTERFACE STRESSES

This section presents the stresses calculated at the interface between the base concrete and the sprayed concrete of the test slab, using the strain measured experimentally.

9.2.1 Experimental set up for strain measurement

As time did not permit an elaborate set up of this experiment, it was kept relatively simple. Test slab B6 was selected for the strain gauge attachment and this was made after the R-C base concrete slab was removed from its casting mould.

A total of six Mortar/Concrete Embedded type strain gauges were attached to the base concrete slab; three on the top face and three on the underside, this is shown in Figure 9.6.

Recesses were made in the slab to accommodate the strain gauges and they were then properly sealed into position by applying a cover to the gauges of grout. This grout also served to protect the gauges from the abrasive action of the grit blasting process. Figure 9.7 shows a strain gauge purposely exposed for observation from the underside of the base slab just before the concrete spraying process (note the grit-blasted finish of the base concrete 's underside and the attachment of the reinforcement for the sprayed concrete layer)

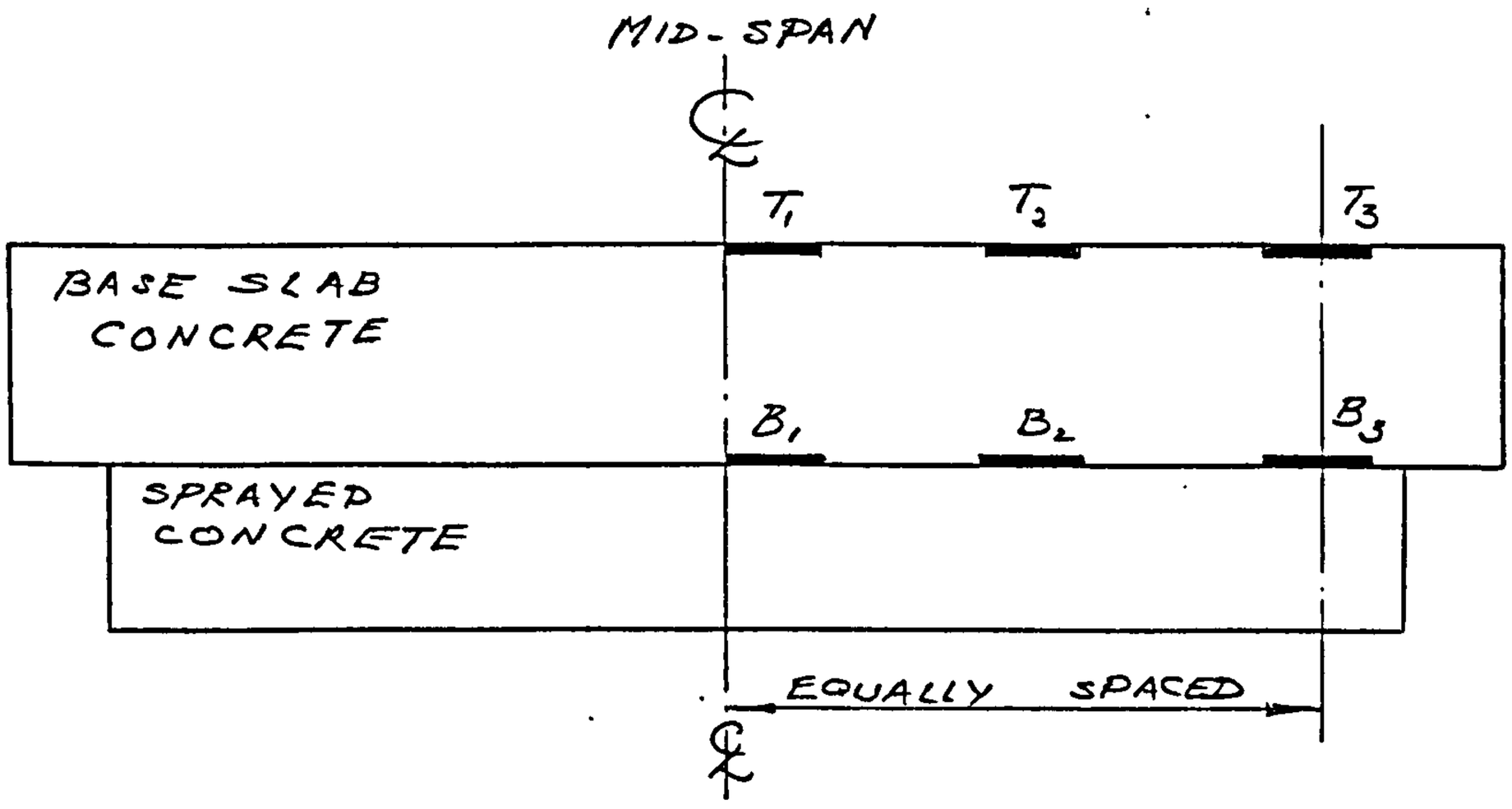

Figure 9.6 - Positions of the strain gauges on the base concrete slab.

Figure 9.7 - A prepared strain gauge attachment, just before the concrete spraying process (looking from below soffit).

All the strain gauges were connected to a strain gauge monitor and the readings were taken immediately after the required sprayed concrete thickness was achieved. Readings were subsequently taken at 24-hour intervals over a period of two and a half months.

Table 9.2 shows the effective strain readings over this period at different points of attachment, based on the following conversion formula (from the strain gauge manufacturer),

$$e = \frac{4 \times V_{out}}{V \times K}$$

Where:

e = Strain in microstrain

V_{out} = Output voltage in microVolts

V = Excitation voltage or bridge voltage

K = Gauge factor

Table 9.2 - Effective strain in the strengthened test slab				
Gauge Position	V_{out} (mV)	Gauge Factor	Excitation Voltage (V)	Effective strain at 2.5 months
T_1	0.92	1.8	5	4.09×10^{-4}
B_1	0.88	1.8	5	3.91×10^{-4}
T_2	1.09	1.8	5	4.84×10^{-4}
B_2	0.78	1.8	5	3.47×10^{-4}
T_3	0.86	1.8	5	3.82×10^{-4}
B_3	0.76	1.8	5	3.38×10^{-4}

9.2.2 Interface stress calculation from experimental strain

Using the simple relationship,

$$E = \frac{\sigma}{\varepsilon}$$

Where:

E = The effective E value

ε = The maximum strain at the interface from Table 9.2.

$$\sigma = E \times \varepsilon$$

$$\sigma_{interface} = 15000 \times (3.91 \times 10^{-4})$$

$$\sigma_{interface} = 5.9 \text{ N/mm}^2$$

Clearly, there is a large difference in comparing this figure and those calculated analytically in Table 9.1 and as a result the author decided not to pursue this discussion further. However, an explanation for this difference is now presented:

Although the gauges used were of the correct type and were properly attached to the test slabs, the apparatus used and the setting up to record the strains were inadequate and perhaps incompatible.

The tight preparation schedule leading up to the arrival of the outside contractor (Structural Repairs Limited) for the major spraying concrete operation in the laboratory did not allow sufficient time to arrange for a compatible data acquisition system for strain gauge measurement.

9.3 PRACTICAL APPLICATION OF THE RECOMMENDED THEORY

This section intends to show the application of the recommended theory in calculating the flexural stresses developed in a structural concrete member due to shrinkage, after strengthening using the technique being researched here and thereby indicates the practicality of this technique of strengthening.

The calculation is based on the strengthened two lane single carriageway bridge modelled in chapter 5.

In order to perform the calculation, a practical layer of reinforced sprayed concrete shall be used and that the composite action that it provides will result in the 30% strengthening factor in the strengthened bridge which was assumed originally to be 30% short of the capacity to carry the new EC load requirement on highway bridges of 40 tons.

It is pointed out that the figure 30% is in fact the general upper bound strengthening factor to which bridges in the UK that were found to have failed the 40 tons load capacity criterion and were subsequently strengthened. It is stressed however, that the 30% figure is by no means the strengthening factor to which bridges in the UK are being strengthened to, but it is the general figure according to practising consulting engineers.

9.3.1 Additional moment capacity required

From QSE grillage analysis of the two-lane single carriageway, in Appendix E, the total maximum design at ULS is:

$$M = \frac{2157}{2.06} \quad \text{KNm / m width of the bridge}$$

$$M = 1047 \quad \text{KNm / m width of the bridge}$$

Assuming that the bridge being modelled is 30% under-strength so that its existing strength is:

$$M = \frac{1047}{1.3} \quad \text{KNm / m width of the bridge}$$

$$M = 805 \quad \text{KNm / m width of the bridge}$$

The additional moment capacity required is:

$$M_{add} = 1048 - 805 \text{ kNm/m}$$

$$M_{add} = 242 \text{ kNm/m}$$

The designed reinforced sprayed concrete layer is to resist this additional moment and therefore the resulting composite action in the strengthened bridge shall replace the 30 % under-strength.

9.3.2 Designing the reinforced sprayed concrete layer

The following calculation is based on BS 8110: Part 1: 1985: Cl 3.4.4.4,

The existing moment capacity of the bridge is 805 kNm/m width.

Assuming 32 mm ∅ bars and 50 mm cover to main bars.

$$d = 750 - 50 - \frac{32}{2} = 684 \text{ mm}$$

$$f_{cu} = 30 \text{ N/mm}^2$$

$$K = \frac{M}{bd^2 f_{cu}} = \frac{805 \times 10^6}{1000 \times 684^2 \times 30}$$

$$K = 0.057 \qquad < K' = 0.156$$

Therefore singly reinforcement provision is OK.

$$z = d\left[0.5 + \sqrt{0.25 - \frac{K}{0.9}}\right]$$

$$z = 684\left[0.5 + \sqrt{0.25 - \frac{0.057}{0.9}}\right]$$

$$z = 637 \text{ mm} \qquad \text{not greater than } 0.95d = 0.95 \times 684 = 650 \text{ mm}$$

$$z = 637 \text{ mm}$$

$$A_s = \frac{M}{0.87 f_y z}$$

$$A_s = \frac{805 \times 10^6}{0.87 \times 460 \times 637}$$

$$A_s = 3162 \text{ mm}^2 / \text{m}$$

$$\text{Total tension force} = \frac{M}{z}$$

$$= \frac{805}{0.93 \times 0.684}$$

$$= 1265.5 \text{ kN/m}$$

Total tension force = Total compression force

$$\text{Depth of stress block} = \frac{1265.5}{0.45 \times 30 \times 1000}$$

Depth of stress block = 93.7 mm, as shown in Figure 9.8

The stress block,

This is based on the yield conditions of the base concrete and its tension reinforcement, assumed 32 mm Ø bars.,

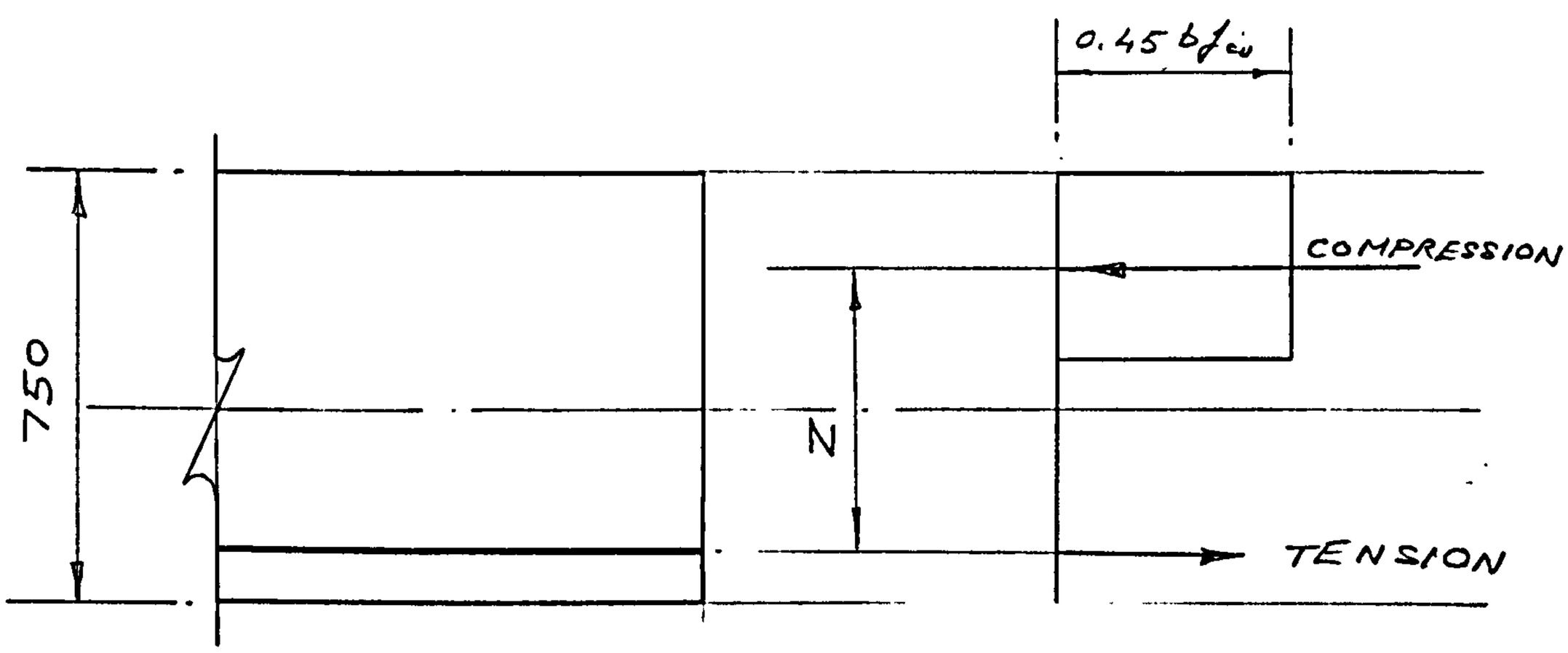

Figure 9.8 - Stress block being used.

Reinforcement in the sprayed concrete layer,

The moment to be resisted by this layer is 242 kNm/m width.

Assuming,

10 mm Ø tension bars

85 mm sprayed concrete layer thickness.

d = 750 + 85 - 50 - 10 = 775m

Assuming,

10 mm Ø tension bars

85 mm sprayed concrete layer thickness.

d = 750 + 85 - 50 - 10 = 775m

Increase the stress block to say, 120 mm

z_1 = 684 - 60 = 624_____Reinf't in the existing bridge slab

z_2 = 775 - 60 = 715_____Reinf't in the sprayed concrete strengthening layer.

M_{total} = 1048 kNm/m

$M_{total} = 1265.5\ z_1 + T_2\ z_2$

$1048 = 1265.5\ (0.624) + T_2\ (0.715)$

T_2 = 361.3 KN/m

$T_2 = 0.87\ f_y\ A_s$

$$A_s = \frac{361.3 \times 1000}{0.87 \times 460}$$

$A_s = 903\ mm^2 / m$

Provide in the sprayed concrete strengthening layer B1131 structural mesh reinforcement.

9.3.3 Designing the reinforcement in the modelled bridge

The reinforcement was designed in accordance with BS 8110. The calculations were similar to those presented in Appendix C.

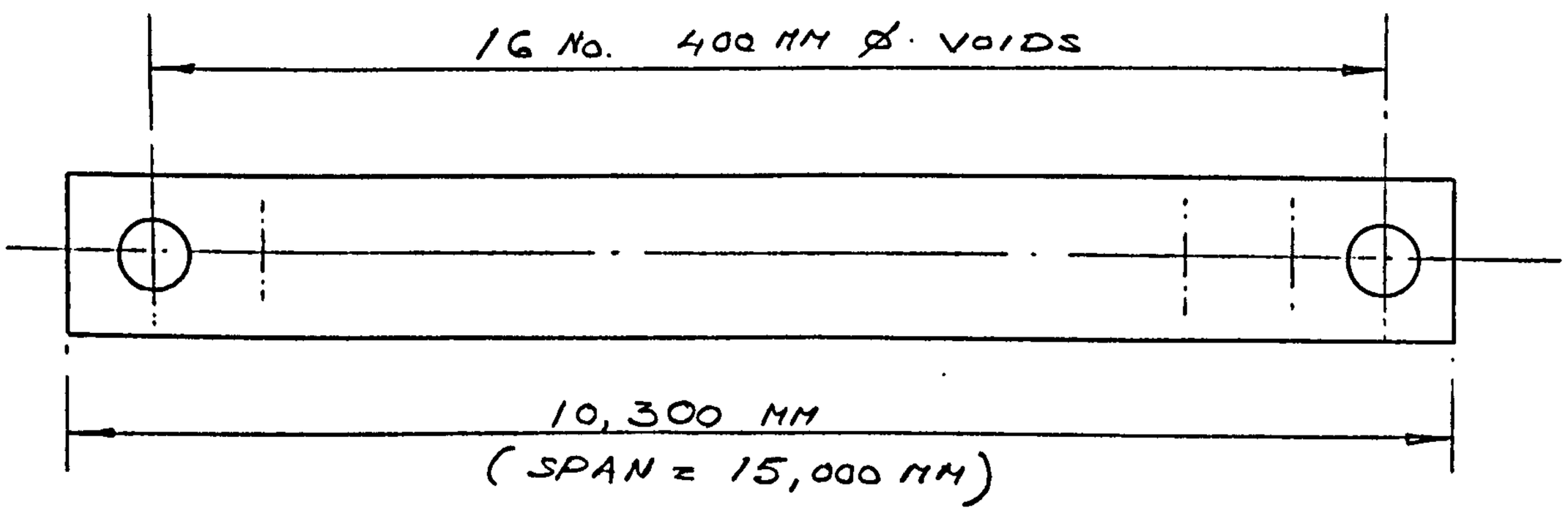

Figure 9.9 - Cross section of the two lane single carriageway.

From figure 9.9,

Tension Reinforcement = 68 T32 @ 150c/c

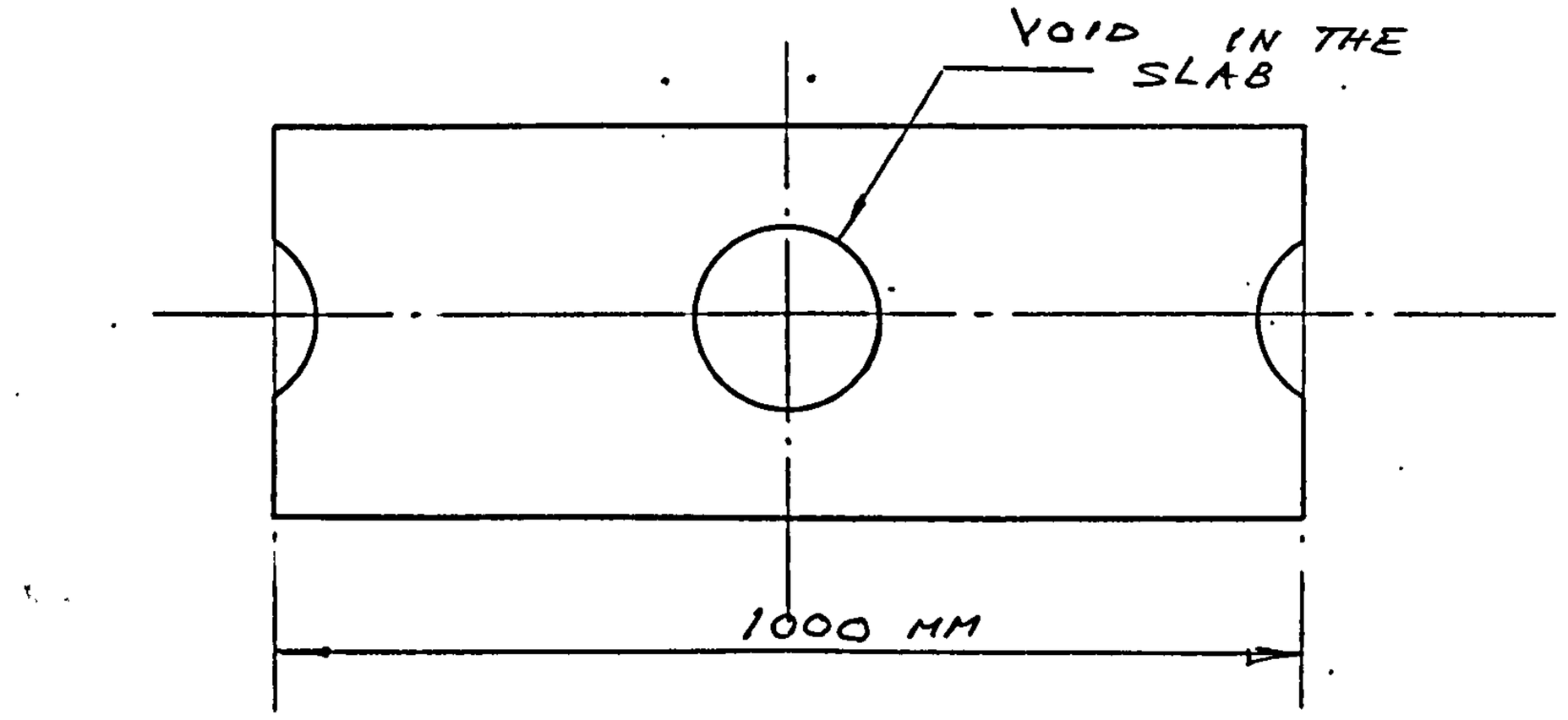

Figure 9.10 - A metre width of the bridge in cross section.

9.3.4 Predicting the shrinkage stresses on the strengthened modelled bridge

From section 9.3.3, the modelled single lane single carriageway is strengthened as shown in Figure 9.11,

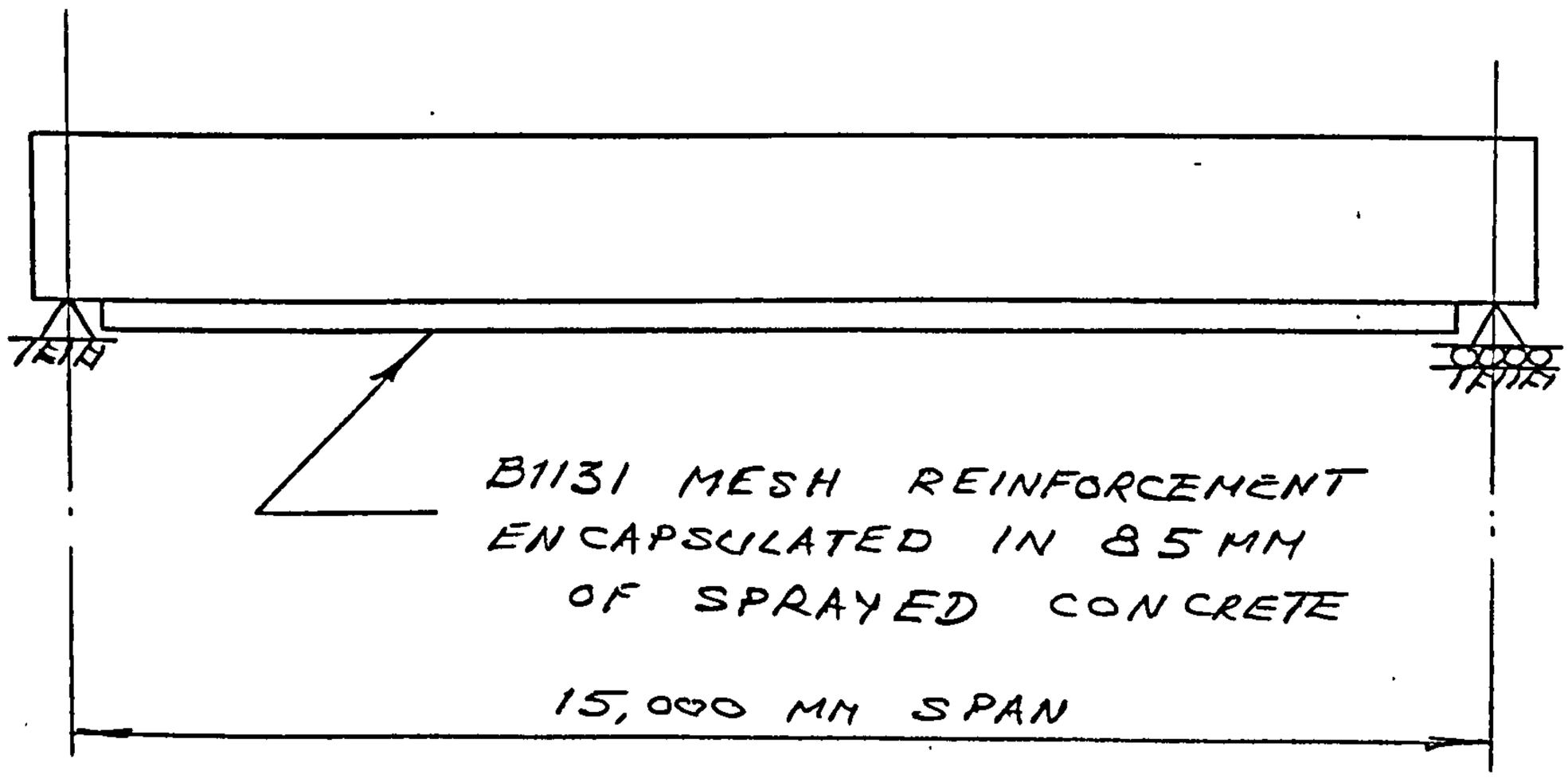

Figure 9.11 - Strengthening of the single lane single carriageway.

The shrinkage stresses are being predicted and presented as follows using the recommended theory as investigated in section 9.1.6 - Yam's theory.

Known parameters

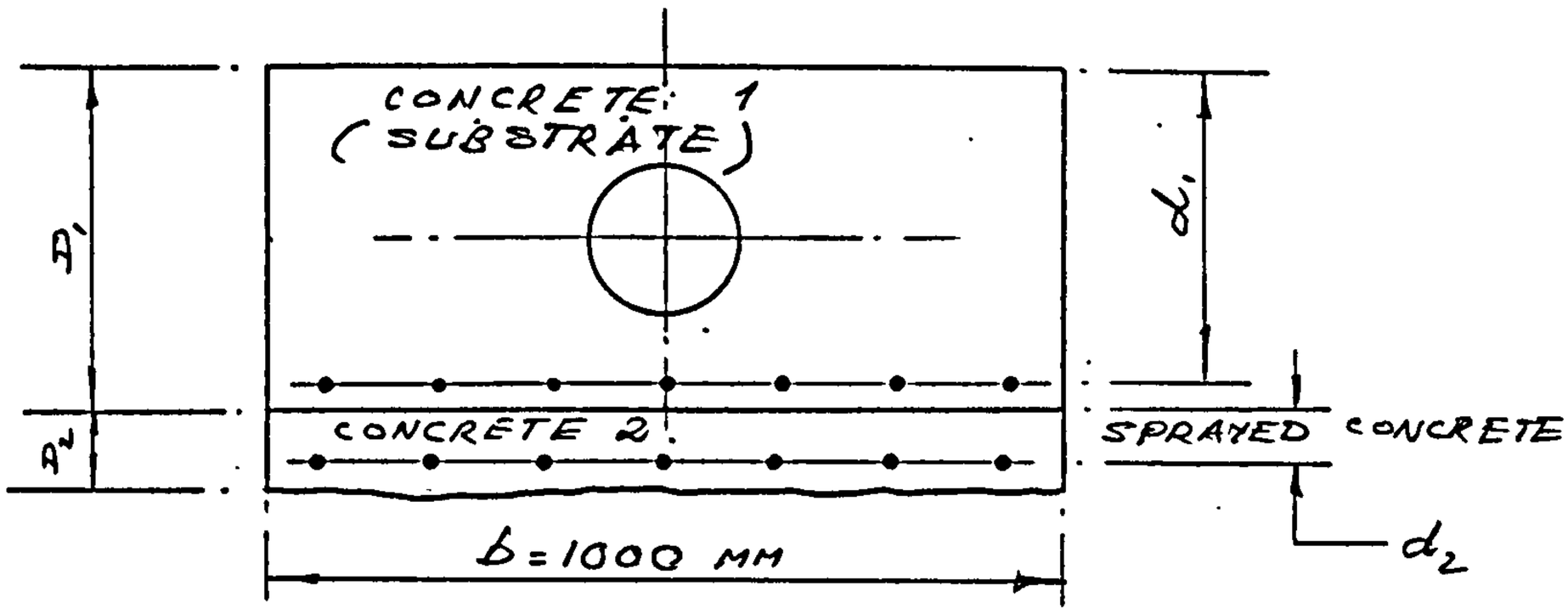

Figure 9.12 - Cross section per metre width.

From Figure 9.12,

$D_1 = 750$ mm

$D_2 = 85$ mm

$d_1 = 750 - 50 - 16 - 16 = 668$ mm

$d_1 = 85 - 50 - 6 = 29$ mm

$\gamma_1 = E_s/E_{c1} = 205/(25*0.5) = 16.4$

$\gamma_2 = E_{c2}/E_{c1} = 25/(25*0.5) = 2$

$A_{s1} = 5630$ mm^2/m

$A_{s2} = 1131$ mm^2/m

$E_{c1} = 12500$ N/mm^2

$E_{c2} = 25000$ N/mm^2

$E_s = 205000$ N/mm^2

Centroid of the transformed section ($\bar{y}$)

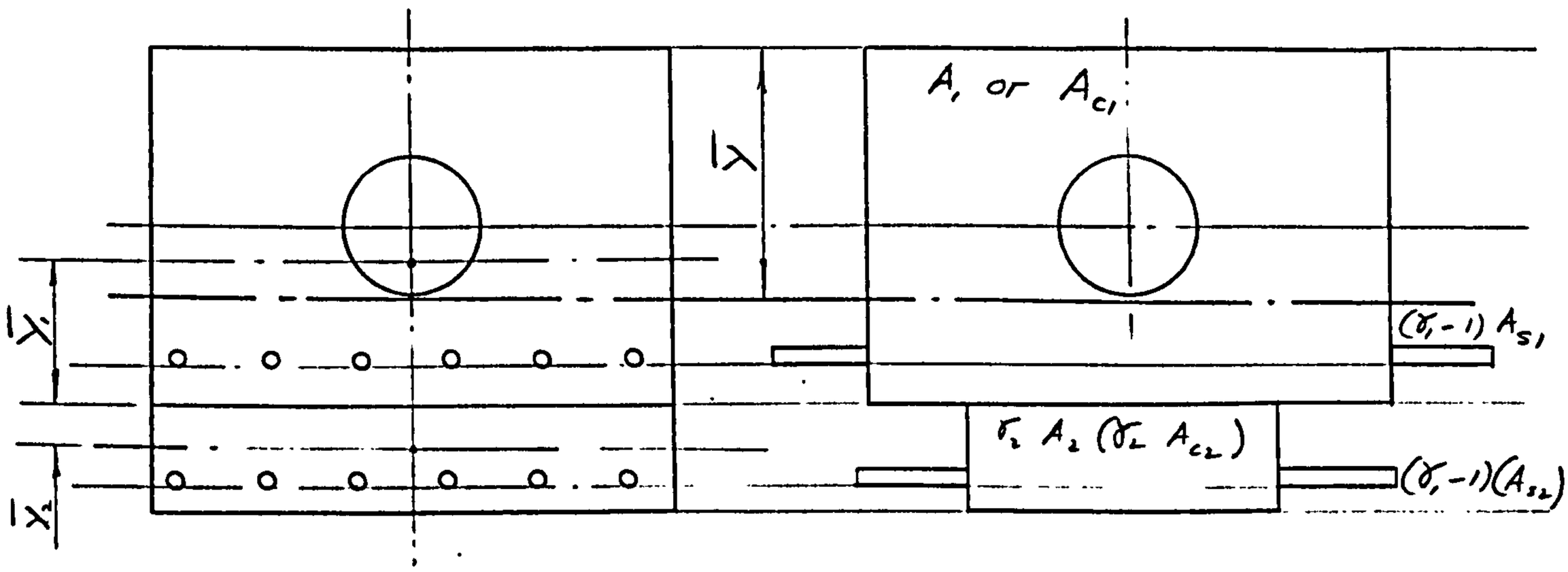

Figure 9.13 - Centroidal position.

From Figure 9.13,

$$\bar{y}[(100\times750)-(\pi\times200^2)+(16.4-1)\times5630+(1000\times85\times2)+(16.4-1)\times1131]$$

$$=\left[(1000\times750)-(\pi\times200^2)\right]\times375+[(16.4-1)\times5630\times668]+\left[2\times1000\times85\times\left(750+\frac{85}{2}\right)\right]$$

$$+[(16.4-1)\times1131\times(750+29)]$$

$$\bar{y}(898456)=4.403\times10^3$$

$$\bar{y}=490\text{ mm}$$

Transformed equivalent areas

$$A_1=(1000\text{ x }750)-(\pi\text{ x }200^2)=6.243\text{ x }10^5\text{ mm}^2$$

$$A_2=2\ (1000\text{ x }85)=1.7\text{ x }10^5\text{ mm}^2$$

$$(\gamma_1-1)A_{s1}=(16.4-1)\ (5630)=8.67\text{ x }10^4\text{ mm}^2$$

$$(\gamma_1-1)A_{s2}=(16.4-1)\ (1131)=1.74\text{ x }10^4\text{ mm}^2$$

Individual centroids of the transformed areas about the base/sprayed concrete interface,

$$\bar{y}[(1000\times750)-(\pi\times200^2)+(16.4-1)5630]=[(1000\times750)-(\pi\times200^2)]\left(\frac{750}{2}\right)$$

$$+(16.4-1)\ (5630\times82)$$

$$\bar{y}_1=339\text{ mm}$$

$$\bar{y}[(1000\times85\times2)+(16.4-1)1131]=\left(1000\times85\times2\times\frac{85}{2}\right)+(16.4-1)\ (1131\times56)$$

$$\bar{y}_2=43.75\text{ mm}$$

$$d_c=339+44=383\text{ mm}$$

Second moment of areas about the centroidal axes of individual concretes

$$I_{c1}=\frac{(1000\times750^3)}{12}-\left[\frac{(\pi\times400^4)}{64}+(16.4-1)(5630)(339-82)^2+(1000\times750)(375-339)^2\right]$$

$$=4.044\times10^{10}\text{ mm}^4$$

$$I_{c1}=\frac{(1000\times85^3)}{12}-(1000\times85)\ (43.75-42.5)^2+(16.4-1)\ (1131)\ (43.75-56)^2$$

$$=5.392\times10^7\text{ mm}^4$$

Force in the shrinking concrete (C)

Similar to section 9.1.3.1, first calculate the composite factor (α),

$E_{c1} = 12500\ N/mm^2$ (effective E value)

$E_{c2} = 25000\ N/mm^2$

$I_{c1} = 4.044 \times 10^{10}\ mm^4$

$I_{c2} = 5.392 \times 10^{7}\ mm^4$

$A_{c1} = [bD_1 - \pi(200)^2] + (\gamma_1-1)A_{s1} = [(1000 \times 750)-\pi(200)^2] + (16.4-1)(5630) = 7.11 \times 10^5\ mm^2$

$A_{c2} = bD_2 + (\gamma_1-1)A_{s2} = (1000 \times 85) + (16.4-1)(1131) = 1.024 \times 10^5\ mm^2$

$d_c = 383\ mm$

$$\alpha = \left[\frac{E_{c1}A_{c1}\,E_{c2}A_{c2}}{E_{c1}A_{c1} + E_{c2}A_{c2}}\right]\left[\frac{d_c^{\,2}}{E_{c1}I_{c1} + E_{c2}I_{c2}}\right]$$

$$\alpha = \left[\frac{(12500)\left(7.11\times10^5\right)(2500)\left(1.024\times10^5\right)}{(12500)\left(7.11\times10^5\right) + (2500)\left(1.024\times10^5\right)}\right]\left[\frac{383^2}{(12500)\left(4.04\times10^{10}\right) + (25000)\left(5.392\times10^7\right)}\right]$$

$$\alpha = 0.575$$

Substituting for α, C is as follows,

$$C = -\frac{\left(E_{c1}A_{c1}\,E_{c2}A_{c2}\right)e_1}{\left(E_{c1}A_{c1} + E_{c2}A_{c2}\right)(1+\alpha)}$$

$$C = -\frac{(12500)\left(7.11\times10^5\right)(25000)\left(1.024\times10^5\right)100\times10^{-6}}{\left[(12500)\left(7.11\times10^5\right) + (25000)\left(1.024\times10^5\right)\right](1+0.575)}$$

$$C = -126191\ N$$

Curvature due to shrinkage

Due to the shrinkage of the sprayed concrete layer, the composite slab will develop an upward curvature of, (assuming the shrinkage strain $e_1 = 100 \times 10^{-6}$)

$$K = \frac{\alpha\, e_1}{(1+\alpha)d_c} = \frac{0.575 \times 100 \times 10^{-6}}{(1+0.575)\,(383)}$$

$$K = 0.0953 \times 10^{-6}.$$

Elastic section modulii (Z)

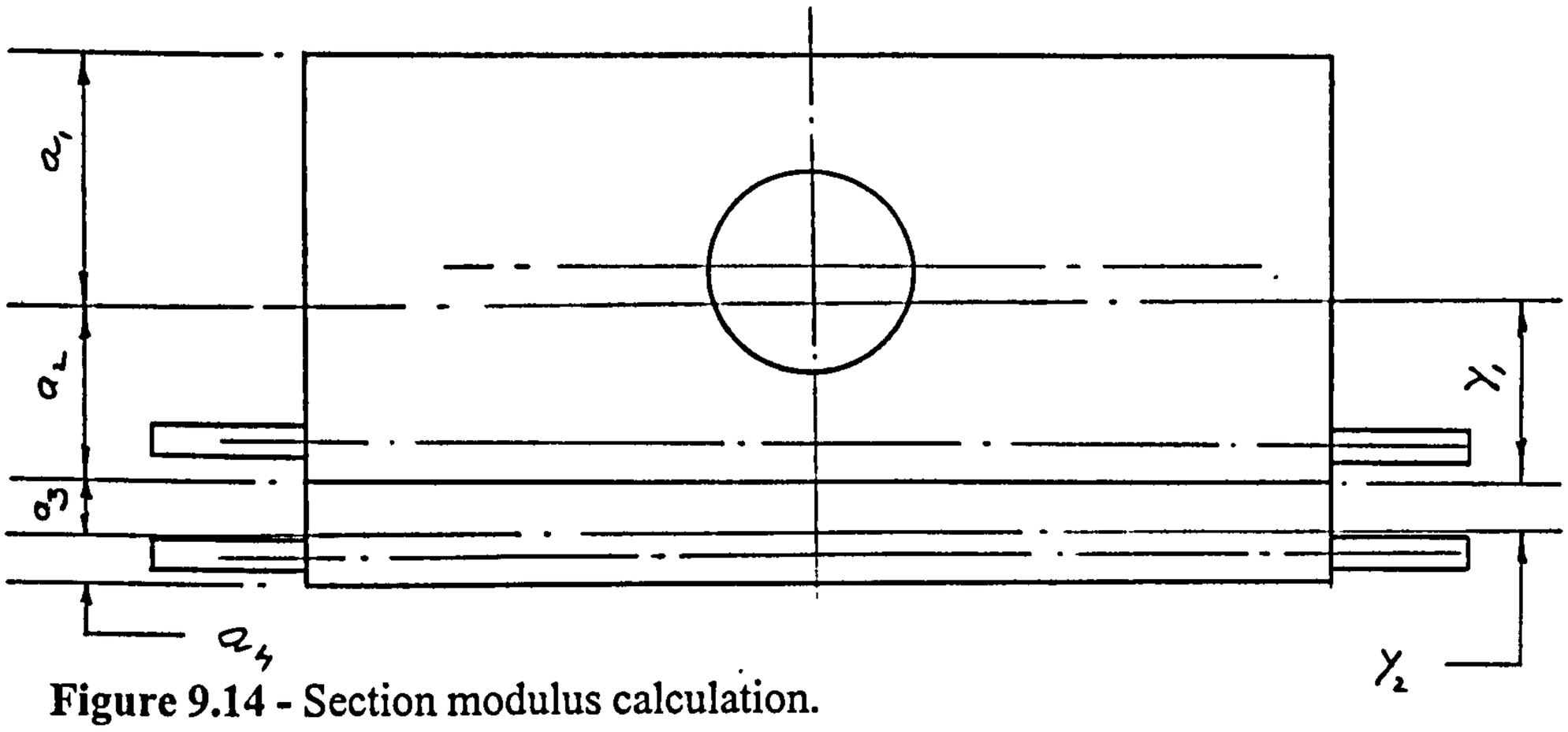

Figure 9.14 - Section modulus calculation.

From Figure 9.14

$y_1 = 339$ mm

$y_2 = 43.75$ m

$a_1 = 750 - 339 = 411$ mm

$a_2 = 339$ mm

$a_3 = 43.75$ mm

$a_4 = 85 - 43.75 = 41.25$ mm

Top of the base concrete, $Z_{c1} = \frac{I_{c1}}{a_1} = \frac{4.044 \times 10^7}{411} = 9.839 \times 10^7 \text{ mm}^3$

Underside of the base concrete, $Z_{c2} = \frac{I_{c1}}{a_2} = \frac{4.044 \times 10^{10}}{339} = 1.193 \times 10^8 \text{ mm}^3$

Top of the sprayed concrete, $Z_{c3} = \frac{I_{c2}}{a_3} = \frac{5.392 \times 10^7}{43.75} = 1.232 \times 10^6 \text{ mm}^3$

Underside of the sprayed concrete, $Z_{c4} = \frac{I_{c2}}{a_4} = \frac{5.392 \times 10^7}{41.25} = 1.307 \times 10^6 \text{ mm}^3$

Stresses due to shrinkage in the composite section

Top of the base concrete,

$$\sigma_1 = \frac{-C}{A_{c1}} - \frac{K\,E_{c1}\,I_{c1}}{Z_{c1}}$$

$$\sigma_1 = \frac{126191}{7.11\times10^5} - \frac{9.532\times10^{-8}\left(4.04\times10^{10}\right)12500}{9.84\times10^7} = -0.31\ \mathrm{N/mm^2}$$

Underside of the base concrete,

$$\sigma_2 = \frac{-C}{A_{c1}} + \frac{K\,E_{c1}\,I_{c1}}{Z_{c2}}$$

$$\sigma_2 = \frac{126191}{7.11\times10^5} + \frac{9.532\times10^{-8}\left(4.04\times10^{10}\right)12500}{1.19\times10^8} = 0.58\ \mathrm{N/mm^2}$$

Top of the sprayed concrete,

$$\sigma_3 = \frac{C}{A_{c2}} - \frac{K\,E_{c2}\,I_{c2}}{Z_{c3}}$$

$$\sigma_3 = \frac{-126191}{1.024\times10^5} - \frac{9.532\times10^{-8}\left(5.39\times10^7\right)25000}{1.23\times10^6} = -1.34\ \mathrm{N/mm^2}$$

Underside of the sprayed concrete,

$$\sigma_4 = \frac{C}{A_{c2}} + \frac{K\,E_{c2}\,I_{c2}}{Z_{c4}}$$

$$\sigma_4 = \frac{-126191}{1.02\times10^5} + \frac{9.532\times10^{-8}\left(5.39\times10^7\right)25000}{1.31\times10^6} = -1.13\ \mathrm{N/mm^2}$$

On comparison with the allowed tensile stresses for pre-stressed concrete detailed in Table 5.4 of BS 8110: Part 1: 1985, cl 5.4.6.2.1, the above calculated figures are perfectly acceptable and should not cause cracking anywhere in the sprayed concrete layer or at the top of the base slab. The use of L. Yam 's theory to predict the induced stresses due to the shrinkage of the strengthening layer of reinforced sprayed concrete is therefore recommended.

CHAPTER 10

DISCUSSIONS, CONCLUSIONS AND RECOMMENDATIONS

10.1 DISCUSSIONS

10.1.1 Static load tests

The load deflection behaviour of all test slabs was found to be very similar to the normally reinforced concrete base slab, see Figure 4.15, indicating that the use of a standard design code such as BS 8110 is acceptable. The differences indicated up to first yield between the normal mix and the proprietary mix test slabs where the former exhibited a steeper initial elastic part with a distinct yield point, compared with a more gradual transition for the latter, are perhaps explained by the lower E values for the proprietary mixes compared to the normal mix, see Table 3.4. However, after first yield all test slabs behave in a similar way.

Strength increase as a result of the strengthening process has been clearly demonstrated with all test slabs maintaining full composite action right up to failure. This significant improvement can be seen in Table 4.2 where the strengthened slab B1 of 212.8 kN is nearly eight times stronger than the unstrengthened slab of 27 kN

It was found that the use of shear connectors has not caused any strength enhancement and this is reflected in the comparison of similar test slabs in Table 4.2 i.e. A2 & A3 and A4, A5 & B4. Also, the use of shear connectors is not necessary in maintaining the full composite action as perfect bond was maintained between the sprayed concrete layer and its base slab even when the interface was subjected to much higher horizontal shear by significantly increasing the reinforcement in the sprayed concrete layer. As seen in slabs B3 and B1 with the reinforcement in the sprayed concrete layer up to nearly three times and four times that in the base slab respectively.

Table 4.2 shows that all test slabs failed at greater flexural strength than theoretically predicted from a standard code, in this case BS 8110 with the ratio of the experimental to theoretical ranging from 1.20 to 1.53. This is attributed to several factors already discussed in section 4.2.2 and these are; a breaking strength of the reinforcement being 1.42 times the design strength used in the calculations; a greater rate of loading of the reinforcement in the slab testing compared with the reinforcement testing in air and to a small extent, the higher cube strength of the base concrete compared with the design value. However, the ratio of experimental to theoretical flexural strength of 1.07 found for slab A4 is possibly due to weakness caused by the spot welding of the mesh reinforcement, torsion induced due to non-planeness of the slab at the support ends and possible variation in density of the sprayed concrete around the reinforcement bars.

A significant increase in flexural strength above that of the base slab can be seen for all test slabs in Table 4.2.

All test slabs displayed multiple flexural cracks and a flexural failure mode occurred when one of these widened under the increasing load and then propagated across the substrate/sprayed concrete interface into the base slab.

Although, the test slabs were under-reinforced with the total area of steel ranging from 0.19 to 0.56, the flexural failure was explosive with the test slabs broken into two halves when the tension steel failed except for slab A5 which failed in a ductile manner and remained intact. On examination of all test slabs which broke into two halves, particularly the B - type slabs which had no shear connectors and had high reinforcement in the sprayed concrete layer (to subject the interface to high horizontal shear), it was found that there was a 'clear' failure without any sign of debonding at the interface. On examination of slab A5 which remained intact, again showed no sign of debonding at the interface as the flexural crack which led to the failure of the slab crossed it.

It appears from the static tests, that grit blasting without the use of shear connectors was a sufficient means of surface preparation to the substrate concrete, to enable full composite action to be maintained right up to failure. Also, proprietary concrete mixes

did not perform better than normal concrete mix in terms of load carrying capacity. However, the mechanical properties from Table 3.4 and freeze-thaw durability are relatively better for the proprietary mixes than normal mix. Therefore, the performance of this technique of strengthening is not dependent on of the type of sprayed concrete mix if exposure to severe weathering is not anticipated.

10.1.2 Fatigue load test

All fatigue tested slabs failed in flexure and broke into two halves due to failure of the reinforcement. No sign of debonding at the interface was observed.

The behaviour of the composite slabs was found to be very similar to a normal reinforced concrete member as indicated by the deflection versus number of load cycle curves of Figures 6.3 to 6.5 and that in a normal concrete bridge, fatigue is not a major problem.

The analytical Table 5.8 tabulates the load range versus the expected number of cycles to failure which was established from the assumed S-N diagram and the modified Goodman diagram. Section 6.3.2 reports the fatigue load test data comparison and this indicates that Table 5.8 is conservative.

A fatigue load study carried out for a typical two lane single carriageway highway bridge using Miner's summation hypothesis to verify that the summation of the ratios of n to N is less than one, in which (n) is the number of load passes and was obtained from the updated current commercial axle load spectrum of BS 5400: Part 10 together with LR 252 to account for overloadings from the 15% commercial vehicle coincidence and (N) is the number of load repetitions causing failure and was obtained from Table 5.8, showed that Miner's summation is less than one, implying that under the current commercial axle spectrum, the typical highway bridge under consideration is still adequate in its load carrying capacity and that its total life expectancy is 922 years. More significant to this research is that as shown in section 6.3.2 the S-N curve of the experimental fatigue data closely follows the analytical curves and together with the finding of similarity in behaviour to a normally reinforced concrete member, it is

reasonably confident to forecast that if this technique is used, the strengthened bridge would have its original design life of 120 years restored with adequate capacity to carry to the current commercial axle load spectrum.

Possible concern that the high longitudinal shear stress concentrations at the re-entrant corner at each end of the sprayed concrete layer, might cause peeling off of this layer at the ends has been shown to be unfounded.

10.1.3 Horizontal shear study

The slant shear test

This test appears to be suitable as a means of comparison in which the slant shear bond strength of the composite specimen is expressed in terms of the compressive strength and compared with the compressive strength of the identical monolithic specimen.

Although the slant shear bond strengths obtained from Table 7.1 can be multiplied by {(cos 30°)x(sin 30°)}, giving 16.3 N/mm^2 at 84 days and 18.9 N/mm^2 at 21 months. These are the component stresses acting along the 30° slanted interface, but these are not the true shear stresses that occur at the substrate/sprayed concrete interface and therefore cannot be compared with the results of the double shear and direct shear tests, described in later sections of this chapter.

However, the author would stress that the slant shear test is a useful comparative test and should be undertaken to assess the bond strength of the sprayed concrete layer to its substrate. In this research, the assessment has shown that monolithic compression failure of the composite specimens were observed as shown in Figures 7.1 and 7.2. suggesting that there was extremely good bond between the sprayed concrete and its substrate when the interface was grit blast prepared. The slant shear bond strength of the composite specimen was 25 % less than the monolithic specimen at 84 days and 8% less at 21 months. This difference is due to the lower strength in the sprayed concrete compared with the substrate concrete, see section 3.3.1 for the results of the pull-off test.

The double shear test

This shear test is believed to be the best simulation of the shearing action in the test slabs and from the results shown in Table 7.2, it can be seen that the bond of the normal mix sprayed concrete to its grit blast prepared substrate was extremely good, comparing well with the values given in BS 8110: Part 1: cl 5.4.7.2. However, it could be argued that this result may not be truly representative of the actual horizontal shear capacity developed in the test slabs, because of the horizontal spraying direction of the shear blocks as opposed to the overhead spraying direction in the test slabs. However, the results given in Table 3.4 for compressive strength and tensile splitting strength showed that there is no difference in the quality of the sprayed concrete whether sprayed overhead or horizontally.

The author would stress that this should be a compulsory test to measure the shear capacity at the substrate/sprayed concrete interface.

Direct shear test

This is another test that closely simulated the shearing action in the test slabs. The results from Table 7.3 show that extremely good bond had been achieved at the substrate/sprayed concrete interface with the shear capacity of the normal mix sprayed concrete specimen 61% that of the monolithic specimen and much higher than that from BS 8110 reproduced in Table 7.2. The possible factors contributing to this difference are:

1. Relatively lower base concrete quality at the soffit level compared to that at the middle level of the base slab where the shear plane of the monolithic specimen was taken.
2. Some pre-stress was set up in the base concrete near the interface due to the shrinkage of the sprayed concrete layer.

From the extremely good bond of the sprayed concrete layer to its substrate concrete, as demonstrated from the results of the discussed three shear tests, it can now be concluded that the formation of the 5mm 'dark' layer near the interface as reported from the petrographic examination, section 3.3.3 , has no detrimental effect to the strengthening reinforced sprayed concrete and that this was a part of the spraying process.

10.1.4 Freeze-thaw durability

As reported in Chapter 8 that very limited data from this test was obtained and this was due to the early deterioration of the base concrete and the normal mix sprayed concrete. The early deterioration was largely due to the very severe testing conditions of the ASTM C666 used, as also found by Morgan[53].

From the results of this test, it was observed that if in addition to the load carrying capacity requirement, there is a likelihood of severe freeze-thaw weathering, then the use of proprietary concrete mix is recommended otherwise, normal mix concrete is adequate. If the use of proprietary mix is necessary, it is recommended that mechanical properties such as the coefficient of linear thermal expansion and the static modulus of elasticity should be similar to those in the substrate concrete in order to minimise the relative deformation which may reduce the bond at the interface as reported in section 8.2

10.1.5 Time dependent study

In the laboratory, when the base concrete slab of 100mm thickness was strengthened with a layer of reinforced sprayed concrete of maximum thickness of 100mm, the shrinkage of the sprayed concrete layer was relieved by the curvature of the composite section. However, on a typical highway bridge, it is expected that the maximum thickness of the reinforced sprayed concrete layer will be relatively thin compared with the existing depth of the bridge which will resist the curvature due to the shrinkage of the sprayed concrete. Therefore, if the recommended theory of induced stress calculations was appropriate, then the calculated induced stresses from the test slab should be less than those calculated from the typical bridge. The following comparison supports the recommended theory.

Section 9.1.6 (test slab):

$\sigma_1 = -0.44$ N/mm^2 Tens

$\sigma_2 = 0.85$ N/mm^2 Comp

$\sigma_3 = -1.08$ N/mm^2 Tens

$\sigma_4 = 0.53$ N/mm^2 Comp

Section 9.3.4 (typical bridge):

$\sigma_1 = -0.31$ N/mm^2 Tens

$\sigma_2 = 0.58$ N/mm^2 Comp

$\sigma_3 = -1.34$ N/mm^2 Tens

$\sigma_4 = -1.13$ N/mm^2 Tens

Unfortunately, the theoretical values were not in agreement with the experimentally obtained shrinkage stresses, but the latter appeared unrealistically high since no distress in the forms of shrinkage cracks or debonding was observed on the test slab.

It appears therefore that the use of Yam's theory to predict the induced stresses due to the shrinkage of the strengthening layer of reinforced sprayed concrete is appropriate.

10.2 CONCLUSIONS

1. Tests from the pre-construction panels revealed that good quality dry mix sprayed concrete was achieved.
2. From petrographic examination, voids behind the reinforcement bars were found but their formation was usually within site tolerance and generally did not significantly affect the bond of the sprayed concrete and the encapsulated reinforcement.
3. Under static loading, the reinforced sprayed concrete layer had successfully strengthened a normally reinforced concrete slab by up to eight times.
4. At the stress levels imposed in this research it was found that the bond between the sprayed concrete layer and the base slab was extremely good from just grit blasting and that shear connectors were not necessary to maintain this bond.
5. Proprietary sprayed concrete mixes did not perform better than the normal concrete mix in either the load carrying capacity or in maintaining the composite action and therefore it can be concluded that unless the exposure conditions were very severe, their use is not necessary.
6. The strengthened slabs behaved almost as a monolithic slab, as full composite action was maintained right up to failure.
7. When this strengthening technique is applied on a real bridge, re-entrant corners at the bearing ends will be created and this was simulated in the laboratory by curtailing the reinforced sprayed concrete layer just before the points of support. No

sign of debonding or 'peeling-off' of the sprayed concrete layer was observed at the point of curtailment under either fatigue or static loading.

8. The analytical table of the number of cycles to failure was found conservative and its use in conjunction with BS 5400's current commercial axle load spectrum and LR 252 gave a total life expectancy of 922 years. The analytical table of the number of cycles to failure was derived from the assumed S-N diagram and its accuracy was successfully verified by the experimental fatigue data. Therefore it can be concluded that the use of this technique of strengthening will at least restore the original design life of a typical highway bridge of 120 years.
9. The double and direct shear tests should be the compulsory tests to measure the horizontal shear capacity at the substrate/sprayed concrete interface. However, the slant shear test should also be undertaken to compare the bond at the interface to a monolithic specimen.
10. The freeze-thaw test of ASTM C666 was very severe and caused early deterioration of the standard C35 designed ready mix substrate concrete as well as the standard pre-packed supplied normal mix sprayed concrete. Bond at the interface was also affected and this effect can be minimised if the mechanical properties such as the coefficient of linear thermal expansion and the static modulus of elasticity were similar to those in the substrate concrete.
11. When using this technique to strengthen a bridge it is recommended that the stresses induced by the shrinkage of the reinforced sprayed concrete layer be calculated from the method outlined in this research, originated from L. Yam.

10.3 RECOMMENDATIONS

The following recommendations for further research are specific to this technique of strengthening concrete bridges.

1. Strengthening an aged base concrete slab whilst it is sustaining static and fatigue loading. This is to simulate the actual site conditions in which the strengthening process is being undertaken whilst the bridge is still open to traffic.
2. Conducting extensive measurement of long term and short term strains induced by the shrinkage of the reinforced sprayed concrete layer.

3. Simulating the actual UK freeze-thaw conditions for experimental testing on the composite specimens.
4. Investigating a means of measuring the degree of roughness from grit blasting the substrate concrete, so that an equation of the horizontal shear capacity or the bond strength as a function of the degree of roughness of the substrate concrete can be established.
5. Strengthening an existing concrete bridge so that a comprehensive cost evaluation between this technique and the alternative plate bonding technique can be fully established.

REFERENCES

1. Abu-Tair A. I. H., "The effectiveness of different concrete repair techniques and materials under static and cyclic loading. PhD thesis, Queen Mary and Westfield college (University of London), London, 1992.

2. Glassgold, I. L., "Shotcrete in the United States: A Brief History", SP 128-14, American Concrete Institute, Detroit, 1991, pp. 289-305

3. ACI Committee 805, "Recommended Practice for the Application of Mortar by Pneumatic Pressure", ACI 805-51, American Concrete Institute, 1951, 11 pp.

4. Stewart, E. P., "New Test Data Aid Quality Control of Gunite", Engineering News - Record, November 1933, 4 pp.

5. Ward, W. H. and Hills, D. L., "Sprayed Concrete: Tunnel Support Requirements and the Dry-Mix Process", Building Research Station, 1977, 23 pp.

6. Parker, Harvey W., "Current Field Research Program on Shotcrete", Use of Shotcrete for Underground Structural Support, SP-45, American Concrete Institute/American Society of Civil Engineers, Detroit, 1974, pp. 330-350.

7. Parker, Harvey W.; Fernandez-Delgado, Gabriel; and Lorig, Loren J., "Field-Oriented Investigation of Conventional and Experimental Shotcrete for Tunnels", Report No. FRA-OR&D 76-06, US Department of Transportation, Washington, D.C., August 1975, 628 pp.

8. Valencia, Fernando E., "Practical Aspects of Shotcrete Application", Use of Shotcrete for Underground Structural Support, SP-45, American Concrete Institute/American Society of Civil Engineers, Detroit, 1974, pp. 114-129.

9. Blumel, O. W.; Lutsch, H.; and Stehno, G., "State of the Art of Shotcrete Technology", Shotcrete for Underground Support III, Engineering Foundation, New York, 1978, pp. 15-26.

10. Ryan, T. F., "Gunite: A Handbook for Engineers", Cement and Concrete Association, Wexham Springs, 1973, 63 pp.

11. ACI Committee 506, "Guide to Shotcrete", (ACI 506R-90), American Concrete Institute, Detroit, 1990, 39 pp.

12. Schrader, E. & Kaden, R. "Durability of Shotcrete", ACI report SP 100-57, 1987, pp 1071 - 1101.

13. BS 8110: Part 2. Code of Practice for Special Circumstances: 1985: "Structural Use of Concrete", British Standards Institution.

14. Marusin, S. L., "Failure of Latex-Modified Shotcrete", Concrete International, October 1990, pp 39-42.

15. ACI Committee 506, "State-of-the-Art Report on Fiber Reinforced Shotcrete", ACI 506.1R-84 (Reapproved 1989), American Concrete Institute, Detroit, 1989, 13 pp.

16. Kirsten, H. A. D., 1993. "Equivalence of Mesh and Fiber-Reinforced Shotcrete at Large Deflections". Canadian Geotechnical Journal. **33**: 418-440.

17. Litvin, Albert and Shideler, Joseph J., "Laboratory Study of Shotcrete", Shotcreting, SP-14, American Concrete Institute, Detroit, 1966, pp. 165-184.

18. Shotcreting, SP-14, American Concrete Institute, Detroit, 1966, 224 pp.

19. Reading, T. J., "Durability of Shotcrete", Concrete International, January 1981, pp 27-33.

20. Morgan, D. R., "Dry-Mix Silica Fume Shotcrete in Western Canada", Concrete International, January 1988, pp 25-32.

21. Berkovitch, I., "Sprayed Concrete Reviewed", Civil Engineering, October 1984, pp 35-38.

22. Humphries E. F., "Specifications and Codes of Practice for Sprayed Concrete", Symposium "Sprayed Concrete" CI 80. Construction Press.

23. "Specification for Sprayed Concrete", Final Draft, The European Federation of National Associations of Specialist Contractors and Material Suppliers for the Construction Industry, (EFNARC), 1993.

24. "Specification for Sprayed concrete", prepared by the Construction and Formwork Committee, The Concrete Society, 1979.

25. ACI Committee 506, "Guide to Certification of Shotcrete Nozzlemen", (ACI 506.3R-82), American Concrete Institute, Detroit, 1982, 25 pp.

26. BS 8110: Part 1. Code of Practice for Design and Construction: 1985: "Structural Use of Concrete", British Standards Institution.

27. BS 1881: Part 120. Method for determination of the compressive strength of concrete cores: 1983: "Testing Concrete", British Standards Institution.

28. BS 1881: Part 117. Method for determination of tensile splitting strength of concrete cores: 1983: "Testing Concrete", British Standards Institution.

29. BS 1881: Part 121. Method for determination of static modulus of elasticity in compression: 1983: "Testing Concrete", British Standards Institution.

30. BS 6319: Part 4. Method for measurement of Bond Strength (Slant Shear Method): 1984: "Testing of Resin Compositions for use in Construction", British Standards Institution.

31. CIRIA Technical Note 139, Standard tests for repair materials and coatings for concrete, Part 1: Pull-off tests, Construction Industry research and Information Association, 1993.

32. The Corps of Engineers, USA, Test for the Coefficient of Linear Thermal Expansion for Concrete (CRD-39).

33. ASTM C 457-90, Standard Test Method for Microscopical Determination of Parameters of the Air-Void System in Hardened Concrete, ASTM, Philadelphia, USA, 1990.

34. "Design and Control of Concrete Mixtures, 13th Edition, Portland Cement Association, Skokie, 1988, 212 pp.

35. Seegebrecht G. W., Litvin A. and Gebler S. H., "Durability of Dry-Mix Shotcrete", Concrete International, January 1989, pp 47-50.

36. Park R. and Paulay T., "Reinforced Concrete Structures", Department of Civil Engineering, University of Canterbury, Christchurch, New Zealand, Wiley-Interscience publication, John Wiley and Sons Inc.

37. ACI Committee 439, "Effect of Steel Strength and Reinforcement Ratio on the Mode of Failure and Strain Energy Capacity of Reinforced Concrete Beams", Journal ACI, Vol. 66, No. 3, March 1969, pp. 165-173.

38. BS 5400: Part 10. Code of Practice for Fatigue: 1980: "Steel, Concrete and Composite Bridges", British Standards Institution.

39. ACI Committee 215, "Consideration for Design of Concrete Structures Subjected to Fatigue Loading", (ACI 506R-74), American Concrete Institute, Detroit, 1986, 25 pp.

40. Departmental Standard BD 37/88: Loads for Highway Bridges, 1994. Department of Transport: Highways and Traffic.

41. Cornelissen H. A. W., "Fatigue of Failure of Concrete in Tension, 1984, Heron, 29(4), 68 pp.

42. Leonard, D. R., "A Traffic Loading and its use in The Fatigue Life Assessment of Highway Bridges", 1972, Transport and Road Research Laboratory Note No. LR 252. Department of the Environment.

43. Holmen J. O., Fatigue of Concrete by Constant and Variable Amplitude Loading, PhD, 1979, NHT, Trondheim, 218 pp.

44. EMACO FOR REPAIRS, 1992, Master Builders Technologies, MBT (UK) Ltd, 42 Sir Thomas Longley Road, Medway City Estate, GB-ROCHESTER, Kent ME2 4DP.

45. ASTM D 905-89, Standard Test Method for Strength Properties of Adhesive Bonds in Shear by Compression Loading, ASTM, Philadelphia, USA, 1989.

46. ASTM C 666-84, Standard Test Method for Resistance of Concrete to Rapid Freezing and Thawing, ASTM, Philadelphia, USA, 1984.

47. BS 1881: Part 203. Recommendation for Measurement of Velocity of Ultrasonic Pulses in Concrete: 1986: British Standards Institution.

48. Neville A. M., "Properties of Concrete", 3rd Edition, 1991, Longman Scientific and Technical, Longman House, Burnt Mill, Harlow.

49. Kong F. K. and Evans R. H., "Reinforced and Prestressed Concrete", 3rd Edition, 1987, Van Nostrand Reinhold (UK) Co. Ltd.

50. Yam, L. C. P., "Design of Composite Steel-Concrete Structures. Published by Surrey University Press, 1981, pp. 17-23 (Chapter 3).

51. Hobbs, D. W. "Shrinkage-Induced Curvature of Reinforced Concrete Members". Wexham Springs, Cement and Concrete Association, November 1979. Technical Report 44.004.

52. Parrott, L. J. "Simplified Methods of Predicting the Deformation of Structural Concrete". Wexham Springs, Cement and Concrete Association, October 1979. Technical Report 44.003.

53. Morgan D. R., "Freeze-Thaw Durability Shotcrete", Concrete International, January 1989, pp 86-93.

54. Hanson J. M., "Design for Fatigue", Handbook of Structural Concrete, Edited by Kong F. K., Evans R. H., Cohen E. and Roll F., 1983, Pitman Publishing Inc.(Massachusetts, USA).

APPENDIX A

MATERIAL ANALYSIS AND PETROGRAPHIC EXAMINATION

This appendix contains the report on the material analysis of the sprayed concrete core specimens and petrographic examination on a prismatic composite specimen extracted from a load tested slab.

TARMAC STRUCTURAL REPAIRS
REPORT ON THE ANALYSIS OF SPRAYED CONCRETE

Reference : 3186

21st April, 1994

CONTENTS

TARMAC STRUCTURAL REPAIRS
REPORT ON THE ANALYSIS OF SPRAYED CONCRETE

Reference - 3186

21st April, 1994

1. INTRODUCTION

1.1 *Samples:*

Twelve samples of sprayed concrete were received on 28th February 1994. Six of the samples were 50 mm diameter cores, five were 70 mm diameter cores and a further lump sample was supplied. Further details of the samples as received are as follows.

Laboratory reference	*Sample number*	*Dimensions*
3186/1	VA1	50 mm in diameter x 70 mm in length
3186/2	VA2	50 mm in diameter x 70 mm in length
3186/3	VA3	50 mm in diameter x 70 mm in length
3186/4	OA1	50 mm in diameter x 80 mm in length
3186/5	OA2	50 mm in diameter x 80 mm in length
3186/6	OA3	50 mm in diameter x 80 mm in length
3186/7	-	220 mm x 160 mm x 45 to 70 mm
3186/8	-	70 mm in diameter x 75 mm in length
3186/9	-	70 mm in diameter x 75 mm in length
3186/10	-	70 mm in diameter x 75 mm in length
3186/11	-	70 mm in diameter x 75 mm in length
3186/12	-	70 mm in diameter x 75 mm in length

Each of the 11 core samples consists of a fine sprayed concrete and has one flat surface containing the impression of formwork and one flat but rough surface. Sample 3186/7 contains an outer layer of some 105 to 110 mm of the fine sprayed concrete adjacent to 110 mm thickness of concrete containing both coarse and fine aggregate. The external surface of the sprayed material is flat but very rough.

1.2 *Objectives:*

It was requested that chloride ingression trials be carried out on Samples 3186/8 to 12, and the air void parameters be calculated for Samples 3186/1 to 6. In addition it was requested that Sample 3186/7 be examined petrographically.

1.3 *Procedures:*

(i) Samples 3186/1 to 6 were sawn in half and the two flat surfaces polished. The polished surfaces were examined with a Zeiss binocular microscope and the air void content and parameters of each sample were calculated according to the ASTM. C-457-71 specification.

(ii) A polished plate and thin section were prepared from Sample 3186/7. The polished surface was examined with a binocular microscope and the thin section was examined with a Zeiss petrological photomicroscope. In addition, the remainder of the sample was examined in hand specimen with the aid of a binocular microscope. Photographs illustrating the sample are given in the Appendix to this report.

(iii) Chloride ingression tests were carried out on Samples 3186/8 to 12. The ingression tests were carried out at 40^{o}C with the sample being analysed after 28, 56 and 84 days immersion in 5 molar sodium chloride solution, and one control sample tested after 28 days in saturated calcium hydroxide solution. A further control was tested for chloride content after 28 days in saturated calcium hydroxide solution followed by 28 days in 5 molar sodium chloride solution.

1.4 *Report structure:*

This report relates to petrography and determination of air void parameters within the sprayed concrete. Results of the chloride ingress trials must be calculated after the 84-day test point and will be reported separately, but interim reports will be produced.

2. DESCRIPTION OF THE SAMPLES

2.1 *General features:*

(3186/7)

(i) *Introduction and structure:*

The sprayed concrete which forms Samples 3186/1 to 6 and 8 to 12, and half of Sample 3186/7 is of very similar structure and appearance and contains a fine siliceous aggregate within a medium grey portland cement paste containing microsilica. The inner concrete is based on a flint gravel and siliceous sand with a binder consisting of portland cement and PFA.

Sections 2.1, 2.2, 2.3, 2.5, and 3 of this report relate directly to observations made upon Sample 3186/7, in particular with the aid of a thin section. The outer sprayed concrete is strongly bonded to an inner concrete containing a partially crushed flint gravel ranging up to 10 mm in diameter, with a siliceous sand in a dense mid-grey portland cement paste of low porosity. The sprayed concrete shows some variation in its appearance and numerous layers can be made out in the hand specimen, and on the polished surface, and also with the aid of the thin section. The sprayed concrete is approximately 107 mm in thickness, and has a dark grey layer of approximately 6 mm adjacent to the inner concrete. This layer is coated with a layer of sprayed concrete of some 10 mm thickness, of very similar appearance to the remainder of the sprayed material. A third layer or group of layers makes up some 60 mm thickness, and a final layer or layers of approximately 35 mm thickness leads to the external surface. Reinforcement rods occur within the outer sprayed concrete at a depth of approximately 30 mm from the external surface and a single rod occurs at approximately 72 mm from the external surface. The majority of the sprayed concrete is strong and robust, and contains a moderate void content, and appears compact. However, there are patchy zones and layers of the concrete which contain a very high porosity and appear weak and friable. Such patches occur at depths of between 50 and 90 mm from the external surface and extend laterally for up to 70 mm: the width of the sample.

(ii) *External surface:*

The external surface of Sample 3186/7 is flat but rough with a variation in relief on the surface of up to 5 mm. The external surface is medium to light grey and has a rough nodular or granular texture, and appears to be coated with a thin layer (less than 0.5 mm) of cement laitance.

(iii) *Cracking:*

There are no macrocracks or other fine cracks within the sample as received. However, during preparation of the polished surface of the

sample the outer sprayed concrete broke at the junction between the first and second layer, between the first dark layer and the outer layers which are of more homogenous appearance.

(iv) *Aggregate type:*

The aggregate is an angular sand with particles ranging up to some 5 mm in diameter.

(v) *Paste type:*

The paste is a medium grey portland cement containing micro-silica.

(vi) *Voids:*

The voids occur in two main forms. The majority of the sprayed concrete is compact and contains voids which range up to 2 mm in diameter, but which are mostly less than 0.5 mm in diameter. The void content is of the order of 4% by volume. The void content and parameters for Samples 3186/1 to 6 are reported in Section 2.4 Composition. Within Sample 3186/7 there are also patches and zones of the sprayed concrete which contain abundant voids or large continuous cavities. These voids range up to 12 mm in depth and range to in excess of 20 mm laterally. There are also areas associated with these cavities which contain numerous tiny voids and which are friable and dusty. The void-rich zones occur within specific layers of the concrete and within the present sample occur in a layer of concrete approximately 10 to 30 mm below the outer series of reinforcement rods.

(vii) *Carbonation:*

Carbonation has penetrated for up to a millimetre from the external surface of the sprayed concrete, but is mostly restricted to less than 0.5 mm from the external surface.

(viii) *Reinforcement*

Sample 3186/7 contains three reinforcement rods at a depth of approximately 32 mm from the external surface. These rods are of approximately 8 mm diameter. The external sprayed concrete also contains a 5 mm reinforcement rod at a depth of approximately 7 mm from the external surface. The internal concrete contains three 8 mm diameter reinforcement rods at a depth of approximately 125 mm from the external surface. In the external sprayed concrete there are voids and cavities within the material which occur in a zone between 0 and 30 mm below the first level of reinforcement rods. Patches of highly porous, almost

honeycombed concrete extend up to the margins of some of the reinforcement rods.

2.2 *Aggregate:*

(i) *Size range and shape:*

The aggregate ranges in size from approximately 0.02 to up to 5 mm in diameter. The majority of the particles are rounded to sub-rounded or irregular in shape, although there are numerous angular particles some of which are elongate. The majority of the particles have aspect ratios of less than 2:1, although there are occasional elongate pieces with aspect ratios in excess of 4:1.

(ii) *Rock types present:*

The majority of the particles larger than 2 mm in diameter are of flint with lesser amounts of vein quartz and occasional particles of ironstone. There are also traces of recrystallized sandstone and metaquartzite granules. The majority of the particles of less than 2 mm are of quartz with lesser amounts of chert, recrystallized sandstone, vein quartz, metaquartzite, and shell and limestone with traces of glauconitic material, hornfels and altered and weathered igneous material.

(iii) *Properties of the lithologies:*

The quartz grains and vein quartz particles show little or no strain. The particles of metaquartzite show varying degrees of strain including pieces which are strongly recrystallized with intersutured grain boundaries and undulose extinction. The pieces of chert are microcrystalline lithologies with occasional patches of chalcedonic quartz, and some contain fine grained ferruginous material. The pieces of sandstone include recrystallized lithologies with intersutured grain boundaries, and most are dominated by grains of quartz with little or no matrix. There are occasional particles of recrystallized chalcedonic sandstone. There are rare particles of dark brown ironstone which are slightly translucent in thin section, and some particles which contain silt and sand sized quartz grains which may be described as ferruginous sandstone and siltstones. The pieces of limestone are mostly fine to medium grained recrystallized micritic lithologies: some are coarser grained and have a sparry matrix. There are occasional fossiliferous fragments including pieces of shell. The glauconitic particles are green and finely granular and mostly of less than 0.1 mm in diameter. The pieces of hornfels are dominated by strongly intersutured quartz crystals showing low degrees of strain, with crystals of amphibole. The altered igneous particles contain lath-shaped crystals of

plagioclase within a fine-grained altered and/or weathered matrix which appears dark and contains iron oxides.

(iv) *Surfaces of the aggregate fragments:*

The majority of the aggregate particles make very sound contact with the cement paste. There are commonly small numbers of tiny crystals of portlandite at the margins of aggregate particles, and occasionally there are very thin discontinuous pellicles of portlandite around margins of some of the aggregate pieces. The crystals are commonly less than 0.01 mm in diameter, and the pellicles of portlandite are almost always less than 0.005 mm in thickness. There are occasional voids which occur around the margins of the aggregate pieces, and there is some tendency for voids to cluster around the margins of individual aggregate particles, particularly within certain void-rich areas of paste. Around the margins of some particles the voids have coalesced to form discontinuous cavities, and such cavities are commonly of the order of 0.05 mm in width. The cavities may be continuous and crack-like, orientated parallel to the junction with the inner concrete and the external surface.

(v) *Evidence of processes of deterioration*

No evidence has been found for deterioration of the aggregate within the sample.

2.3 *Paste:*

(i) *General structure and appearance:*

The paste in hand specimen is a medium grey and appears dense and strong. In thin section the majority of the paste is very dark in colour, contains abundant residual clinker grains, and has a very low level of porosity and contains very few microcracks. The paste varies very slightly in colour and appearance with different layers of the sprayed concrete: the densest paste containing the most abundant clinker occurs in the thin darkest layer adjacent to the internal concrete. The paste at depths of between 55 and 95 mm from the external surface contain zones which contain numerous voids. The paste within these zones is friable and dusty.

(ii) *Portlandite:*

Portlandite occurs as fine crystals within the paste and as slightly coarser crystals around the numerous particles of residual unhydrated clinker and around some of the fine aggregate particles as both fine crystals and as thin discontinuous pellicles. There is very little portlandite in the dark paste immediately adjacent to the inner concrete.

(iii) *Unhydrated cement grains:*

The sample contains abundant residual unhydrated cement clinker, and numerous particles of partially hydrated cement clinker.

(iv) *Hydrated cement:*

The hydrates have a slightly patchy colour which varies from layer to layer of the sprayed concrete. However, the vast majority of the material has a very low porosity and contains very few microcracks.

(v) *Microcracking:*

The level of microcracking within the sample is exceptionally low, with less than 2 microcracks encountered upon each 40 mm traverse of the thin section. However, there are occasional clusters of voids which occur around aggregate margins and some clusters of voids which form elongate cavities, which are orientated parallel to the external and internal surfaces and which are discontinuous and continuous over several millimetres. These cavities commonly run through the paste and around margins of aggregate pieces.

(vi) *Voids:*

The paste contains numerous voids, which are mostly very tiny. The voids are empty and commonly cluster around the margins of particles of the aggregate, as previously reported. Further details related to the voids are given in the following section.

(vii) *Dark layer:*

The dark layer at the interface with the substrate concrete has virtually none of the coarser size ranges of the aggregate but has a normal component of fines. The paste has much more residual unhydrated cement than the remainder of the repair concrete and its structure is in keeping with a lower water/cement ratio.

2.4 *Composition:*

(i) *Volume proportions:*

The volume proportions have been determined by point counting on the polished surfaces of Samples 3186/1 to 6. In addition the void size distribution and parameters have been calculated from examination of these polished surfaces. The results are as follows.

Sample	*3186/1*	*3186/2*	*3186/3*	*3186/4*	*3186/5*	*3186/6*
Aggregate	57.2	57.2	54.7	54.6	54.4	57.4
Paste	38.9	38.5	41.3	40.9	42.3	39.6
Total air void content	3.9	4.3	4.0	4.4	3.3	3.0
Number of voids per mm	0.23	0.27	0.21	0.16	0.19	0.17
	5.6	6.9	5.3	4.1	4.8	4.3
Average chord intercept	0.17	0.16	0.19	0.27	0.18	0.17
Specific surface in mm to -1	23.3	24.7	21.5	14.8	22.6	22.9
Spacing factor (mm)	0.34	0.27	0.34	0.51	0.33	0.34
Entrained air to paste/ratio	0.10	0.11	0.10	0.11	0.08	0.08

These results show a standard deviation for the paste content of 1.4% by volume. The effective water/cement ratio is estimated to be 0.40 and this points to a total cementitious content of about 500 kg/m^3 and total aggregate of about 1450 kg/m^3.

3. DISCUSSION

3.1 *Aggregate:*

The aggregate within the sample is a siliceous sand containing various lithologies which include the chert, metaquartzite, recrystallized sandstone and chalcedonic sandstone, ironstone and hornfels. No evidence of deterioration of the aggregate has been found.

3.2 *Paste:*

The paste is largely strong and coherent and has a very low level of porosity and contains very few microcracks. However, there are areas of the sprayed concrete, particularly below the reinforcement rods, where the

material contains abundant voids, cavities, and dusty and friable areas of paste. These zones appear to result from screening of the inner concrete by the reinforcement rods, producing a local patch of lower quality concrete below the rods. There are also numerous voids within the paste which are very small. These void show some tendency to cluster around the margins of aggregate particles, reducing the bond strength between the aggregate and the paste. In addition, further weakening of the material may have resulted from where the voids have coalesced to form larger cavities, particularly elongate cavities which pass through the paste and along the surfaces of aggregate particles.

3.3 *Deterioration:*

The occurrence of clustered voids around particles of the fine aggregate, and the tendency for cavities to occur in zones parallel to the external and internal surfaces, running through the paste and around the margins of aggregate pieces is potentially deleterious to the strength and long-term durability of the material.

The sprayed concrete contains zones beneath the reinforcement rods which are friable and dusty, and which contain abundant voids and some cavities which may be many millimetres in diameter. These areas of concrete are much weaker and much less robust than the majority of the concrete and may be the result of interference of the reinforcement rods with the spraying process. These zone are deleterious in terms of both strength and durability of the material, in particular because they occur near to or are in contact with steel reinforcement rods. The more porous concrete would also be susceptible to carbonation and recrystallization.

4. CONCLUSIONS

4.1 The twelve samples are of a sprayed concrete repair material containing a siliceous aggregate ranging up to 5 mm in diameter, in a medium grey portland cement containing microsilica.

4.2 The majority of the paste has very low porosity and contains very few microcracks.

4.3 The paste contains numerous voids, the abundance and distribution of which are summarized in in Section 2.4. The voids show some tendency to cluster around the margins of fine aggregate pieces, and may form discontinuous and continuous cavities which are orientated parallel to the internal and external surfaces.

4.4 The majority of the material is strong and robust, but there are patches of weak and friable, and highly. porous concrete below the reinforcement rods. This poorer quality material is considered to be the result of interference from the rods with the spraying of the concrete.

TARMAC STRUCTURAL REPAIRS
REPORT ON THE ANALYSIS OF SPRAYED CONCRETE

Reference - 3186

21st April, 1994

5. APPENDIX

5.1 *Photographs illustrating the samples:*

Figure 1:

Sample 3186/7

Scale: The ruler is engraved in millimetres and centimetres.

This view shows part of the outer sprayed material adjoining the inner concrete towards the base of the photograph. A layer of dark grey sprayed material occurs adjacent to the concrete, and robust layers of sprayed concrete with low levels of porosity occur around I3 and B3. The layers of sprayed material around E3 are friable and weak and contain a high void content.

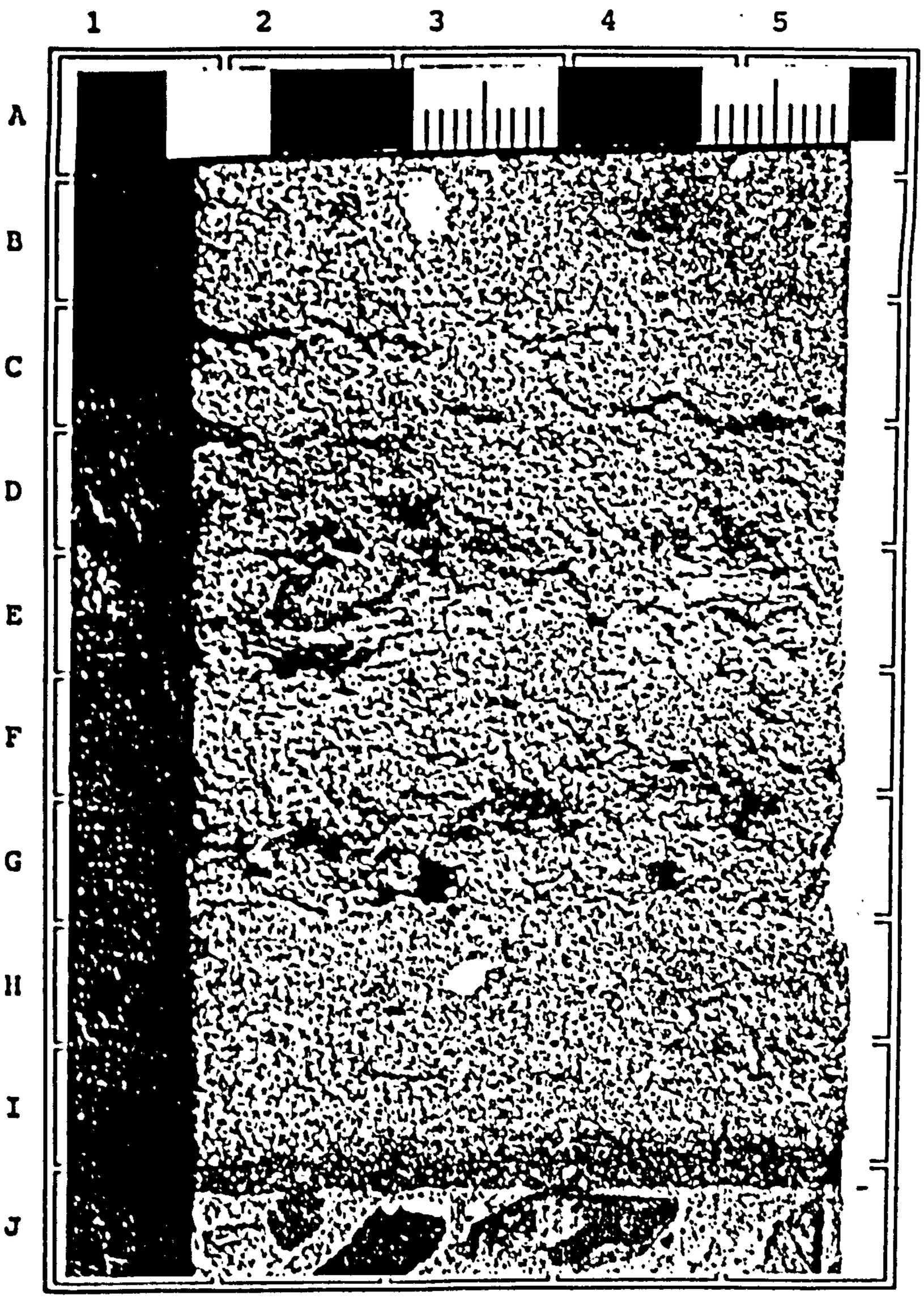

Figure 2:

Sample 3186/7

Scale: The ruler is engraved in millimetres and centimetres.

This view shows part of the sprayed external concrete with the external surface at the base of the view. A reinforcement rod occurs in F2 to F4, and the material directly below the reinforcement rod, centred around D2, contains cavities and numerous voids.

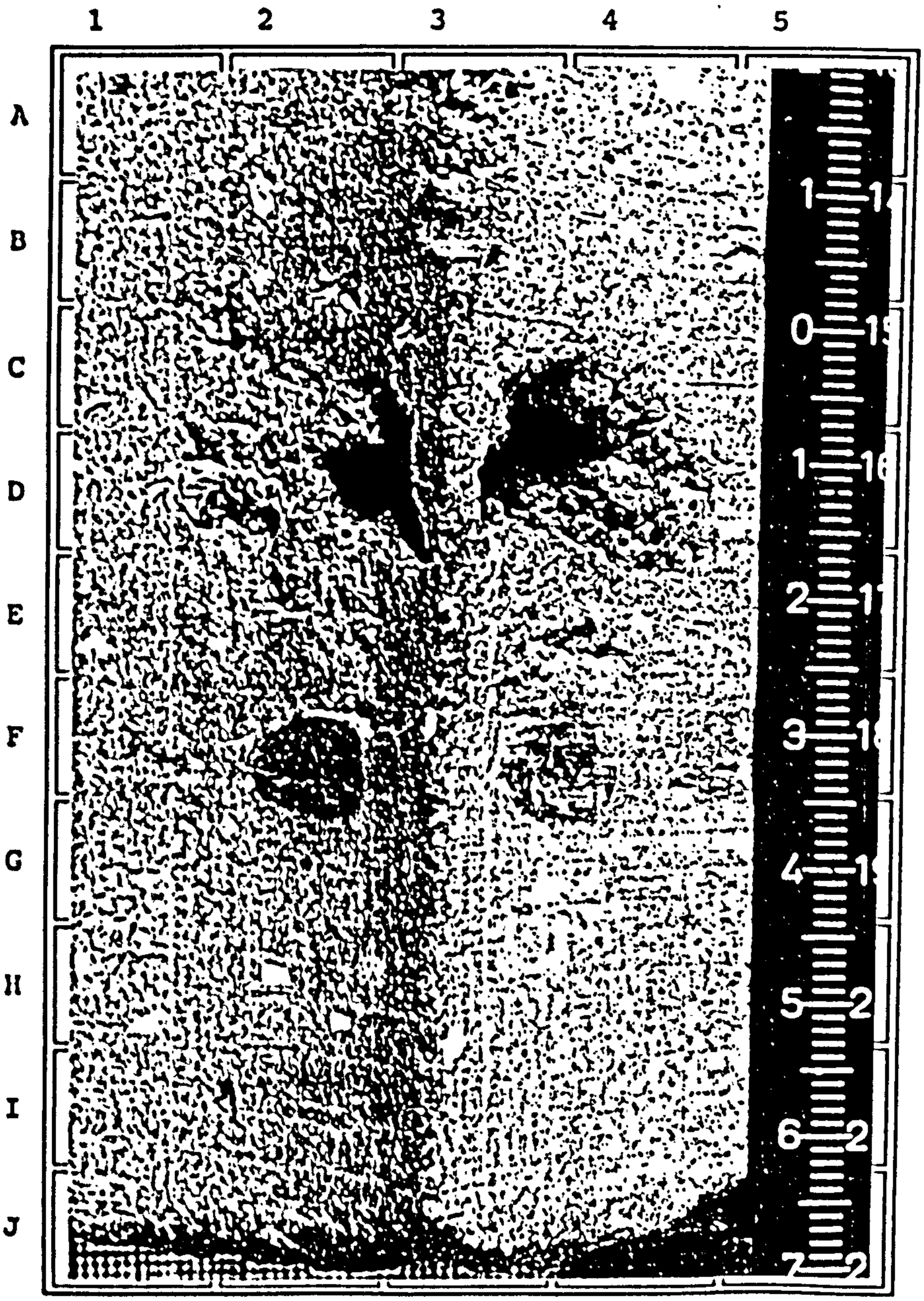

Figure 3:

Sample 3186/7

Scale: The width of the photograph represents 10 mm.

This is a detail of the weak, friable sprayed concrete showing numerous voids and cavities at A2, F1, F3, E4, etc.

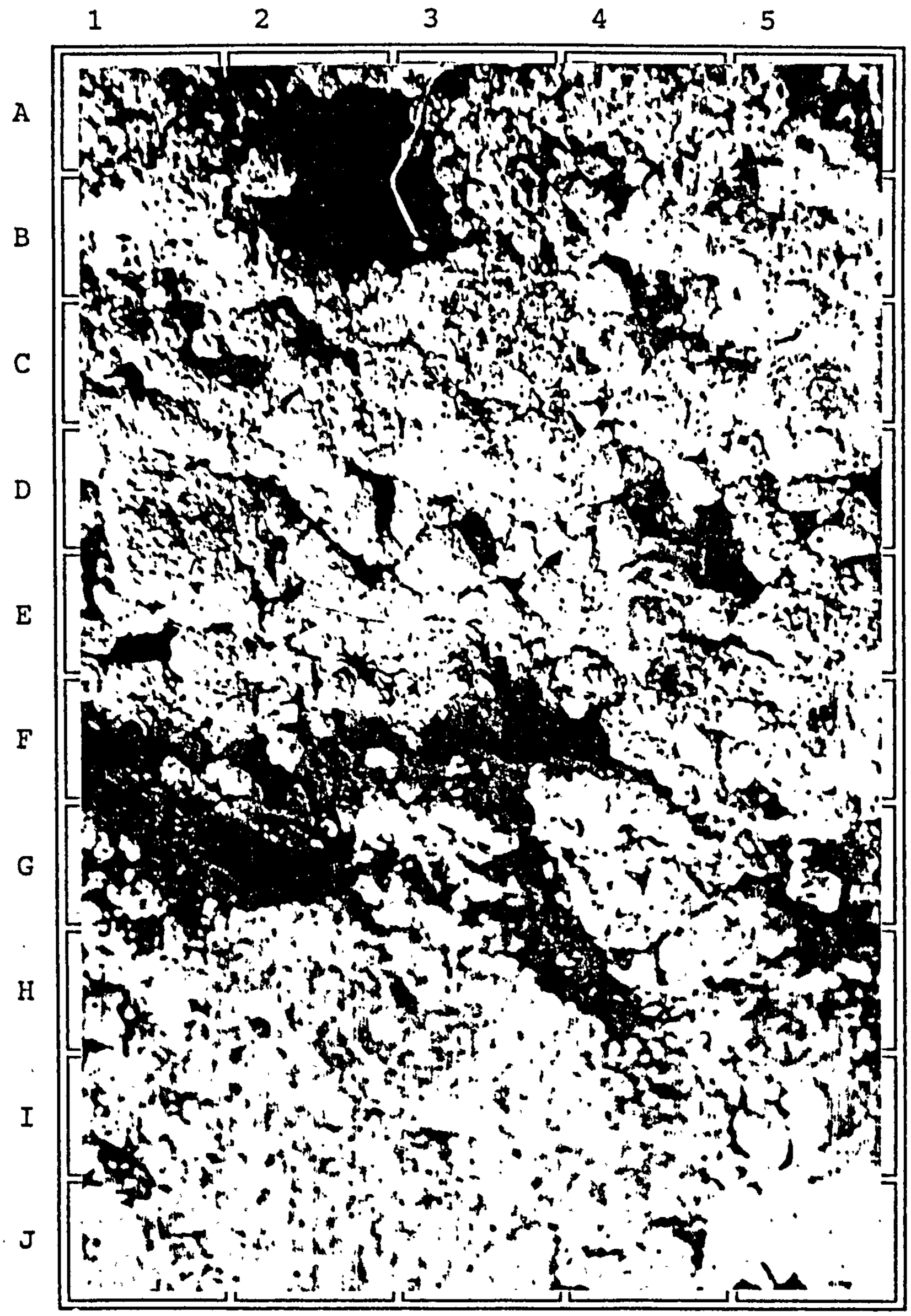

Figure 4:

Sample 3186/7

Scale: The width of the photograph represents 10 mm.

This view is of a sawn surface of the sample and show the junction between the internal concrete in the lower half of the view and the first layer of dark grey sprayed concrete in the upper half of the view. The junction appears very sound and no cavities or cracks occur at the junction.

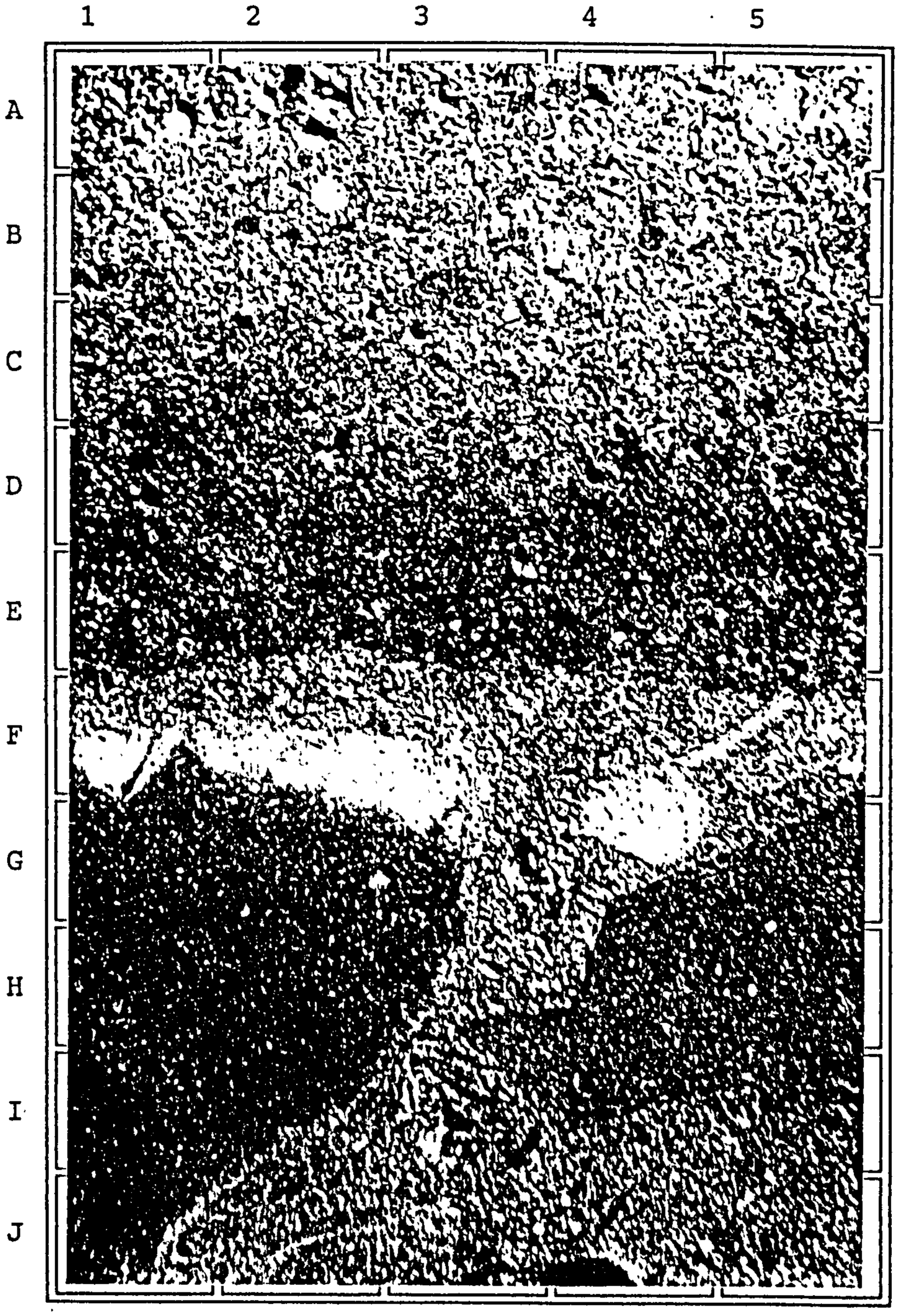

Figure 5:

Sample 3186/7

Scale: The ruler is engraved in millimetres and centimetres.

Polished plate. This view shows the polished surface of the specimen with the junction with the internal concrete at the base of the view. Layers are visible within the sprayed material running parallel to the internal and external surfaces, for example in A2, D2, I2 and J2. The polished plate has broken towards the junction with the internal concrete, where the dark first layer of sprayed material meets the remaining lighter coloured sprayed layers.

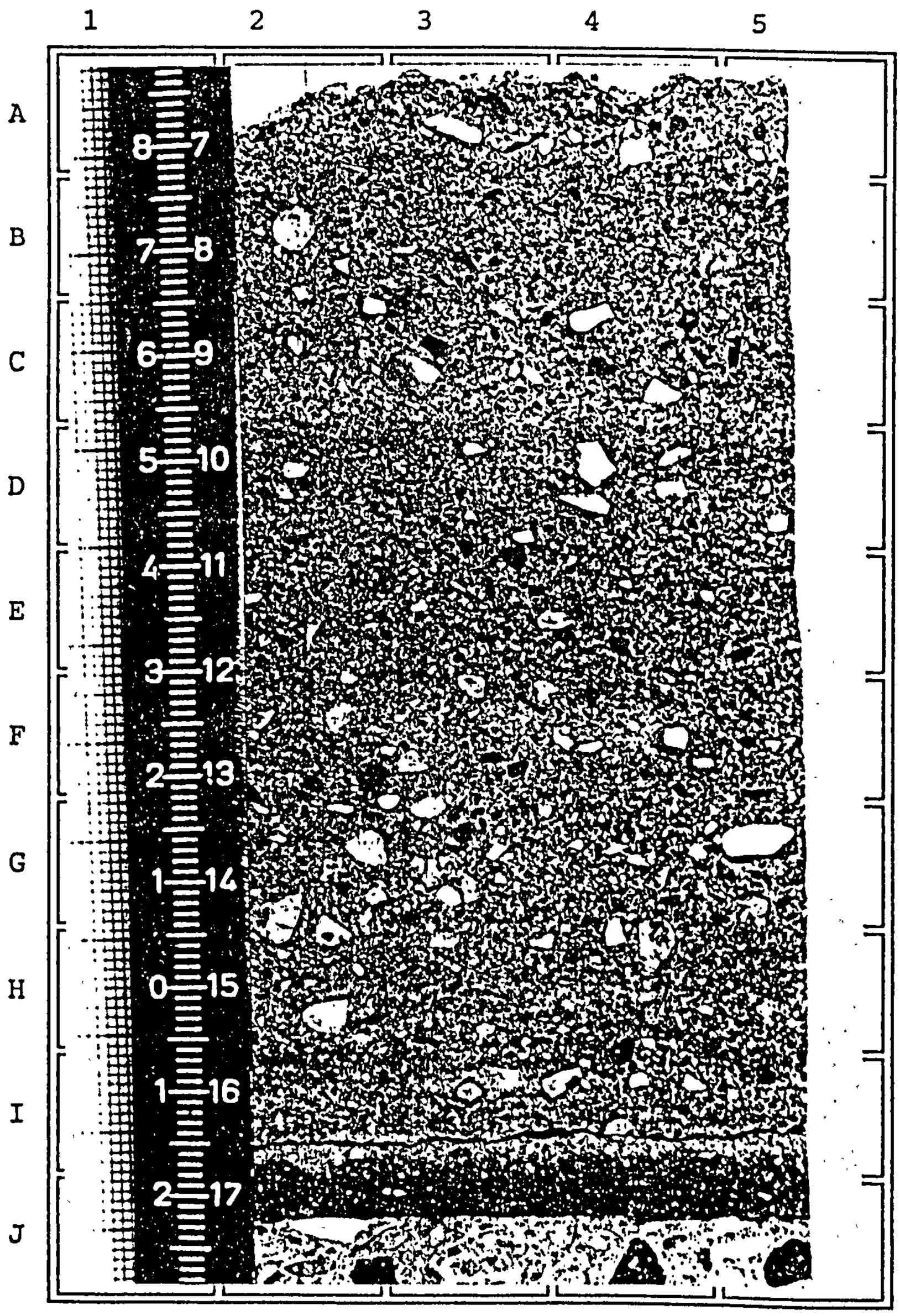

Figure 6:

Sample 3186/7

Scale: The width of the photograph represents 1 mm.

Thin section, transmitted light. This is a view of the sprayed material at approximately 10 mm from the junction with the concrete. The material to the left of the view is towards the junction with the internal concrete and the material on the right of the view is towards the external surface. A microcrack passes through the paste and around particles of aggregate from A2 to J3.

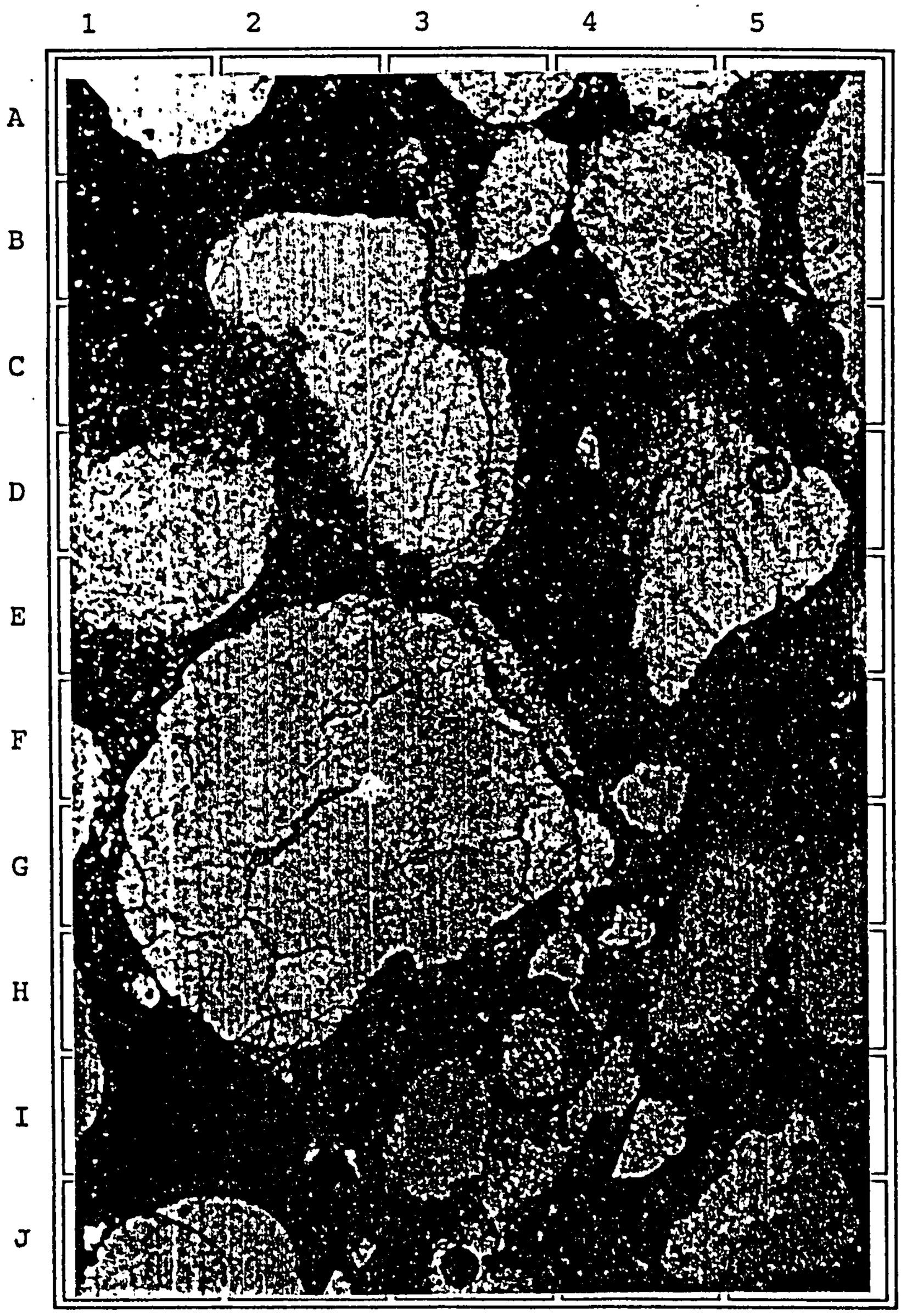

Figure 7:

Sample 3186/7

Scale: The width of the photograph represents 0.5 mm.

Thin section, transmitted light. This view is of the paste within the dark layer of sprayed material adjacent to the concrete. The paste is very dense and contains numerous residual unhydrated cement clinker particles. The paste is of very low porosity and contains very few microcracks.

Figure 8:

Sample 3186/7

Scale: The width of the photograph represents 0.5 mm.

Thin section, transmitted light. This view is of paste at approximately 10 mm from the junction with the internal concrete and shows slightly less dense paste than that illustrated in Figure 7. This paste contains abundant residual clinker particles and has very low porosity.

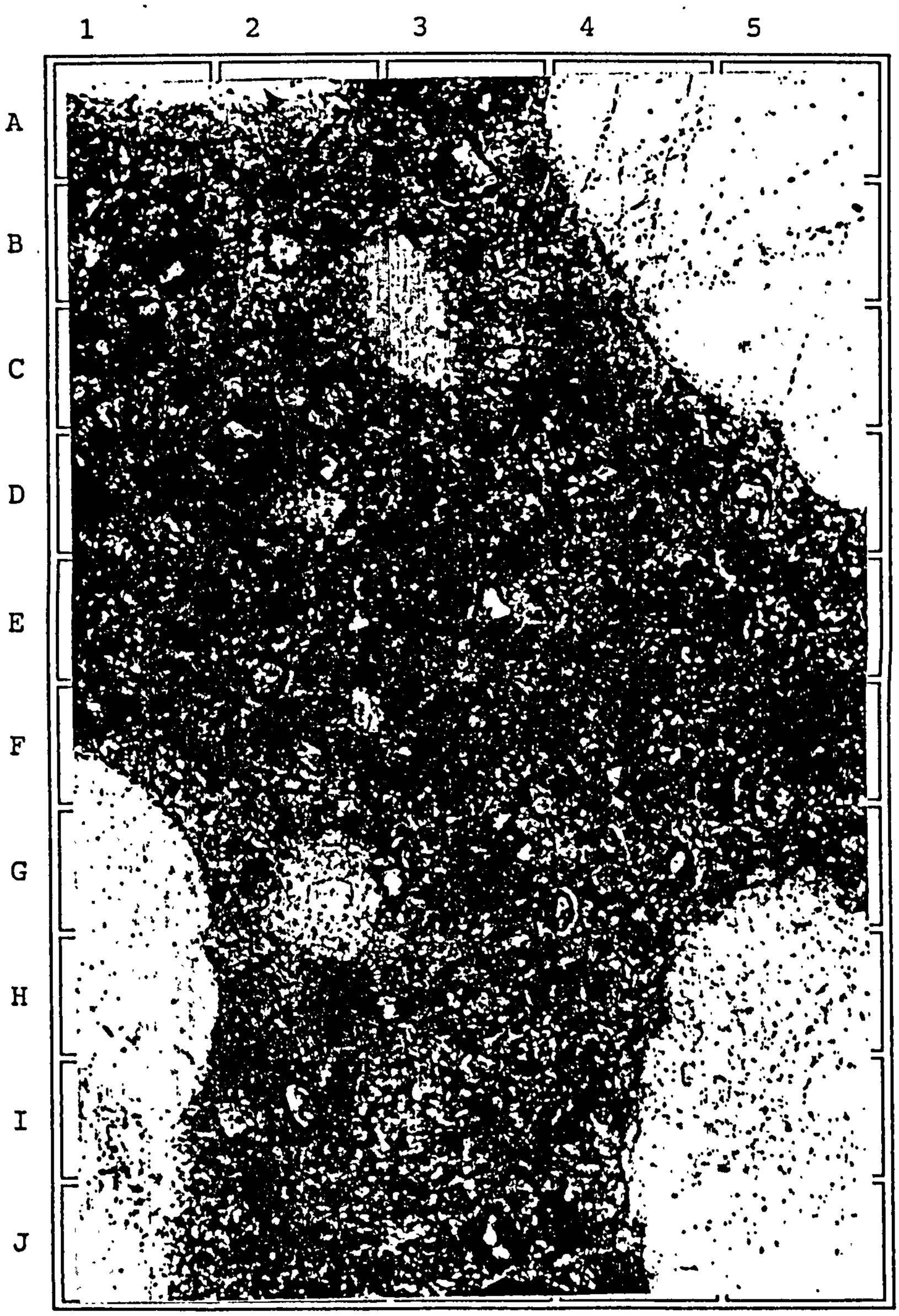

Figure 9:

Sample 3186/7

Scale: The width of the photograph represents 1 mm.

Thin section, fluorescent light. This view illustrates the junction between the internal concrete on the left of the view and the first layer of sprayed concrete on the right of the view. The concrete on the left has a paste which appears grey/green and is of low porosity, but contains microcracks running through the paste and around aggregate margins, for example from J2 to G2. The paste in the sprayed concrete is very dense and of exceptionally low porosity and contains no microcracks.

Figure 10:

Sample 3186/7

Scale: The width of the photograph represents 1 mm.

Thin section, fluorescent light. This view is of sprayed concrete approximately 5 mm from the junction with the internal concrete and shows a paste which is very dark and of very low porosity but contains a microcrack passing through the paste and around an aggregate margin from A3 to J4. A void is centred around B2/3.

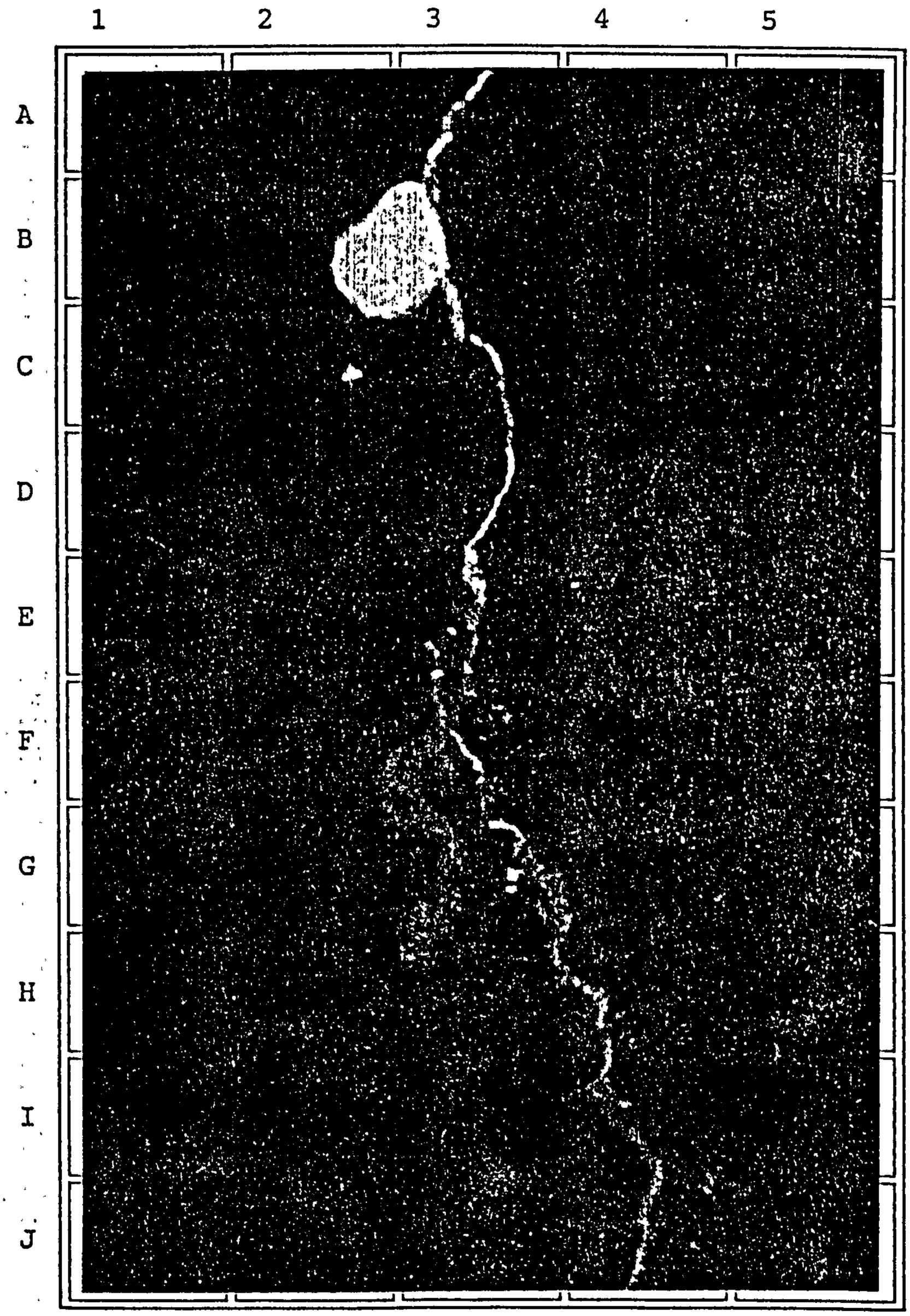

Figure 11:

Sample 3186/7

Scale: The width of the photograph represents 1 mm.

Thin section, fluorescent light. This view is of paste approximately 20 mm from the junction with the concrete and shows numerous voids centred around a particle of aggregate at F3. These voids have coalesced to form a cavity which is linked to a crack or series of cracks passing from A1 and A3 to J2 and J4.

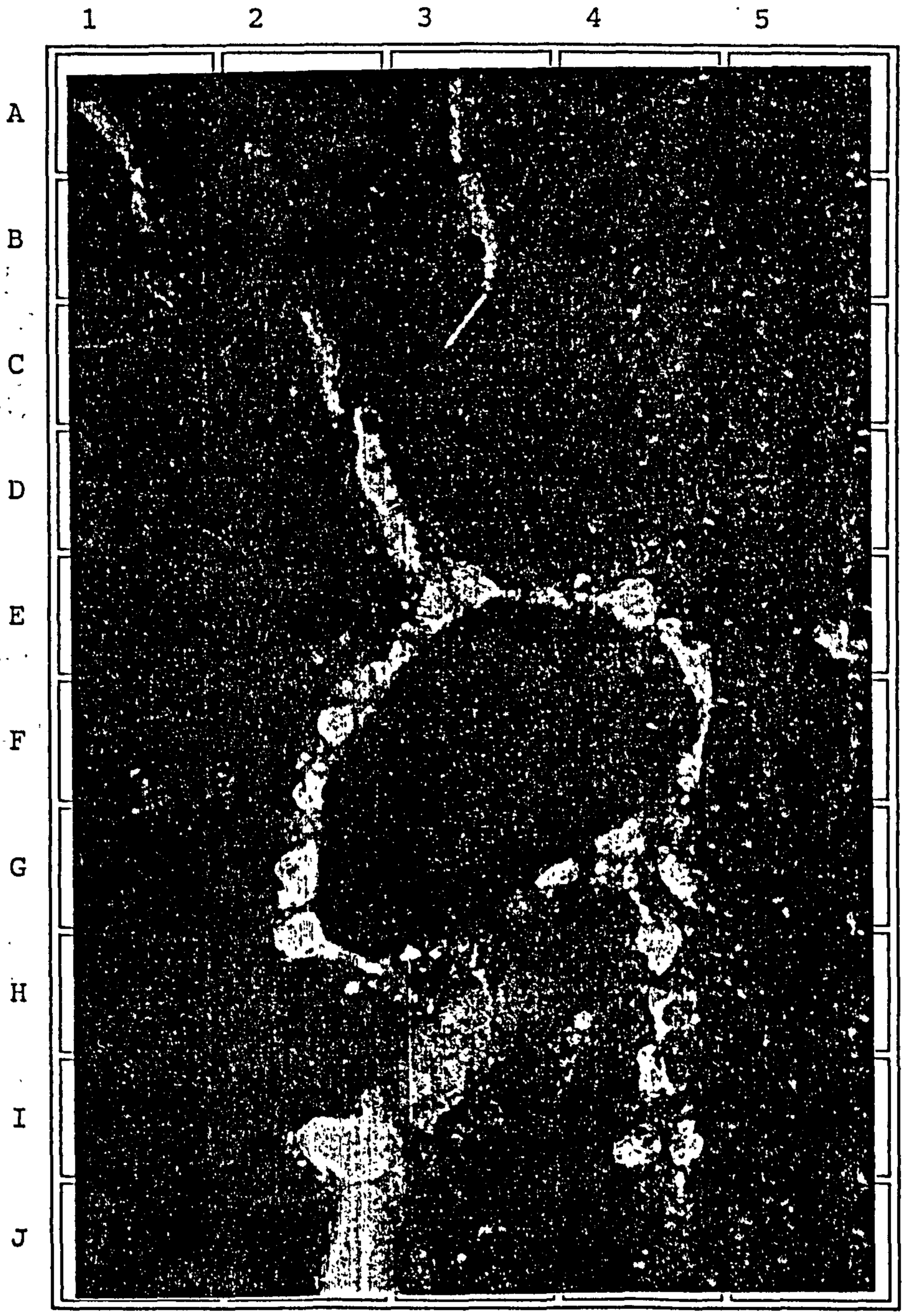

Figure 12:

Sample 3186/7

Scale: The width of the photograph represents 1 mm.

Thin section, fluorescent light. This view is of paste within the friable porous layers of sprayed concrete, and shows a highly porous and microcracked structure. Microcracks are visible within the paste passing from J2 and J4 to B3.

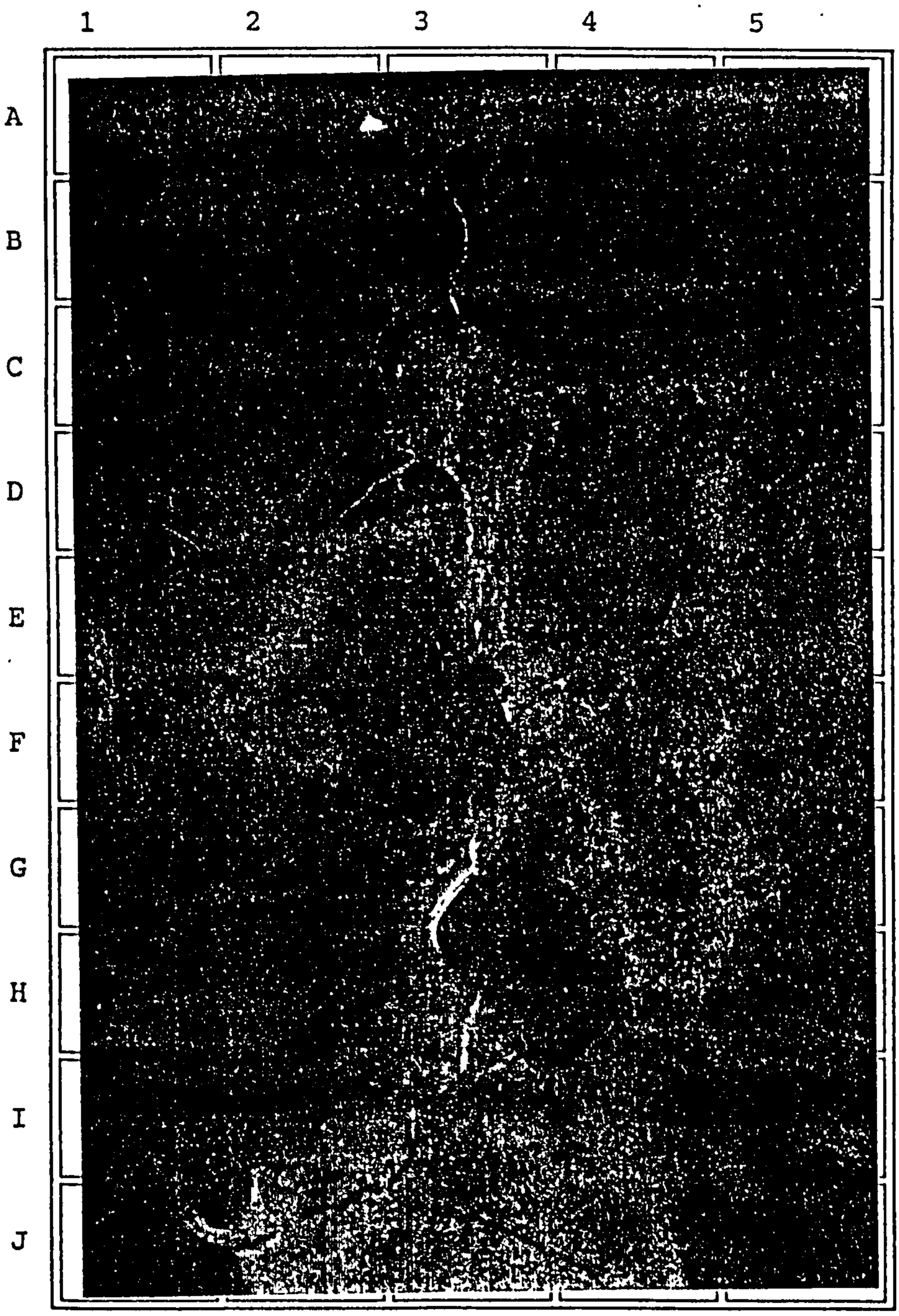

APPENDIX B

CHLORIDE INGRESSION TESTING

This appendix contains the report on Chloride Ingression testing on the sprayed concrete core specimens extracted from the pre-construction test panels.

TARMAC STRUCTURAL REPAIRS
REPORT ON CHLORIDE INGRESSION INTO SAMPLES OF SPRAYED CONCRETE

Reference - 3186A

18th July, 1994

CONTENTS

TARMAC STRUCTURAL REPAIRS
REPORT ON CHLORIDE INGRESSION INTO SAMPLES OF SPRAYED CONCRETE

Reference - 3186A

18th July, 1994

1. INTRODUCTION

1.1 *Samples:*

Five core samples of sprayed concrete measuring 100 mm in length by 75 mm diameter were provided on 28th February 1994.

1.2 *Objectives:*

It was requested that the samples be studied by the method of chloride ingression and that the effective diffusion coefficient be calculated.

1.3 *Procedures:*

(i) A thin layer of grease was placed on the curved surfaces of the cores and they were sealed into cans so that only the external surface was exposed

(ii) All the samples were conditioned by placing them in saturated $Ca(OH)_2$ solution for 24 hours.

(iii) Two samples were left in the $Ca(OH)_2$ solution for 28 days.

(iv) The other three samples were placed in a saturated $Ca(OH)_2$ solution containing NaCl at a concentration of 5 Molar.

(v) One of the samples was removed from this NaCl solution after 28 days and both samples were removed from the $Ca(OH)_2$ saturated solution after 28 days. One of the latter was placed in the NaCl solution; the other was used as a control to establish background chloride level.

(vi) The two samples taken from the two solutions at 28 days were dried by towelling. They were then cut and ground dry to produce a flat surface measuring over 30 mm wide and 25 mm deep and cut at right angles to the external surface and axially through the samples.

(vii) These two flat surfaces were analysed using the electron microprobe in zones parallel to the outer surface and with each zone being 4 mm wide. This showed that the traverse in the outermost 4 mm of the sample taken from the NaCl solution was the only traverse to have more than background chloride.

(viii) The plate exposed to chloride was therefore analysed again in zones 1 mm wide and parallel to the outer surface.

(ix) After 56 days two further samples were removed from the chloride solution. One of these was that preconditioned for 28 days in the $Ca(OH)_2$ solution while the second had been in the NaCl solution for 56 days.

(x) These two samples were analysed in zones 1 mm wide to a depth of 5 mm.

(xi) After 84 days the final sample was removed from the NaCl solution and analysed in the same way as the 56 day sample.

1.4 *Calculation:*

There are various factors that influence the chloride ingression including:

simple diffusion
diffusion with reaction
imbibition
temperature

The temperature of all these experiments was 38°C. Ideally the diffusion coefficient can be calculated from the Arrhenius equation if the tests have been carried out under two or more temperatures. For the present measurements only derivations from Fick's law can be applied. Two approaches have been used, one assuming pure diffusion, the other assuming reaction taking in chloride. It must be assumed that no carbonation or other alteration has occurred, since this will enhance chloride penetration. The calculations have been summarized in BCA (C & CA) Technical Report 544 by C. D. Lawrence. For simple diffusion the formula is

$$C/C_o = \text{erfc}[X/(2(Dt)^{0.5})] .$$

where C_o is the concentration in the solution outside the specimen, C the concentration inside the specimen, X the distance from the surface, D the diffusion coefficient, and t the time in seconds.

For diffusion with reaction the formula is

Y is obtained from $gY = (1 - C_X/C_1)/(C_X/C_1)$ and $2W = X/(Dt)^{0.5}$

where C_1 is the concentration of the ion in the outermost layer and C_X is the amount of the ion taken into combination by reaction and gY is a derivative of erfY.

For the present purpose C_X has been taken to be half of the concentration in the outermost layer (i.e. $C_X/C_1 = 0.5$). D is expressed in m^2/sec.

2. RESULTS

2.1 *Analytical data:*

The chloride concentrations found are given in Tables 1 to 4. The background chloride is low at 0.02% by weight of dry concrete. Though the background is low it is included in calculations, since it will contribute to the total chloride concentration affecting the infiltration and diffusion. The observations made show that the penetration of chloride is very low with penetration at significant levels occurring at less than 5 mm from the surface. The analytical data are measured as the percentage of the dry weight of the concrete. For the calculations this has been corrected by assuming that there is 7% of water by weight of concrete.

2.2 *Simple diffusion:*

Applying the simple diffusion equation is unreliable when the penetration is very low because the outermost layers could be affected by carbonation, bleeding and laitance segregation..

The results of this calculation are given in Tables 1 to 4. Typical values of D range from 1.1E-12 to 2.1E-12 m/sec. The overall mean is 1.56E-12 m^2/sec.

2.3 *Diffusion with reaction:*

The diffusion coefficients for this calculation are listed in Tables 1 to 4. The results centre around D = 1.0E-12 m^2/sec. This assumes that the chloride taken through reaction is half of that in the surface layer. The overall mean result is 1.02E-12 m^2/sec.

3. DISCUSSION

The diffusion coefficient found is similar to but less than that normally encountered in concrete which is about 5×10^{-12} m/sec. The profile is very steep and the surface concentration is considered to be less than might be expected from an ambient chloride concentration of 5M and at a

temperature of 38°C. The diffusion coefficient tends to increase slightly with depth into the concrete and to decrease slightly with time. Comparison is made with a typical gradient expected for high quality concrete in Figure 1. In this the dark points represent the expected gradient while the open squares are the 84 day results for the present samples. Considering the mean of all three times of analysis shows that this concrete gives a result almost identical with that expected for high quality concrete. The variation found in the outer 3 mm reflects variation in aggregate proportion which is more erratic than that of the bulk of the material. The inner data are more systematic and suggest a steady rate of penetration of the chloride front (producing 0.1% chloride 0.08% above background) of less than about 0.02 mm/day. This results in very close to that expected for high quality concrete.

TABLE 1 CHLORIDE CONCENTRATION IN OUTER 6 MM AFTER 28 DAYS

Depth (mm)	Weight % chloride (dry)					Mean	Mean (wet)	D m^2/s simple	D(m^2/s) with reaction
0 to 1	0.942	1.528	1.449	1.500	1.261	1.336	1.242		
1 to 2	0.482	0.516	0.476	0.735	0.478	0.5374	0.500	2.89E-13	1.88E-13
2 to 3	0.175	0.151	0.433	0.517	0.330	0.3212	0.299	7.16E-13	4.65E-13
3 to 4	0.172	0.163	0.281	0.381	0.211	0.2416	0.225	1.39E-12	9.00E-13
4 to 5	0.059	0.028	0.179	0.077	0.145	0.0976	0.091	1.92E-12	1.25E-12
5 to 6	0.052	0.017	0.091	0.049	0.078	0.0574	0.053	2.82E-12	1.83E-12
6 to 7	0.024	0.02	0.02	0.02	0.02	0.0208	0.019	1.28E-12	8.31E-13
						mean		1.4E-12	9.11E-13

TABLE 2 CHLORIDE CONCENTRATION IN OUTER 5 MM AFTER 28 DAYS (+28 days in CaCl soln.)

Depth (mm)	Weight % chloride (dry)					Mean	Mean (wet)	D m^2/s simple	D(m^2/s) with reaction
0 to 1	0.455	0.930	0.892	0.831	1.178	0.8572	0.797		
1 to 2	0.643	0.897	0.596	0.607	0.663	0.6812	0.634	2.45E-12	1.59E-12
2 to 3	0.412	0.391	0.468	0.219	0.159	0.3298	0.307	1.09E-12	7.09E-13
3 to 4	0.120	0.100	0.228	0.037	0.074	0.1118	0.104	1.23E-12	7.99E-13
4 to 5	0.030	0.042	0.046	0.012	0.018	0.0296	0.028	1.77E-12	1.15E-12
							mean	1.64E-12	1.06E-12

TABLE 3 CHLORIDE CONCENTRATION IN OUTER 5 MM AFTER 56 DAYS

Depth (mm)	Weight % chloride (dry)					Mean	Mean (wet)	D m^2/s simple	D(m^2/s) with reaction
0 to 1	0.975	1.187	0.939	0.683	0.753	0.907	0.844		
1 to 2	0.896	1.077	0.805	0.477	0.355	0.722	0.671	1.24E-12	8.04E-13
2 to 3	0.505	0.482	0.431	0.353	0.274	0.409	0.380	6.85E-13	4.45E-13
3 to 4	0.586	0.455	0.243	0.307	0.215	0.361	0.336	1.28E-12	8.34E-13
4 to 5	0.066	0.424	0.150	0.174	0.078	0.178	0.166	1.28E-12	8.32E-13.
5 to 6	0.067	0.338	0.042						
6 to 7		0.162							
7 to 8		0.136				mean		1.12E-12	7.29E-13
8 to 9		0.000							

TABLE 4 CHLORIDE CONCENTRATION IN OUTER 7 MM AFTER 84 DAYS

Depth (mm)	Weight % chloride (dry)					Mean	Mean (wet)	D m^2/s simple	D(m^2/s) with reaction
0 to 1	0.632	0.883	0.782	0.766	0.749	0.7624	0.709		
1 to 2	0.558	0.785	0.388	0.530	0.693	0.5908	0.549	6.8E-13	4.42E-13
2 to 3	0.847	0.590	0.627	0.567	0.539	0.634	0.590	4.86E-12	3.16E-12
3 to 4	0.406	0.500	0.492	0.346	0.552	0.4592	0.427	1.96E-12	1.27E-12
4 to 5	0.351	0.360	0.258	0.374	0.336	0.3358	0.312	1.76E-12	1.14E-12
5 to 6	0.149	0.248	0.151	0.214	0.213	0.1950	0.181	1.55E-12	1.01E-12
6 to 7	0.092	0.131	0.113	0.181	0.056	0.1146	0.107	1.72E-12	1.12E-12
							mean	2.09E-12	1.3567E-12

Figure 1:

Chloride concentration in the concrete sample tested at 84 days (open squares) and that expected for high quality concrete (picked squares).

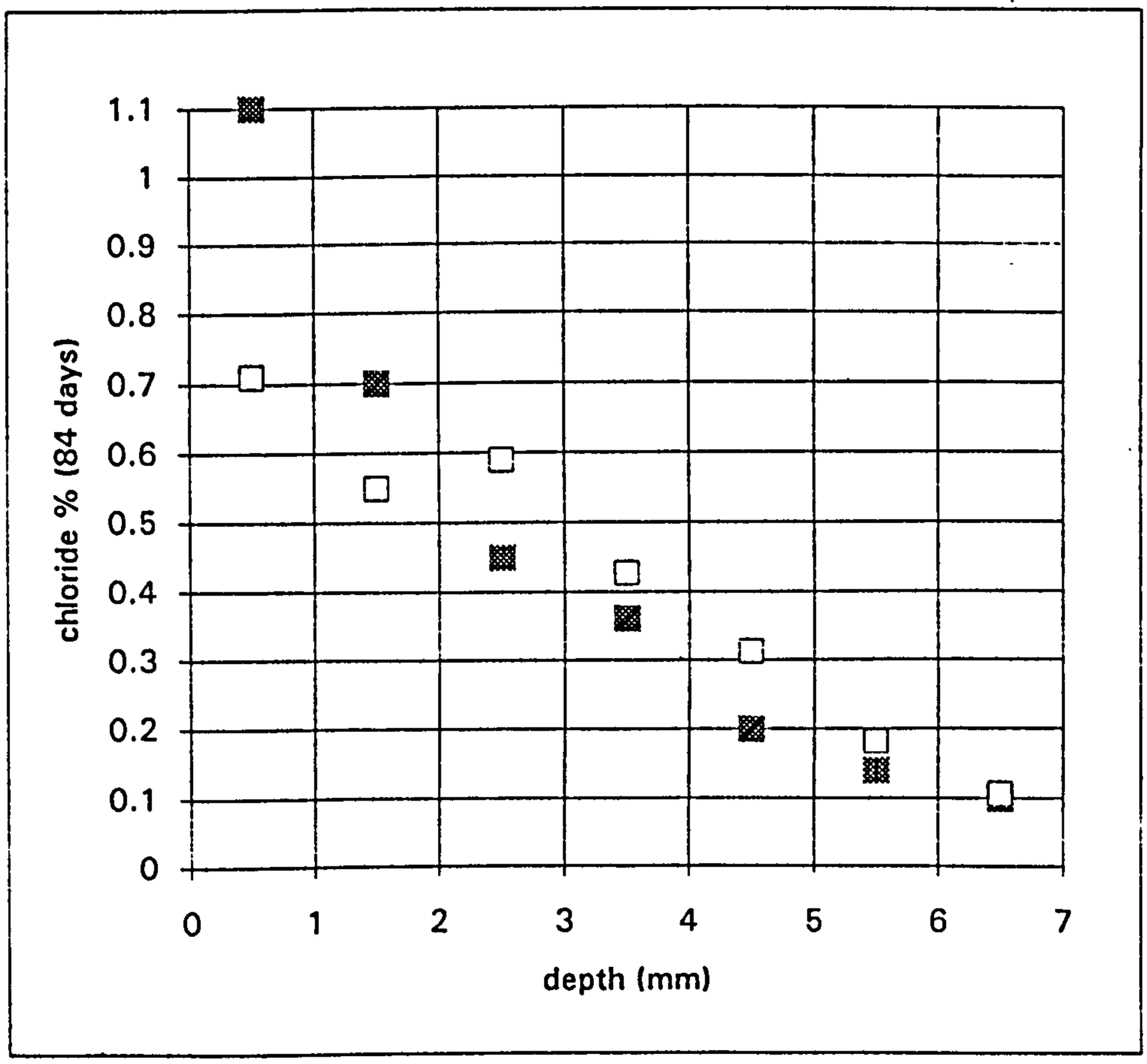

APPENDIX C

MOMENT CAPACITY OF A TYPICAL TEST SLAB

This appendix contains the calculations of the moment capacity of a typical test slab, A4, in accordance with BS 8110.

Test slab A4 is under-reinforced and assuming that all the reinforcement has yielded, the strain diagram and the BS 8110 simplified stress block are taken as shown in Figure C1,

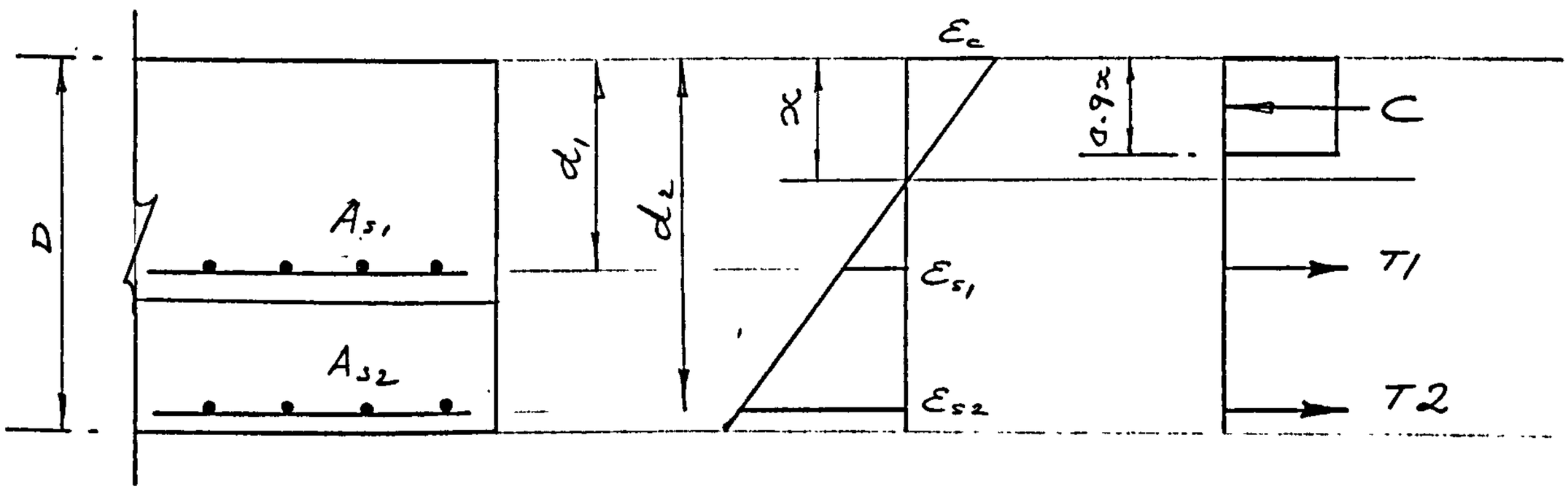

Figure C1 - Strain diagram and BS 8110 simplified stress block.

The stress diagram of the yielded steel is as shown in Figure C2.

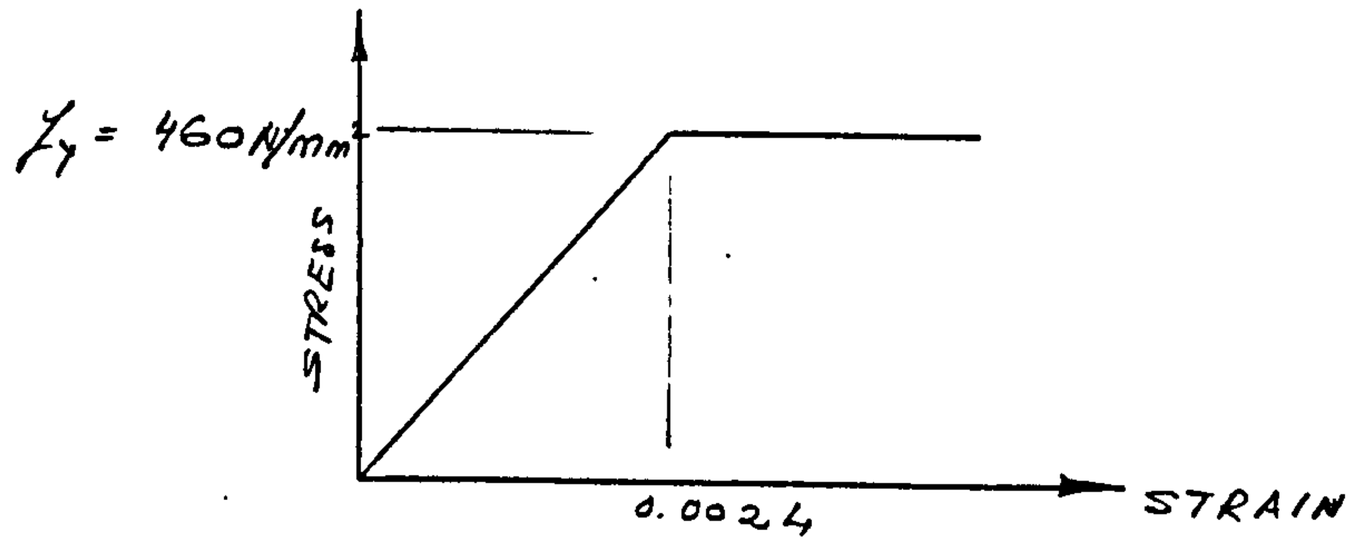

Figure C2 - Yielded steel.

Test slab data:

$D = 175$ mm (actual)

$d_1 = 100 - 15 - (0.5 \times 7) = 81.5$ mm

$d_2 = 175 - 25 - (0.5 \times 10) = 145$ mm

$b = 1000$ mm

$A_{s1} = 192.4$ mm^2/m

$A_{s2} = 392.7$ mm^2/m

$f_{cu} = 35$ N/mm^2

$f_y = 460$ N/mm^2

Position of the centroid at x:

$$C = T1 + T2$$

$$(0.45) \,.\, f_{cu} \,.\, b \,.\, (0.9x) \,.\, (1.5) = (0.87) \,.\, f_y \,.\, \{392.7 + 192.4\} \,.\, (1.15)$$

$$(0.45) \,.\, 35 \,.\, b \,.\, (0.9x) \,.\, (1.5) = (0.87) \,.\, 460 \,.\, \{392.7 + 192.4\} \,.\, (1.15)$$

$$x = 12.72 \text{ mm}$$

Lever arms:

$$z_1 = d_1 - \{0.5 \,.\, (0.9x)\} = 81.5 - \{(0.5) \,.\, (0.9) \,.\, (12.72)\} = 75.78 \text{ mm}$$

$$z_2 = d_2 - \{0.5 \,.\, (0.9x)\} = 145 - \{(0.5) \,.\, (0.9) \,.\, (12.72)\} = 139.28 \text{ mm}$$

Taking moment about the centre of the stress block C:

The moment capacity M_{BS8110} is,

$$M_{BS8110} = (T_1 \,.\, z_1) + (T_2 \,.\, z_2)$$

$$M_{BS8110} = (0.87) \,.\, 460 \,.\, \{(192.4).(75.78) + (392.7).(139.28)\} \,.\, (1.15)$$

$$M_{BS8110} = 32 \text{ kNm}$$

APPENDIX D

EXTRACTS FROM BS 5400: PART 10:1980

This appendix contains the original copy of Table 1 and the modified and updated Table 11 extracted from BS 5400: Part 10:1980.

Table 1. Annual flow of commercial vehicles ($n_c \times 10^6$)

Category of road			Number of millions of vehicles per lane, per year (n_c)	
Type	Carriageway layout	Number of lanes per carriageway	Each slow lane	Each adjacent lane
Motorway	Dual	3	2.0	1.5
Motorway	Dual	2	1.5	1.0
All purpose	Dual	3		
All purpose	Dual	2		
Slip road	Single	2		
All purpose	Single	3	1.0	Not applicable
All purpose	Single (10 m*)	2		
Slip road	Single	1		
All purpose	Single (7.3 m*)	2	0.5	Not applicable

*The number of vehicles in each lane of a single carriageway between 7.3 m and 10 m wide should be obtained by linear interpolation.

7.2.3.5 *Method of loading.* Only one vehicle should be assumed to be on the structure at any one time and each lane should be traversed separately. The effects of combinations of vehicles are allowed for in clause 8.

7.2.4 *Allowance for impact.* Where a discontinuity occurs in the road surface, e.g. at an expansion joint, the static stress at every point affected by a wheel, at or within 5 m of the discontinuity, should be increased by magnifying the relevant influence line, as shown in figure 7.

7.2.5 *Centrifugal forces.* The effects of any centrifugal force associated with the fatigue loading defined in 7.2.2 need only be considered for substructures ; the force should be taken as acting at and parallel to the road surface. The magnitude of the force should be calculated at the appropriate design speed of the particular road, for the individual vehicles of the standard load spectrum shown in table 11 as follows :

$$\text{the centrifugal force per axle} = \frac{W v^2}{127 r} \text{ (kN)}$$

where

W is the axle load of the vehicle (kN)
v is the design speed of the road (km/h)
r is the radius of curvature at the particular lane on which the vehicles are assumed to travel (m)

The force assumed for any vehi

$$\frac{30\,000}{r + 150} \text{ kN}$$

7.3 Railway loading

7.3.1 *General.* The loads to b appropriate combination of the lurching and centrifugal force, British Standard.

In welded members the dead lc considered. In unwelded meml have to be considered in deterr range when compression stres

7.3.2 *Application of loadin* applied to the appropriate leng influence lines of not more thai the algebraic maximum and mi detail under consideration.

Table 11. Typical commercial vehicle groups

Total axles	Chassis type	Average axle spacings, m	Loading Group	Total weight, kN	Axle loads, kN	No. in each group per million commercial vehicles	Vehicle designation
18	Girder Trailer and 2 tractors	4.5 1.5 4.0 7.5 13.5 7.5 4.0 4.5 1.5	H	3 680	80 160 160 240 (6 no.) 240 (6 no.) 80 160 160	10	18GT-H
			M	1 520	80 160 160 60 (6 no.) 60 (6 no.) 80 160 160	30	18GT-M
9	Tray Trailer and tractor	4.5 1.5 4.0 1.5 1.5 1.5 1.5 1.5	H	1 610	70 140 140 210 210 210 210 210 210	20	9TT-H
			M	750	50 110 110 80 80 80 80 80 80	40	9TT-M
7	Girder Trailer and tractor	4.5 1.5 4.0 2.0 10.0 2.0	H	1 310	70 140 140 240 240 240 240	30	7GT-H
			M	680	60 130 130 90 90 90 90	70	7GT-M
	Articulated	3.0 1.5 9.5 1.5 1.5 1.5	H	790	70 100 100 130 130 130 130	20	7A-H
5	Articulated	3.0 1.5 13.5 1.5	H	630	70 130 130 150 150	280	5A-H
		3.0 1.5 5.0 1.5 1.5	M	360	60 70 70 80 80 80	14 500	5A-M
			L	250	40 45 45 60 60	15 000	5A-L
	Articulated	3.0 6.5 1.5	H	335	55 100 90 90	90 000	4A-H
			M	260	45 85 65 65	90 000	4A-M
			L	145	35 50 30 30	90 000	4A-L
4	Rigid	1.5 3.5 1.5	H	280	50 50 90 90	15 000	4R-H
			M	240	40 40 80 80	15 000	4R-M
			L	120	20 20 40 40	15 000	4R-L
	Articulated	2.5 4.5	H	215	45 85 85	30 000	3A-H
			M	140	30 55 55	30 000	3A-M
			L	90	20 35 35	30 000	3A-L
3	Rigid	4.0 1.5	H	240	60 90 90	15 000	3R-H
			M	195	55 70 70	15 000	3R-M
			L	120	40 40 40	15 000	3R-L
2	Rigid	4.0	H	135	50 85	170 000	2R-H
			M	65	30 35	170 000	2R-M
			L	30	15 15	180 000	2R-L

TRACTOR + TRAILER

◉ Standard axle, 4 tyre, 1.8 m track ◎ Steering axle, 2 tyre, 2.0 m track O Special axle, 2 to 8 tyres, up to 3.4 m outer track

APPENDIX E

THE 15M SPAN TWO LANE SINGLE CARRIAGEWAY SLAB BRIDGE

BRIDGE UNDER CONSIDERATION

A 15 m two lane single carriageway slab bridge.

BRIDGE CONSTRUCTION

As shown in Figure E1 using:

$$\frac{\text{Span}}{\text{Depth}} = 20 \qquad \text{and} \qquad \text{Span} = 15\ \text{m}$$

$$\text{Depth} = 750\ \text{mm}$$

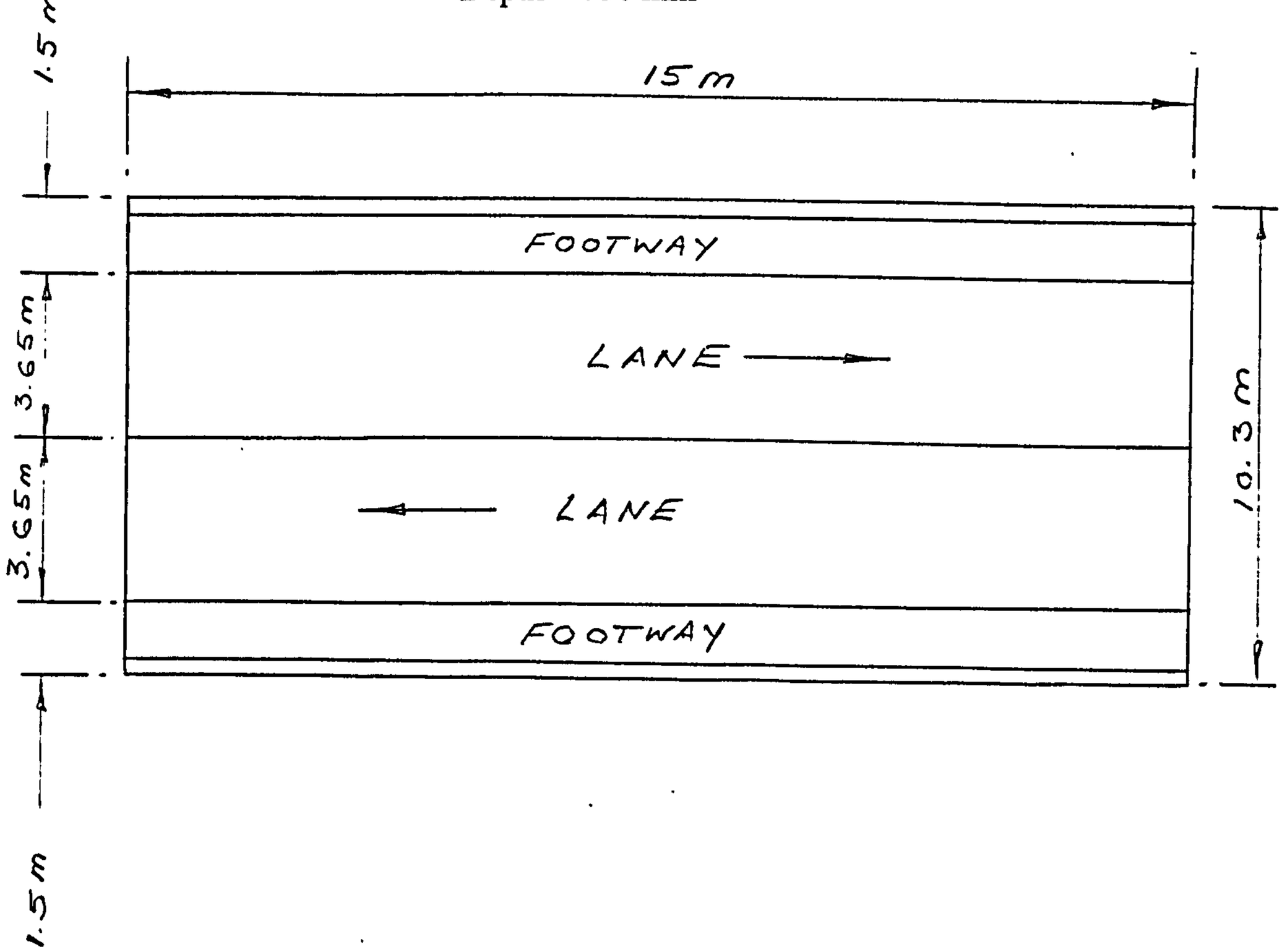

Figure E1 - A 15 m two lane single carriageway slab bridge.

BRIDGE LOADING

This is to be considered in accordance with BD 37/88: Loading for highway structures:

The bridge deck is to be designed to resist the most severe effect of either,

1. Design HA loading.
2. Design HA loading combined with design HB loading.

Case 2. is being adopted here.

Application of load case 2. in accordance with BD 37/88

Where the HB vehicle lies wholly within the notional lane, as shown in Figure E2, type HB loading is assumed to displace part of HA loading in the lane. No other live loading shall be considered for 25 metres in front of the leading axle to 25m behind the rear axle of the HB vehicle. The remainder of the loaded length of the lane or lanes thus occupied by the HB vehicle shall be loaded with HA udl only; HA KEL to be omitted

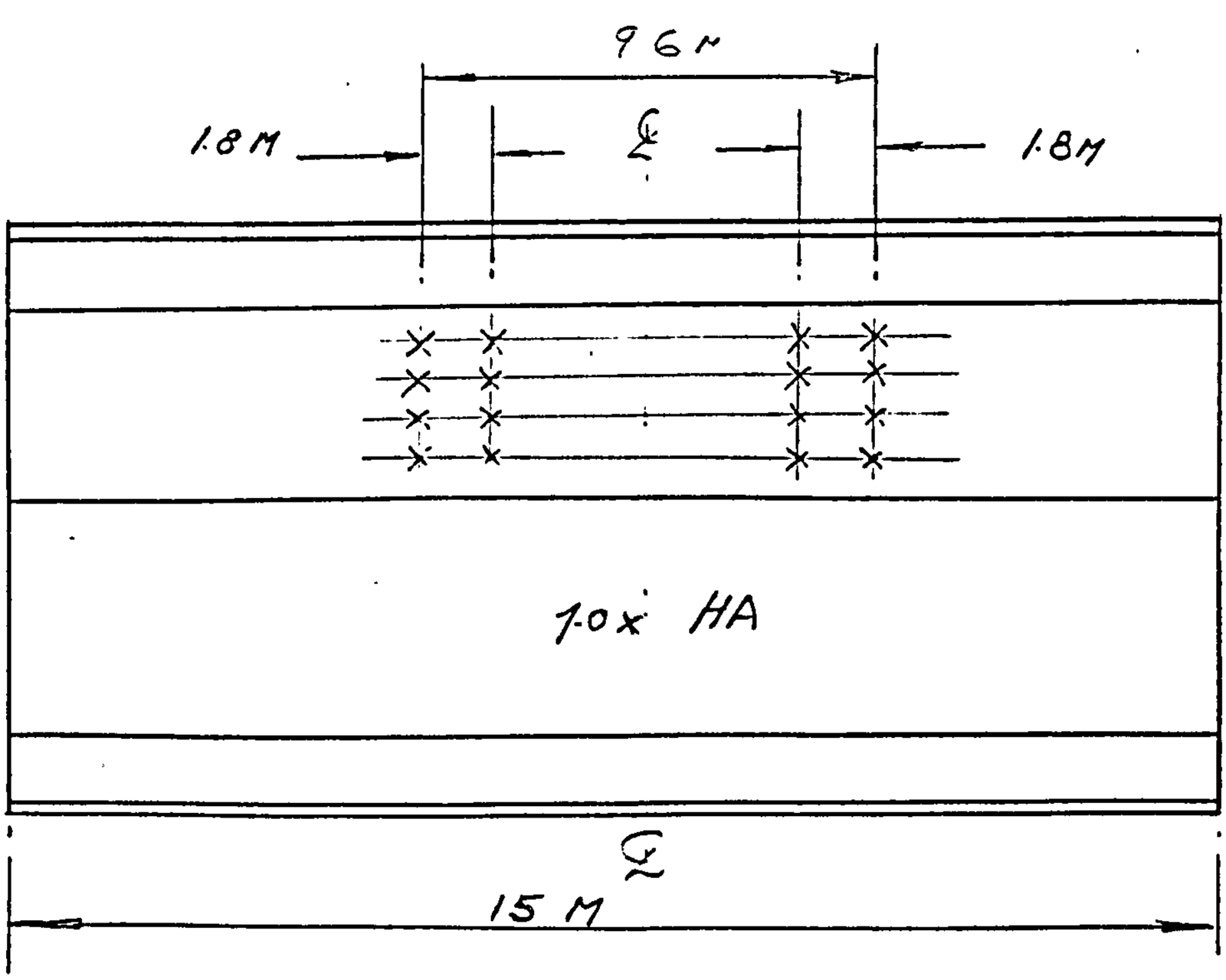

Figure E2 - Bridge loading for the 15 m two lane single carriageway slab bridge.

LOAD FACTOR

β_1 = HA Lane factor, from Table 14 of BD 37/88 = α_1.

$\beta_1 = \alpha_1 = 0.274$ x (notional lane width in m).

$\beta_1 = 0.274$ x 3.65.

$\beta_1 = 1$ (to be applied to HA udl and KEL).

$\beta_3 = 0.6$

$\gamma_{fl} = 1.3$ for both HA and HB when applied together.

$\gamma_{fl} = 1.15$ for concrete (unit weight = 24 kN/m^3).

$\gamma_{fl} = 1.5$ for footway (5 kN/m^2) and HA applied alone.

$\gamma_{fl} = 1.75$ for road surfacing (2 kN/m^2).

Note: HA comprises HA udl + KEL.

CHARACTERISTIC LOAD VALUE

Live load

$$\omega_{HA} = 336\left(\frac{1}{15}\right)^{0.67} \text{ kN/m of notional lane.}$$

KEL = 120 kN/ notional lane.

Abnormal load

HB = 45 Units (1 HB unit = 10 kN/axle).

HB = 450 kN/axle (each axle comprises 4 wheels).

Dead load

$\omega_{footpath} = 1.5$ x 2 x 5 = 15 kN/m of notional lane.

$\omega_{surfacing} = 7.3$ x 2 = 14.6 kN/m.

$\omega_{concrete}$ = (24 x 10.3 x 0.75) - (24 x 16 x π x 0.2^2) kN/m of notional lane.

Moment due to characteristic dead load

$$M_{deadload} = [(14.6) + (24 \times 10.3 \times 0.75) - (24 \times 16 \times \pi \times 0.2^2)]\, 15^2/8.$$

$M_{deadload} = 4.27$ x 10^3 kNm.

FACTORED LOAD VALUE

Live load

$$\omega_{HA} = 1.3 \times 336\left(\frac{1}{15}\right)^{0.67} = 71.17 \text{ kN/m.}$$

$$KEL = 120 \times 1.3 = 156 \text{ kN/m.}$$

$$\omega_{footpath} = 15 \times 1.5 = 22.5 \text{ kN/m.}$$

Abnormal load

$$HB = 450 \times 1.3 = 585 \text{ kN/axle.}$$

Dead load

$$\omega_{surfacing} = 14.6 \times 1.75 = 25.55 \text{ kN/m.}$$

$$\omega_{concrete} = (24 \times 10.3 \times 0.75 \times 1.15) - (24 \times 16 \times \pi \times 0.2^2 \times 1.15).$$

$$\omega_{concrete} = 157.72 \text{ kN/m.}$$

FACTORED MOMENT DUE TO FACTORED LOAD

Dead load

$$M_{deadload} = (157.72 + 25.55) \times 15^2/8 = 5154 \text{ kNm.}$$

Live load

$$M_{HA} = 71.17 \times 15^2/8 \text{ for single notional lanes of HA.}$$

$$M_{HA} = 2002 \text{ kNm.}$$

$$M_{KEL} = 7.5 \times 156/2.$$

$$M_{KEL} = 585 \text{ kNm.}$$

$$M_{footpath} = 22.5 \times 15^2/8 = 632.81 \text{ kNm.}$$

Abnormal load

$M_{HB} = 5967$ kNm from normal static with HB vehicle in the most severe position on the bridge).

TOTAL FACTORED MOMENT

$$M_{factored} = 2002 + 585 + 633 + 5967 + 5154.$$

$$M_{factored} = 1.43 \times 10^4 \text{ kNm.}$$

GRILLAGE ANALYSIS FOR THE ULTIMATE BENDING MOMENT ON THE BRIDGE BEING MODELLED

Grillage analysis was carried out using the computer package QSE Structural Analysis. In using this computer package, the bridge deck was modelled as shown in Figure E3

with the main feature comprising 5 No. longitudinal grids @ 2060 mm c/c by 8 No. transverse grids @ 1875 mm c/c.

Load value

Using the factored udl value,

$\beta_1 HA = 1 \times 71.17 = 71.17$ kN/m of notional lane.

$\omega_{footpath} = 22.5/2$ kN/m for each side of pedestrian footpath.

$\omega_{footpath} = 11.25$ kN/m.

$\omega_{surfacing} = 25.55$ kN/m.

$\omega_{concrete} = 157.72/5$ kN/m for each hypothetical beam in the grillage.

$\omega_{concrete} = 31.54$ kN/m.

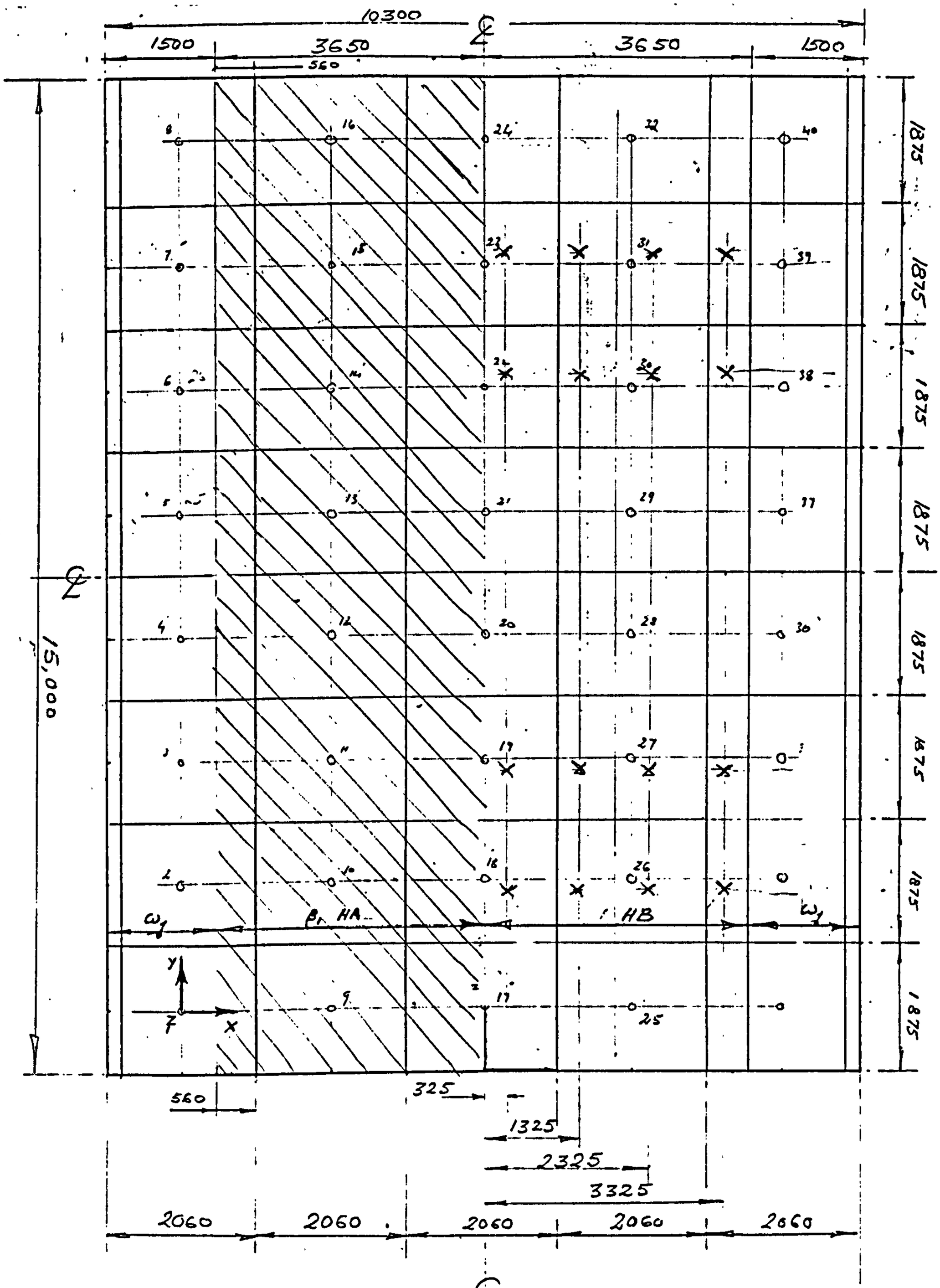

Figure E3 - Computer modelling of the 15m span bridge deck.

Abnormal factored load

A section is taken across the bridge at mid-span of Figure E3, with the HB vehicle in the position on the left lane. HB load being 585 kN/axle, the load distribution of this axle load on the hypothetical grillage is as follows:

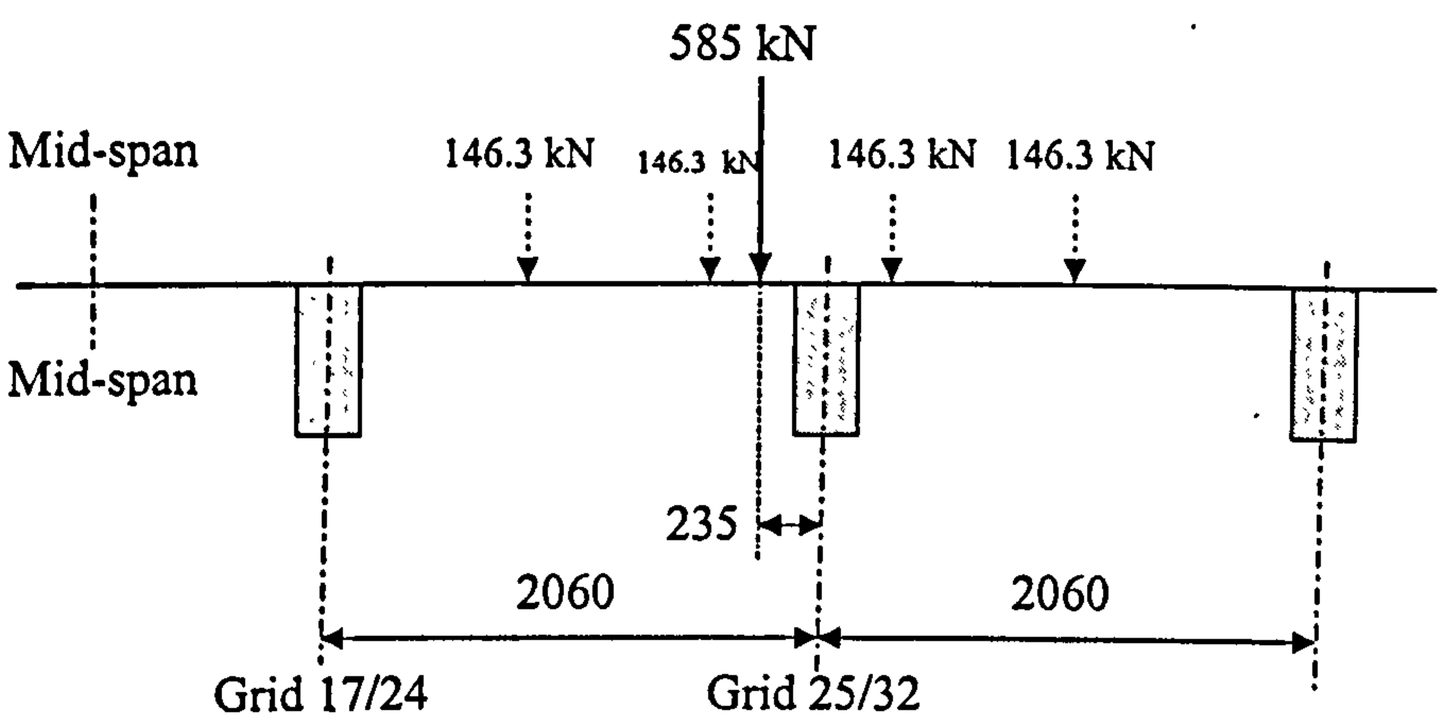

$$HB_{25/32} = 585 \times 235/2060 = 66.74 \text{ kN.}$$

$$HB_{17/24} = 585 \times 1825/2060 = 518.26 \text{ kN.}$$

KEL factored load

KEL point load is to be positioned at mid-span on each lane as shown in Figure E2. The position of each KEL point load relative to the hypothetical grid of Figure E3 and its load distribution is calculated as below, KEL = 156 kN/notional lane. Note that factors β_1 & β_3 are being applied if KEL falls into such zone.

1st notional lane from HB vehicle,

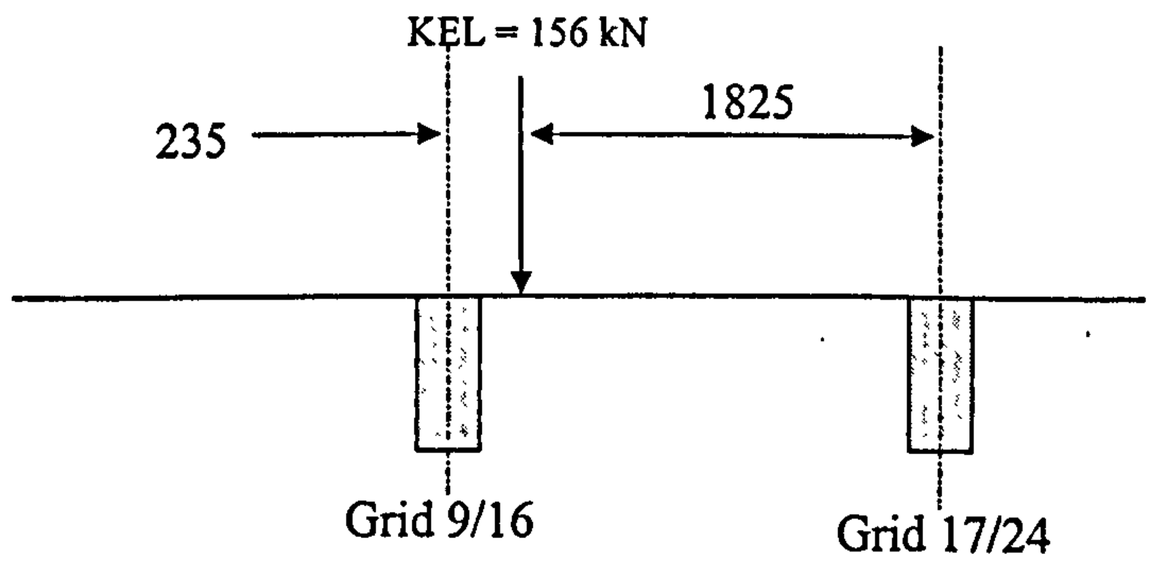

$$\beta_1 KEL_{17/24} = 1 \times 156 \times 235/2060 = 17.8 \text{ kN.}$$

$$\beta_1 KEL_{9/16} = 1 \times 156 \times 1825/2060 = 138.2 \text{ kN.}$$

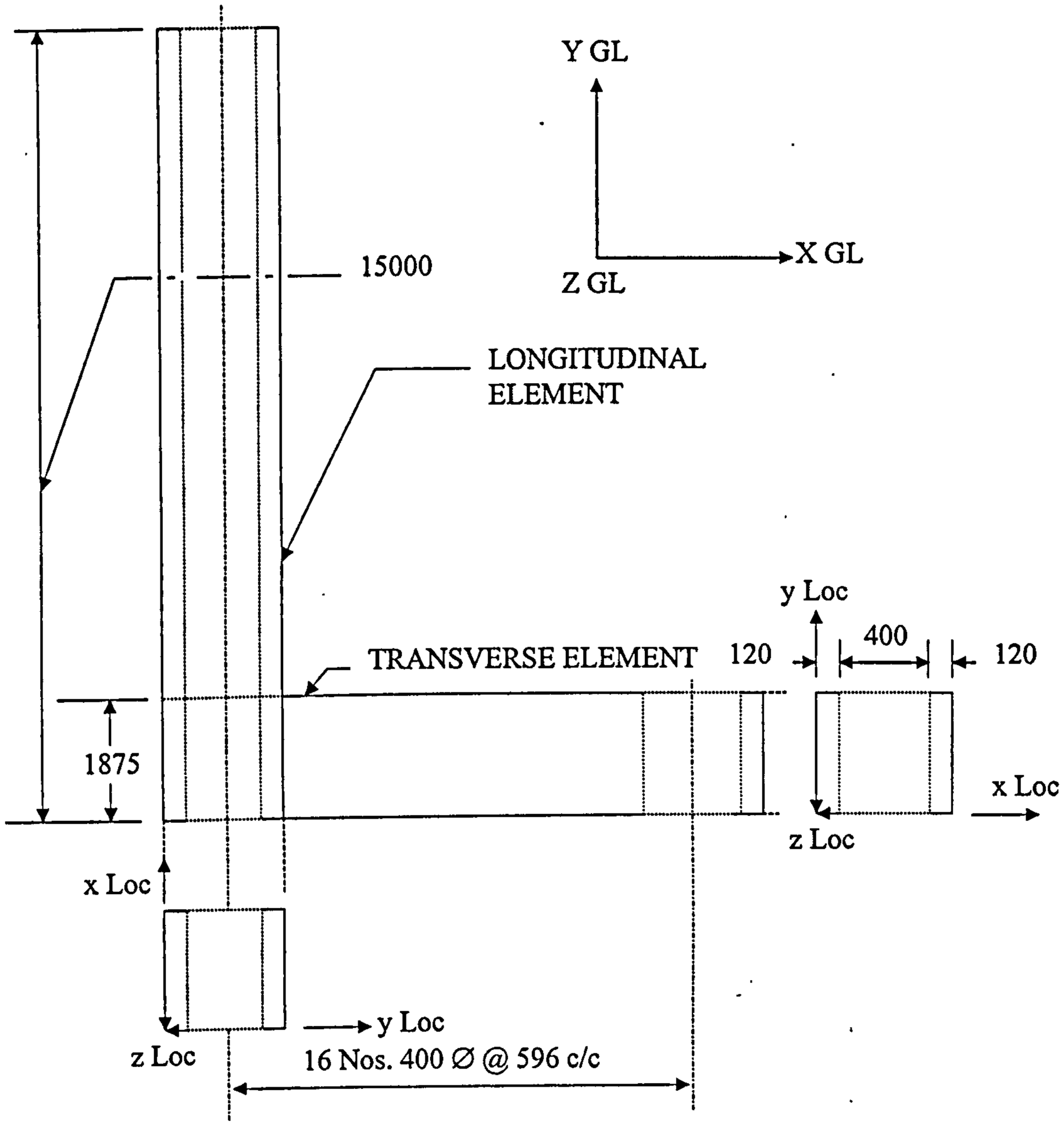

Figure E4 - Orientation of axes for bridge.

Longitudinal element

$$I_{YY} = \frac{bd^3}{12} = \frac{10300 \times 750^3}{12} = 3.62 \times 10^{11}\,mm^4 \text{ gross cross section.}$$

$I_{YY} = 3.62 \times 10^{11} - (16 \times \pi \times 400^4/64) = 3.42 \times 10^{11}\ mm^4$ Net cross section.

$I_{YY} = 3.42 \times 10^{11} / 5 = 6.84 \times 10^{10}\ mm^4$ for each longitudinal element.

$$I_{XX} = \frac{bd^3}{12} = \frac{1875 \times 750^3}{12} - \frac{1875 \times 400^3}{12} = 5.59 \times 10^{10}\,mm^4 \text{ net cross section.}$$

$$I_{ZZ} = \frac{750 \times 10300^3}{12} = 6.83 \times 10^{13}\ mm^4 \text{ gross cross section.}$$

$I_{ZZ} = 6.83 \times 10^{13}/5 = 1.37 \times 10^{13}$ mm^4 for each element.

$$J = \frac{1}{3}bh^3 - \frac{\pi}{2}r^4$$

$$J = \frac{1}{5}\left[\frac{10300 \times 750^3}{3} - \frac{\pi \times 16}{2}\left(\frac{400}{2}\right)^4\right] \text{ net cross section of each element.}$$

$J = 2.82 \times 10^{11}$ mm^4.

Transverse element

$$I_{YY} = \frac{1875}{12}750^3 - \frac{1875}{12}400^3 = 5.59 \times 10^{11} \text{ mm}^4 \text{ Net cross section.}$$

$$I_{XX} = \frac{1}{5}\left[\frac{10300 \times 750^3}{12} - \frac{16 \times \pi \times 400^4}{64}\right] = 6.84 \times 10^{10} \text{ mm}^4$$

$$I_{ZZ} = \frac{2 \times 175 \times 1875^3}{12} = 1.92 \times 10^{11} \text{mm}^4$$

$$J = \frac{1}{3}bh^3 = 2\left(\frac{1875 \times 175^3}{3}\right) = 6.7 \times 10^9 \text{ mm}^4.$$

LOAD DATA FOR COMPUTING

Table E details the computing data.

Table E - Computing data.

Grid line, refer to Fig E3	**UDL (kN/m)**	**KEL (kN)**	**HB load (kN)**
1/8	$\frac{560}{3650}(71.2 + 25.6) + 11.3 + 31.5 = 57.6$	-	-
9/16	$\frac{2060}{3650}(71.2 + 25.6) + 31.5 = 86.$	138.2	-
17/24	$\frac{1030}{3650}(71.2) + \frac{2060}{3650}(25.6) + 31.5 = 66.0$	17.8	66.74 @ four positions along span direction
25/32	$\frac{2060}{3650}(25.6) + 31.5 = 45.9$	-	518.26 @ four positions along span direction
33/40	$\frac{560}{3650}(25.6) + 31.5 + 11.3 = 46.7$	-	1

APPENDIX F

THE 20M SPAN TWO LANE DUAL CARRIAGEWAY SLAB BRIDGE

BRIDGE UNDER CONSIDERATION

A 20m span two lane dual carriageway slab bridge.

BRIDGE CONSTRUCTION

As shown in Figure F1 using:

$$\frac{\text{Span}}{\text{Depth}} = 20 \qquad \text{and} \qquad \text{Span} = 20\text{m}$$

$$\text{Depth} = 1000\text{mm}$$

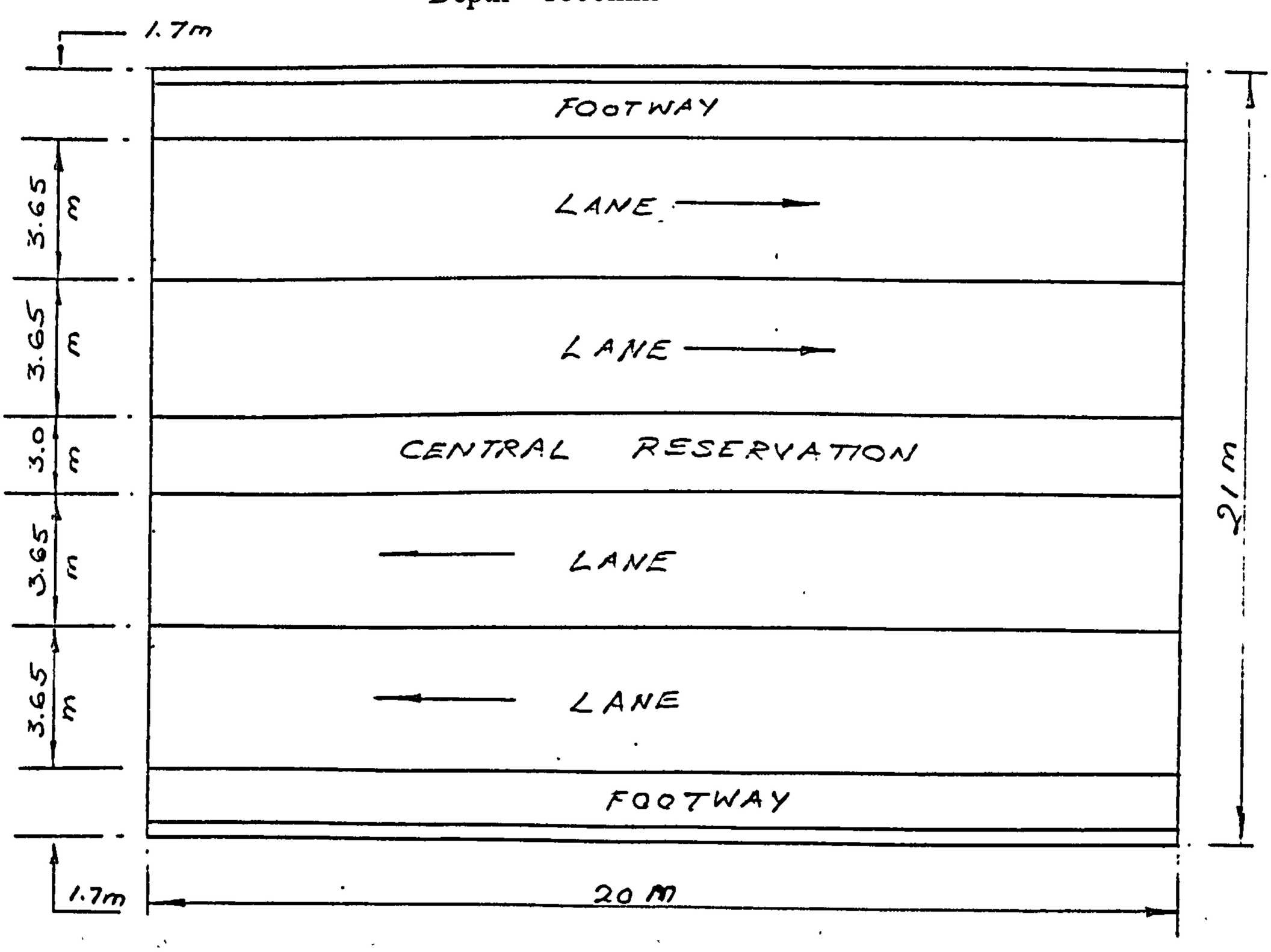

Figure F1 - A 20m span two lane dual carriageway slab bridge.

BRIDGE LOADING

This is to be considered in accordance with BD 37/88: Loading for highway structures:

The bridge deck is to be designed to resist the most severe effect of either,

1. Design HA loading.
2. Design HA loading combined with design HB loading.

Case 2. is being adopted here.

Application of load case 2. in accordance with BD 37/88

Where the HB vehicle lies wholly within the notional lane, as shown in Figure F2, type HB loading is assumed to displace part of HA loading in the lane. No other live loading shall be considered for 25 metres in front of the leading axle to 25m behind the rear axle of the HB vehicle. The remainder of the loaded length of the lane or lanes thus occupied by the HB vehicle shall be loaded with HA udl only; HA KEL to be omitted

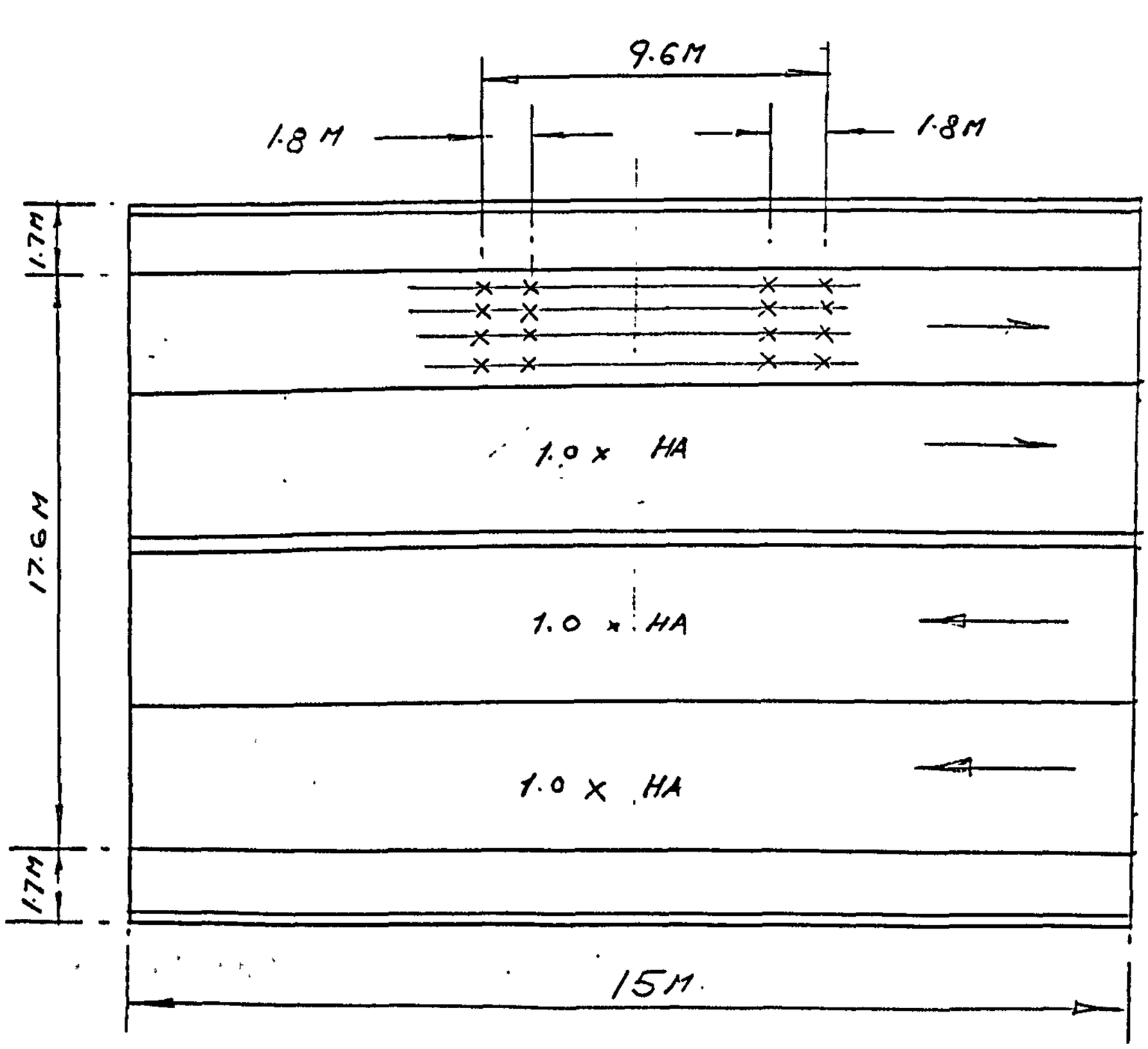

Figure F2 - Bridge loading for the 20m span dual carriageway slab bridge.

LOAD FACTOR

β_1 = HA Lane factor, from Table 14 of BD 37/88 = α_1.

$\beta_1 = \alpha_1 = 0.274$ x (notional lane width in m).

$\beta_1 = 0.274 \times 3.65$.

$\beta_1 = 1$ (to be applied to HA udl and KEL).

$\beta_3 = 0.6$

$\gamma_{fl} = 1.3$ for both HA and HB when applied together.

$\gamma_{fl} = 1.15$ for concrete (unit weight = 24 kN/m^3).

$\gamma_{fl} = 1.5$ for footway (5 kN/m^2) and HA applied alone.

$\gamma_{fl} = 1.75$ for road surfacing (2 kN/m^2).

Note: HA comprises HA udl + KEL.

CHARACTERISTIC LOAD VALUE

Live load

$$\omega_{HA} = 336\left(\frac{1}{20}\right)^{0.67} \text{ kN/m of notional lane.}$$

KEL = 120 kN/ notional lane.

Abnormal load

HB = 45 Units (1 HB unit = 10 kN/axle).

HB = 450 kN/axle (each axle comprises 4 wheels).

Dead load

$\omega_{footpath} = 3.4 \times 5 = 17$ kN/m of notional lane.

$\omega_{surfacing} = 17.6 \times 2 = 35.2$ kN/m.

$\omega_{concrete} = (24 \times 21 \times 1) - (24 \times 21 \times \pi \times 0.38^2)$ kN/m of notional lane.

Moment due to characteristic dead load

$$M_{deadload} = [(35.2) + (24 \times 21 \times 1) - (24 \times 21 \times \pi \times 0.38^2)] \, 20^2/8.$$

$M_{deadload} = 1.56 \times 10^4$ kNm.

FACTORED LOAD VALUE

Live load

$$\omega_{HA} = 1.3 \times 336\left(\frac{1}{20}\right)^{0.67} = 58.7 \text{ kN/m.}$$

$$KEL = 120 \times 1.3 = 156 \text{ kN/m.}$$

$$\omega_{footpath} = 3.4 \times 5 \times 1.5 = 25.5 \text{ kN/m.}$$

Abnormal load

$$HB = 450 \times 1.3 = 585 \text{ kN/axle.}$$

Dead load

$$\omega_{surfacing} = 17.6 \times 2 \times 1.75 = 61.6 \text{ kN/m.}$$

$$\omega_{concrete} = (24 \times 21 \times 1 \times 1.15) - (24 \times 21 \times \pi \times 0.38^2 \times 1.15).$$

$$\omega_{concrete} = 317 \text{ kN/m.}$$

FACTORED MOMENT DUE TO FACTORED LOAD

Dead load

$$M_{deadload} = (317 + 61.6) \times 20^2/8 = 18930 \text{ kNm.}$$

Live load

$$M_{HA} = 3 \times 58.7 \times 20^2/8 \text{ for three notional lanes of HA.}$$

$$M_{HA} = 8805 \text{ kNm.}$$

$$M_{KEL} = 10 \times 3 \times 156/2.$$

$$M_{KEL} = 2340 \text{ kNm.}$$

$$M_{footpath} = 25.5 \times 20^2/8 = 1275 \text{ kNm.}$$

Abnormal load

$M_{HB} = 8897$ kNm from normal static with HB vehicle in the most severe position on the bridge).

TOTAL FACTORED MOMENT

$$M_{factored} = 19830 + 1275 + 8805 + 2340 + 8897.$$

$$M_{factored} = 4.025 \times 10^4 \text{ kNm.}$$

GRILLAGE ANALYSIS FOR THE ULTIMATE BENDING MOMENT ON THE BRIDGE BEING MODELLED

Grillage analysis was carried out using the computer package QSE Structural Analysis. In using this computer package, the bridge deck was modelled as shown in Figure F3 with the main feature comprising 7 No. longitudinal grids @ 3000 mm c/c by 8 No. transverse grids @ 2500 mm c/c.

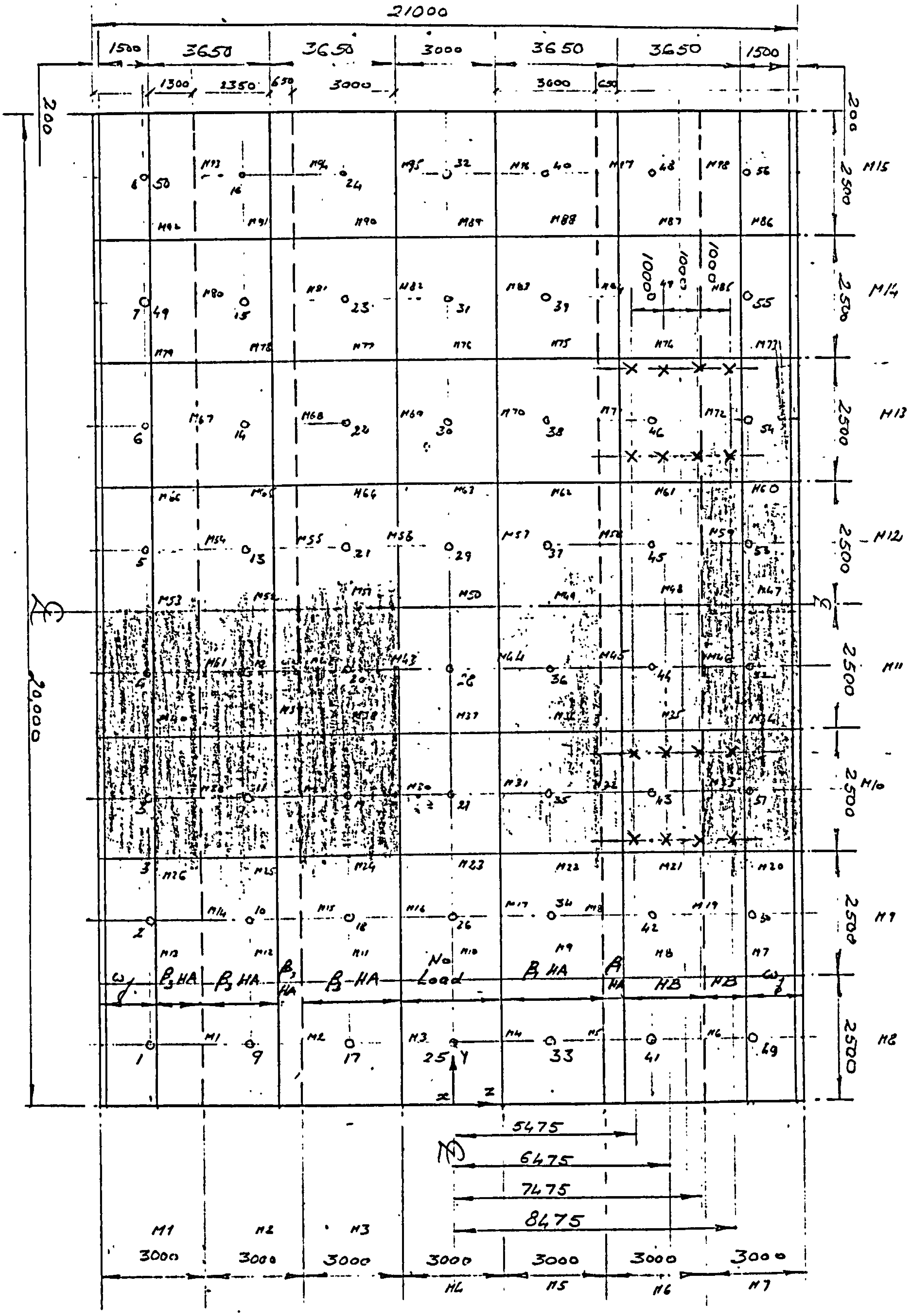

Figure F3 - Computer modelling of the 20m span bridge deck.

Load value

Using the factored udl value,

β_1HA = 1 x 58.7 = 58.7 kN/m of notional lane.

β_3HA = 0.6 x 58.7 = 35.2 kN/m of notional lane.

$\omega_{footpath}$ = 25.5/2 kN/m for each side of pedestrian footpath.

$\omega_{footpath}$ = 12.75 kN/m.

$\omega_{surfacing}$ = 61.6 kN/m.

$\omega_{concrete}$ = 317/7 kN/m for each hypothetical beam in the grillage.

$\omega_{concrete}$ = 45.3 kN/m.

Abnormal factored load

A section is taken across the bridge at mid-span of Figure F3, with the HB vehicle in the position on the left lane. HB load being 585 kN/axle, the load distribution of this axle load on the hypothetical grillage is as follows:

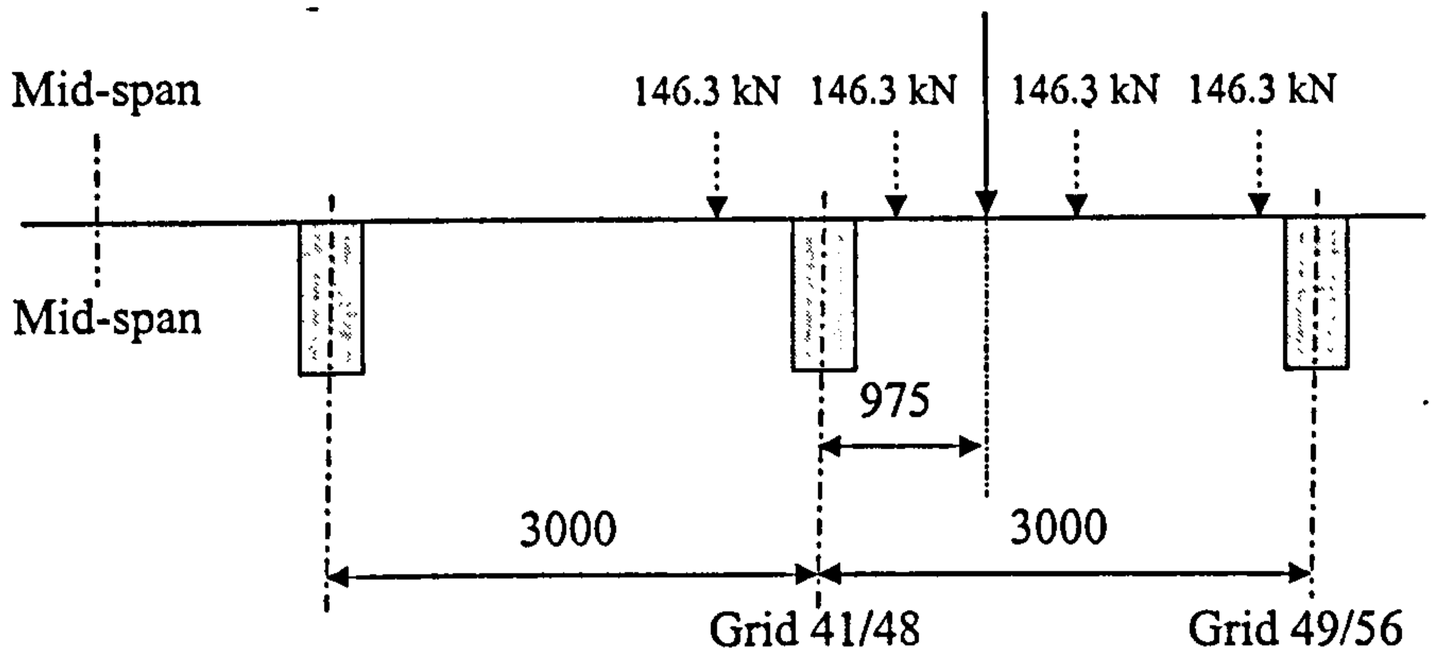

$HB_{41/48}$ = 585 x 2025/3000 = 395 kN.

$HB_{49/56}$ = 585 x 975/3000 = 190 kN.

KEL factored load

KEL point load is to be positioned at mid-span on each lane as shown in Figure F2. The position of each KEL point load relative to the hypothetical grid of Figure F3 and its load distribution is calculated as below, KEL = 156 kN/notional lane. Note that factors β_1 & β_3 are being applied if KEL falls into such zone.

1st notional lane from HB vehicle,

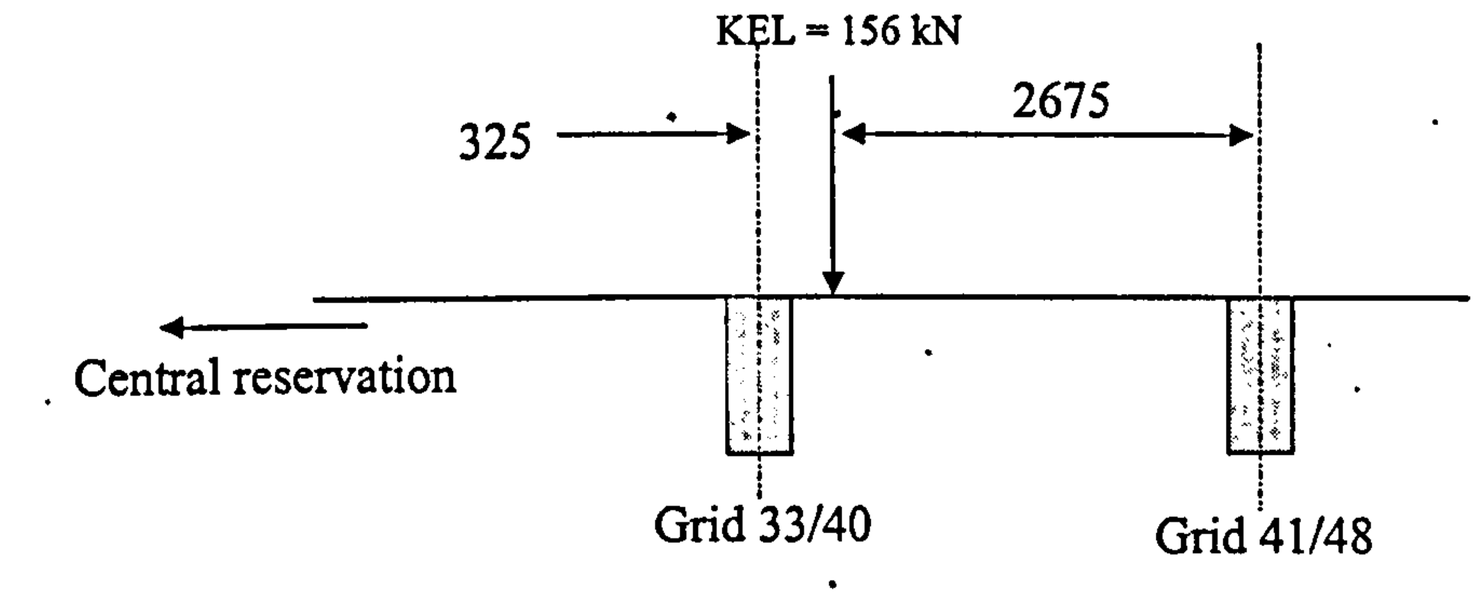

$\beta_1 KEL_{33/40} = 1 \times 156 \times 2675/3000 = 139.1$ kN.

$\beta_1 KEL_{41/48} = 1 \times 156 \times 325/3000 = 16.9$ kN.

2nd notional lane from the HB vehicle,

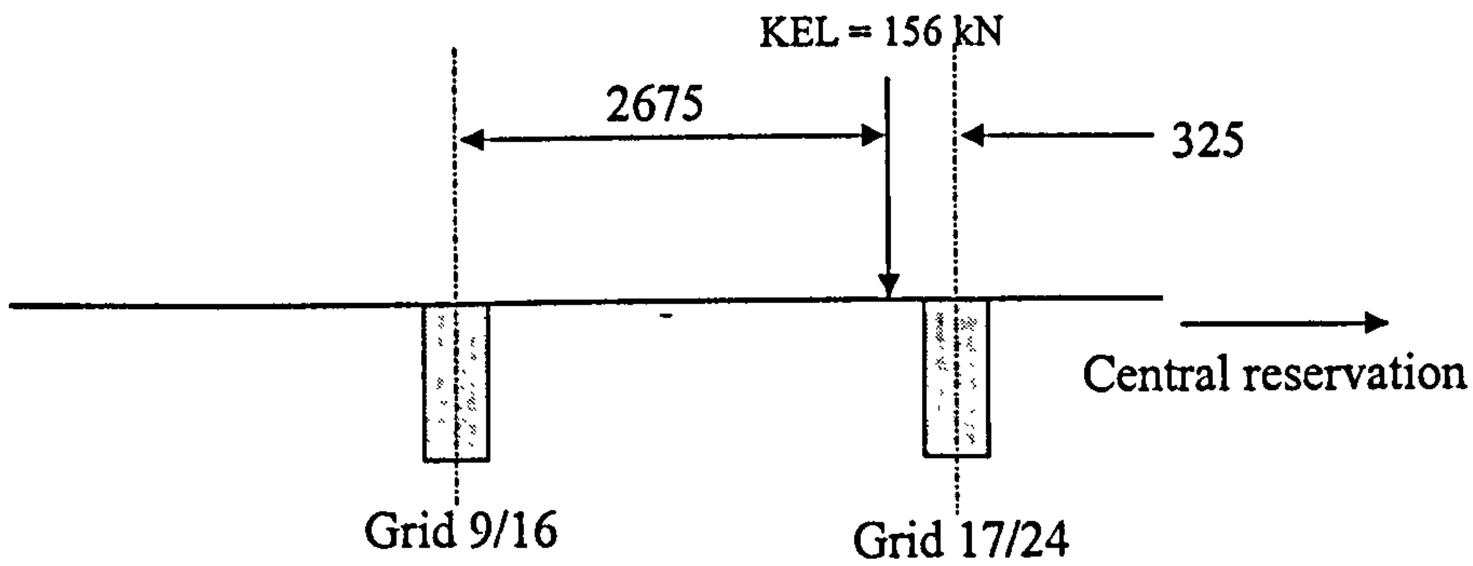

$\beta_3 KEL_{17/24} = 0.6 \times 156 \times 2675/3000 = 83.46$ kN.

$\beta_3 KEL_{9/16} = 0.6 \times 156 \times 325/3000 = 10.14$ kN.

3rd notional lane from the HB vehicle,

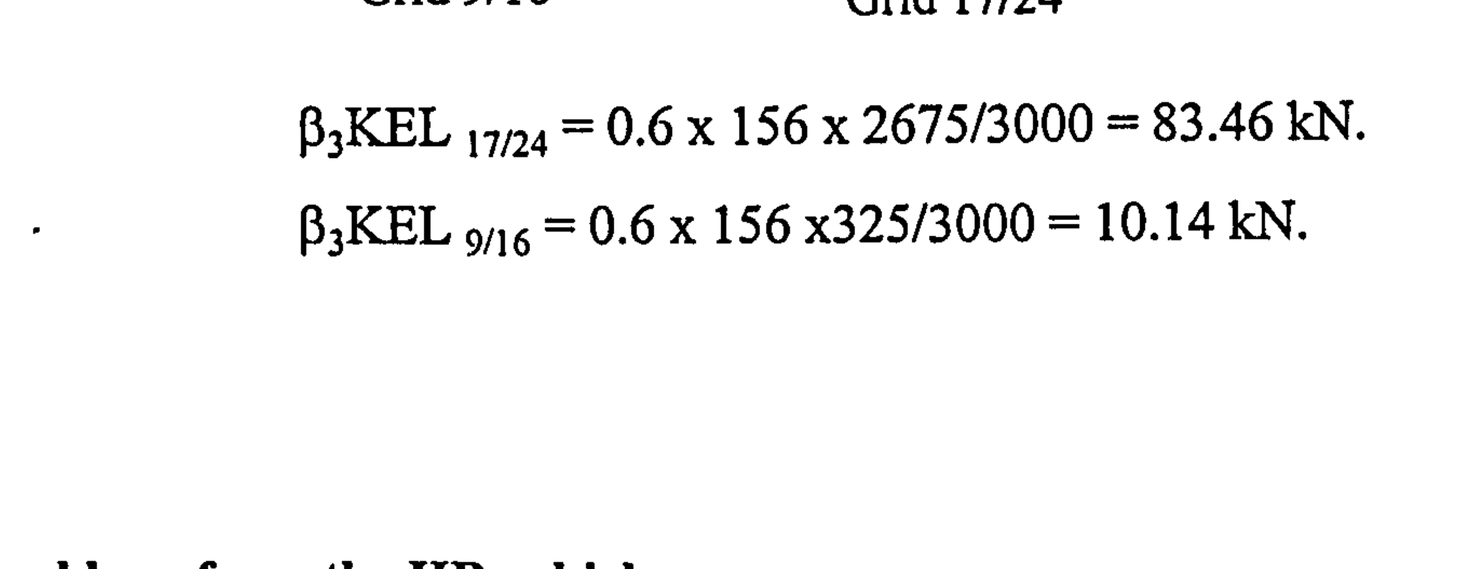

$\beta_3 KEL_{1/8} = 0.6 \times 156 \times 975/3000 = 30.42$ kN.

$\beta_3 KEL_{9/16} = 0.6 \times 156 \times 2025/3000 = 63.18$ kN.

SECTION PROPERTIES OF THE BRIDGE BEING CONSIDERED

With reference to Figure F3 and the following Figure F4,

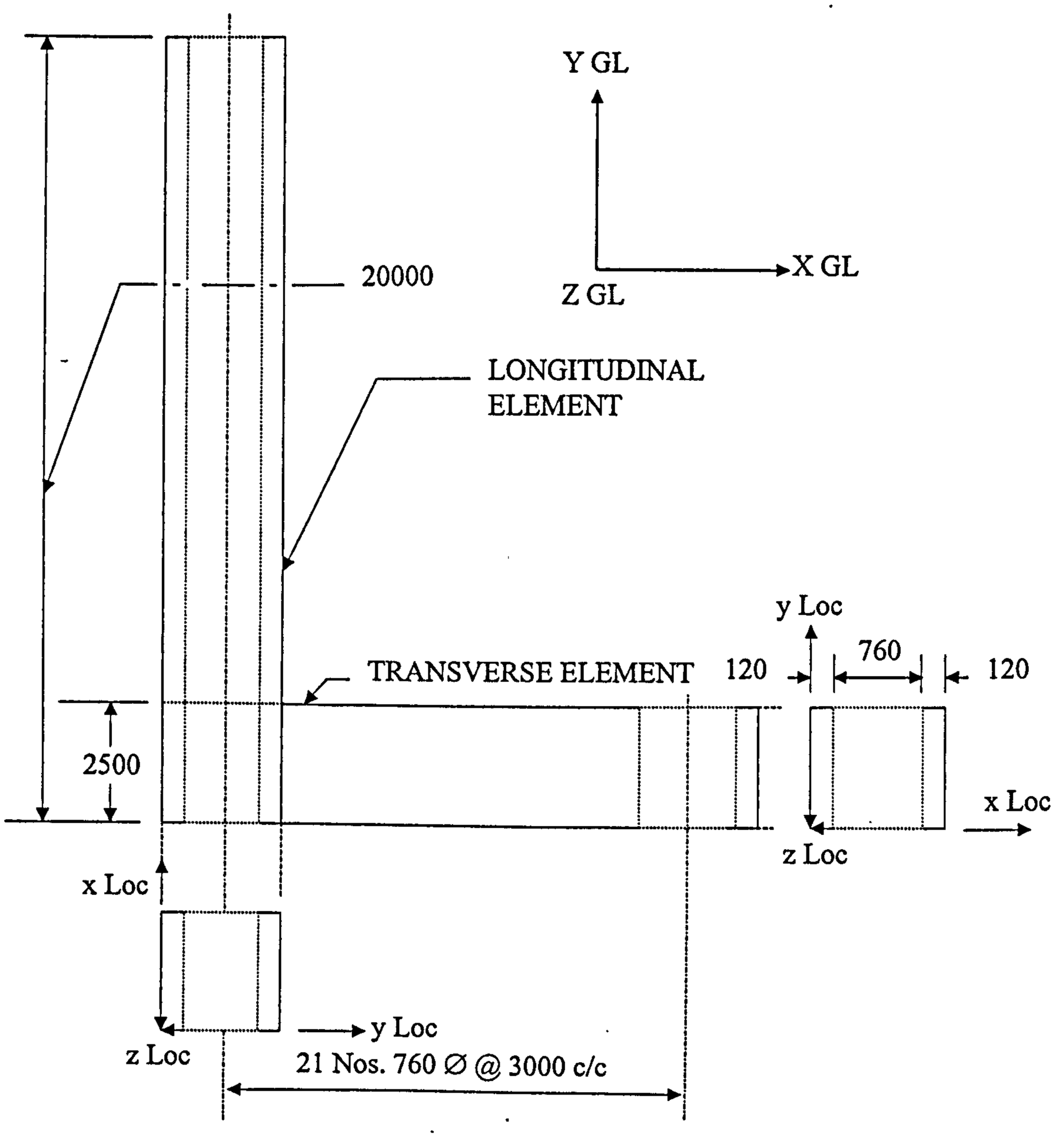

Figure F4. - Orientation of axes for bridge.

Longitudinal element

$$I_{YY} = \frac{bd^3}{12} = \frac{21000 \times 1000^3}{12} = 1.75 \times 10^{12}\ mm^4 \text{ gross cross section.}$$

$I_{YY} = 1.75 \times 10^{12} - (21 \times \pi \times 760^4/64) = 1.41 \times 10^{12}\ mm^4$ Net cross section.

$I_{YY} = 1.41 \times 10^{12}/7 = 2.014 \times 10^{11}\ mm^4$ for each longitudinal element.

$$I_{xx} = \frac{bd^3}{12} = \frac{2500 \times 1000^3}{12} - \frac{2500 \times 760^3}{12} = 1.17 \times 10^{11}\ mm^4 \text{ net cross section.}$$

$$I_{zz} = \frac{1000 \times 21000^3}{12} = 7.72 \times 10^{14}\ mm^4 \text{ gross cross section.}$$

$I_{ZZ} = 7.72 \times 10^{14}/7 = 1.102 \times 10^{14}\ mm^4$ for each element.

$$J = \frac{1}{3}bh^3 - \frac{\pi}{2}r^4$$

$$J = \frac{1}{7}\left[\frac{21000 \times 1000^3}{3} - \frac{\pi \times 21}{2}\left(\frac{760}{2}\right)^4\right] \text{ net cross section of each element.}$$

$J = 9.02 \times 10^{11}\ mm^4$.

Transverse element

$$I_{YY} = \frac{2500}{12}1000^3 - \frac{2500}{12}760^3 = 1.17 \times 10^{11}\ mm^4 \text{ Net cross section.}$$

$I_{XX} = 1.41 \times 10^{12}/7 = 2.014 \times 10^{11}\ mm^4$ net cross section.

$$I_{zz} = \frac{2 \times 120 \times 2500^3}{12} = 3.13 \times 10^{11} mm^4.$$

$$J = \frac{1}{3}bh^3 = 2\left(\frac{2500 \times 120^3}{3}\right) = 2.88 \times 10^9\ mm^4.$$

LOAD DATA FOR COMPUTING

Table F details the computing data.

Table F - Computing data.

Grid line, refer to Fig F3	**UDL (kN/m)**	**KEL (kN)**	**HB load (kN)**
1/8	$\frac{1300}{3650}(35.2+61.6)+12.75+45.3=92.53$	30.42	-
9/16	$\frac{3000}{3650}(35.2+61.6)+45.3=124.86$	63.18 + 10.14 = 73.32	-
17/24	$\frac{3000}{3650}(35.2+61.6)+45.3=124.86$	83.46	-
25/32	$\frac{3000}{3650}(61.6)+45.3=95.9$	-	-
33/40	$\frac{3000}{3650}(58.7+61.6)+45.3=144.18$	139.1	1
41/48	$\frac{650}{3650}(58.7)+\frac{3000}{3650}(61.6)+45.3=106.4$	16.9	395 @ four positions along span direction
49/56	$\frac{1300}{3650}(61.6)+12.75+45.3=80.00$	-	190 @ four positions along span direction